Towards rapid self-healing polymer organogelators for electrophoretic type displays

A thesis submitted to The University of Manchester for the degree of
Doctor of Philosophy
in the Faculty of Science and Engineering

Submitted 2016

Melody Obeng

School of Materials

Contents

List of Figures 5

List of Schemes 10

List of Tables 12

List of Equations 13

List of Abbreviations 16

List of Symbols 19

Thesis Abstract 23

Declaration 24

Copyright statement 24

Dedication 25

Acknowledgments 26

Preface 27

1 Introduction 29

1.1 Aim of the study 29

1.2 Survey of thesis 29

1.3 References 31

2 Background information and literature review 32

2.1 Industrial potential of polymer organogelators in electrophoretic paper technology 32

2.1.1 Properties of electronic paper devices 32

2.1.2 Functions of EPDs 33

2.1.3 Proposed function of a polymer organogelator in an EPD 36

2.1.4 Properties of bistable gels in EPD technology 37

2.2 Various pathways to achieve gelation from polymer organogelators 37

2.2.1 Low molecular weight gelators 37

2.2.2 Self-assembly of low molecular weight gelators 43

2.2.3 Self-assembly of polymers containing LMWGs 46

2.2.4 Self-assembly of non-ionic amphiphilic linear copolymers 47

2.2.5 Assemblies of non-ionic amphiphilic graft copolymers 54
2.3 The evolution of radical polymerisation 56
2.3.1 Conventional free radical polymerisation 56
2.3.2 Controlled radical polymerisation 58
2.3.2.1 CRP based on degenerative transfer 59
2.3.2.2 CRP based on the persistent radical effect 63
2.4 Concluding remarks 69
2.5 References 71
3 Key methods and characterisation techniques 77
3.1 ATRP 77
3.1.1 Initiating system 77
3.1.2 Halogen exchange method 80
3.1.3 Solvent polarity and polymerisation temperature 81
3.1.4 The initial presence of deactivator species/ reducing agents 82
3.2 Physical characterisation 82
3.2.1 Proton nuclear magnetic resonance 82
3.2.2 Gel permeation chromatography 84
3.2.3 Dynamic light scattering 85
3.2.4 Rheology 87
3.2.5 Transmission electron microscopy 89
3.2.6 Elemental analysis 90
3.3 References 90
4 Results and Discussion 92
Proposed Publication Paper 1 93
Proposed Publication Paper 2 94
Proposed Publication Paper 3 95
5 Conclusions and future work 96
5.1 Work overview 96

5.2 Future work 97

Word count: 49,072

List of Figures

Fig. 1.1 Depiction of the linear copolymer approach (a) and the graft copolymer approach (b) towards developing polymer gelators with a LMWG segment. The diblock copolymer is represented by the blue and green segments whilst the purple star indicates the LMWG. Page 30

Fig. 1.2 Depiction of an amphiphilic linear diblock copolymer gelator comprising of two distinct polymer blocks signified by the blue and red segments. The blue and red segment represents the solvophillic and the solvophobic parts of the macromolecule, respectively. Self-assembled nano-objects with spherical, worm-like and vesicle morphologies are obtained depending on the ratio of the solvophobic block to the solvophillic the block. Page 30

Fig. 1.3 Depiction of an amphiphilic graft copolymer. The polymer side chains are indicated by the blue (PLMA) and the red (PBzMA) segments. The black (PBiBEA) and blue segments represent the solvophillic blocks whilst the red segment represents the solvophobic block. Large spherical assemblies are obtained for a graft copolymer structure that possess longer side chains with respect to the polymer backbone. Page 31

Fig. 2.1 A thin and bendable colour EPD possessing an image memory property developed by Fujitsu. Page 33

Fig. 2.2 Amazon Kindle that displays black text on white coloured background. Page 33

Fig. 2.3 Illustration of an EPD with E-ink containing white and black charged microparticles. Page 34

Fig. 2.4 A depiction of inside a coloured EPD. Page 35

Fig. 2.5 ALS gelator (a) and (*R*)-12-hydroxystearic acid (b). The number '17' indicates the carbon atom number to which the steroid group is attached. Page 38

Fig. 2.6 Dibenzylidene-monosaccharide. Page 41

Fig. 2.7 N^{ε}-lauroyl-*L*-lysine. Page 42

Fig. 2.8 Cyclo(*L*-aspartyl-*L*-phenylalanyl) that comprises of *L*-phenylalanine and *L*-aspartic acid constituents. Page 43

Fig. 2.9 Hydrogen bonding between carboxylic groups of neighbouring amino acid derived LMWGs. Page 43

Fig. 2.10 Polymer gelator containing LMWGs. Page 46

Fig. 2.11 Morphologies formed from amphiphilic surfactants. Page 48

Fig. 2.12 Illustration of the relationship between the packing parameter and morphologies of non-ionic amphiphilic diblock copolymers. Page 49

Fig. 2.13 Worms-to-sphere transition. The red arrows (b) indicate the presence of spheres. Page 53

Fig. 2.14 Architectural comparison between a linear and graft copolymer. Page 54

Fig. 2.15 Bowl-shaped morphologies obtained from TEM studies of graft copolymer based on polystyrene (core-forming block). Page 54

Fig. 2.16 Graphical representation of the relationship between number-average molecular weight (M_n) with conversion. The blue and red lines represent conventional free radical polymerisation and controlled radical polymerisation, respectively. Page 58

Fig. 2.17 TEMPO nitroxide radical. Page 63

Fig. 2.18 Illustration of well-defined polymer topologies, composition and functionalities prepared by ATRP. The varying compositions are distinguished by darker and lighter circles denoting differing monomer units. Chain end functionality is represented by moieties (X or Y). Page 67

Fig. 3.1 Various initiators with their respective rate constants of activation in brackets. The ATRP reactions conducted at 35 °C for the study shown in the figure above used the catalyst/ligand complex $Cu^{I}X$/PMDETA (X = Br or Cl) and the solvent acetonitrile. The initiators with 3° structures are red whilst those with 2° and 1° structures are blue and black, respectively. Isocyanate/thiocyanate can be seen to the left of the figure with half-filled symbols. Chloride-based initiators are signified by open symbols, bromide-based initiators are represented by filled symbols whilst iodide-based initiators are indicated by bottom half-filled symbols. The structure of the radical stabilising group is indicated like so: amide (∇), benzyl ester (Δ), ester (sqaure), nitrile (circle) and phenyl ester (◊). Page 77

Fig. 3.2 The ATRP equilibrium constants (K_{ATRP}) plotted for common ATRP multidentate nitrogen-based ligands. The ATRP reactions were conducted at 22 °C using $Cu^{I}Br$ catalyst in acetonitrile. The direction of the black arrow indicates faster rates of ATRP. Page 79

Fig. 3.3 $Cu^{I}Br$/PMDETA in a non-polar media forms a neutral complex (a) and an ion pair (b). Page 80

Fig. 3.4 Orientation of protons in an external magnetic field. Page 82

Fig. 3.5 Diagram of the dynamic light scattering theory. Page 85

Fig. 3.6 Depiction of shear stress on an object. Page 86

Fig. 3.7 Newtonian, non-Newtonian and Bingham fluids viscosity in response to a constant shear rate taken from ref. Bingham fluids are strictly non-Newtonian before displaying Newtonian fluid-like behaviour when under minimum stress. The symbols $\eta_0$and η_∞represent zero shear rate viscosity and infinite shear rate viscosity, respectively. Page 87

Proposed publication paper 1

Fig. 1 ^{1}H NMR spectra for LA_8 (a) and L_{10} (b). The signals labelled with *, ** and *** signify the impurities water, DMF and vinyl groups belonging to unreacted LA, respectively. Page 17

Fig. 2 GPC chromatograms for LA_8 (a) and L_{10} (b). The chromatograms were obtained using THF eluent and polystyrene standards. Page 18

Fig. 3 ^{1}H NMR spectra for the homopolymer L_{43} (a) and the diblock copolymers L_{10}-H_{10} (b) and L_{10}-H_5 (c). The signals labelled with * and ** represent water and DMF, respectively. A co-solvent blend of the deuterated solvents $CDCl_3$ and undeuterated DMF was required for ^{1}H NMR characterisation of L_{10}-H_y copolymers. Page 21

Fig. 4 GPC chromatograms for L_{43} and the diblock copolymer L_{10}-H_5. Signs of L_{10} that lacked further chain extension of LMA repeat units is indicated by the arrow. The chromatograms were obtained using THF eluent and polystyrene standards. Page 22

Fig. 5 ^{1}H NMR spectra for L_{10}-H_5 (a) and L_{10}-H_5-$CONHCOC(Cl)_3$ (b) following the addition of trichloroacetyl isocyanate, that results in a proportion of substituted OH groups. Page 24

Fig. 6 ^{1}H NMR spectra for PMA_6 (a), PMA_6-$AlOH_1$ (b) PMA_6-$AlOH_1$-$CONHCOC(Cl)_3$ (c). Page 26

Fig. 7 ^{1}H NMR spectra for Aspartame (a) and CAP (b) and the diblock copolymer gelator, L_{10}-H_5-CAP_z (c). Page 27

Fig. 8 ^{1}H NMR spectra for HEA (a) and HEATMS (b) $PHEATMS_{21}$ (c) and the macroinitiator P_{21} (d). Page 29

Fig. 9 GPC chromatograms for PH_{21} (a) and the macroinitiator P_{21} (b). The chromatograms were obtained using THF eluent and polystyrene standards. Page 30

Fig. 10 ^{1}H NMR spectra for the graft copolymers $(P\text{-}LA_7)_{21}$ (a) and $(P\text{-}L_{33})_{21}$ (b). Page 33

Fig. 11 Image of the graft copolymer, $(P\text{-}LA_7)_{21}$, that precipitated from solution during polymerisation of LA from the macroinitiator P_{21}. Page 34

Fig. 12 GPC chromatograph of $(P\text{-}L_{33})_{21}$. Signs of the macroinitiator P_{21} that lacked grafted LMA repeat units is indicated by the arrow. The chromatograms were obtained using THF eluent and polystyrene standards. Page 35

Proposed publication paper 2

Fig. 1 ^{1}H NMR spectra for the macroinitiator (L_{14}) and the diblock copolymers. The identities are shown. The peak labelled with * was due to water. Page 9

Fig. 2 GPC chromatograms for the macroinitiator (L_{14}) and the diblock copolymers (L_{14}-B_{34} – L_{14}-B_{74}). The chromatograms were obtained using THF eluent and polystyrene standards. Page 10

Fig. 3 TEM images of diblock copolymer nano-objects deposited from *n*-dodecane dispersions. The samples were stained with ruthenium tetra-oxide. The scale bars in the main and inset figures represent 200 and 20 nm, respectively. Page 11

Fig. 4 Low magnification TEM images of diblock copolymer nano-objects deposited from *n*-dodecane dispersions containing (a) L_{14}-B_{34}, (b) L_{14}-B_{46}, (c) L_{14}-B_{64} and (d) L_{14}-B_{74}. The samples were stained with ruthenium tetra-oxide. The arrows in (d) highlight small vesicles. Page 12

Fig. 5 Phase diagram comparing ATRP-based $PLMA_{14}$-$PBzMA_y$ diblock copolymer nano-objects from the present study (black diamonds and labels) with those prepared by non-aqueous RAFT dispersion polymerisation from Fielding *et al.* (Ref: *J. Amer. Chem. Soc.*, 136, 5790, 2014) (red diamonds and labels). Page 13

Fig. 6 Variable-temperature ^{1}H NMR spectra for dilute dispersions of (a) L_{14}-B_{34} and (b) L_{14}-B_{64} in dodecane-d_{26}. The temperature was increased from 25 to 115 °C before cooling to 25 °C. (c) Signal integral ratios of **j** to **f** for the dispersions containing L_{14}-B_{34} spheres (red circles) and L_{14}-B_{64} worms (black squares). Page 16

Fig. 7 Variable-temperature DLS data for dispersions of (a) L_{14}-B_{34} spheres and (b) L_{14}-B_{64} worms. The *z*-average diameter is represented by blue circles, while the polydispersity index is represented by red squares. The arrows indicate the directions of temperature ramps. The initial and final temperatures were 20 °C. Page 17

Fig. 8 (a) Concentrated dispersions of $PLMA_{14}$-$PBzMA_y$ diblock copolymers in *n*-dodecane (20 % w/w) at room temperature. Dispersions of L_{14}-B_{34} and L_{14}-B_{74} were free-flowing liquids. The vesicles in L_{14}-B_{74} showed evidence of sedimentation. L_{14}-B_{46} and L_{14}-B_{64} formed self-supporting gels with the former being less turbid. (b) L_{14}-B_{46} de-gelled when heated to 90 ^{o}C to form a free-flowing liquid which subsequently re-gelled when cooled. Page 19

Fig. 9 (a) Dynamic frequency-sweep rheology data for the physical gels formed from L_{14}-B_{64} and L_{14}-B_{46} dispersed in *n*-dodecane (20 % w/w). The G' (storage modulus) and G'' (loss modulus) values are indicated by closed and open data points, respectively. (b) Variation of tan δ (= G'' / G') with frequency for L_{14}-B_{64} and L_{14}-B_{46}. All data were measured at 20 ^{o}C. Page 20

Fig. 10 Variable temperature dynamic rheological data for (a) L_{14}-B_{46} and (b) L_{14}-B_{64} dispersed in *n*-dodecane (20 % w/w). The G' (storage modulus) and G'' (loss modulus) values are indicated by closed data points and open data points, respectively. T_{soft} and CGT are the gel softening temperature and critical gelation temperatures, respectively (See text). Page 21

Fig. 11 Variation of tan δ (= G'' / G', where G'' and G' are the loss and storage modulus, respectively) with temperature for (a) L_{14}-B_{46} and (b) L_{14}-B_{64} dispersed in *n*-dodecane (20 % w/w). The measurements started at 20 ^{o}C. Page 22

Proposed publication paper 3

Fig. 1 Design strategies for previous work (a) described in the second proposed publication in Chapter 4 and current work (b). The solvophilic and solvophobic blocks are represented by the blue and red segments, respectively. The solvophilic core (PBiBEA) is exclusive to the graft copolymer and represented by the black segment. Page 3

Fig. 2 ^{1}H NMR for the macroinitiator P_{21} (a) and the graft copolymers $(P\text{-}L_{15})_{21}$ (b), $(P\text{-}L_{15}\text{-}B_4)_{21}$ (c) and $(P\text{-}L_{15}\text{-}B_{31})_{21}$ (d). The peaks labelled with an asterix are identified as residual water (*), acetone (**) and benzyl methacrylate vinyl groups (***), respectively. Page 10

Fig. 3 GPC chromatograms for the macroinitiator P_{21} and the graft copolymers $(P\text{-}L_{15})_{21}$, $(P\text{-}L_{15}\text{-}B_4)_{21}$ and $(P\text{-}L_{15}\text{-}B_{31})_{21}$. The chromatograms were obtained using THF and linear polystyrene standards. The arrows indicate evidence of dead polymeric chains. Page 11

Fig. 4 TEM images for $(P\text{-}L_{15}\text{-}B_4)_{21}$ (a) and $(P\text{-}L_{15}\text{-}B_{31})_{21}$ (b) graft copolymer assemblies. Scrutiny of the core-shell morphology is indicated by a yellow arrow (core) and an orange arrow (shell). The white arrow specifies smaller assemblies. Page 16

Fig. 5 Variable-temperature ^1H NMR studies for dilute dispersions of the graft copolymers $(P\text{-}L_{15}\text{-}B_4)_{21}$ (a) $(P\text{-}L_{15}\text{-}B_{31})_{21}$ (b). The temperature increased every 15 ^oC from 25 ^oC to 115 ^oC before returning to the starting temperature. (c) Signal integral ratio for **k** and **f´** for $(P\text{-}L_{15}\text{-}B_4)_{21}$ (B4) and $(P\text{-}L_{15}\text{-}B_{31})_{21}$ (B31). Page 19

Fig. 6 Variable-temperature DLS studies of the graft copolymers $(P\text{-}L_{15}\text{-}B_4)_{21}$ (a) and $(P\text{-}L_{15}\text{-}B_{31})_{21}$ (b). The *z*-average diameter is represented by black circles, whilst the PDI is represented by red squares. The arrows indicate the direction of the temperature ramps. The temperature ramp began and ended at 20 °C. Page 20

List of Schemes

Scheme 2.1 Proposed self-healing concept of the physical gel in an EPD. Page 36

Scheme 2.2 Reversible mechanism of LMWGs forming a three-dimensional network. Page 44

Scheme 2.3 Mechanism for the formation of spherulitic or fibrous network SAFINS (self-assembled fibrillary network) formed from heating a solution containing the LMWGs 5α-cholestan-3β-yl *N*-(2-naphthyl) carbamate (CNC) or 3β-cholesteryl *N*-(2-naphthyl) carbamate (CeNC) in *n*-alkane or ethyl acetate. Page 45

Scheme 2.4 Kinetic steps for initiation (a), propagation (b) and termination (c) for conventional radical polymerisation. Page 56

Scheme 2.5 Kinetics for degenerative transfer CRP reactions. Page 59

Scheme 2.6 Kinetics for RAFT polymerisation. Page 60

Scheme 2.7 Kinetics for activation-deactivation CRP reactions. Page 62

Scheme 2.8 Kinetics for copper mediated ATRP. Page 65

Scheme 3.1 Depiction of the kinetic pathways for ISET and OSET. ISET-C and OSET-C occur in a concerted fashion whilst OSET-SW is a stepwise process. The ions are indicated with respective anionic or cationic charges. Page 78

Scheme 3.2 Kinetics of the halogen exchange principle in copper mediated ATRP. Page 80

Scheme 3.3 Depiction of gel permeation chromatography. Page 83

Scheme 3.4 Proposed mechanism for the reaction between cyclohexene and ruthenium tetra-oxide results in adipaldehyde and ruthenium dioxide. Page 89

Proposed publication paper 1

Scheme 1 Depiction of the synthesis of the diblock copolymer strategy. (a) The first step involved ATRP of LA to form PLA_8. (b) LMA was used in place of LA to form $PLMA_{10}$. Further chain extension of LMA from $PLMA_{10}$ resulted in $PLMA_{43}$. (c) Subsequent polymerisation of HEMA from $PLMA_{10}$ formed $PLMA_{10}$-$HEMA_y$ prior to the introduction of CAP that resulted in the diblock copolymer gelator, $PLMA_{10}$-$HEMA_y$-CAP_z. Page 5

Scheme 2 Depiction of the synthesis of CAP from Aspartame. Page 6

Scheme 3 Depiction of the series of steps required to synthesise PBiBEA from 2-hydroxethyl acrylate (HEA). Page 6

Scheme 4 Depiction of the synthesis of the graft copolymer strategy. (a) The first step involved grafting LA from PBiBEA to form $(PBiBEA\text{-}PLA_7)_{21}$. (b) LMA was also grafted from PBiBEA in place of LA to form $(PBiBEA\text{-}PLMA_{33})_{21}$. (c) The proposed steps for synthesising the graft copolymer gelator, $(PBiBEA\text{-}\ PLMA_x\text{-}HEMA_y\text{-}CAP_z)_{21}$. Page 7

Scheme 5 Depiction of the alcoholysis reaction between L_{10}-H_5 and trichloroacetyl isocyanate, that results in a proportion OH groups being substituted with a urethane bond.
Page 24

Proposed publication paper 2

Scheme 1 (a) Depiction of the synthesis of poly(lauryl methacrylate) macroinitiator ($PLMA_{14}$-Br) *via* solution ATRP using α-bromoisobutyrate (EBiB) and subsequent addition of benzyl methacrylate (BzMA) *via* halogen exchange through the use of CuCl/PMDETA to form $PLMA_{14}$-$PBzMA_y$. (b) Self-assembly of nano-objects was achieved by post-polymerisation transfer which involved replacing a volatile good solvent for both blocks (chloroform, Step 1) with a selective solvent (*n*-dodecane) for PLMA (Step 2). Spherical, worm-like or vesicle-like nano-objects assembled depending on the value for *y*. Page 4

Proposed publication paper 3

Scheme 1 (a) The synthesis of the graft copolymer $(PBiBEA\text{-}PLMA_{15}\text{-}PBzMA_y)_{21}$. The first step was the ATRP-based graft solution polymerisation of LMA from the multibrominated macroinitator ($PBiBEA_{21}$). The next step was chain extension using BzMA and halogen exchange. (b) Macromicelles assemblies of the graft copolymer obtained by post-polymerisation transfer involved replacing a good solvent for all three blocks (chloroform, Step 1) with a selective solvent (*n*-dodecane) for PLMA (Step 2). Page 5

List of Tables

Proposed publication paper 1

Table 1 Compositions and characterisation data for the synthesised homopolymers, diblock copolymer, macroinitiator and graft copolymers. Compositions determined from [a] ^{1}H NMR spectroscopy and [b] GPC studies Page 19

Proposed publication paper 2

Table 1 Compositions and characterisation data for the macroinitiator and copolymers. [a] Compositions determined from ^{1}H NMR spectroscopy. [b] Apparent sphere-equivalent *z*-average diameter of the diblock copolymers measured at 20 ^{o}C. [c] Morphologies based on TEM data (Fig. 2) Page 7

Proposed publication paper 3

Table 1 Compositions and characterisation data for the multibrominated macroinitiator and graft copolymers. [a] Compositions of P_{21} and the graft copolymers determined from GPC studies. [b] The spheres z-average diameters were measured at 20 °C *via* DLS. [c] The graft copolymer morphologies were determined from TEM data (Fig. 4) Page 12

List of Equations

$$p = \frac{V}{a_0 l_c} \quad \textbf{(2.1)}$$

$$N_{agg} = \frac{M_{w\ polymeric\ micelle}}{M_{w}\ polymer} \quad \textbf{(2.2)}$$

$$R_p = k_p[M]\left(\frac{f k_d[I]}{k_t}\right)^{\frac{1}{2}} \quad \textbf{(2.3)}$$

$$DP = \frac{k_p[M]}{(1+q)(f k_d[I])^{\frac{1}{2}}} \quad \textbf{(2.4)}$$

$$R_p = k_p K_{ATRP}\left(\frac{[P_n X][Cu^I/L]\,[M]}{[XCu^{II}/L]}\right) \quad \textbf{(2.5)}$$

$$\frac{M_w}{M_n} = 1 + \left(\frac{k_p[P_n X]}{k_{deact}[XCu^{II}/L]}\right)\left(\frac{2}{p} - 1\right) \quad \textbf{(2.6)}$$

$$M_n = \frac{\Sigma N_i M_i}{\Sigma N_i} \quad \textbf{(3.1)}$$

$$M_w = \frac{\Sigma N_i M_i^2}{\Sigma N_i M_i} \quad \textbf{(3.2)}$$

$$PDI = \frac{M_w}{M_n} \quad \textbf{(3.3)}$$

$$G(\tau) = \langle I(t).I(t+\tau)\rangle \quad \textbf{(3.4)}$$

$$G(\tau) = A + B\exp(-2\Gamma\tau) \quad \textbf{(3.5)}$$

$$\Gamma = Dq^2 \quad \textbf{(3.6)}$$

$$q = \frac{4\pi n}{\lambda}\sin\left(\frac{\theta}{2}\right) \quad \textbf{(3.7)}$$

$$d = \frac{kT}{3\pi\eta D} \quad \textbf{(3.8)}$$

$$\varepsilon = \frac{dl}{l_o} \quad \textbf{(3.9)}$$

$$\eta = \frac{\tau}{\dot{\gamma}} \quad \textbf{(3.10)}$$

$$G = \frac{\tau}{\gamma} \quad \textbf{(3.11)}$$

$$\tan\delta = \frac{G''}{G'} \quad \textbf{(3.12)}$$

Proposed publication paper 1

$$x = \frac{1}{6}\left(\left(\frac{A_h + A_c}{A_a}\right) - 2\right) \quad \textbf{(1)}$$

$$x = \frac{M_n - 195}{240} \quad \textbf{(2)}$$

$$x = \frac{M_n - 195}{254} \quad \textbf{(3)}$$

$$y = (9x + 3)\left(\frac{A_{g^*}}{A_h + A_c}\right) \quad \textbf{(4)}$$

$$y = \frac{M_n - (254x) - 151}{130} \quad \textbf{(5)}$$

$$y = x\left(\frac{A_{g^*}}{A_f}\right) \quad \textbf{(6)}$$

$$x = \frac{A_f}{A_a} \quad \textbf{(7)}$$

$$y = 3x\ \left(\frac{A_{g^*}}{A_f}\right) \quad \textbf{(8)}$$

$$z = \frac{1}{5}\left(\left(\frac{A_{t^{**}}}{A_{g^*}}\right)\ 2y\right) \quad \textbf{(9)}$$

$$z = y\left(\frac{A_{n^{**}} + A_{q^{**}}}{A_{g^*}}\right) \quad \textbf{(10)}$$

$$x = 3\left(\frac{A_{f^{**}}}{A_{c^*}}\right) \quad \textbf{(11)}$$

$$x = \frac{M_n - 195}{188} \quad \textbf{(12)}$$

$$n = \frac{3}{2}\left(\frac{{A_f}^{**} + {A_g}^{*}}{A_c}\right) \quad \textbf{(13)}$$

$$\text{chain end fidelity} = \left(\frac{A_{h^*}}{A_{c^*}} \times \frac{1}{n}\right) \times 100 \quad \textbf{(14)}$$

$$n = \frac{M_n - 195}{265} \quad \textbf{(15)}$$

$$x = \frac{2}{9}\left(\left(\frac{A_c + A_{c^*} + A_h}{A_f + A_g}\right) - \frac{1}{3}\left(1 + \frac{1}{n}\right)\right) \quad \textbf{(16)}$$

$$x = \frac{M_n - (265n) - 195}{254n} \quad \textbf{(17)}$$

Proposed publication paper 2

$$y = (9x + 3)\left(\frac{A_j}{A_h + A_c}\right) \quad \textbf{(2)}$$

$$l = 0.125\ \times\ 2 \quad \textbf{(3)}$$

$$l_{stretch} = yl \quad \textbf{(4)}$$

$$d_{max} = 2l_{stretch} \quad \textbf{(5)}$$

$$m_{sphere} = \frac{\pi \rho_{PBzMA} d_{TEM}^3}{6} \quad \textbf{(6)}$$

$$m_{PBzMA} = \frac{MW_{PBzMA}}{N_A} \quad \textbf{(7)}$$

$$N_{agg} = \frac{m_{sphere}}{m_{PBzMA}} \quad \textbf{(8)}$$

$$A_{sphere} = \pi d_{TEM}^2 \quad \textbf{(9)}$$

$$A_{chain} = \frac{A_{sphere}}{N_{agg}} \quad \textbf{(10)}$$

Proposed publication paper 3

$$x = \frac{3}{2}\left(\frac{A_f + A_g}{A_c}\right) \quad \textbf{(1)}$$

$$\text{chain end fidelity} = \left(\frac{A_h}{A_c} \times \frac{1}{n}\right) \times 100 \quad \textbf{(3)}$$

$$n_{MI} = \frac{m_{MI}}{M_n} \quad \textbf{(5)}$$

$$\bar{n}_{MI} = \frac{N_A\, n_{MI}}{V} \quad \textbf{(6)}$$

$$H = \left(\frac{1}{\bar{n}_{MI}}\right)^{\frac{1}{3}} \quad \textbf{(7)}$$

$$x' = \sin(54.75)Q \quad \textbf{(8)}$$

$$L = xm \quad \textbf{(9)}$$

$$m = 1(0.8Q) \quad \textbf{(10)}$$

$$y = \frac{M_n - (265n) - (254xn) - 195}{176} \quad \textbf{(11)}$$

$$L = (x + y)m \quad \textbf{(12)}$$

$$d_{cal} = \left(\frac{6m_{chain}}{\rho\pi}\right)^{\frac{1}{3}} \quad \textbf{(13)}$$

$$m_{chain} = \frac{M_n}{N_A} \quad \textbf{(14)}$$

List of Abbreviations

Abbreviation	Full meaning
ARGET	activators regenerated by electron transfer
ATRA	atom transfer radical addition
ATRP	atom transfer radical polymerisation
CRP	controlled radical polymerisation
Cu	copper
CuCl	copper chloride
DLS	dynamic light scattering
DMF	*N*, *N*-dimethylformamide
DP_n	number-average degree of polymerisation
EPD	electrophoretic type display
GPC	gel permeation chromatography
ISET	inner sphere electron transfer
IUPAC	International Union of Pure and Applied Chemistry
K_{ATRP}	ATRP equilibrium constant
L	ligand
LMWG(s)	low molecular weight gelator(s)
ALS	aromatic, linker and steroidal groups
MWD	molecular weight distribution
OSET	outer sphere electron transfer
PDI	polydispersity index
PCS	photon correlation spectroscopy
PISA	polymerisation induced self-assembly
PMDETA	*N,N,N′,N′′,N′′*-pentamethyldiethylenetriamine
PRE	persistent radical effect

^{1}H NMR	proton nuclear magnetic resonance
NMP	nitroxide-mediated polymerisation
SFRP	stable free radical polymerisation
RAFT	reversible addition-fragmentation chain transfer
RDRP	reversible-deactivation radical polymerisation
RP	radical polymerisation
SEC	size exclusion principle

Proposed Publication paper 1

Abbreviation	Full meaning
PLMA	poly(lauryl methacrylate)
CAP	cyclo(*L*-aspartyl-*L*-phenylalanyl)
LA	lauryl acrylate
LMA	lauryl methacrylate
PLMA-PHEMA	poly(lauryl methacrylate)-*b*-poly(2-hydroxyethyl methacrylate)
PHEMA	poly(2-hydroxyethyl methacrylate)
PLA	poly(lauryl acrylate)
PBiBEA	poly(2-bromoisobutyryloxyethyl acrylate)
HEMA	2-hydroxyethyl methacrylate
HEA	2-hydroxyethyl acrylate
HEATMS	Trimethylsilyloxyethyl acrylate
PHEATMS	poly(trimethylsilyloxyethyl acrylate)
PMA	poly(methyl acrylate)
PMA-AlOH	poly(methyl acrylate)-*b*-poly(allyl alcohol)

Proposed Publication paper 2

Abbreviation	Full meaning
PLMA-PBzMA	poly(lauryl methacrylate)-*b*-poly(benzyl methacrylate)
PBzMA	poly(benzyl methacrylate)
BzMA	benzyl methacrylate

Proposed Publication paper 3

Abbreviation	Full meaning
PBiBEA-PLMA-PBzMA	poly(2-bromoisobutyryloxyethyl acrylate)-*g*-poly(lauryl methacrylate)-*b*-poly(benzyl methacrylate)

List of Symbols

Symbol	Meaning
a_0	surface area
A	area
[Cu^I/L]	concentration of activators
d	particle diameter
D	diffusion coefficient
dl	change in length
ε	strain
l_0	original length
f	initiator efficiency
F_p	parallel component force
G	shear modulus
G'	storage modulus
G''	loss modulus
[I]	initiator concentration
k	Boltzmann's constant
T	temperature
η	viscosity
I	intensity scattered light
τ	shear stress or delay time
Γ	decay rate
$G(\tau)$	autocorrelation function
H_0	external magnetic field
k_{act}	rate constant of activation
k_{deact}	rate constant of deactivation

k_{ex}	reversible degenerative exchange
k_d	rate constant of decomposition
k_i	rate constant of initiation
k_p	rate constant of propagation
k_t	rate constant of termination
I	characteristic spin of nucleus
l_c	length of the insoluble block
[M]	monomer concentration
M_n	number average molecular weight
M_w	weight average molecular weight
N_{agg}	aggregation number
N_i	number of chains
θ	scattering angle
ϕ	phase angle
n	refractive index
p	packing parameter or monomer conversion
λ	wavelength
V	volume
$[P_nX]$	concentration of dormant species
q	quantitative measure of the fraction of termination reactions due to disproportionation
q^2	modulus of scattering vector
R_p	rate of polymerisation
μ	nuclear magnetic moment
$[X\text{-}Cu^{II}/L]$	concentration of deactivators

Proposed Publication 1

Symbol	Meaning
x	number-average degree of polymerisation for the first polymer segment
y	number-average degree of polymerisation for the second polymer segment
z	number-average degree of polymerisation for the third molecular segment
n	number-average degree of polymerisation for the polymer backbone
A_a	integral value for a protons
A_c	integral value for c protons
A_c'	integral value for c′ protons
A_f	integral value for f protons
A_f''	integral value for f′′ protons
A_g	integral value for g protons
A_g'	integral value for g′protons
A_h	integral value for h protons
A_h'	integral value for h′ protons
A_n''	integral value for n′′ protons
A_q''	integral value for q′′protons
A_t''	integral value for t′′ protons

Proposed Publication 2

Symbol	Meaning
d_{TEM}	number-average diameter measured by TEM
l	repeat unit length for polymer length
d_{max}	number-average diameter measured by TEM
d_z	z-average of a spherical particle
$l_{stretch}$	fully stretched polymer segment
m_{PBzMA}	mass of PBzMA chain
m_{sphere}	mass of an average spherical particle

A_{sphere}	surface area of a sphere
A_{chain}	area per chain
N_A	Avogadro's constant
A_f	integral value for f protons
A_j	integral value for j protons
A_j / A_f	ratio of integrals for j and f protons

Proposed Publication 3

Symbol	Meaning
n_{MI}	number of moles for the macroinitiator
m_{MI}	mass of the macroinitiator
$\bar{n}_{MI}$	number of molecules of macroinitiator
H	distance between two centres
x'	unit length of polymer segment
Q	bond length
L	length of side chains
m	number of polymer segments
d_{cal}	calculated diameter
ρ	density
m_{chain}	mass of a chain
A_k / A_f'	ratio of integrals for k and f′ protons

Thesis Abstract

Towards rapid self-healing polymer organogelators for electrophoretic type displays

Abstract of thesis submitted by Melody Obeng to the School of Materials, The University of Manchester for the degree of Doctor of Philosophy, 2016

This thesis explores the development of rapid self-healing polymer organogelators that were proposed to sustain the function of an electrophoretic paper display (EPD). Two distinct topologies of the polymer gelators, prepared by atom transfer radical polymerisation (ATRP), were investigated. One was based on a linear copolymer and the second concerning a graft copolymer. Compositional differences of the copolymers established the pathways in which gelation from a non-polar organic solvent was pursued. One approach relied on the incorporation of a low molecular weight gelator (LMWG) onto a copolymer segment, whilst the other relied upon the amphilicity of diblock copolymers.

In the first part of the project a linear copolymer organogelator containing the LMWG cyclo(*L*-aspartyl-*L*-phenylalanyl) (CAP) was targeted. The block copolymer composition was based on poly(lauryl methacrylate)-*b*-poly(2-hydroxyethyl methacrylate) (PLMA-PHEMA). Preliminary trichloroacetyl isocyanate experiments implied that the hydroxyl proton belonging to HEMA would be absent in ^{1}H NMR spectroscopy studies following esterification. This observation was later confirmed, along with the emergence of a methylene proton signal at a chemical shift of 3.9 ppm, which strongly suggested successful synthesis of the diblock copolymer organogelator. Some of the PLMA-based graft copolymer organogelator was realised and confirmed *via* ^{1}H NMR spectroscopy and gel permeation chromatography, despite evidence of poor control over the polydispersity value (PDI = 2.21). Before ATRP conditions could be optimised, the project direction was changed to a less complex method of developing a polymer organogelator.

The second part of the project focused on preparing an amphiphilic linear polymer gelator based on poly(lauryl methacrylate)-*b*-poly(benzyl methacrylate (PLMA-PBzMA). When the PLMA degree of polymerisation (x) was fixed at 14 and the PBzMA degree of polymerisation (y) was varied, spheres (y = 34), mixed spheres and worms (y = 46) and pure worms (y = 64) in *n*-dodecane were observed *via* transmission electron microscopy (TEM). Concentrated gels (i.e., 20 wt. % PLMA-PBzMA) were formed from the mixed phase and the worms phase. Tube inversion tests of the mixed phase gel exhibited reversible de-gelation when heated to 90 $^{\circ}$C. Dilute dispersion studies *via* variable-temperature ^{1}H NMR spectroscopy and dynamic light scattering (DLS) studies showed thermo-reversibility of the nano-objects increased with decreasing lengths of y.

The third part of the project followed from the success of the linear diblock copolymer gelator approach. The PLMA-PBzMA-based graft copolymers formed spherical core-shell micellar clusters in *n*-dodecane that were revealed by TEM. Variable-temperature ^{1}H NMR spectroscopy showed that dilute dispersions showed thermo-reversibility irrespective of increasing lengths of y. However, variable-temperature DLS studies generally displayed kinetically frozen spheres at 90 $^{\circ}$C.

Finally, future design strategies based on the mixed phase composition were discussed towards achieving transparent gel forming organogelators. The potential for solution ATRP to prepare self-assembling copolymers for non-information display technology was also discussed.

Declaration

I hereby declare that no portion of the work referred to in this thesis has been submitted in support of an application for another degree or qualification of this or any other university or other institute of learning.

Copyright statement

i. The author of this thesis (including any appendices and/or schedules to this thesis) owns certain copyright or related rights in it (the "Copyright") and she has given The University of Manchester certain rights to use such Copyright, including for administrative purposes.

ii. Copies of the this thesis, either in full or in extracts and whether in hard or electronic copy, may be made only in accordance with the Copyright, Designs and Patents Act 1988 (as amended) and regulations issued under it or, where appropriate, in accordance with licensing agreements which the University has from time to time. This page must form part of any such copies made.

iii. The ownership of certain Copyright, patents, designs, trademarks and other intellectual property (the "Intellectual Property") and any reproductions of copyright works in the thesis, for example graphs and tables ("Reproductions"), which may be described in this thesis, may not be owned by the author and may be owned by third parties. Such Intellectual Property and Reproductions cannot and must not be made available for use without prior written permission of the owner(s) of the relevant Intellectual Property and/or Reproductions.

iv. Further information on the conditions under which disclosure, publication and commercialisation of this thesis, the Copyright and any Intellectual Property and/or reproductions described in it may take place is available in the University IP Policy (see http://documents.manchester.ac.uk/DocuInfo.aspx?DocID=487), in any relevant Thesis restriction declarations deposited in the University Library, The University Library's regulations (see http://www.library.manchester.ac.uk/aboutus/regulations) and in The University's policy on Presentation of Theses.

Dedication

I would like to dedicate this thesis to all my family and friends who have provided immense support during the last 4 years. To my exceptional mother Mary, thank you for your words of wisdom and reminding me that my faith is what makes all experiences worthwhile. To my siblings Michael and Megan for making me laugh in the face of impending deadlines. To my father Noah for inspiring me to take the family name as far as I can. To my uncles Funky and Junior, who continued to believe in me despite my feelings of discouragement. To my cousins Rachel, Joseph and Akua who reminded me that good food and jokes are all I need to overcome anything.

To Dayna and Tosin, I am grateful for having met you because my experience in Manchester wouldn't have been the same. To Deborah, Obioma and Dami, who were there for me through the fluctuations of life and declined every invitation to extended pity parties.

Finally, I would like to dedicate this thesis to my extended family and friends too numerous to name – I wouldn't have gotten this far without your input!

Acknowledgments

There are many people that contributed in many ways throughout my PhD project. The first, being my supervisor Prof. Brian Saunders. I would like to express my deepest gratitude to him for granting me the opportunity to work as a part of his research group, and also his immense support throughout my PhD project. He is surely one of a kind!

I would like to express my thanks to my co-supervisor Stephen Yeates for access to his research group's lab facilities and other staff at The School of Chemistry. I would also like to extend my thanks to Louise Farrand and Mark Goulding at Merck for their support. I greatly acknowledge the funding that was provided for this project from Merck and the EPSRC iCASE grant (Voucher 12220937).

I would like to acknowledge Polly Greensmith who passed down her knowledge of lab techniques to me and Dr Basile Khara for allowing me to pinch supplies from the teaching lab (I did always replace everything….overtime). I would also like to extend my thanks to Dr Lee Fielding for his input in submitting my first paper to a peer-reviewed journal.

I must thank my research colleagues Dr Naur Nabilah Shahidan, Dr Kyriaki Pafiti, Dr Silviya Halavecha, Dr Amirhossein Milani, Muhamad Sharan Musa and Zhenxing Cui whose lab experience helped my project immensely. I would like to thank my other research colleagues Mingning Zhu, Wenkai Wang, Nam Nguyen who made it enjoyable working in the lab. I also would like to extend my appreciation to other members of the research group.

Finally, I would like to extend my gratitude and appreciation to my family and friends who encouraged me to keep going no matter what the challenge.

Preface

The author of this thesis has obtained a Bachelor's degree in Biomedical Materials Science with a 1st class classification at The University of Manchester. Prior to this PhD project the author had undergraduate level experience in Colloidal research. Current research skills of the author include conducting atom transfer radical polymerisation. The author is also a confident interpreter of the characterisation studies used in this thesis.

“There’s no such thing as a failed experiment,
only experiments with unexpected outcomes.”

R. Buckminster Fuller

1 Introduction

1.1 Aim of the study

This study was a collaborative project with Merck Group[1] who sought to develop a new smart material based on electrophoretic paper display (EPD) technology. The aim of this project was to prepare a polymer gelator *via* copper-mediated atom transfer radical polymerisation (ATRP)[2]. It was hypothesised that the polymer gelator can form a transparent physical gel from the dielectric medium found in EPDs, which is typically a non-polar organic fluid. This process of gelation is exclusive to polymer organogelators, which is implied throughout this thesis. The successful application of the polymer organogelator in an microencapsulated EPD would result in Merck attaining their commercial goal of developing the next generation of EPDs, that could potentially compete with the market leader e-ink[3].

E-ink are the creators of electronic ink technology which is used in the Amazon Kindle. The technology involves pigmented microparticles that move between electrodes. The particle size is in the region of 0.15 – 0.5 μm and the dielectric medium forming the continuous phase is *n*-dodecane. It is hypothesised that the polymer gelator can form a physical gel from *n*-dodecane. EPDs must have good on / off stability so that the particles are held in place immediately after the electric field is switched off. Rheologically speaking, this indicates that the resultant gel can exhibit shear-thinning behaviour. It is important that the locally broken gel begins to reform as soon as the electric field is switched off. It was essential that the developed polymer organogelators displayed potential that complemented the design requirements of an ED. The aim of this project was to make such a gel.

1.2 Survey of thesis

This thesis begins with a literature review in Chapter 2 that outlines the theories and background information pertinent to this project. Chapter 3 gives a description of key methods that were employed in this project and the physical characterisation techniques used to analyse the (macro)molecules.

In Chapter 4, the analysis of the results obtained for this project are presented in a format suited for publication in a peer-reviewed journal. The alternative thesis format was adopted to distinguish the experimental pathways, while making the flow of the thesis coherent for the reader. There are three proposed publication papers detailed in Chapter 4.

For the first proposed publication paper two strategies were postulated as shown in Fig. 1.1. Polymer gelators based on poly(lauryl methacrylate)-*b*-poly(2-hydroxyethyl methacrylate) (PLMA-PHEMA) that contained the low molecular weight gelator (LMWG) cyclo(*L*-aspartyl-*L*-phenylalanyl) (CAP)[4, 5] were explored. This type of polymer gelator would cause gelation through intermolecular forces between LMWG segments. The first strategy involved the preparation of a linear diblock copolymer gelator whilst the second was centred on a graft copolymer gelator.

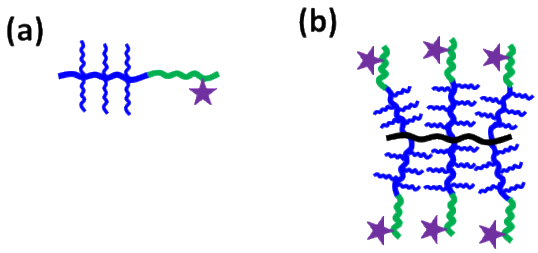

Fig. 1.1 Depiction of the linear copolymer approach (a) and the graft copolymer approach (b) towards developing polymer gelators with a LMWG segment. The diblock copolymer is represented by the blue and green segments, whilst the purple star indicates the LMWG.

The second proposed publication paper embarked on synthesising polymer gelators based on amphiphilic copolymers of poly(lauryl methacrylate)-*b*-poly(benzyl methacrylate) (PLMA-PBzMA)[6]. The relative ratio of the solvophillic (PLMA) and the solvophobic (PBzMA) macromolecular blocks resulted in various self-assembled nano-objects in a selective solvent suitable for the solvophillic block (Fig. 1.2). The solvophillic block acted as stabiliser for the block copolymers. Self-assembly driven by the amphiphilicity of this type of polymer gelator was discussed.

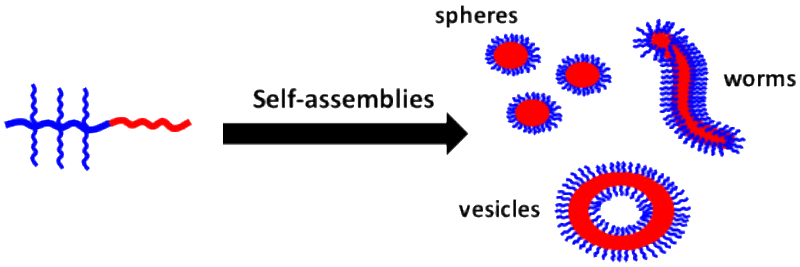

Fig. 1.2 Depiction of an amphiphilic linear diblock copolymer gelator comprising of two distinct polymer blocks, signified by the blue and red segments. The blue and red segments represent the solvophillic and the solvophobic parts of the macromolecule, respectively. Self-assembled nano-objects with spherical, worm-like and vesicle morphologies are obtained depending on the ratio of the solvophobic block to the solvophillic block.

The third proposed publication was focused towards the development of a polymer gelator based on an amphiphilic graft copolymer structure. The multibrominated macroinitiator poly(2-bromoisobutyryloxyethyl) acrylate (PBiBEA)[7] was used to grow PLMA-PBzMA side chains. The assembly of (PBiBEA-*g*-PLMA-*b*-PBzMA) graft copolymers in a selective solvent suitable for the solvophillic (PBiBEA and PLMA) blocks of the macromolecule are shown in shown in Fig. 1.3. The large-scale association of the amphiphilic graft copolymers were studied and discussed.

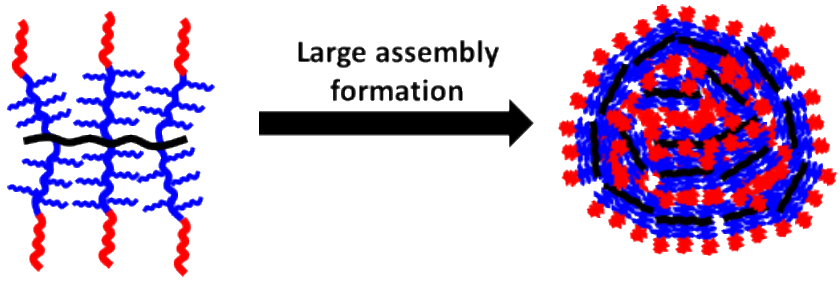

Fig. 1.3 Depiction of an amphiphilic graft copolymer. The polymer side chains are indicated by the blue (PLMA) and the red (PBzMA) segments. The black (PBiBEA) and blue segments represent the solvophillic blocks, whilst the red segment represents the solvophobic block. Large spherical assemblies are obtained for a graft copolymer structure that possess longer side chains with respect to the polymer backbone.

1.3 References

1. Merck Group, http://www.merckgroup.com/en/index.html, (accessed 18th December, 2016).
2. F. Isaure, P. A. G. Cormack, S. Graham, D. C. Sherrington, S. P. Armes and V. Butun, *Chem Commun*, 2004, 1138-1139.
3. E.-I. Coporation, http://www.eink.com/index.html, (accessed 18th December, 2016).
4. H. Hoshizawa, M. Suzuki and K. Hanabusa, *Chem Lett*, 2011, **40**, 1143-1145.
5. K. Hanabusa, M. Matsumoto, M. Kimura, A. Kakehi and H. Shirai, *J Colloid Interf Sci*, 2000, **224**, 231-244.
6. L. A. Fielding, J. A. Lane, M. J. Derry, O. O. Mykhaylyk and S. P. Armes, *J Am Chem Soc*, 2014, **136**, 5790-5798.
7. A. Nese, J. Mosnacek, A. Juhari, J. A. Yoon, K. Koynov, T. Kowalewski and K. Matyjaszewski, *Macromolecules*, 2010, **43**, 1227-1235.

2 Background information and literature review

2.1 Industrial potential of polymer organogelators in electrophoretic paper technology

The context of the project worked towards advancing the potential of electrophoretic type display devices by incorporating a self-healing gel within its structure[1]. This section delves into the properties and function of electrophoretic display (EPD) technology before describing the hypothesised purpose of polymer organogelators in EPDs.

2.1.1 Properties of electronic paper devices

Electronic ink technology[2], created by E-ink in the 1970s, operates on the process of electrophoresis to display information from an electronic device that emulates the appearance of 'ink on paper'. Electrophoresis in electrophoretic displays involves the motion of charged particles through a medium[3]. Particle migration is induced by the application of an electric field and results in image formation. The name for EPDs, also known as e-papers, derives from the design of the display to possess similar physical properties to paper, such as being lightweight and flexible as shown in Fig. 2.1. E-papers are admired for their advantageous property of operating on significantly less power compared to liquid crystal displays[4]. This is possible as the device only requires energy when the page is being changed and not for image retention. The prior description is reminiscent of passive e-paper displays, whereas active e-paper displays provide dynamic content at a given rate. As e-papers lack a backlight feature they are considered as reflective displays that possess enhanced contrast of an image or text for viewers[5]. This energy efficient property is optimised in the presence of an external light source.

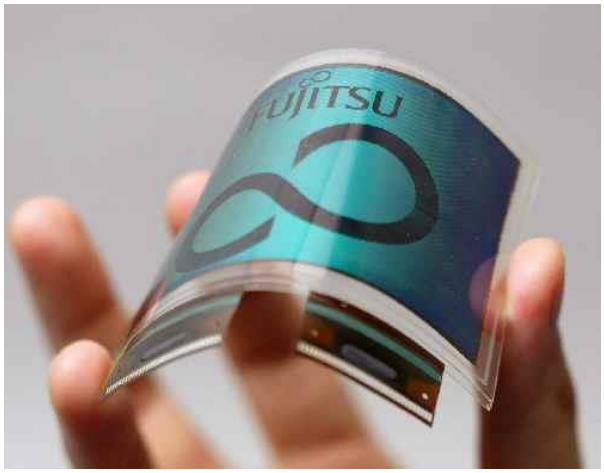

Fig. 2.1 A thin and bendable colour EPD possessing an image memory property developed by Fujitsu [6].

2.1.2 Functions of EPDs

An electronic-reader, also known as an e-reader, is a type of e-paper device that possesses a larger memory capacity for storing material within the device. A popular e-reader in the twenty-first century is the Amazon Kindle, which functions as an electronic analogue to a book. (Fig. 2.2).

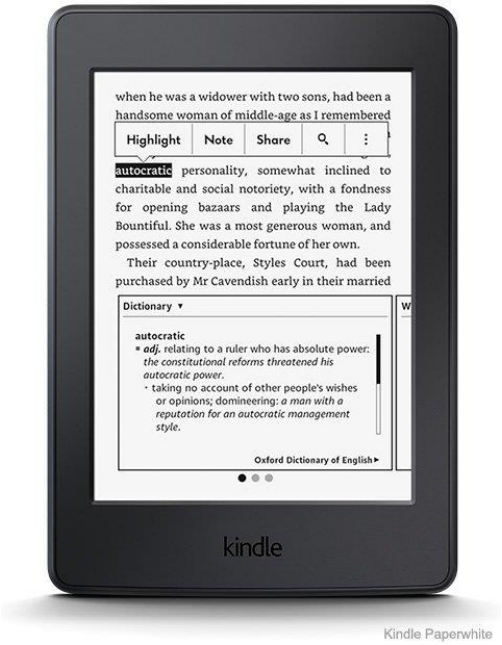

Fig. 2.2 Amazon Kindle that displays black text on white coloured background [7].

The fundamental components of an EPD possessing microencapsulated particles can be simplified to three distinct parts: the transparent top electrode, electronic ink and the bottom electrode (Fig. 2.3). The electronic ink is responsible for generating viewable content. It is made up of multiple microcapsules that consist of charged pigmented microparticles suspended in colourless dielectric medium. The microcapsules serve the function of hindering lateral drift and agglomeration of charged particles as a means of preserving image formation[8]. The aim of the project was to develop a physical gel that has potential to provide a rheological barrier when formed from the dielectric medium. It can be seen in Fig. 2.3 that the electrodes above and below the microcapsule generate a positive or negative electric field causing the pigmented microparticles to rearrange due to repulsive and attractive forces[9]. In the case that a negative electric field is created at the bottom electrode, the negatively charged black microparticles will migrate away from the bottom electrode whilst the positively charged white particles move towards it. Reversing the electric field will lead to inevitable migration of the black particles in the direction of the bottom electrode. Optical contrast is therefore realised through the migration of oppositely charged particles. In the absence of an electric field particle rearrangement is repressed, however, this does not compromise the visibility of an image on an e-paper. The term bistability[5] is used to describe the distinguishable feature of EPD technology. It implies the sustained display of an image without the use of energy. This makes e-papers, and therefore e-readers, energy efficient devices compared to emissive forms of technology, such as an electronic tablet.

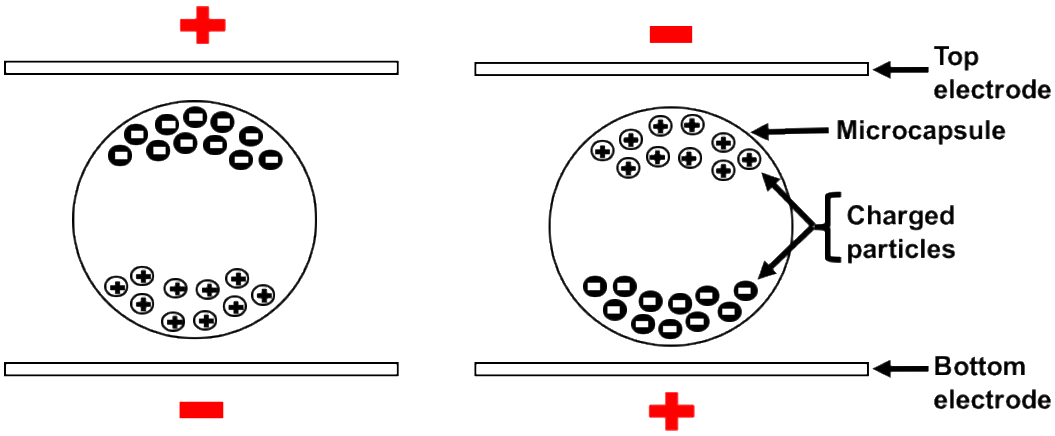

Fig. 2.3 Illustration of an EPD with E-ink containing white and black charged microparticles[2].

Tailoring the design of an EPD, in terms of its thickness and particle pigmentation, generated the interest of developing e-papers for specific applications. Chen *et al.*[9] developed a considerably thinner (0.3 mm) e-paper display that can withstand bending and maintain good

resolution (96 pixels per inch). These properties were suited for e-paper displays used for a person's identification, wearable computer screens and electronic newspapers. A thin film transistor composed of steel foil imparted flexibility and allowed the e-paper display to be low in weight.

Typically, white charged particles within the microcapsules are composed of the rutile type of titanium dioxide (TiO_2)[10]. TiO_2 is used due to the advantages of possessing high brightness, along with, good scattering properties and chemical stability[11]. However, its high density and predisposition to gravitation, as well as its strong interaction with metallic electrodes, has led others[12] to coat TiO_2 with a polymeric shell to overcome the aforementioned drawbacks. Since the creation of E-ink, coloured EPDs have also been investigated. A feasible approach appears to be the incorporation of a colour filter array to a black and white EPD. However, this approach has limited success due to reduced reflectivity, lightness and resolution. It is for this reason E-ink's advanced colour e-paper technology[13] is a favoured alternative method. This coloured EPD technology comprises of three coloured charged particles (cyan, magenta and yellow) and a light-scattering white charged particle with opposing charges. Image formation occurs due to the relative positioning of the coloured particles with respect to the white particles. Similarly, Kim *et al.*[14] prepared microcapsules containing charged white and coloured microparticles, as illustrated in Fig. 2.4. Coloured printer toner particles were chosen due to their brightness and low-weight.

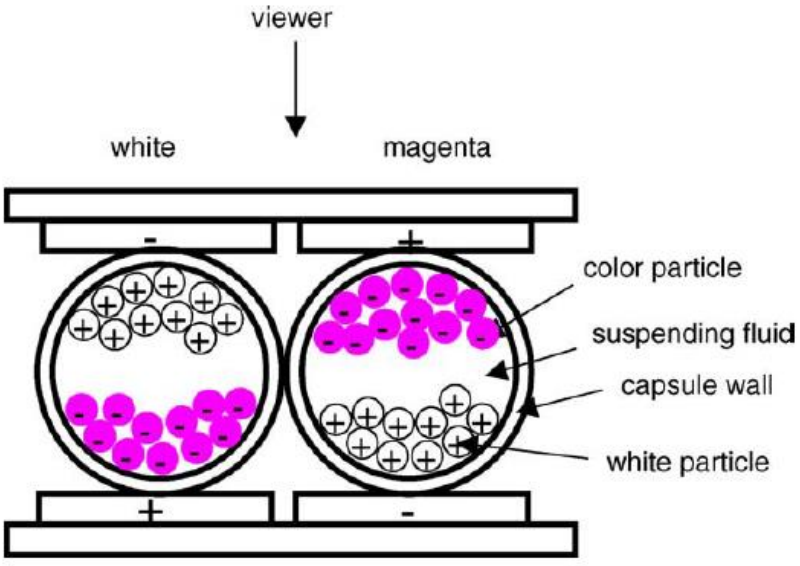

Fig. 2.4: A depiction of inside a coloured EPD [9].

2.1.3 Proposed function of a polymer organogelator in an EPD

As described above, the potential of a polymer organogelator in EPD technology was pertinent to this project. For this thesis, the reference 'polymer organogelator' derived from the hypothesis that a polymer gelator can form a physical gel from a non-polar dielectric medium. It is essential that the resultant gel is transparent so that it will not interfere with the high contrast performance of an EPD. Furthermore, the gel is expected to exhibit fast localised breakdown and reformation to adhere to the principle of bistability. The proposed concept of gel breakdown is shown in Scheme 2.1.

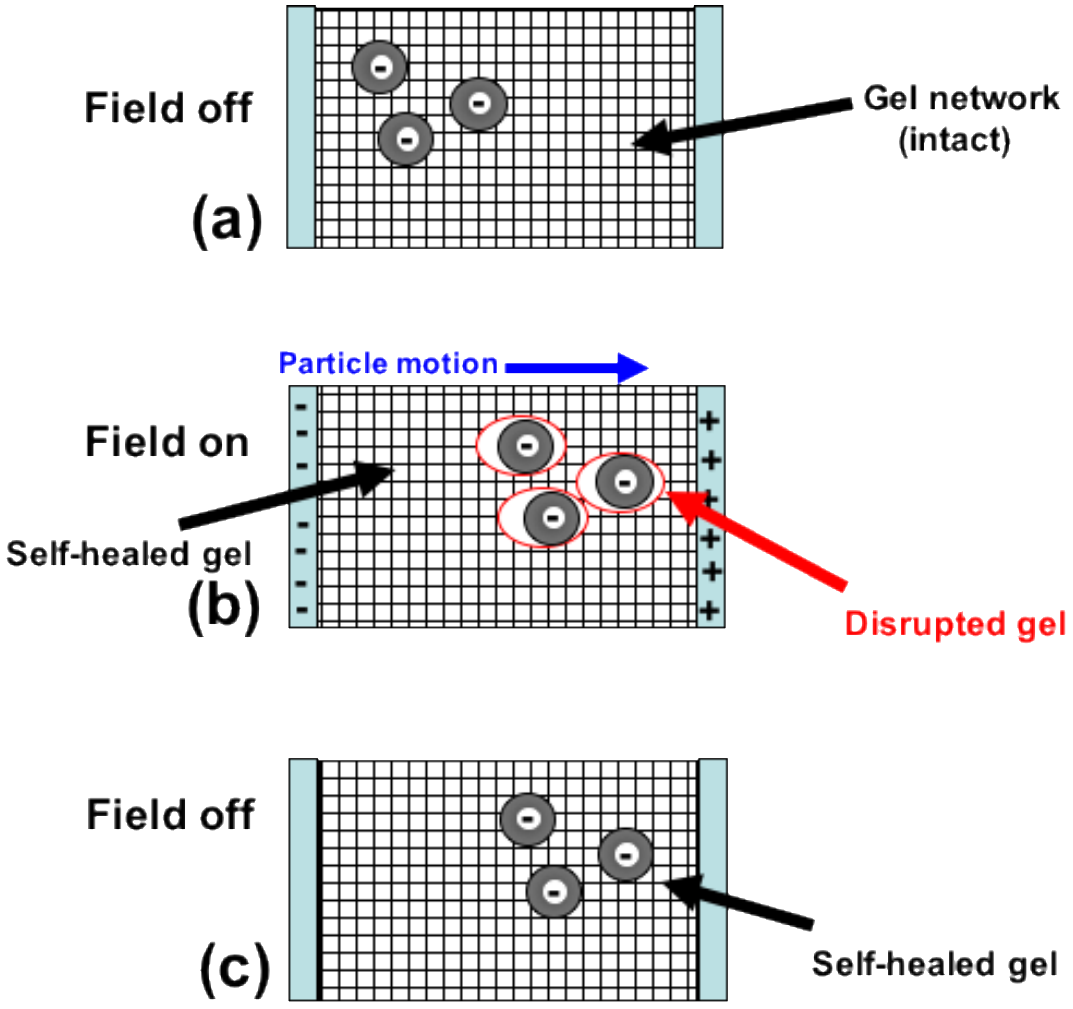

Scheme 2.1 Proposed self-healing concept of the physical gel in an EPD.

In Scheme 2.1a the absence of an electric field implies that the gel is intact and can support the stationary microparticles (0.15 – 0.5 μm). Once an electric field is applied (Scheme 2.1b), the motion of the particles will cause the gel to break down locally and it is in this way the

gel serves as a rheological barrier. It is proposed that the area that the microparticles have left can reform quickly with complete reformation of the gel network evidenced within milliseconds after the electric field is turned off (Scheme 2.1c). The proposed concept was envisaged to produce a new type of EPD that can compete with leading market e-readers, such as the Amazon Kindle.

2.1.4 Properties of bistable gels in EPD technology

Along with the development of the gel displaying the aforementioned properties, it is necessary that the gel can function efficiently after repetitive cycles of an applied electric field (i.e., >> 10^3). The gel must also be compatible with the charged particles and electric field strength of 0.5 V μm^{-1}. It is proposed that the gel ought to also contain a high particle concentration (i.e. > 20 wt. %) in *n*-dodecane or other non-polar solvents (e.g. *n*-decane) that are typically used as dielectric medium in EPD technology. Lastly, the self-healing property of the stable gel should display shear thinning behaviour in response to particle migration.

There are specific properties the proposed polymer gelator is envisaged to possess. The following sections of this chapter delves into types of polymer organogelators and their respective mechanism of gelation. Methods of preparing the polymer segment of the polymer organogelator is also explored with concluding remarks of this chapter being addressed finally.

2.2 Various pathways to achieve gelation from polymer organogelators

To date, there are numerous reports concerning the gelation of polymers from water and non-aqueous solvents, whereby the latter is better suited for the application of this project. This section highlights the various pathways of forming a physical organogel through the self-assembly of non-ionic polymer organogelators. The term 'organogel' in the context of this thesis describes a physical gel formed from an organic solvent[15].

2.2.1 Low molecular weight gelators

Low molecular weight gelators (LMWGs) are a class of gelator molecules that are typically $<$ 3000 g / mol[16] and are capable of forming a physical gel with aqueous[17] and non-aqueous solvents[18]. A vast majority of discovered LMWGs has been serendipitous. Furthermore, the spectrum of LMWGs that can gelate organic fluids makes it challenging to describe favourable characteristics. However, it is notable that amphiphilicity is a common feature for

successful LMWGs to encourage gelation through a variety of non-covalent interactions, such as van der Waals forces, $\pi - \pi$ stacking and hydrogen bonding[19].

There are several classes of LMWGs that possess various functionalities (i.e., amide, urea, aromatic and hydroxyl groups) that enable intermolecular interactions to occur between neighbouring groups towards the goal of achieving gelation. The largest class of LMWGs are ALS derived compounds. This type of gelator consists of an aromatic group (A), connected *via* a functionalised linker (L) to a steroid group (S) that is usually cholesterol (Fig. 2.5a). Typically, the characteristic features such as, a minimum of three aromatic rings linearly fused together and a C_8H_{17} alkyl chain connected to the C17 of the steroid group, encourages gelation with multiple organic fluids[20]. Weiss and co-workers[21] reported one of the first ALS gelators, cholestryl-4-(2-anthryloxy) butanoate, that formed translucent gels with organic fluids. Mukkamala *et al.*[22] found that the molecular structure of ALS gelator played an important role in gelation because as soon as 2-anthryl was substituted with 9-anthryl, 2-naphthyl or biphenyl groups gelation was absent. This observation was related to a reduction in $\pi - \pi$ stacking interactions between aromatic groups of neighbouring ALS gelators.

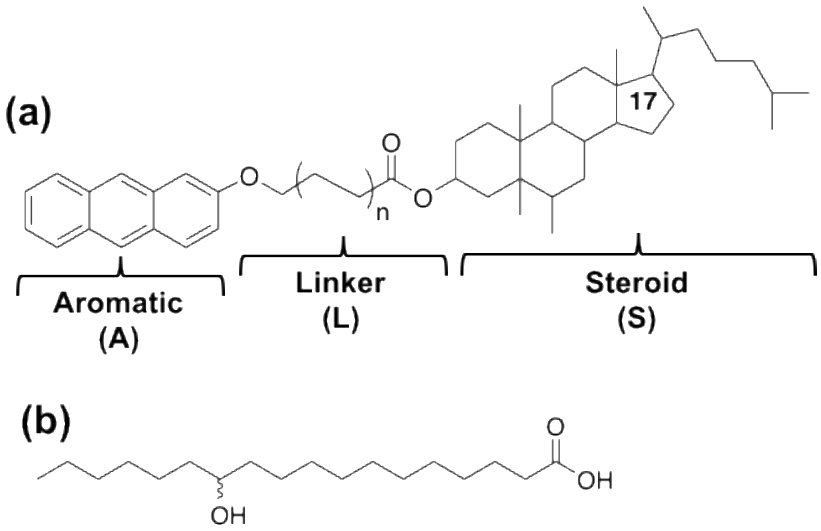

Fig. 2.5 ALS gelator (a) and (*R*)-12-hydroxystearic acid (b). The number '17' indicates the carbon atom number to which the steroid group is attached[23].

The progressive development towards $A(LS)_2$ gelators, which consist of two cholesterol groups symmetrically connected to an aromatic group, has also shown favourable gelation ability in many organic fluids. Hou *et al.*[24] described an $A(LS)_2$ gelator that was based on an ALS compound with expected gelation ability and 3-cholesteryloxycarbonylpropanoic acid. The $A(LS)_2$ compound gelled many alcohol and aromatic solvents and formed a partial gel

(i.e., coexisting solution and solid-like system) with ethyl acetate. The gelation behaviour of this new compound differed from that of the isolated ALS component. It was hypothesised that a lack of a hydrogen-bonded group in the ALS compound was a contributory factor to its poor gelation ability.

Simplifying the structure of ALS-type gelators to AL[25] (i.e., containing an aromatic and a functionalised linking group) and LS[26] (i.e., containing a linker and a steroid group) compounds have displayed limited gelation ability, with the stability of the gel being dependent on the nature of the organic fluid. Systematic elimination of aromatic, steroidal and alkyl groups from ALS gelators led to the development of the structurally simplest LMWG, known as *n*-alkanes. Abdallah *et al*.[27] reported the ability of hexatriacontane gelating *n*-alkanes and other fluids, such as silicone oil. Rogers *et al*.[28] described that the gelation ability of *n*-alkanes diminishes with decreasing length of the hydrocarbon chain, due the cumulative effect of reducing van der Waals forces.

Steroidal gelators are class of LMWGs closely related to ALS gelators, except that they do not consist of an aromatic and linker group. Peng *et al*.[29] reported cholesterol derived gelators that were discovered accidently following their ability to gel *n*-alkanes, such as *n*-heptane, *n*-octane, *n*-nonane and *n*-dodecane and also commercial fuels. The cholesterol derived gelator also acted as a thickener and could form gel-like emulsions with water and organic liquid mixtures. Similarly, Liu *et al*.[30] observed that cholesteryl glycinate gelators displayed optimised gelation ability with a variety of non-polar solvents in the presence of neutralising ammonium salts.

Another class of LMWGs stem from amphiphilic fatty acid compounds that comprise of a long alkyl chain and polar functional groups. An example of an extensively investigated fatty acid gelator is (*R*)-12-hydroxystearic acid (Fig. 2.5b). This type of gelator is distinguished by an interior hydroxyl group and a terminal carboxylic acid group. Mallia *et al*.[31] discovered that, compounds that were structurally related to stearic acid but lacked a hydroxyl group, exhibited reduced gelation ability as extra hydrogen bonding sites were absent. It was also concluded that the transformation of a terminal carboxylic acid group into a primary amide could improve the stability of the gels with *n*-alkanes, higher molecular mass alcohols (i.e., 1-octanol) and aromatic solvents. Interestingly, gelation ability was compromised once a secondary amine was introduced. Li *et al*.[32] also modified (*R*)-12-hydroxystearic acid by substituting a carboxylic group with hydrazide functionality. The modified gelator exhibited substantial gelation efficiency in a variety of solvents, such as toluene, lower molecular mass

alcohols (i.e., ethanol and methanol) and polar solvents like nitrobenzene, ethylene glycol and dimethyl sulfoxide. However, further modification involving the incorporation of a *n*-alkyl group to the terminal nitrogen atom of the hydrazide group resulted in limited gelation. Although the diverse structures of fatty acid gelators has made it challenging to establish a model structure-gelation relationship, it is well known that gelation ability is largely influenced by its chain length[33]. Pa *et a*l.[34] observed that long chain fatty acid amides based on amino acids were capable of gelling *n*-hexane, *n*-heptane and toluene. This was attributed to the long alkyl chain and amide bond participating in van der Waals forces and hydrogen bonding, respectively, to mediate gel formation.

Urea derivatives also make for good LMWGs in organic fluids. Complementary hydrogen bonding between neighbouring functional groups (i.e., C=O and N-H) mediates the self-assembly of this class of gelators[35]. George *et al*.[36] described that the smallest LMWG (M_w = 88 g/mol) was *N*,*N*´-dimethylurea. *N*,*N*´-dialkylureas demonstrated efficient gelation depending on the length of the alkyl chain. It was discovered that with increasing carbon length from dimethyl to dipropyl, gelation ability consequently improved. However, for *N*,*N*´-dibutylurea gelation ability reduced before increasing again after the number of carbon atoms exceeded ten. The combination of dipolar interactions and hydrogen bonding was considered to dominate the self-assembly of gels based on *N*,*N*´-dialkylureas. Huang *et al*.[37] also drew some conclusions for the gelation ability of benzoyl thiourea derivatives, stating that a suitable length of the alkyl side chains encouraged van der Waals forces, which in conjunction with hydrogen bonding, enhanced the gelation efficiency of the LMWGs.

The potential of carbohydrate based LMWGs comes from the presence of multiple polar regions that encourage hydrogen bonding. It is for this reason it could be argued that this class of gelator molecules has superior gelation abilities compared to the ones described earlier. However, the limited literature reporting would suggest that their success is few and far between. Nonetheless, the diversity of dibenzylidene-monosaccharides is an example of the promising nature of this class of gelator (Fig. 2.6). Yoza *et al*.[38] reported good gelation ability of this type of gelator and observed that the gelation efficiency was related to saccharide structure. The presence of numerous hydroxyl groups was essential to encouraging multiple hydrogen bonding interactions in organic fluids[39]. It was found that the α- and β-isomers of *D*-galactose were able to gel a variety of organic fluids through H-bonding interactions that mediated organised assembly of the gelator molecules. This superiority compared to other derivatives (i.e., *D*-glucose) was ascribed to the *L*-

configuration being less resistant to intermolecular aggregation. Gronwald *et al.*[40] went on further to describe that methyl 4,6-*O*-benzylidene galactose and mannose derivatives can be expected to display optimal gelation efficiency in a broader range of organic fluids. The possibility of these gelators acting as "supergelators" was also addressed due to their ability to gel hydrocarbons at very low solids content (i.e., 0.03-0.05 wt. %). In recent years, methyl 4,6-*O*-benzylidene galactose and mannose derivatives are still proving to be effective gelators with emerging thixotropic properties of their resultant gels[41].

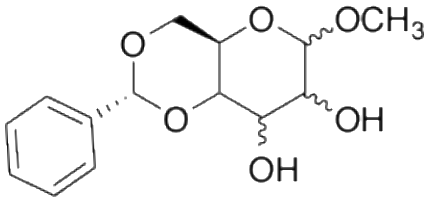

Fig. 2.6 Dibenzylidene-monosaccharide[23].

The 20 naturally occurring α-Amino acids with *L*-configuration represents an additional collection of gelator molecules. Their incorporation as gelators has popularised over recent years because, similar to carbohydrate derived gelators, they are biodegradable and inexpensive to prepare from commercially available starting materials[42]. Suzuki *et al.*[43] described the facile preparation of *L*-lysine derived LMWGs from the esterification of N^{ε}-lauroyl-*L*-lysine (Fig 2.7). Further reactions with alkyl isocyanates served the role of providing differing lengths of alkyl chains to diversify the resulting gelator molecules. The gelation abilities of *L*-lysine derived gelators with a range of organic fluids were studied. It was determined that the presence of the urea bond significantly improved the gelation abilities[44]. In addition, it was discovered that the position and the length of the alkyl chain had interesting effects on their gelation ability. If a long alkyl chain was positioned close to the α-amino group, gelation ability increased through van der Waals forces. However, this behaviour diminished when there was increasing length of the alkyl chain proceeding the ester group. This was presumably because van der Waals forces dominating at the ester position are insufficient to encourage hierarchal self-assembly. The same research group addressed previously that the optimum balance of hydrogen bonding sites and the length of the alkyl chain length is an important parameter for *L*-lysine derived gelators[45].

Brosse and co-workers[46] also discovered that gelation of *L*-phenylalanine based gelators with non-polar solvents was driven by a combination of polar (i.e., amide group) and hydrophobic (i.e., aromatic and alkyl groups) portions of the gelator. The research group were able to describe a relationship between the structure of the *L*-amino acid and the solvent. It was concluded that for aromatic solvents, such as toluene, an aromatic group is also advised to exist within the structure of the LMWG to encourage gelation *via* $\pi - \pi$ stacking interactions[47].

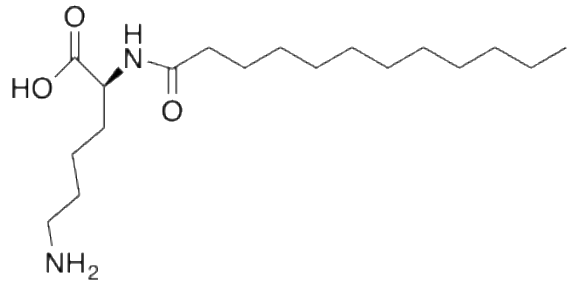

Fig. 2.7 N^{ε}-lauroyl-*L*-lysine[43].

Following the successful gelation efficiency of *L*-amino acids, the development of cyclic dipeptides has shown comparable results. The key feature regarding the composition of a dipeptide is that it must comprise of two structurally distinct amino acids, as a means of hindering crystallisation[48]. Hanabusa *et al.*[49] focused on the gelation ability of various cyclic dipeptides in orgainic fluids and reported that a cyclo(dipeptide) comprising of two neutral amino acids, such as *L*-phenylalanine and *L*-leucine, displayed good gelation ability. However, when replaced by a neutral and acidic amino acids (i.e., *L*-phenylalanine and *L*-aspartic acid, Fig. 2.8) gelation ability was enhanced due to more hydrogen bonding interactions. Introduction of branching to *L*-glutamic or *L*-aspartic acid based cyclo(dipeptides) also resulted in improved gelation efficiency due to van der Waals forces between alkyl chains contributing to hierarchal self-assembly.

Another interesting property of gels formed from cyclic dipeptides, is the ability to display a reversible shear-thinning characteristic after being shaken (i.e., thixotropic). Hoshizawa *et al.*[50] described the thixotropic property of gels based on cyclo(*L*-aspartyl-*L*-phenylalanyl) that self-healed when left to stand for one hour at ambient temperature. The gel-sol-gel transformations were mediated by hydrogen bonding and van der Waals forces, however weaker van der Waals interactions were disrupted when the gel was subject to shearing forces.

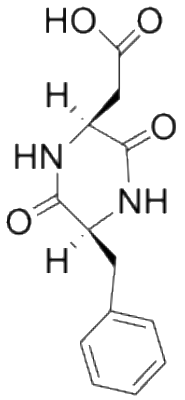

Fig. 2.8 Cyclo(*L*-aspartyl-*L*-phenylalanyl) that comprises of *L*-phenylalanine and *L*-aspartic acid constituents[50].

2.2.2 Self-assembly of low molecular weight gelators

A successful LMWG can be characterised by the following criteria: (1) the ability to exhibit good solubility at elevated temperatures and encourage gelation or thickening of fluids, (2) to induce gelation with a low concentration of gelator molecules, (3) the resultant gel is temperature responsive and exhibits reversible gel breakdown and reformation and lastly, (4) gelation is driven by weak intermolecular interactions[48]. The occurrence of non-covalent interactions, such as van der Waals forces, $\pi - \pi$ stacking and hydrogen bonding, is responsible for the self-assembly of neighbouring LMWGs (Fig. 2.9) prior to the formation of supramolecular structures[51].

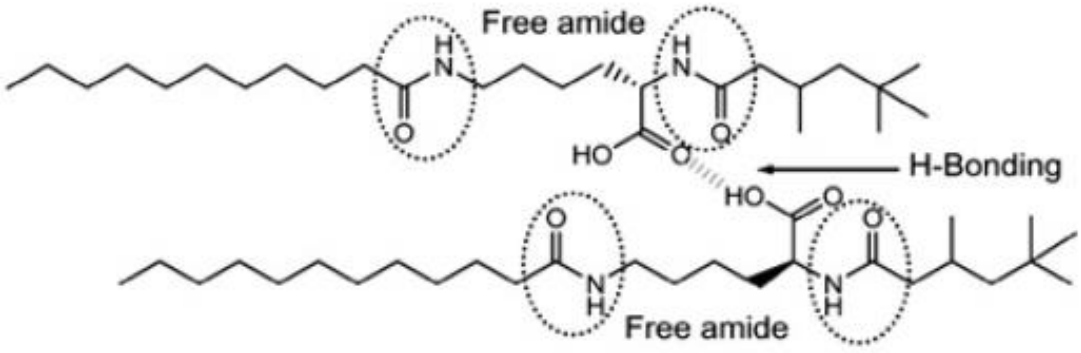

Fig. 2.9 Hydrogen bonding between carboxylic groups of neighbouring amino acid derived LMWGs[52].

As there is usually more than one polar portion[53] that can partake in non-covalent bonding, the formation of the resultant three-dimensional network can be explained by the assembly of hierarchal structures[54]. The self-assembly of LMWGs shown in Scheme 2.2 involves three distinct steps to form a three-dimensional network. The first being the formation of one-dimensional fibre-like aggregates mediated by intermolecular interactions, such as hydrogen bonding. The second, concerns bundle formation of these fibres through van der Waals forces or other intermolecular interactions and finally, further entanglements to create a porous three-dimensional network.

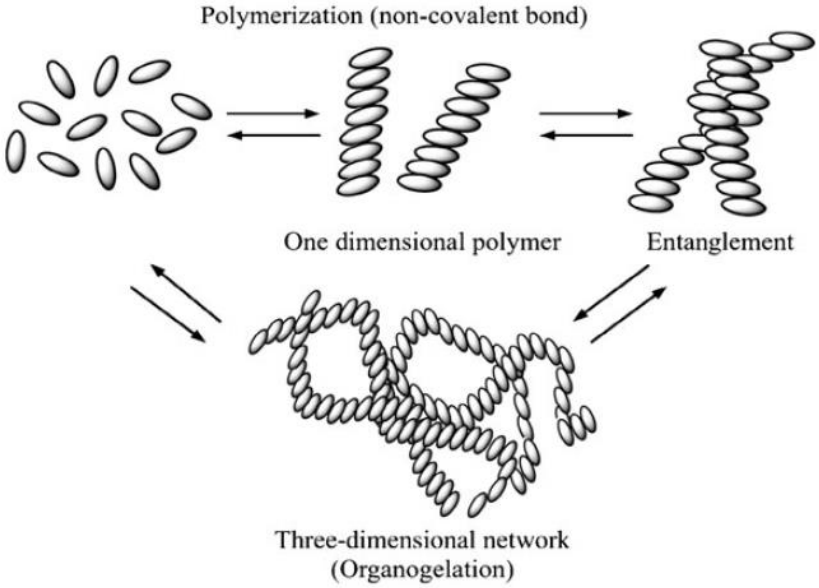

Scheme 2.2 Reversible mechanism of LMWGs forming a three-dimensional network[54].

Immobilisation of a fluid within the interstices of three-dimensional network results in a physical gel[55]. For gelation to be encouraged, a mixture comprising of typically a low solids content ($\lesssim$ 1 wt %)[56] of LMWGs and the organic solvent, must be heated to form a homogeneous solution prior to gelation upon cooling to room temperature. The organogels tend to be transparent or opaque, depending on the gelator and solvent type[48]. As these gels are sustained by non-covalent interaction, gel breakdown and reformation can be rationalised by the disruption and occurrence of the intermolecular forces described above. For example, van der Waals are expected to break before the hydrogen bonding that forms one-dimensional structures[45]. Alternatively, in the absence of an external stimulus the gel is expected to exhibit good stability. Although the context of this thesis concerns EPD technology, the temperature-responsive nature of LMWG bears insight into the self-healing smart functional material this project envisages[57].

2.2.2.1.1 Kinetic contributions to the self-assembly of LMWGs

The work of Huang *et al.*[58] and others[59] has helped to gain further insight into the kinetic factors that affect the self-assembly of LMWGs. The proposed mechanism for gelation first assumes instantaneous nucleation that derives from the intermolecular interactions between neighbouring LMWGs. This is then followed by one-dimensional fibres growing from nucleation points, and lastly branched fibres forming a three-dimensional network as the fibres intertwine. The latter stage is where the relationship between the arrangement of LMWGs, to form crystalline structures or less ordered structures that are apparent in gels, is established. As mentioned above, the gels are produced upon cooling (i.e., in a matter of minutes or hours). Once cooled below 28 ºC, spherulites aggregate to exhibit less ordered structures that drive gelation[58]. Above 30 ºC these structures begin to elongate to make fibrous networks with increased order that inhibit organogelation[60]. Interestingly, an organogel can display a thixotropic property depending on subsequent self-assembly of the fibres. Spherulites exhibit partial destruction under shear stress whilst fibrous networks become fragmented and exist as predominately single fibres. For this reason, spherulitic assemblies are better suited for thixotropic organogels as reversibility is predicted (Scheme 2.3). Despite better understanding of the kinetics, the variety of LMWGs and the intermolecular interactions highlight the difficulty in outlining a universal kinetic pathway[58].

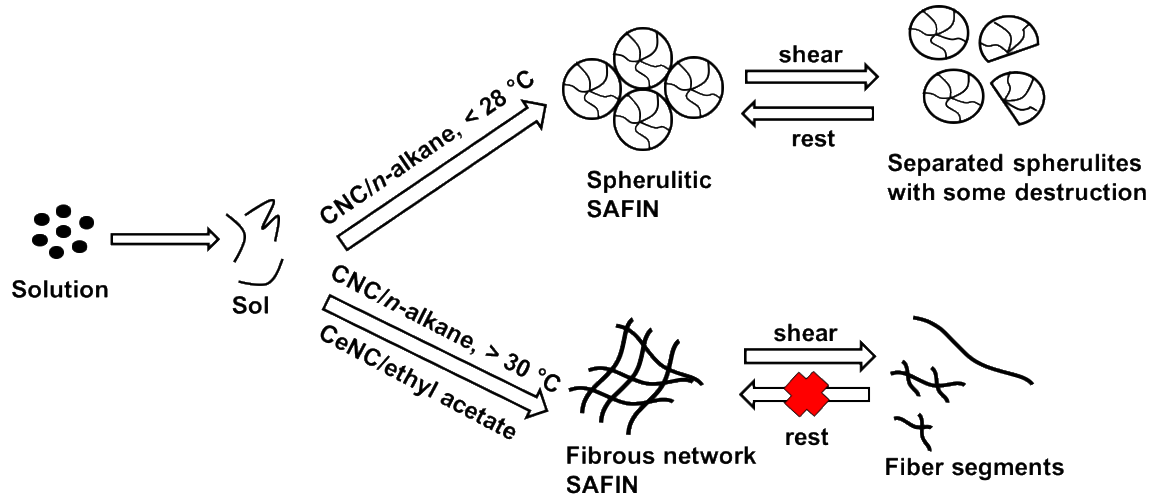

Scheme 2.3 Mechanism for the formation of spherulitic or fibrous network SAFINS (self-assembled fibrillary network) formed from heating a solution containing the LMWGs 5α-cholestan-3β-yl *N*-(2-naphthyl) carbamate (CNC) or 3β-cholesteryl *N*-(2-naphthyl) carbamate (CeNC) in *n*-alkane or ethyl acetate[58].

LMWGs can form an organogel from a variety of polar and apolar solvents. Lee *et al.*[61] discovered that the critical gel concentration (cgc) of LMWGs should be above 2 wt. % in order to form an organogel from a variety of *n*-alkane solvents. For this project, the architecture of the polymer gelator was tailored to encourage gelation from a non-polar solvent. This is advantageous as intermolecular interactions between polar potions of neighbouring LMWGs can be optimised as competing interactions with polar solvent molecules would be absent[62].

2.2.3 Self-assembly of polymers containing LMWGs

The incorporation of the LMWG segment onto a polymer results in a polymer gelator with enhanced gelation abilities[63]. This is due to the polymer segment preventing crystallisation and providing wider interstices for trapping the organic fluid[64]. The presence of a polymer segment alleviates the critical drawback that LMWGs form metastable gels. This is because for polymers and oligomers their molecular weight distribution and entanglements of chains inhibit crystallisation. This differs for LMWGs that are smaller molecules that tend to form ordered structures and thus crystallise within a short or prolonged time frame[48].

LMWG molecules are added onto a polymer segment by the introduction of a covalent bond *via* esterification[65] or hydrosilylation reactions. Fig. 2.10 represents a polysiloxane based polymer gelator mediated by a Si-H bond between methylhydrosiloxane-dimethylsiloxane and a *L*-isoleucine derived LMWG. Hydrosilylation can occur provided that an unsaturated C=C bond is introduced onto the LMWG[66].

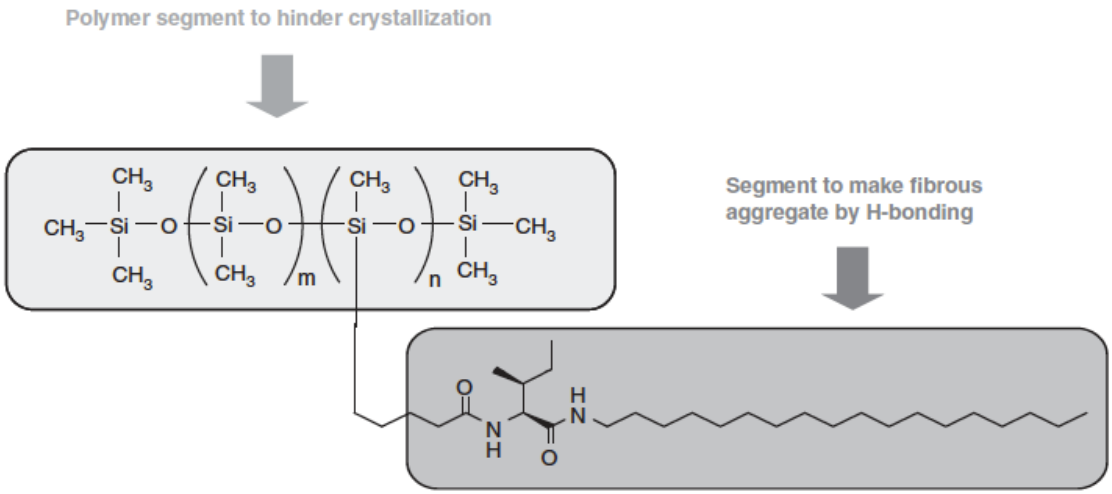

Fig. 2.10 Polymer organogelator containing LMWGs[48].

For polymer gelators the LMWG portion drives gelation[67]. It is necessary that the gelation property is preserved after the introduction of the LMWG onto a polymer. Another factor to consider is the proportion of LMWGs to the length of the polymer segment.

Ihara *et al.*[66] showed that the influence of steric interactions became larger with increasing lengths of the poly(methyl acrylate) block and therefore compromised gelation. However, once the ratio of the polymer segment to the LMWG was suitable, the polymer organogelators formed transparent thermoresponsive organogels.

The versatility of the LMWG segment in causing gel formation from multiple non-polar solvents was optimised due to the presence of a polymer segment[63]. The gels also display a shear thinning behaviour which is suited to the application of such gels in EPD technology. Hoshizawa *et al.*[68] prepared a polymer organogelator based on cyclodipeptides that formed thixotropic organogels from decane. The thixotropic property was related to breakdown and reassembly of fibril-like structures that further assembled into spherulites.

2.2.4 Self-assembly of non-ionic amphiphilic linear copolymers

The self-assembly of amphiphilic surfactants[69] is an interesting behavioural phenomenon that paved the way for the development of linear diblock copolymer gelators. In an aqueous environment, surfactant molecules undergo specialised rearrangement to form aggregates driven by the insolubilities of the hydrophobic tail and the hydrophilic head group. The structures of these micelles are made up of an inner hydrophobic layer shielded from unfavourable interactions with water molecules, and an outer hydrophilic layer facing the water molecules. These distinct layers are identified as the core and corona and are apparent in the form of spherical, globular-like, rod-like or spherical bilayer morphologies[70] as shown in Fig. 2.11.

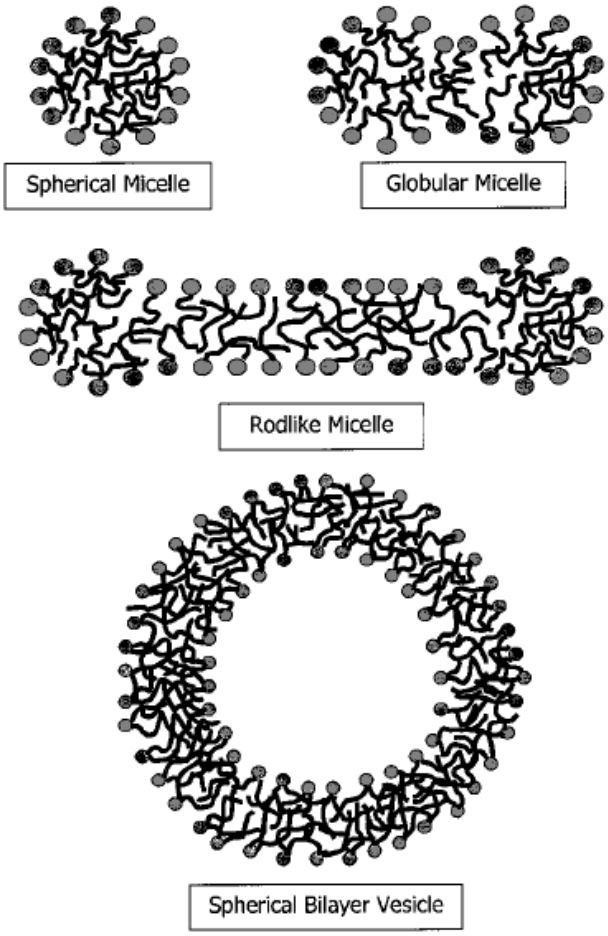

Fig. 2.11 Morphologies formed from amphiphilic surfactants[70].

Ionic surfactants also form various aggregates in low and high strength ionic environments. However, the principle behind the self-assembly of non-ionic surfactants will only be discussed further and can be assumed in the context of the proceeding sub-sections.

2.2.4.1.1 Thermodynamic contribution to the self-assembly of non-ionic amphiphilic diblock copolymers

The reports given by Israelachvili *et al.*[71] and Tanford *et al.*[72] have been instrumental in understanding the thermodynamic influence on the geometry of aggregated non-ionic surfactants. A similar rationale was applied to the self-assembly of non-ionic amphiphilic diblock copolymers in aqueous environments or in a selective organic solvent for one of the polymer blocks. In both instances the insoluble and soluble block would form the core and corona, respectively.

Self-assembly is influenced by the ratio of the insoluble and soluble parts of the macromolecule, which in turn, dictates the two dominant free energies; surface energy and entropic energy[73]. Within the congested core the insoluble block would prefer to be fully stretched; however, this conformation is compromised for entropic reasons resulting in the insoluble block being somewhat stretched to minimise the entropic energy. The surface energy is reduced by the prevention of the solvophobic block partaking in unfavourable interactions with solvent molecules[74]. The minimised surface and entropic energy results in an overall lowered free energy of the polymeric micelle. The packing parameter (p) quantitatively defines the preferred morphology of a polymeric micelle as expressed by Equation (2.1)[75]:

$$p = \frac{V}{a_0 l_c} \qquad \textbf{(2.1)}$$

where V and l_c represent the volume and the length of the insoluble block, respectively, and a_0 is the surface area of the insoluble block at the interface between the insoluble and soluble blocks. Therefore, for a fixed length of the soluble block, increasing V/l_c reduces the volume the insoluble block can occupy and increases the packing parameter. In this way predominantly spheres are obtained when $p < \frac{1}{3}$ and worms and vesicles are observed $\frac{1}{3} \leq p \leq \frac{1}{2}$ and $\frac{1}{2} \leq p \leq 1$, respectively[76] (Fig 2.12).

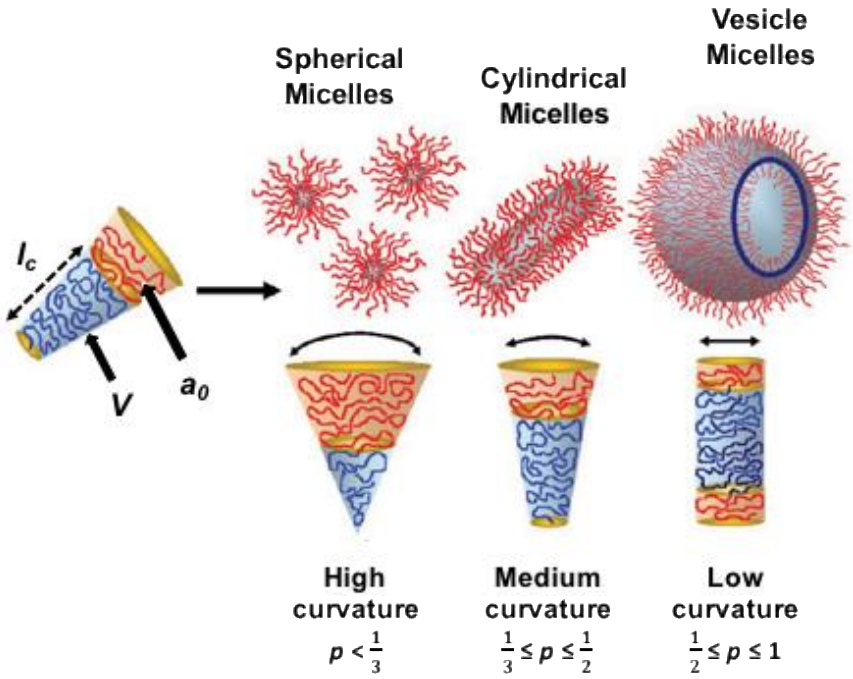

Fig. 2.12 Illustration of the relationship between the packing parameter and morphologies of non-ionic amphiphilic diblock copolymers[77].

2.2.4.1.2 Kinetic contribution to the self-assembly of non-ionic amphiphilic diblock copolymers

Kinetic pathways that lead to the morphologies of non-ionic amphiphilic diblock copolymers have been reported to be slower than thermodynamically driven contributions. The proposed methods of lowering the two free energies once a critical micelle concentration (cmc) has been reached, is by individual polymer molecules being exchanged between aggregated micelles[78] or through the integration of aggregated micelles[79]. The debate over which method is favourable suggests that both theories provide a qualitative analysis of kinetically driven self-assembly. Non-ionic surfactants are considered as dynamic as the kinetic pathways occur more quickly for a given experimental time length, unlike larger kinetically frozen non-ionic amphiphilic diblock copolymers[80]. This is because the core forming block tends to have a higher glass transition temperature (T_g) than the corona forming block, resulting in slower kinetic contributions to self-assembly. The aggregation number (N_{agg}) can be calculated using Equation (2.2) [81]:

$$N_{agg} = \frac{M_{w\ polymeric\ micelle}}{M_{w\ polymer}} \qquad \textbf{(2.2)}$$

where M_w is the weight-average molecular weight. Using the above equation relates to the number of macromolecules that make up a polymeric micelle. The value for N_{agg} for spherical polymeric micelles can range from tens to hundreds with possibly greater values for cylindrical micelles[81].

2.2.4.1.3 Gelation of worm-like non-ionic amphiphilic diblock copolymers

Diblock copolymer compositions that exhibited worm-like morphologies were of interest in this project as they can behave as polymer gelators. One of the earlier reports from Zheng *et al*.[82] uses reversible addition-fragmentation polymerisation (RAFT) to prepare nano-objects based on polystyrene macro-RAFT agents. It was discovered that with increasing molecular weight of the polystyrene block large and highly anisotropic micelle formation would exist and encourage gelation with tetrahydrofuran. Since then, numerous investigations employing RAFT dispersion polymerisation has been explored with *in situ* self-assembled worms in aqueous[83] and non-aqueous environments[84]. To adhere to the context of this section of the literature review, gelation with non-aqueous solvents will only be described further.

Generally, polymerisation induced self-assembly (PISA) during RAFT dispersion allows for the growth of the second polymer block at elevated temperatures (e.g. 70 °C), for a fixed length of the first polymer block, to form nano-object morphologies[85]. Provided that the length of the first (solvophillic) polymer block has a number-average degree of polymerisation (DP) below the critical value for accessing various morphologies, pure worm phases become increasingly attainable[86]. Zhao *et al*.[87] reported that for macro-RAFT agents based on poly(ethylene glycol) methyl ether (meth)acrylate that were used to polymerise styrene in isopropanol, when the DP value was greater than 20, only spherical morphologies were observed. He *et al*.[88] seldom observed worm-like structures based on self-assembled poly(acrylic acid)-*b*-polystyrene particles in methanol, due to the DP of poly(acrylic acid)-based RAFT agent being equivalent to 61. It could be reasoned that a longer repeat unit of the stabilising component imposed greater steric stabilisation, which prevented morphologies with reduced curvature to be present[89].

The worms phase is a narrow region, with its positioning being dependent on the diblock copolymer composition and the type of dispersion solvent[90]. Derry *et al*.[91] concluded that poor solvent quality can result in higher DP values of the solvophobic block being obtained

prior to worm-like formation. For poly(lauryl methacrylate)-*b*-poly(benzyl methacrylate) (PLMA-PBzMA) diblock copolymers, whereby the DP of PLMA subtly varied from 17 to 18, it was observed that the DP of PBzMA had to be within the range of 50-70 in *n*-heptane to obtain worms. However, the DP of PBzMA reduced to 37-47 when mineral oil was the chosen solvent. It was presumed that mineral oil was a poorer solvent for PBzMA in comparison to *n*-heptane, as longer BzMA chains were required for worm-like structures to exist. Further investigation of the worms phase boundary was investigated in mineral oil and poly(α-olefin). It was discovered that, when the DP of PLMA and PBzMA was 18 and 45 respectively, a pure worms phase was obtained in mineral oil that formed a physical gel at a high solids content (i.e., 20 wt. %). This contrasted with the mixed spheres, worms and vesicle morphologies that formed when poly(α-olefin) was the selected solvent for the same diblock copolymer composition.

Mixed phases are commonly seen in literature of self-assembled diblock copolymers. It is reasoned that it is the result of fusion events between multiple micelles. However, it is also possible that the broadness of molecular weight distribution of the copolymer chains plays a part in overlapping phase boundaries[92]. Highly anisotropic worms form non-covalent inter-worm contacts that entrap solvent molecules and lead to gelation. Some mixed spheres and worms are also able to gel an organic fluid, suggesting that a critical worms concentration formed from inter-sphere fusion is a key feature in encouraging gelation[93]. A less convenient approach to forming physical gels based on fixed diblock copolymer compositions, is through increasing diblock copolymer concentration. By isolating formulations of poly(stearyl methacrylate)-*b*-poly(3-phenylpropyl methacrylate) Pei *et al*.[94] demonstrated that at 30 and 40 wt. % solids contents in *n*-tetradecane, stable physical gels were attainable at ambient temperature. Alternatively, at lower solids contents (i.e., 10 and 20 wt. %) free-flowing solutions were apparent. The contrasting observations were related to worm-like structures dominating at higher solid contents, while spheres were exclusive to lower solid contents of the diblock copolymer. Similar conclusions were drawn in the work of Cunningham *et al*.[95], where it was reported that worm-like morphologies are obtainable at 15 wt. % of poly(stearyl methacrylate)-*b*-poly(*N*-2-(methacryloyloxy) ethyl pyrrolidine in *n*-dodecane.

RAFT dispersion polymerisation *via* PISA has been conducted using acrylate and methacrylate monomers[96]. Namely, acrylate based diblock copolymer compositions exhibit broader molecular weight distributions due to chain transfer reactions[97]. Nevertheless, both

systems can form worms, spheres and vesicle nano-objects, with a high concentrations of the copolymer worms resulting in physical gels that exhibit temperature-responsive behaviour. Ratcliffe *et al*.[98] reported the reversible thermo-sensitivity of translucent coloured gels based on poly(lauryl acrylate)-*b*-poly(benzyl acrylate) (PLA-PBzA) in *n*-alkanes. The pigmentation of the gels was attributed to the sulphur containing group in PLA macro-RAFT agents[99]. The gels turned into free-flowing solution when it was heated to ~ 67 °C but transformed into the gel state at ~15 °C. Fielding *et al*.[100] also demonstrated that gels based on PLMA-PBzMA were thermoresponsive, and displayed reversible gel-sol-gel transition when heated to 70 °C and allowed to cool to 20 °C. The gel breakdown and reformation was characterised by a morphological worms-to-sphere transition as shown by Fig. 2.13

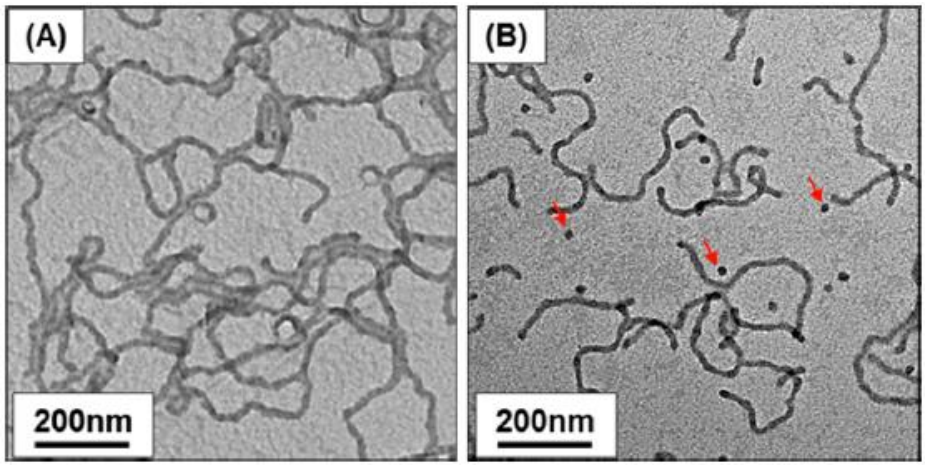

Fig. 2.13 Worms-to-sphere transition. The red arrows (b) indicate the presence of spheres[100].

The phase transformation upon heating was ascribed to delegation, a process whereby a series of spheres separate from the worm-like structure. Upon cooling of the solution, it was hypothesised that these spheres participated in fusion events to form anisotropic worms, which would once again trap the solvent molecules[81]. These temperature-responsive morphological transformations relied on maintaining the lowest free energy for a given polymeric micelle[101].

It is well known that RAFT dispersion polymerisation is the leading method of synthesising self-assembling non-ionic diblock copolymers[102]. Controlled polymerisation techniques, such as ATRP has also proven to be a successful method in preparing functionalised non-ionic amphiphilic diblock copolymers[103]. However, the number of reports are considerably limited[104].

2.2.5 Assemblies of non-ionic amphiphilic graft copolymers

Graft copolymers consisting of amphiphilic side chains can form assemblies in a selective solvent for one of the polymer blocks. The assemblies that can form differs from linear block copolymers due to presence of a polymer backbone. Fig. 2.14 (b) depicts the position of the polymer backbone, which can place restrictions on the obtainable morphologies[105] of the graft copolymer in a selective solvent.

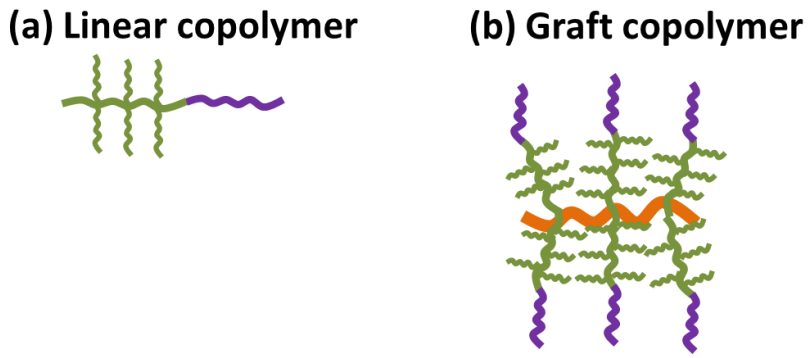

Fig. 2.14 Architectural comparison between a linear and graft copolymer.

The morphologies of densely grafted copolymers display interesting nano-objects with the report of spheres[106, 107] being most common. Jiang *et al.*[108] described bowl-shaped morphologies formed from graft copolymers based on polystyrene (Fig 2.15). The bowl-shaped macromicelles were obtained once the hydrophobic polystyrene side chains were exposed to water. As the hydrophilic polymer backbone prevented self-assembly in the way that a linear copolymer would allow, the morphology was related to multiple graft copolymers aggregating to minimise unfavourable interactions between polystyrene and water molecules[109].

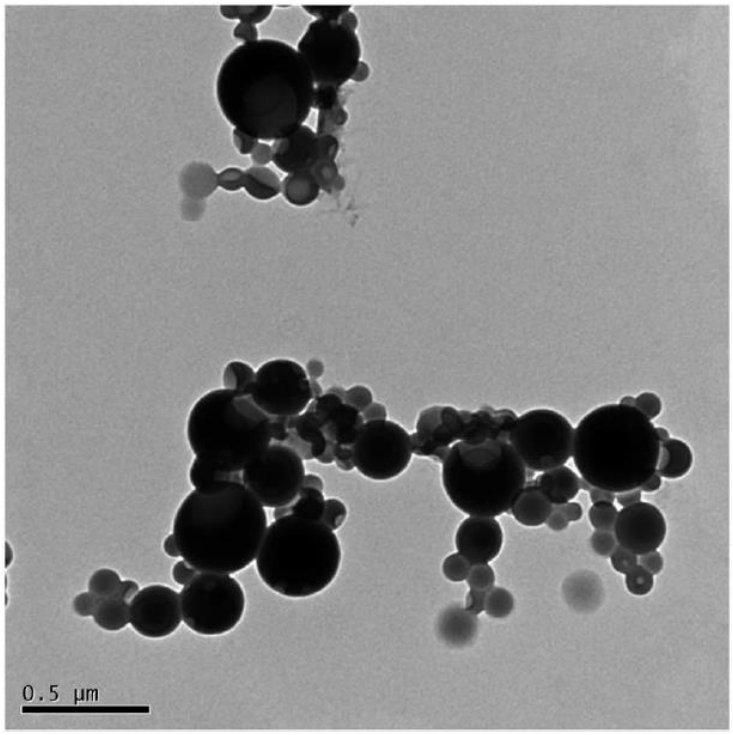

Fig. 2.15 Bowl-shaped morphologies obtained from TEM studies of graft copolymer based on polystyrene (core-forming block)[108].

Although the mechanism for linear copolymer self-assembly in a selective solvent is more understood, the obtained morphologies can be insightful for the predicted morphologies of graft copolymers. Eisenberg *et al.*[110] reported that linear copolymers based on polystyrene exhibited similar spherical-like aggregates as shown in Fig. 2.15. This suggests that the preferred graft copolymer aggregate morphology is similarly dictated by reducing the free energy of the micelle system[73]. Zhai *et al.*[111] observed that increasing lengths of hydrophobic side chains resulted in larger spheres to reduce the surface energy between unfavourable solvent molecules and the hydrophobic block. Alternatively, graft copolymers can exhibit worm-like assemblies in solution, provided that the length of the side chains is greater than the polymer backbone. Vlcek *et al.*[112] synthesised densely grafted copolymers with methyl methacrylate side chains in 1,4- dioxane *via* ATRP. The graft copolymers formed worms with lengths of 350 – 400 nm and widths of 70 – 90 nm. Similarly, lauryl methacrylate based double-grafted copolymers prepared in anisole exhibited worm-like structures *via* atomic force microscopy[113]. However, once the length of the LMA chains were reduced spherical morphologies were obtainable.

Therefore, considering the position of the solvophobic block in a graft copolymer widens the contributions thermodynamic and kinetic pathways may have on graft copolymer assembly.

However, the architectural complexity of a graft copolymer has also shown to impose morphological limitations in solution.

2.3 The evolution of radical polymerisation

The development of radical polymerisation (RP) provided the route to synthesise polymers. A polymer is a macromolecule that comprises of monomer units joined by covalent bonds. There are two mainly recognised types of polymerisation employed to synthesise polymers[114]. Addition (or chain-growth) polymerisation is notable for forming polymers that are based on repeat units of entire monomers. Alternatively, condensation (or step-growth) polymerisation involves the joining of two monomers, sometimes at the expense of eliminating atoms. Addition polymerisation has further developed into more advanced mechanisms used to synthesise the polymer gelators for this project.

2.3.1 Conventional free radical polymerisation

In the case of radical based addition polymerisation, polymer chain growth is dependent on the early creation of free radicals. For conventional RP[79] there are three distinct steps towards the preparation of a polymer (Scheme 2.4).

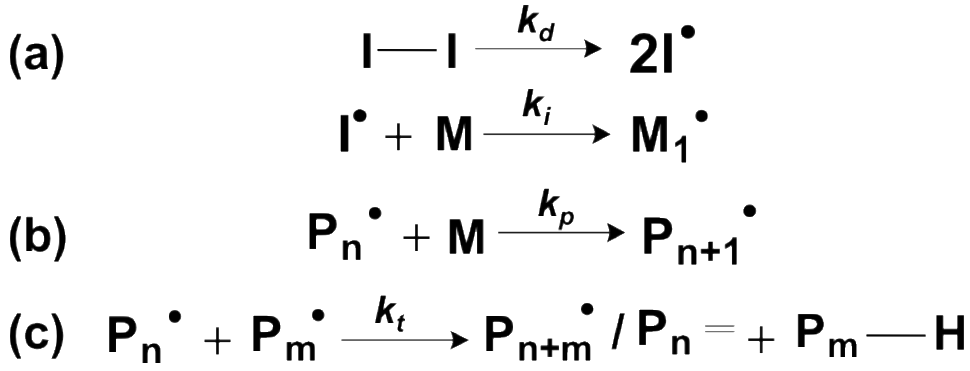

Scheme 2.4 Kinetic steps for initiation (a), propagation (b) and termination (c) for conventional radical polymerisation[115].

The initiation step involves the thermal, photochemical or chemical decomposition of an initiator (I) to generate free radicals ($I^{\cdot}$) followed by the reaction between a free radical and a monomer (M) to form active species ($M_1^{\cdot}$) (Scheme 2.4a). Thereafter more monomer units add onto propagating chain ($P_n^{\cdot}$) which is represented by polymer chain growth ($P_{n+1}^{\cdot}$) (Scheme 2.4b). Finally, termination describes the end of polymer chain growth *via* combination (P_{n+m}) or disproportionation (P_n= + P_m-H) (Scheme 2.4c). Termination becomes

increasingly apparent during polymer chain growth as more free radicals are created. This happens because termination is proportional to square of the active centre concentration[116].

In conventional RP the rate constant of decomposition (k_d), specifically referring to the homolysis of the initiator, is the rate limiting step as it occurs at a slower rate. As a monomer reacts with a free radical the rate constant of initiation (k_i) increases due to the highly reactive nature of free radicals. It then follows that the rate constant of propagation (k_p) becomes faster rate than k_i. As the number-average degree of polymerisation (DP) for a polymer increases the rate constant of termination (k_t) progressively increases. Chain transfer is another possible chain breaking reaction. However, it is seldom significant in free radical systems and can be minimised by low polymerisation temperatures[115].

Assuming negligible chain transfer, steady state conditions occur once the rate of initiation is equal to the rate of termination. This occurs after a short time period as the increasing concentration of radical species favours termination. The short lifetime of free radicals is why the polymers synthesised by conventional RP are shorter polymers with broad molecular weight distributions (MWD) [117, 118].

The rate of polymerisation (R_p) for conventional radical polymerisation reaction is described by Equation (2.3)[119]:

$$R_p = k_p[M]\left(\frac{f k_d[I]}{k_t}\right)^{\frac{1}{2}} \qquad \textbf{(2.3)}$$

where f and [I] are the initiator efficiency and initiator concentration, respectively. k_d is the initiator decomposition rate constant. From the equation above, it follows that the rate of polymerisation is proportional to the monomer concentration, yet dependent on the square root of the initiator concentration and initiator efficiency. This implies that the rate of polymerisation is given by monomer consumption during propagation. However, due to biomolecular termination between active species and the value for f usually being between 0.5-0.8[119], the rate of polymerisation is given by the square root of initiator concentration and initiator efficiency.

The DP of a polymer synthesised *via* conventional RP can also be calculated using Equation (2.4)[116]:

$$DP = \frac{k_p[M]}{(1+q)(f k_d[I])^{\frac{1}{2}}} \qquad \textbf{(2.4)}$$

where q is a quantitative measure of the fraction of termination reactions due to disproportionation and k_p is the propagation rate constant. Similar to Equation (2.3), the number-average degree of polymerisation is proportional to the monomer concentration. However, the degree of polymerisation is inversely proportion to the square root of the initiator concentration and initiator efficiency. In the case of the latter relationship, DP decreases by a factor of the square root as the initiator concentration and initiator efficiency increases. This is a result of inevitable biomolecular termination as the concentration of the active species increases during polymerisation. Consequently, the polymer chains can range from oligomers to short polymer chains. This is reflected in the broad molecular weight distribution and high polydispersity of these polymers[118].

2.3.2 Controlled radical polymerisation

Conventional radical polymerisation possesses the advantages of ease application, in addition to the ability to polymerise a broad range of monomers under diverse conditions[119]. However, the limitations in conventional RP drove polymer science in the direction of controlled radical polymerisation (CRP). Namely for conventional radical polymerisation, the short lifetime of active species means that the initial increase in molecular weight instantaneously plateaus with increasing monomer conversion. This is due to the prevalence of the steady-state condition. This behaviour is absent in CRP reactions as the lifetime of growing chains becomes extended to several hours or more because of the introduction of a dynamic equilibrium to the conventional RP system[120]. This results in the molecular weight of polymers synthesised *via* CRP displaying a linear relationship to monomer conversion in contrast to the non-linear curve that is typified for conventional RP (Fig. 2.16).

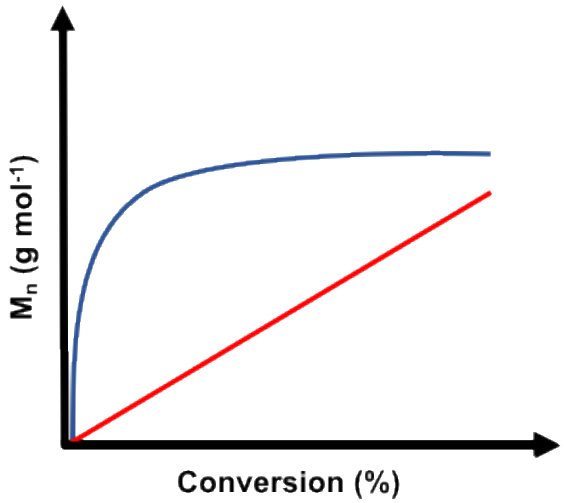

Fig. 2.16 Graphical representation of the relationship between number-average molecular weight (M_n) with conversion. The blue and red lines represents conventional free radical polymerisation and controlled radical polymerisation, respectively[121].

The term "CRP" is now recommended by the International Union of Pure and Applied Chemistry (IUPAC) to be referred to as "reversible-deactivation radical polymerisation" (RDRP)[122]. However, throughout this thesis the abbreviation CRP will be used as it is still widely used in polymer chemistry literature. Since the development of CRP, well-defined (co)polymers[123-125] have been synthesised through the contribution of dormant species and intermittent reversible activation. The presence of a dynamic equilibrium maintains a low concentration of radicals which supresses large amounts of termination during chain growth. Although termination is not eliminated, a satisfactory degree of control is imparted over the molecular weights (MW) and MWD of a polymer. The term "control" in this context is ascribed to the ability of a polymer chemist to manipulate one or many architectural properties of the resultant polymer, and obtain MWs that correspond to theoretical calculations despite some termination. Unlike conventional RP, CRP techniques can be described as "living" due to the prolonged lifetime of propagating species reacting with most monomer units. There are two approaches in which control is favoured in a CRP system[126]; the first employing degenerative transfer and the second being based on the persistent radical effect (PRE)

2.3.2.1 CRP based on degenerative transfer

For CRP techniques that involve degenerative chain transfer[120], such as reversible addition-fragmentation chain transfer (RAFT)[99], an exchange between the active species ($P_n^{\cdot}$) and

dormant species (P_m-X) takes place. This results in the production of more dormant species (P_n-X*)* that are available to react with active species ($P_m^{\cdot}$). Despite unavoidable termination (k_t) of the few propagating radicals, reversible degenerative exchange (k_{ex}) is optimised with a high concentration of transfer agent that behaves as a dormant specie. This exchange is also fast enough to satisfy CRP conditions, resulting in precise high MW polymers with a narrow MWD (Scheme 2.5).

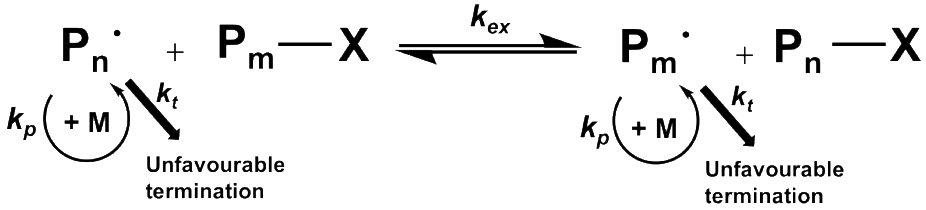

Scheme 2.5 Kinetics for degenerative transfer CRP reactions[120].

2.3.2.1.1 RAFT polymerisation

RAFT polymerisation employs a transfer agent, in the form of a thiocarbonylthio compound, to form well-defined polymers[127]. The S=C(Z)S- moiety of a RAFT agent is transferred between dormant and active species *via* addition-fragmentation reactions, in order to maintain the 'livingness' of the polymerisation reaction (Scheme 2.6).

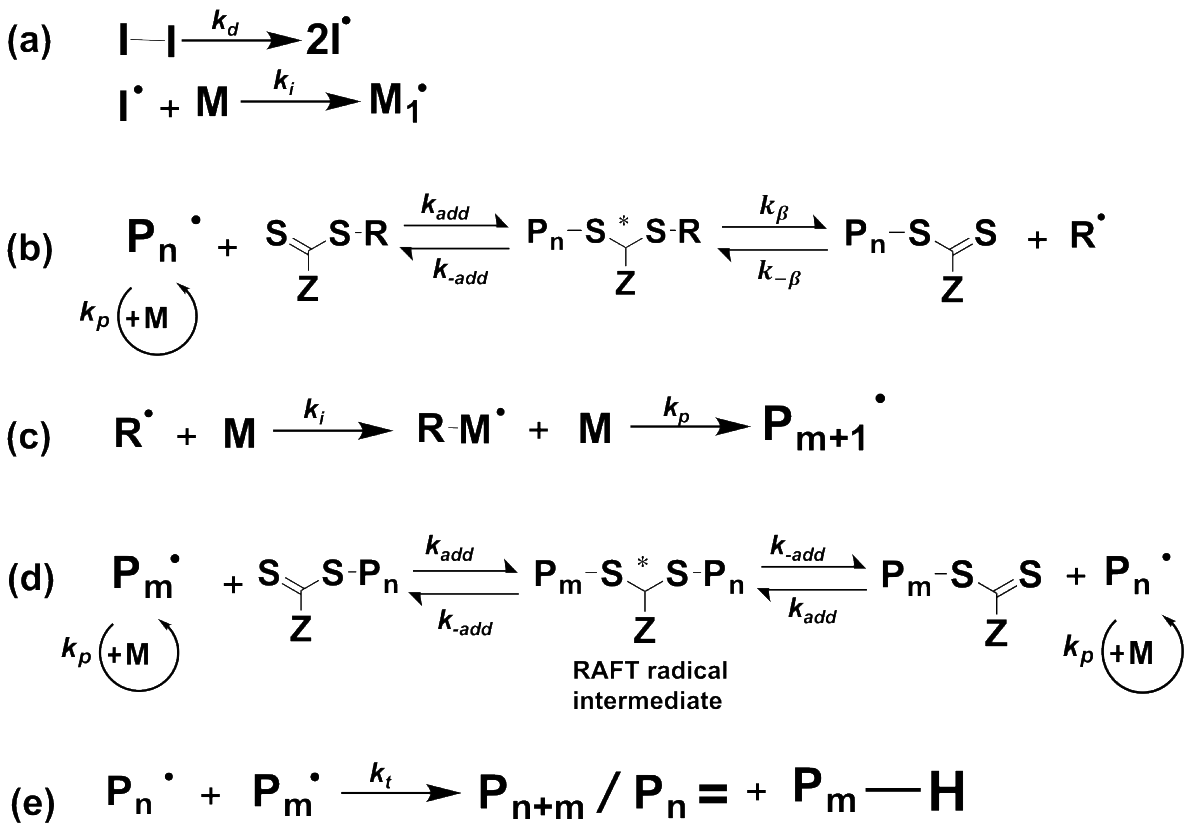

Scheme 2.6 Kinetics for RAFT polymerisation[128].

Similar to conventional RP, RAFT polymerisation begins with an initiating step that involves the decomposition of an initiator to provide free radicals. In turn, these active species can react with several monomer units (Scheme 2.6a). The following step, which is regarded as the pre-equilibrium stage, describes the addition of active species in the form of an oligomeric macro-radical to an initial RAFT agent (S=C(Z)S-R). This results in an intermediate radical (P_n-S-C(Z)S-R) that can undergo β-scission to release another radical ($R^{\cdot}$) and a dormant macro-RAFT agent (P_m-S(Z)C=S) (Scheme 2.6b). The re-initiation step involves the leaving group radical formed in the previous step, reacting with monomer units to form more active species ($P_{m+1}^{\cdot}$) (Scheme 2.6c) that can participate in the main equilibrium step Scheme 2.6d[128]. The main RAFT equilibrium differs significantly from the PRE-based equilibrium because both forward and backward reactions encourage equal growth of all polymer chains during the polymerisation reaction. This is achieved through propagating chains ($P_m^{\cdot}$) reacting with a dormant species (S=C(Z)S-P_n), that consequently forms an intermediate radical (P_m-S-C(Z)S-P_n) prior its transformation into more dormant (P_m-S(Z)C=S) and active ($P_n^{\cdot}$) species.

In the case of a less ideal RAFT reaction, increasing stability of intermediate radicals can have a negative impact on the kinetics of the reaction, thereby producing shorter than expected polymer chains exhibiting poor control. For RAFT reactions mediated by dithiobenzoate compounds (i.e., a type of Z group), the high addition rate towards active species, which is an attribute effective for controlled polymerisation, is also responsible for encouraging rate retardation. This is because enhanced stability of the intermediate radical, through its delocalisation into the phenyl group[129], results in increased self-termination between intermediate radicals and cross-termination between intermediate radicals and propagating chains[130]. Slower fragmentation rate constants (k_{-add}) are also arguably a plausible contributor towards rate retardation, despite its rapidity being determined in the order of 10^4 s^{-1} [131]. The formation of intermediate radicals is a characteristic feature of RAFT polymerisation, that is absent in NMP and ATRP. Although the presence of intermediate radicals suggests that termination is not supressed, an impressive degree of control during RAFT polymerisation is maintained through higher concentrations of dormant thiocarbonylthio-containing polymers compared to initiator-derived polymer chains[132].

RAFT polymerisation is widely recognised as a versatile technique that is favoured for its impressive tolerance to a broader variety of monomers and reaction conditions compared to ATRP and NMP[133]. This is because, aside from the incorporation of a RAFT agent, RAFT polymerisation is closely related to conventional RP, making it an advantageous technique that can easily be adopted by industries. In order to not undermine the significance of the presence of a RAFT agent, it is noteworthy to highlight its inclusion is responsible for creating a dynamic equilibrium far greater than the steps involved in conventional RP[134].
Another benefit to employing RAFT polymerisation is, provided that the appropriate initial RAFT agent and reaction conditions are selected for a polymerisation reaction, longer polymer chains with narrow molecular weight distributions can be obtained. This is because the main RAFT equilibrium is what enables the synthesis of well-defined polymers, rather than the suppression of biomolecular termination which is used to its advantage in PRE-based CRP methods. Furthermore, the preservation of RAFT end groups in the polymeric product implies that in themselves they are RAFT dormant agents that can be used for subsequent polymerisation reaction. This underpins the "livingness" of RAFT polymerisation and has opened the pathway for synthesising diverse and complexed polymers[135]. However, the presence of the thiocarbonylthio groups implies two disadvantages for the resultant polymers. Firstly, that they may be discoloured and secondly, they have increased potential to release

and odour over a prolonged period[136]. Even though these drawbacks can be alleviated by appropriate selection of the initial RAFT agent, employing post-polymerisation modification procedures is an alternative option[137].

2.3.2.2 CRP based on the persistent radical effect

CRP techniques based on PRE, are distinguished by the forward reaction driving the reversible termination of transient radicals by persistent radicals (X), as a means of supressing unfavourable termination[138]. There are two CRP methods that adhere to PRE-principle; ATRP and stable free radical polymerisation (SFRP), whereby the most commonly known form of the latter CRP method is nitroxide mediated polymerisation (NMP). After the initiation stage, free radicals react with monomers to form propagating chains ($P_n^{\cdot}$). These active species can revert to the dormant state (P_n-X) after several monomer units have been added prior its reversible reaction with the deactivator specie (X). The latter specie is represented differently for NMP and ATRP, with further details being addressed below. The reversibility of this equilibrium implies that for further chain growth free radicals need to be generated. This occurs through the activation of P_n-X by the application of heat. The concurrence of persistent radicals (X) with transient active species ($P_n^{\cdot}$) is responsible for the kinetic feature present in PRE-based radical systems (Scheme 2.7).

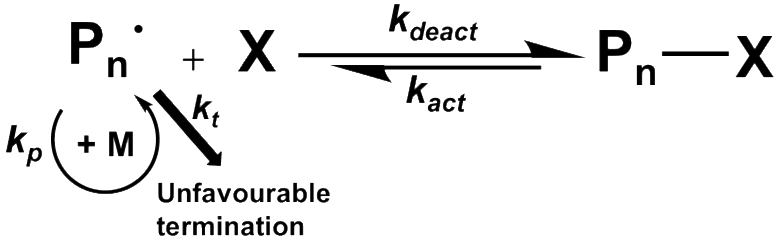

Scheme 2.7 Kinetics for activation-deactivation CRP reactions[120].

In this approach, PRE[139, 140] affords a self-regulating process in which persistent radicals continuously form dormant species. Generally over the course of the CRP reaction, termination reduces following a 1/3 power law that favours an increase in the concentration of dormant species in response to a high radical concentration, until a significant concentration of persistent radicals exists[120]. Consequently, a low steady radical concentration is attained by the position of the equilibrium being shifted towards the formation of dormant species. Kinetically speaking, it is important for there to be faster rates of deactivation (k_{deact}) compared to activation (k_{act}) to ensure a low active centre (radical)

concentration and low termination rates. Thus, all the polymer chains can grow at the same time to produce a narrow MWD.

2.3.2.2.1 Nitroxide-mediated polymerisation

NMP technique was initially discovered then followed other CRP methods, RAFT and ATRP[141]. This CRP technique involves stable nitroxide radicals reacting with propagating radicals so that polymer chain growth is favoured and termination reactions are minimised. This is achieved through the nitroxide radical, which can be represented as X in Scheme 2.7, reacting with active species to form a dormant specie. The nitroxide radical, 2,2,6,6-Tetramethyl-1-piperidinoxyl (TEMPO, Fig. 2.17), has been studied extensively and has proven to be the most efficient radical[142]. Although use of the term "nitroxide" and "nitroxide mediated polymerisation" is now recommended by IUPAC to be referred to as "aminoxyl" and "aminoxyl-mediated radical polymerisation, "[122] respectively, nitroxide and NMP will be referred to as such in this thesis as they are still used widely in literature[143].

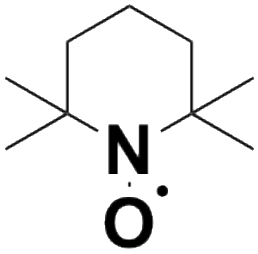

Fig. 2.17 TEMPO nitroxide radical[142].

Mechanistically, NMP is an analogue to ATRP because the presence of the dynamic equilibrium supresses irreversible termination as a means of ensuing uniform polymer chain growth. NMP also comprises of initiation, propagation and termination steps. However, the initiating system for NMP does not include an organic halide initiator and a transition metal complex as they are exclusive to ATRP. For NMP, the initiation system consists of either; an alkoxyamine that undergoes thermal decomposition to provide the nitroxide radical or, an initiator mixture of a conventional radical (e.g., benzoyl peroxide) and the nitroxide radical[121]. In the latter case, for example, benzoyl peroxide can react with TEMPO to generate initial active species quicker than the thermal decomposition of benzoyl peroxide[144]. As the stabilisation of nitroxide radicals is high, in both instances it cannot undergo irreversible bimolecular termination with itself. In this way, nitroxide radicals are free to

react with propagating chains during polymerisation in order to discourage irreversible termination between transient radicals.

There are several dissimilarities that exist between NMP and ATRP. One being that polymerisation reactions are conducted at higher temperatures (125-145)[145] due to slow polymerisation kinetics. Similar to conventional RP, the rate of polymerisation for nitroxide mediated reactions is determined by k_p. Elevated temperatures are used to help increase the rate of homolysis of the C-ON bond to allow equal polymer chain growth (i.e., an increase in k_p), in an effort to increase R_p[146]. The slow polymerisation kinetics also influences the duration of NMP reactions, which are reported to last up to 1-3 days[147]. Despite these disadvantages NMP remains as the simplest CRP technique to conduct, with successful reports on the controlled polymerisation of styrene[148]. Also, without the presence of sulfur-containing polymers, like in RAFT, or the use of transition metals, like in ATRP, the polymers prepared *via* NMP are less odoriferous and exhibit no discolouration or metal contamination. However, the few initiators and limited monomers that can form polymers with low polydispersities makes NMP the least versatile technique of all CRP methods. To date, NMP can display good control over the polymerisation of acrylates, acrylamides, 1,3-dienes and acrylonitriles and limited control over methacrylates[149]. In particular for TEMPO mediated NMP, it is hypothesised that the reaction between the nitroxide radical and methacrylate results in the abstraction of a β-hydrogen atom from a propagating chain, leading to the formation of a dead methacrylate chain and hydroxylamine[150]. On the contrary, copolymerisation reactions with low fraction of styrene[151] or the use of other nitroxide-derived radicals[152] can alleviate the 20% of methacrylate-based radicals that are expected to terminate prematurely[153]. Further development of NMP reaction conditions to prepare complex architectures in dispersed systems at lowered polymerisation temperatures helps to increase the robustness of this technique[154, 155].

2.3.2.2.2 Atom Transfer Radical Polymerisation

The self-regulating principle of PRE is also relevant to ATRP[156]. However, it is noteworthy to clarify that for ATRP, when considering Scheme 2.7, X is not a radical but rather a halogen atom (i.e., bromine or chlorine). ATRP mechanistically resembles the radical based organic synthetic process of atom transfer radical addition (ATRA)[157]. In copper (Cu) mediated ATRP[158] a catalyst/ligand complex is formed from Cu coordinating with a ligand (L). The Cu/L complex in the lower oxidation state (Cu^I/L), then reacts with dormant

molecules (P_n-X). Dormant molecules in ATRP are alkyl halide initiators or macroinitiators that have a halogenated moiety. The activation of the alkyl halide creates active species ($P_n^{\cdot}$) to which monomer units can add onto slowly and the catalyst/ligand complex at a higher oxidation state (X-Cu^{II}/L). Transient active species ($P_n^{\cdot}$) are inclined to terminate *via* combination, however, in the presence of X-Cu^{II}/L deactivator species they can return to the dormant state for the process of activation to repeat. This periodic and repetitive cycle of activation and deactivation by catalytic means ensures that PRE-based dynamic equilibrium is maintained during polymer growth so that termination is supressed (Scheme 2.8).

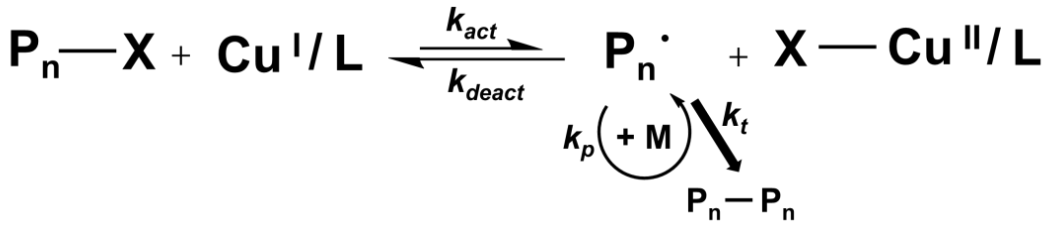

Scheme 2.8 Kinetics for copper mediated ATRP[159].

For an ATRP reaction, the rate of polymerisation is described by Equation (2.5)[159]:

$$R_p = k_p K_{ATRP}\left(\frac{[P_nX][Cu^I/L]\,[M]}{[XCu^{II}/L]}\right) \qquad \textbf{(2.5)}$$

where [P_nX] and K_{ATRP} are the concentration of dormant species and ATRP equilibrium constant, respectively. Also, [Cu^I/L] represents the concentration of activators whilst [X-Cu^{II}/L] refers to the concentration of deactivators. Similar to conventional RP, it is observed that R_p is determined by k_p. However, the concentration of deactivators has an inversely proportional relation to R_p. This implies that with increasing concentration of deactivators the rate of polymerisation is reduced as more propagating chains transform into dormant species. Conversely, when the concentration of deactivator species is decreased to an acceptable level, R_p increases as polymer chain growth by a few monomer units is permitted. The ratio of the constants of activation and deactivation directly affect the value of K_{ATRP}. Control over the polymerisation reaction would imply $k_{deact} >> k_{act}$, to maintain low radical concentration and therefore minimal termination reaction. This would result in a small K_{ATRP} value (10^{-9} to 10^{-4})[160] for an acceptable R_p.

In addition, the narrow MWD of a polymer synthesised *via* ATRP is enhanced by faster rates of deactivation that maintain relatively small values of k_p/ k_{deact}. This ratio is lowered by slow monomer addition, high monomer conversion and higher concentration of deactivator species during polymerisation[161]. In the case of longer and complex macromolecules, a reduction in the concentration of dormant species would be an additional factor to aid uniform chain growth.

The uniformity of a polymer chain refers to the dispersity of the weight-average and number-average molecular weights (M_w/M_n). The polydispersity index (PDI) describes the degree to which the polymer chains are uniform. Equation 2.6 describes how the PDI is dependent on the ATRP reaction parameters[158]:

$$\frac{M_w}{M_n} = 1 + \left(\frac{k_p[P_nX]}{k_{deact}[XCu^{II}/L]}\right)\left(\frac{2}{p} - 1\right) \qquad \textbf{(2.6)}$$

where p represents the monomer conversion and $[P_nX]$ is the concentration of dormant species. A low PDI is formed by high k_{deact} values. Good control over an ATRP reaction is evidenced by PDI values for polymers that are within the range of $1.04 \leq \text{PDI} \leq 1.5$[162]. This degree of control is vastly superior to the polymers prepared by conventional RP, which usually have a PDI ≥ 1.8[163]. Furthermore, in an investigation to explore the degree of control over the polymerisation of *N, N*-dimethylacrylamide, ATRP could be used to prepare poly(*N, N*-dimethylacrylamide) with a PDI of 1.09, which was comparatively better than when RAFT was conducted (e.g., PDI = 1.1) and considerably greater than when NMP was employed (e.g., PDI = 3.2)[164].

2.3.2.2.2.1 Versatility of polymers synthesised by ATRP

ATRP is suited to synthesising copolymers with controlled topologies as evidenced by linear copolymers, graft copolymers and other complex structures (Fig. 2.18). Linear copolymers comprise of two or more chemically distinct polymer blocks with resultant molecular weights generally ranging from 10^3 to 10^4 g/mol. Similar to RAFT, the formation of dormant species in ATRP allows for sequential polymerisation of subsequent monomers *in situ* or after purification to produce block, statistical and gradient copolymers[165]. In the case of ATRP reaction, the purification step is key to the remove transition metal from the polymer mixture. This can be achieved by flash chromatography using alumina or silica gel[166]. However, on an industrial scale this limits the widespread application of ATRP, despite efforts to remove all traces of the catalyst by additional means[167]. Furthermore, isolating the polymer through

precipitation methods increases the time scale for extracting the polymer product and general wastage of solvents, thereby decreasing the cost-effectiveness of ATRP[168]. Nevertheless, ATRP is still considered as a competitive technology to RAFT, with low potential of the polymers to release volatile sulphur-based compounds over long periods[169].

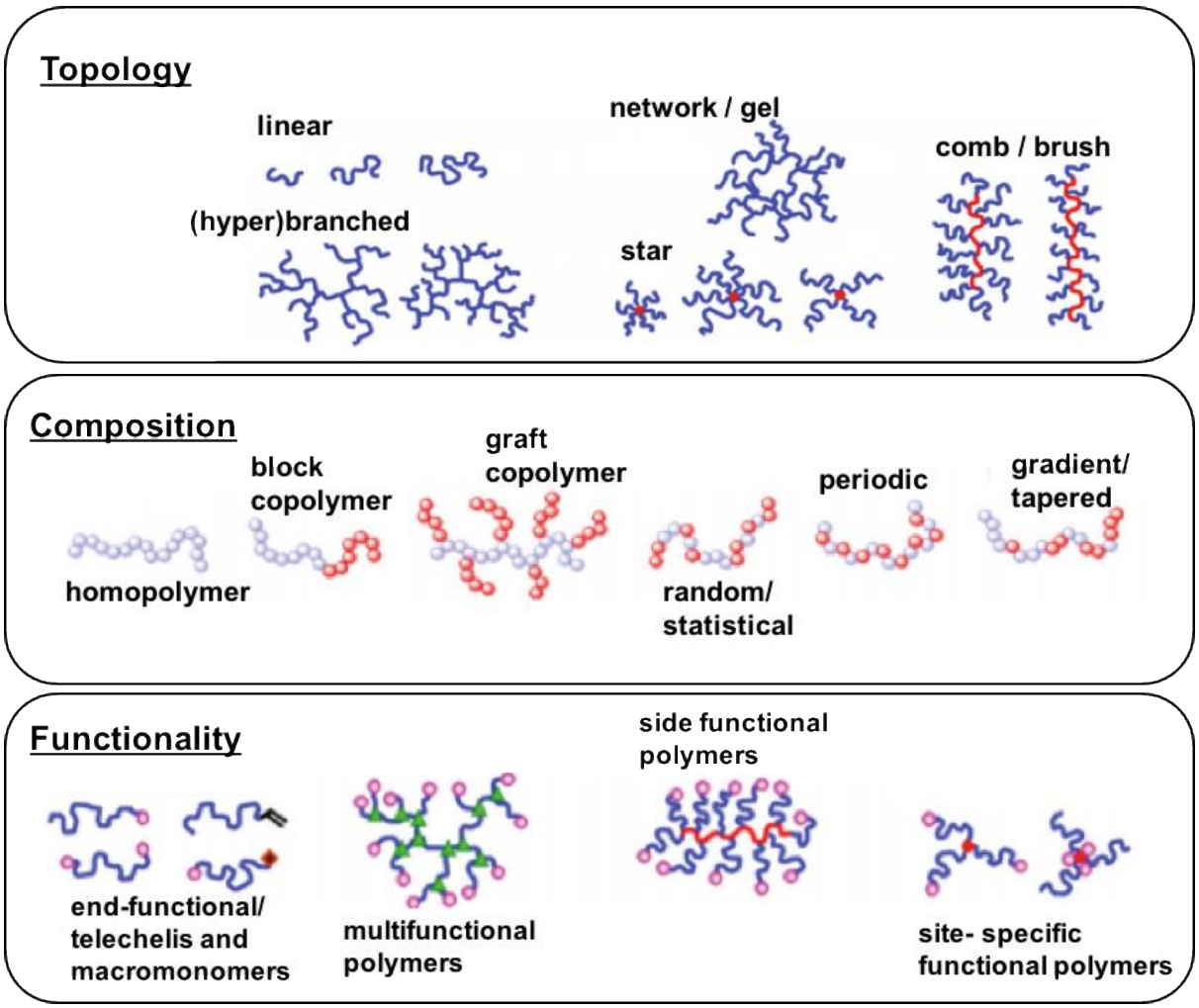

Fig. 2.18 Illustration of well-defined polymer topologies, composition and functionalities prepared by ATRP. The varying compositions are distinguished by darker and lighter circles denoting differing monomer units. Chain end functionality is represented by moieties (X or Y)[158].

The ability for one to adjust an initiating system to meet the needs of a given ATRP reaction puts ATRP in a recognisably distinct league compared to other CRP methods. This is supported by the investigation Schumers *et al.*[170] carried out to polymerise *o*-Nitrobenzyl (meth)acrylate monomers using CRP methods. Despite *o*-Nitrobenzyl acrylate being the more difficult monomer to polymerise, ATRP could synthesise the homopolymer but with poor control. In the case of *o*-Nitrobenzyl methacrylate, ATRP displayed good control over the

polymerisation kinetics at low monomer conversion (i.e., 30 %), provided that the reaction conditions were appropriately adjusted.

The variety of (macro)initiators and ligands that are available for ATRP conditions have shown that ATRP can also provide good control over the polymerisation of styrene[171, 172], various (meth)acrylates[173, 174] and other monomers[175] due to its tolerance to various functionalities. LMA is the most frequently investigated monomer for ATRP reactions[176]. Raghunadh *et al.*[177] discovered that the homopolymerisation of LMA in toluene helped to solubilise the catalyst/ligand complex in the lower oxidation state, thereby allowing ideal ATRP polymerisation kinetics to prevail. Similarly, Chatterjee *et al.*[178] polymerised LMA in the non-polar solvent anisole and discovered that the presence of tricaprylylmethylammonium chloride, alongside the catalyst/ligand complex, resulted in a well-defined homopolymer. It is reported that fast polymerisation in ATRP accommodates for the cross-propagation of methacrylates, which is a known limitation for NMP[179].

For branched polymer structures, such as graft copolymers, a macroinitiator is used to synthesise well-defined polymer side chains[180, 181]. A limitation to using ATRP to synthesise more complex architecture is that multiple variables must be considered to ensure that the ATRP mechanism will maintain ideal CRP principles, which often is perfected through trial and error[182]. Both NMP and RAFT possess the benefit of being conveniently conducted. Howvever, in contrast to NMP, the faster polymerisation kinetics of ATRP means that this CRP technique can operate at lower polymerisation temperatures and polymers can be synthesised within shorter reaction times[183]. In contrast with RAFT, the absence of intermediate radicals in ATRP reduces the potential for biomolecular termination of propagating complex copolymers and ensures that the resultant polymer will not display a characteristic red/pink/yellow colour that is indicative of RAFT-end groups[184].

2.4 Concluding remarks

The background information and the literature review presented in this chapter indicates that the presence of a polymer segment is crucial to form stable gels for EPD technology. There were two types of amphiphilic polymer organogelators that were addressed in this chapter. One containing a LMWG and the second based on non-ionic diblock copolymer composition. Depending on the pathway of developing the proposed polymer organogelator, it is understood that non-covalent interactions drive gelator molecules to self-assemble and thus encourages gelation with a non-polar solvent. In the case of the polymer organogelators

containing a LMWG, gelation is obtainable with low solids content of LMWG molecules ($\lesssim$ 1 wt. %). The LMWG portion is responsible for driving self-assembly *via* hydrogen bonding, $\pi - \pi$ stacking and van der Waals interactions, whilst the polymer segment inhibits crystallisation. For non-ionic diblock copolymer organogelators, the packing parameter influences observable morphologies. In a solvent that is good for the corona-forming block, spheres, worms or vesicle nano-objects become apparent, with the possibility of mixed phases also emerging due to inter-micelle interactions and polydispersity effects. The worms phase is expected to encourage gelation with higher solids content of the diblock copolymer (>10 wt. %) *in situ via* PISA or following concentration studies of the formulation mixture. Stable concentrated gels are desired for this project as a means of complying with the principle of bistability. The diblock copolymer gelator pathway would therefore be a more suitable route as crystallisation is preventable due to the presence of exclusively polymer chains. This is an important characteristic for the proposed polymer organogelator in EPD technology so that image retention is possible and gel breakdown is only evident during particle migration when a new image is forming. The reversible nature of the polymer organogelators was addressed by means of stimuli responsive behaviour, such as temperature changes and time-dependent shear-thinning studies. It is understood that the method of self-assembly is kinetically quicker for polymer organogelators containing a LMWG in comparison to diblock copolymer organogelators.

The development of conventional RP into more controlled methods provided scope for preparing a plethora of polymer chains with increasing complexity and unprecedented molecular weight distributions. CRP methods share the common feature of a dynamic equilibrium that encourages equal growth of all polymer chain. Categorisation of CRP methods into those based on degenerative transfer and PRE are acknowledged according to the presence of a transfer agent (i.e., RAFT) or a persistent radical (i.e., NMP and RAFT), respectively. Arguably RAFT and ATRP are the most versatile CRP techniques. RAFT dispersion is a central technique used to prepare the diblock copolymer organogelators. The resultant polymers containing RAFT end-groups tend to be coloured and emit odours over time due to the presence of sulphur groups. There are limited reports on the use of ATRP to prepare diblock copolymer organogelators, however, the retention of halogenated species in the macroinitiator implies polymer organogelators can be prepared using ATRP. ATRP conditions are difficult to control compared to RAFT and NMP, however, the absence of sulphur-containing compounds and the fast polymerisation kinetic suggests that ATRP is a

suitable technique to prepare well-defined polymer organogelators, that form unpigmented gels through efficient purification.

2.5 References

1. J. A. Rogers and Z. Bao, *J Polym Sci Pol Chem*, 2002, **40**, 3327-3334.
2. E-Ink Coporation, How our ink works, http://www.eink.com/technology.html, (accessed 4 December, 2016).
3. in *A Guide to Protein Isolation*, Springer Netherlands, Dordrecht, 2002, pp. 115-149.
4. X. W. Meng, F. Q. Tang, B. Peng and J. Ren, *Nanoscale Res Lett*, 2010, **5**, 174-179.
5. B. Comiskey, J. D. Albert, H. Yoshizawa and J. Jacobson, *Nature*, 1998, **394**, 253-255.
6. F. L. Ltd, http://www.fujitsu.com/global/about/resources/news/press-releases/2005/0713-01.html, (accessed 24th December, 2016).
7. Amazon, https://www.amazon.co.uk/Amazon-Kindle-6-Inch-4GB-E-Reader/dp/B0186FESVC, (accessed 27th December, 2016).
8. S. Inoue, H. Kawai, S. Kanbe, T. Saeki and T. Shimoda, *Ieee T Electron Dev*, 2002, **49**, 1532-1539.
9. Y. Chen, J. Au, P. Kazlas, A. Ritenour, H. Gates and M. McCreary, *Nature*, 2003, **423**, 136-136.
10. C. X. Wang, H. Y. Mao, C. X. Wang and S. H. Fu, *Ind Eng Chem Res*, 2011, **50**, 11930-11934.
11. M. P. L. Werts, M. Badila, C. Brochon, A. Hebraud and G. Hadziioannou, *Chem Mater*, 2008, **20**, 1292-1298.
12. D. G. Yu and J. H. An, *Colloid Surface A*, 2004, **237**, 87-93.
13. S. J. Telfer and M. D. McCreary, *42-4: Invited Paper: A Full-Color Electrophoretic Display*, 2016.
14. C. A. Kim, M. J. Joung, S. D. Ahn, G. H. Kim, S. Y. Kang, I. K. You, J. Oh, H. J. Myoung, K. H. Baek and K. S. Suh, *Synthetic Met*, 2005, **151**, 181-185.
15. C. Tomasini and N. Castellucci, *Chem Soc Rev*, 2013, **42**, 156-172.
16. M. Dama and S. Berger, *J Phys Chem B*, 2013, **117**, 5788-5791.
17. G. J. Wang and A. D. Hamilton, *Chem Commun*, 2003, 310-311.
18. X. Y. Yang, G. X. Zhang and D. Q. Zhang, *J Mater Chem*, 2012, **22**, 38-50.
19. M. George and R. G. Weiss, *Accounts Chem Res*, 2006, **39**, 489-497.
20. Y. Lin, B. Kachar and R. G. Weiss, *J Am Chem Soc*, 1989, **111**, 5542-5551.
21. Y. C. Lin and R. G. Weiss, *Macromolecules*, 1987, **20**, 414-417.
22. R. Mukkamala and R. G. Weiss, *Langmuir*, 1996, **12**, 1474-1482.
23. K. J. Skilling, F. Citossi, T. D. Bradshaw, M. Ashford, B. Kellam and M. Marlow, *Soft Matter*, 2014, **10**, 237-256.
24. Q. F. Hou, S. C. Wang, L. B. Zang, X. L. Wang and S. M. Jiang, *J Colloid Interf Sci*, 2009, **338**, 463-467.
25. T. Brotin, R. Utermohlen, F. Fages, H. Bouaslaurent and J. P. Desvergne, *J Chem Soc Chem Comm*, 1991, 416-418.
26. L. D. Lu and R. G. Weiss, *Chem Commun*, 1996, 2029-2030.
27. D. J. Abdallah, S. A. Sirchio and R. G. Weiss, *Langmuir*, 2000, **16**, 7558-7561.
28. M. A. Rogers and R. G. Weiss, *New J Chem*, 2015, **39**, 785-799.
29. J. X. Peng, H. Y. Xia, K. Q. Liu, D. Gao, M. Yang, N. Yan and Y. Fang, *J Colloid Interf Sci*, 2009, **336**, 780-785.

30. K. Q. Liu, N. Yan, J. X. Peng, J. Liu, Q. H. Zhang and Y. Fang, *J Colloid Interf Sci*, 2008, **327**, 233-242.
31. V. A. Mallia, M. George, D. L. Blair and R. G. Weiss, *Langmuir*, 2009, **25**, 8615-8625.
32. J. J. Li, M. H. Zhang and R. G. Weiss, *Chem-Asian J*, 2016, **11**, 3414-3422.
33. J. Daniel and R. Rajasekharan, *J Am Oil Chem Soc*, 2003, **80**, 417-421.
34. A. Pal, Y. K. Ghosh and S. Bhattacharya, *Tetrahedron*, 2007, **63**, 7334-7348.
35. M. Yamanaka, *J Incl Phenom Macro*, 2013, **77**, 33-48.
36. M. George, G. Tan, V. T. John and R. G. Weiss, *Chem-Eur J*, 2005, **11**, 3243-3254.
37. Y. D. Huang, X. L. Dong, L. L. Zhang, W. Chai and J. Y. Chang, *J Mol Struct*, 2013, **1031**, 43-48.
38. K. Yoza, N. Amanokura, Y. Ono, T. Akao, H. Shinmori, M. Takeuchi, S. Shinkai and D. N. Reinhoudt, *Chem-Eur J*, 1999, **5**, 2722-2729.
39. S. Datta and S. Bhattacharya, *Chem Soc Rev*, 2015, **44**, 5596-5637.
40. O. Gronwald and S. Shinkai, *Chem-Eur J*, 2001, **7**, 4328-4334.
41. F. Ono, H. Watanabe and S. Shinkai, *Rsc Adv*, 2014, **4**, 25940-25947.
42. G. L. Feng, H. H. Chen, J. H. Cai, J. W. Wen and X. B. Liu, *Soft Mater*, 2014, **12**, 403-410.
43. M. Suzuki and K. Hanabusa, *Chem Soc Rev*, 2009, **38**, 967-975.
44. E. Yilgor, E. Burgaz, E. Yurtsever and I. Yilgor, *Polymer*, 2000, **41**, 849-857.
45. M. Suzuki, Y. Nakajima, M. Yumoto, M. Kimura, H. Shirai and K. Hanabusa, *Langmuir*, 2003, **19**, 8622-8624.
46. N. Brosse, D. Barth and B. Jamart-Gregoire, *Tetrahedron Lett*, 2004, **45**, 9521-9524.
47. G. Bastiat and J. C. Leroux, *J Mater Chem*, 2009, **19**, 3867-3877.
48. K. Hanabusa and M. Suzuki, *Polym J*, 2014, **46**, 776-782.
49. K. Hanabusa, M. Matsumoto, M. Kimura, A. Kakehi and H. Shirai, *J Colloid Interf Sci*, 2000, **224**, 231-244.
50. H. Hoshizawa, Y. Minemura, K. Yoshikawa, M. Suzuki and K. Hanabusa, *Langmuir*, 2013, **29**, 14666-14673.
51. F. d. r. Fages and K. Araki, *Low molecular mass gelators : design, self-assembly, function*, Springer, Berlin ; New York, 2005.
52. M. Suzuki, M. Yumoto, H. Shirai and K. Hanabusa, *Tetrahedron*, 2008, **64**, 10395-10400.
53. B. O. Okesola and D. K. Smith, *Chem Soc Rev*, 2016, **45**, 4226-4251.
54. M. Suzuki and K. Hanabusa, *Chem Soc Rev*, 2010, **39**, 455-463.
55. L. Z. Rogovina, V. G. Vasil'ev and E. E. Braudo, *Polym Sci Ser C+*, 2008, **50**, 85-92.
56. J. K. Gupta, D. J. Adams and N. G. Berry, *Chem Sci*, 2016, **7**, 4713-4719.
57. S. Saha, J. Bachl, T. Kundu, D. D. Diaz and R. Banerjee, *Chem Commun*, 2014, **50**, 3004-3006.
58. X. Huang, P. Terech, S. R. Raghavan and R. G. Weiss, *J Am Chem Soc*, 2005, **127**, 4336-4344.
59. M. Singh, G. Tan, V. Agarwal, G. Fritz, K. Maskos, A. Bose, V. John and G. McPherson, *Langmuir*, 2004, **20**, 7392-7398.
60. X. Huang, S. R. Raghavan, P. Terech and R. G. Weiss, *J Am Chem Soc*, 2006, **128**, 15341-15352.
61. J. Lee, J. E. Kwon, Y. You and S. Y. Park, *Langmuir*, 2014, **30**, 2842-2851.
62. G. Y. Zhu and J. S. Dordick, *Chem Mater*, 2006, **18**, 5988-5995.
63. D. J. Abdallah and R. G. Weiss, *Adv Mater*, 2000, **12**, 1237-+.
64. D. J. Adams, K. Morris, L. Chen, L. C. Serpell, J. Bacsa and G. M. Day, *Soft Matter*, 2010, **6**, 4144-4156.
65. E. P. Boden and G. E. Keck, *J Org Chem*, 1985, **50**, 2394-2395.

66. H. Ihara, M. Takafuji, T. Sakurai, M. Katsumoto, N. Ushijima, T. Shirosaki and H. Hachisako, *Org Biomol Chem*, 2003, **1**, 3004-3006.
67. P. Terech and R. G. Weiss, *Chem Rev*, 1997, **97**, 3133-3159.
68. H. Hoshizawa, M. Suzuki and K. Hanabusa, *Chem Lett*, 2011, **40**, 1143-1145.
69. R. Nagarajan and E. Ruckenstein, *Langmuir*, 1991, **7**, 2934-2969.
70. R. Nagarajan, *Langmuir*, 2002, **18**, 31-38.
71. J. N. Israelachvili, D. J. Mitchell and B. W. Ninham, *J Chem Soc Farad T 2*, 1976, **72**, 1525-1568.
72. R. Smith and C. Tanford, *P Natl Acad Sci USA*, 1973, **70**, 289-293.
73. G. Riess, *Prog Polym Sci*, 2003, **28**, 1107-1170.
74. Y. Y. Mai and A. Eisenberg, *Chem Soc Rev*, 2012, **41**, 5969-5985.
75. M. Karayianni and S. Pispas, *Springer Ser Fluores*, 2016, **16**, 27-63.
76. Y. W. Wang, J. T. He, C. C. Liu, W. H. Chong and H. Y. Chen, *Angew Chem Int Edit*, 2015, **54**, 2022-2051.
77. A. Blanazs, S. P. Armes and A. J. Ryan, *Macromol Rapid Comm*, 2009, **30**, 267-277.
78. Y. Y. Won, H. T. Davis and F. S. Bates, *Macromolecules*, 2003, **36**, 953-955.
79. T. Nicolai, O. Colombani and C. Chassenieux, *Soft Matter*, 2010, **6**, 3111-3118.
80. S. Jain and F. S. Bates, *Macromolecules*, 2004, **37**, 1511-1523.
81. J. P. Patterson, M. P. Robin, C. Chassenieux, O. Colombani and R. K. O'Reilly, *Chemical Society reviews*, 2014, **43**, 2412-2425.
82. G. H. Zheng and C. Y. Pan, *Macromolecules*, 2006, **39**, 95-102.
83. S. Sugihara, A. Blanazs, S. P. Armes, A. J. Ryan and A. L. Lewis, *J Am Chem Soc*, 2011, **133**, 15707-15713.
84. Y. W. Pei, N. C. Dharsana, J. A. Van Hensbergen, R. P. Burford, P. J. Roth and A. B. Lowe, *Soft Matter*, 2014, **10**, 5787-5796.
85. B. Charleux, G. Delaittre, J. Rieger and F. D'Agosto, *Macromolecules*, 2012, **45**, 6753-6765.
86. L. Houillot, C. Bui, C. Farcet, C. Moire, J. A. Raust, H. Pasch, M. Save and B. Charleux, *Acs Appl Mater Inter*, 2010, **2**, 434-442.
87. W. Zhao, G. Gody, S. M. Dong, P. B. Zetterlund and S. Perrier, *Polym Chem-Uk*, 2014, **5**, 6990-7003.
88. W. D. He, X. L. Sun, W. M. Wan and C. Y. Pan, *Macromolecules*, 2011, **44**, 3358-3365.
89. L. A. Fielding, M. J. Derry, V. Ladmiral, J. Rosselgong, A. M. Rodrigues, L. P. D. Ratcliffe, S. Sugihara and S. P. Armes, *Chem Sci*, 2013, **4**, 2081-2087.
90. V. J. Cunningham, Y. Ning, S. P. Armes and O. M. Musa, *Polymer*, 2016, **106**, 189-199.
91. M. J. Derry, L. A. Fielding and S. P. Armes, *Polym Chem-Uk*, 2015, **6**, 3054-3062.
92. A. Blanazs, A. J. Ryan and S. P. Armes, *Macromolecules*, 2012, **45**, 5099-5107.
93. A. P. Lopez-Oliva, N. J. Warren, A. Rajkumar, O. O. Mykhaylyk, M. J. Derry, K. E. B. Doncom, M. J. Rymaruk and S. P. Armes, *Macromolecules*, 2015, **48**, 3547-3555.
94. Y. Pei, L. Thurairajah, O. R. Sugita and A. B. Lowe, *Macromolecules*, 2015, **48**, 236-244.
95. V. J. Cunningham, S. P. Armes and O. M. Musa, *Polym Chem-Uk*, 2016, **7**, 1882-1891.
96. S. L. Canning, G. N. Smith and S. P. Armes, *Macromolecules*, 2016, **49**, 1985-2001.
97. N. M. Ahmad, B. Charleux, C. Farcet, C. J. Ferguson, S. G. Gaynor, B. S. Hawkett, F. Heatley, B. Klumperman, D. Konkolewicz, P. A. Lovell, K. Matyjaszewski and R. Venkatesh, *Macromol Rapid Comm*, 2009, **30**, 2002-2021.
98. L. P. D. Ratcliffe, B. E. McKenzie, G. M. D. Le Bouedec, C. N. Williams, S. L. Brown and S. P. Armes, *Macromolecules*, 2015, **48**, 8594-8607.

99. D. J. Keddie, G. Moad, E. Rizzardo and S. H. Thang, *Macromolecules*, 2012, **45**, 5321-5342.
100. L. A. Fielding, J. A. Lane, M. J. Derry, O. O. Mykhaylyk and S. P. Armes, *J Am Chem Soc*, 2014, **136**, 5790-5798.
101. A. Blanazs, J. Madsen, G. Battaglia, A. J. Ryan and S. P. Armes, *J Am Chem Soc*, 2011, **133**, 16581-16587.
102. Y. W. Pei and A. B. Lowe, *Polym Chem-Uk*, 2014, **5**, 2342-2351.
103. D. J. Siegwart, J. K. Oh and K. Matyjaszewski, *Prog Polym Sci*, 2012, **37**, 18-37.
104. H. F. Yu, A. Shishido, T. Iyoda and T. Ikeda, *Macromol Rapid Comm*, 2007, **28**, 927-931.
105. V. Abetz, V. Abetz and SpringerLink, *Block copolymers II*, 2005.
106. J. X. Zhang, L. Y. Qiu and K. J. Zhu, *Macromol Rapid Comm*, 2005, **26**, 1716-1723.
107. D. Peng, G. L. Lu, S. Zhang, X. H. Zhang and X. Y. Huang, *J Polym Sci Pol Chem*, 2006, **44**, 6857-6868.
108. X. Y. Jiang, X. Jiang, G. L. Lu, C. Feng and X. Y. Huang, *Polym Chem-Uk*, 2014, **5**, 4915-4925.
109. Z. W. Xu, J. P. Lin, Q. Zhang, L. Q. Wang and X. H. Tian, *Polym Chem-Uk*, 2016, **7**, 3783-3811.
110. X. Y. Liu, J. S. Kim, J. Wu and A. Eisenberg, *Macromolecules*, 2005, **38**, 6749-6751.
111. S. J. Zhai, J. Shang, D. Yang, S. Y. Wang, J. H. Hu, G. L. Lu and X. Y. Huang, *J Polym Sci Pol Chem*, 2012, **50**, 811-820.
112. P. Vlcek, M. Janata, P. Latalova, J. Dybal, M. Spirkova and L. Toman, *J Polym Sci Pol Chem*, 2008, **46**, 564-573.
113. Y. Y. Xu, H. Becker, J. Y. Yuan, M. Burkhardt, Y. Zhang, A. Walther, S. Bolisetty, M. Ballauff and A. H. E. Muller, *Macromol Chem Physic*, 2007, **208**, 1666-1675.
114. F. W. Harris, *J Chem Educ*, 1981, **58**, 837-843.
115. D. Greszta, D. Mardare and K. Matyjaszewski, *Macromolecules*, 1994, **27**, 638-644.
116. R. J. Young and P. A. Lovell, *Introduction to polymers*, 2011.
117. K. Matyjaszewski, *J Phys Org Chem*, 1995, **8**, 197-207.
118. A. Goto and T. Fukuda, *Prog Polym Sci*, 2004, **29**, 329-385.
119. K. Matyjaszewski and T. P. Davis, *Handbook of Radical Polymerization*, Wiley, 2003.
120. W. A. Braunecker and K. Matyjaszewski, *Prog Polym Sci*, 2007, **32**, 93-146.
121. G. Odian, *Principles of Polymerization*, 2004.
122. A. D. Jenkins, R. G. Jones and G. Moad, *Pure Appl Chem*, 2010, **82**, 483-491.
123. X. P. Chen and K. Y. Qiu, *Chem Commun*, 2000, 233-234.
124. K. A. Davis and K. Matyjaszewski, *Macromolecules*, 2000, **33**, 4039-4047.
125. J. Chiefari, Y. K. Chong, F. Ercole, J. Krstina, J. Jeffery, T. P. T. Le, R. T. A. Mayadunne, G. F. Meijs, C. L. Moad, G. Moad, E. Rizzardo and S. H. Thang, *Macromolecules*, 1998, **31**, 5559-5562.
126. K. Matyjaszewski, S. Gaynor, D. Greszta, D. Mardare and T. Shigemoto, *J Phys Org Chem*, 1995, **8**, 306-315.
127. G. Moad, J. Chiefari, Y. K. Chong, J. Krstina, R. T. A. Mayadunne, A. Postma, E. Rizzardo and S. H. Thang, *Polym Int*, 2000, **49**, 993-1001.
128. G. Moad, E. Rizzardo and S. H. Thang, *Aust J Chem*, 2009, **62**, 1402-1472.
129. C. Barner-Kowollik, M. Buback, B. Charleux, M. L. Coote, M. Drache, T. Fukuda, A. Goto, B. Klumperman, A. B. Lowe, J. B. Mcleary, G. Moad, M. J. Monteiro, R. D. Sanderson, M. P. Tonge and P. Vana, *J Polym Sci Pol Chem*, 2006, **44**, 5809-5831.
130. I. Altarawneh, S. Rawadieh and V. G. Gomes, *Des Monomers Polym*, 2014, **17**, 430-437.

131. Y. Kwak, A. Goto, Y. Tsujii, Y. Murata, K. Komatsu and T. Fukuda, *Macromolecules*, 2002, **35**, 3026-3029.
132. M. R. Hill, R. N. Carmean and B. S. Sumerlin, *Macromolecules*, 2015, **48**, 5459-5469.
133. P. B. Zetterlund, S. C. Thickett, S. Perrier, E. Bourgeat-Lami and M. Lansalot, *Chem Rev*, 2015, **115**, 9745-9800.
134. D. J. Keddie, *Chem Soc Rev*, 2014, **43**, 496-505.
135. C. Barner-Kowollik, *Handbook of RAFT polymerization*, Wiley-VCH, Weinheim, 2008.
136. Y. K. Chong, G. Moad, E. Rizzardo and S. H. Thang, *Macromolecules*, 2007, **40**, 4446-4455.
137. H. Willcock and R. K. O'Reilly, *Polym Chem-Uk*, 2010, **1**, 149-157.
138. H. Fischer, *J Polym Sci Pol Chem*, 1999, **37**, 1885-1901.
139. H. Fischer, *Macromolecules*, 1997, **30**, 5666-5672.
140. B. E. Daikh and R. G. Finke, *J Am Chem Soc*, 1992, **114**, 2938-2943.
141. C. J. Hawker, *J Am Chem Soc*, 1994, **116**, 11185-11186.
142. G. Moad and E. Rizzardo, *Rsc Polym Chem Ser*, 2016, 1-44.
143. V. Sciannamea, R. Jerome and C. Detrembleur, *Chem Rev*, 2008, **108**, 1104-1126.
144. R. P. N. Veregin, M. K. Georges, P. M. Kazmaier and G. K. Hamer, *Macromolecules*, 1993, **26**, 5316-5320.
145. K. A. Payne, P. Nesvadba, J. Debling, M. F. Cunningham and R. A. Hutchinson, *Acs Macro Lett*, 2015, **4**, 280-283.
146. M. X. Zhou, N. T. McManus, E. Vivaldo-Lima, L. M. F. Lona and A. Penlidis, *Macromol Symp*, 2010, **289**, 95-107.
147. C. J. Hawker, A. W. Bosman and E. Harth, *Chem Rev*, 2001, **101**, 3661-3688.
148. T. Fukuda, T. Terauchi, A. Goto, K. Ohno, Y. Tsujii, T. Miyamoto, S. Kobatake and B. Yamada, *Macromolecules*, 1996, **29**, 6393-6398.
149. J. Nicolas, Y. Guillaneuf, C. Lefay, D. Bertin, D. Gigmes and B. Charleux, *Prog Polym Sci*, 2013, **38**, 63-235.
150. C. Burguiere, M. A. Dourges, B. Charleux and J. P. Vairon, *Macromolecules*, 1999, **32**, 3883-3890.
151. D. Benoit, V. Chaplinski, R. Braslau and C. J. Hawker, *J Am Chem Soc*, 1999, **121**, 3904-3920.
152. Y. Guillaneuf, D. Gigmes, S. R. A. Marque, P. Astolfi, L. Greci, P. Tordo and D. Bertin, *Macromolecules*, 2007, **40**, 3108-3114.
153. M. Souaille and H. Fischer, *Macromolecules*, 2000, **33**, 7378-7394.
154. S. Tomoeda, Y. Kitayama, J. Wakamatsu, H. Minami, P. B. Zetterlund and M. Okubo, *Macromolecules*, 2011, **44**, 5599-5604.
155. A. Darabi, P. G. Jessop and M. F. Cunningham, *Macromolecules*, 2015, **48**, 1952-1958.
156. A. Limer and D. M. Haddleton, *Prog React Kinet Mec*, 2004, **29**, 187-241.
157. K. Thommes, B. Icli, R. Scopelliti and K. Severin, *Chem-Eur J*, 2007, **13**, 6899-6907.
158. K. Matyjaszewski, *Macromolecules*, 2012, **45**, 4015-4039.
159. K. Matyjaszewski, *Isr J Chem*, 2012, **52**, 206-220.
160. W. Tang, N. V. Tsarevsky and K. Matyjaszewski, *J Am Chem Soc*, 2006, **128**, 1598-1604.
161. G. Litvinenko and A. H. E. Muller, *Macromolecules*, 1997, **30**, 1253-1266.
162. K. Matyjaszewski, *Macromol Symp*, 1996, **111**, 47-61.
163. T. E. Patten, J. H. Xia, T. Abernathy and K. Matyjaszewski, *Science*, 1996, **272**, 866-868.

164. J. F. Lutz, D. Neugebauer and K. Matyjaszewski, *J Am Chem Soc*, 2003, **125**, 6986-6993.
165. S. H. Qin, J. Saget, J. R. Pyun, S. J. Jia, T. Kowalewski and K. Matyjaszewski, *Macromolecules*, 2003, **36**, 8969-8977.
166. F. Canturk, B. Karagoz and N. Bicak, *J Polym Sci Pol Chem*, 2011, **49**, 3536-3542.
167. K. Matyjaszewski, T. Pintauer and S. Gaynor, *Macromolecules*, 2000, **33**, 1476-1478.
168. S. Faucher, P. Okrutny and S. P. Zhu, *Macromolecules*, 2006, **39**, 3-5.
169. G. Moad, E. Rizzardo and S. H. Thang, *Aust J Chem*, 2012, **65**, 985-1076.
170. J. M. Schumers, C. A. Fustin, A. Can, R. Hoogenboom, U. S. Schubert and J. F. Gohy, *J Polym Sci Pol Chem*, 2009, **47**, 6504-6513.
171. M. Al-Harthi, L. S. Cheng, J. B. P. Soares and L. C. Simon, *J Polym Sci Pol Chem*, 2007, **45**, 2212-2224.
172. J. Tom, B. Hornby, A. West, S. Harrisson and S. Perrier, *Polym Chem-Uk*, 2010, **1**, 420-422.
173. P. V. Mendonca, A. C. Serra, J. F. J. Coelho, A. V. Popov and T. Guliashvili, *Eur Polym J*, 2011, **47**, 1460-1466.
174. A. Carlmark, R. Vestberg and E. M. Jonsson, *Polymer*, 2002, **43**, 4237-4242.
175. M. Teodorescu and K. Matyjaszewski, *Macromol Rapid Comm*, 2000, **21**, 190-194.
176. G. Cayli and M. A. R. Meier, *Eur J Lipid Sci Tech*, 2008, **110**, 853-859.
177. V. Raghunadh, D. Baskaran and S. Sivaram, *Polymer*, 2004, **45**, 3149-3155.
178. D. P. Chatterjee and B. M. Mandal, *Polymer*, 2006, **47**, 1812-1819.
179. R. B. Grubbs, *Polym Rev*, 2011, **51**, 104-137.
180. J. Burdynska, Y. C. Li, A. V. Aggarwal, S. Hoger, S. S. Sheiko and K. Matyjaszewski, *J Am Chem Soc*, 2014, **136**, 12762-12770.
181. S. Yamamoto, J. Pietrasik and K. Matyjaszewski, *Macromolecules*, 2008, **41**, 7013-7020.
182. M. Billing and F. H. Schacher, *Macromolecules*, 2016, **49**, 3696-3705.
183. A. Ramakrishnan, R. Dhamodharan and J. Ruhe, *J Polym Sci Pol Chem*, 2006, **44**, 1758-1769.
184. C. P. Jesson, C. M. Pearce, H. Simon, A. Werner, V. J. Cunningham, J. R. Lovett, M. J. Smallridge, N. J. Warren and S. P. Armes, *Macromolecules*, 2017, **50**, 182-191.

3 Key methods and characterisation techniques

3.1 ATRP

The polymers studied in this thesis were synthesised *via* ATRP. This polymerisation technique was employed for the advantages of preparing polymer organogelators based on diblock and graft copolymers architectures. To maintain active Cu^{I} catalyst in copper-mediated ATRP it was important that all reactions were conducted under inert conditions[1] so that Cu^{I} would become oxidised after reacting with free radicals rather than oxygen[2]. In addition, repetitive freeze-pump-thaw cycles[3] were carried out to remove oxygen from the reaction mixture.

To gain enhanced control over an ATRP reaction it is assumed that K_{ATRP} is optimised. Certain conditions[4] like the type of alkyl halide initiator, catalyst/ligand complex, solvent polarity, polymerisation temperature and the use of reducing agents/deactivators were tailored to achieve control over the polymerisation of the (meth)acrylates presented in this thesis. A detailed description of the methods is outlined in the experimental sections of the proposed publication papers in Chapter 4.

3.1.1 Initiating system

The activity of an initiator is affected by the atomic mass of the halogen atom and the structure of the alkyl halide[5] (Fig 3.1). The order of activity for the halogen atoms increases in the order of Cl < Br < I[6]. The exception to the order of reactivity is benzyl bromide, which is more reactive than thiocyanate/isocyanate. Furthermore, tertiary (3°) alkyl halides are the most reactive when compared to secondary (2°) alkyl halides and lastly primary (1°) alkyl halides[7]. To encourage faster rates of initiation, tertiary alkyl halide (macro)initiators were used in this work.

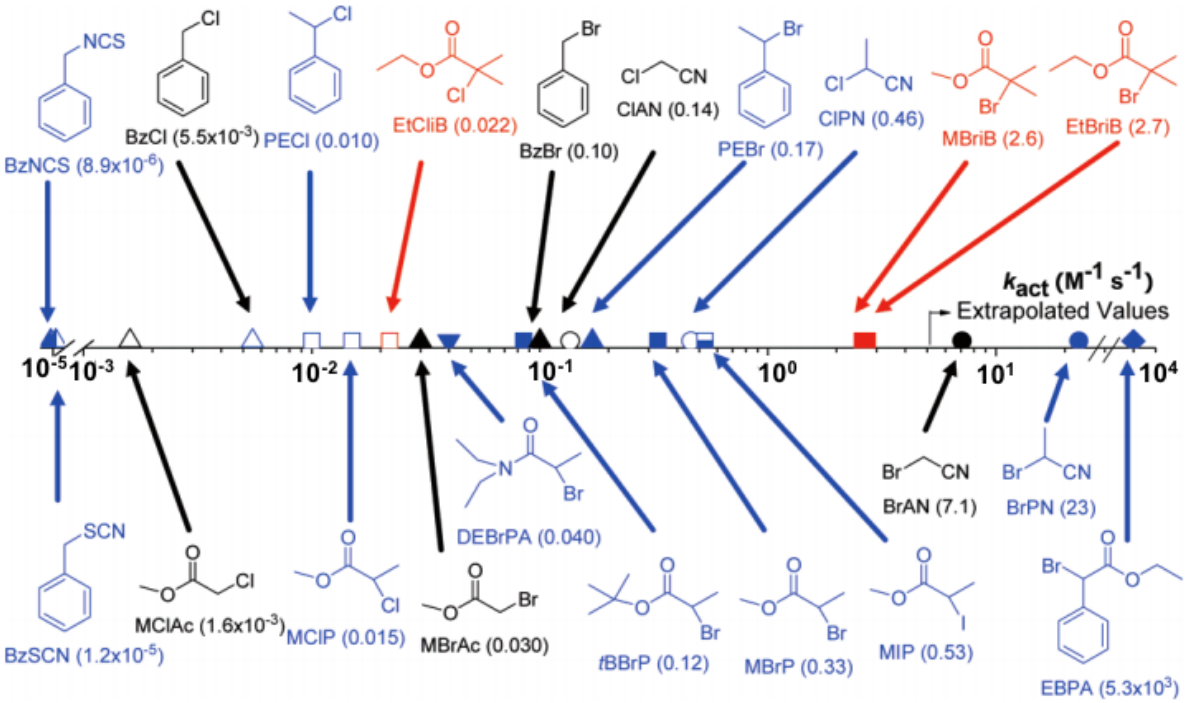

Fig. 3.1 Various initiators with their respective rate constants of activation in brackets. The ATRP reactions conducted at 35 °C for the study shown in the figure above used the catalyst/ligand complex $Cu^{I}X$/PMDETA (X = Br or Cl) and the solvent acetonitrile. The initiators with 3° structures are red whilst those with 2° and 1° structures are blue and black, respectively. Isocyanate/thiocyanate can be seen to the left of the figure with half-filled symbols. Chloride-based initiators are signified by open symbols, bromide-based initiators are represented by filled symbols whilst iodide-based initiators are indicated by bottom half-filled symbols. The structure of the radical stabilising group is indicated like so: amide (∇), benzyl ester (Δ), ester (sqaure), nitrile (circle) and phenyl ester (◊)[7].

The type of $Cu^{I}X$/L complex (where X = Br or Cl) that was employed in this study was important as it formed both the activator and deactivator species. The work in this thesis was concerned with copper-mediated ATRP[8], although there are reports of successfully prepared polymers that have utilised an iron catalyst[9, 10] or other unconventional metals[11]. For copper-mediated ATRP, activation and deactivation can occur *via* two concerted electron transfer processes[12] as shown in Scheme 3.1.

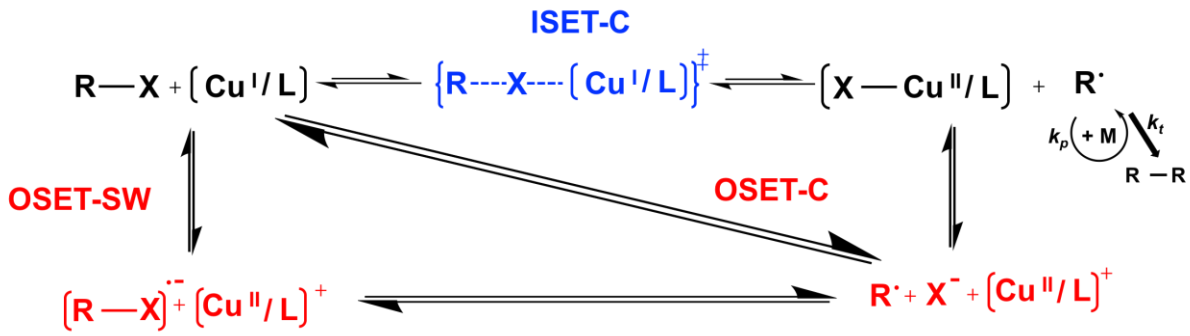

Scheme 3.1 Depiction of the kinetic pathways for ISET and OSET. ISET-C and OSET-C occur in a concerted fashion whilst OSET-SW is a stepwise process. The ions are indicated with respective anionic or cationic charges[13].

Inner sphere electron transfer (ISET) involves homolytic cleavage of the halogen atom from the alkyl halide and its transfer to the catalyst/ligand complex and vice versa. Outer sphere electron transfer (OSET) concludes with radical and anion formation after halogen dissociation. If OSET occurs it can do so *via* a stepwise or a concerted manner, whereby the latter is proposed to be energetically favourable in an ATRP system[5]. Overall, ISET is the preferred process as the intermediate is less likely to participate in side reactions[13].

The ligand *N,N,N′,N′′,N′′′*-pentamethyldiethylenetriamine (PMDETA) was chosen for the work in this thesis to form part of the $Cu^{I}X$/L complex. PMDETA is an inexpensive ligand[14] that is commonly used for copper-mediated ATRP of (meth)acrylates[15, 16]. Multidentate nitrogen-based ligands, like PMDETA, serve the purpose of effectively solubilising Cu^{II} species and altering the activity of Cu to favour a high k_{deact} to suppress high amounts of termination during ATRP[14, 17]. The rate constants of activations for various ligands were determined in structure-reactivity studies[18]. This showed that the order of activity for various multidentate ligand structures increases in the order of bidentate < tridentate < tetradentate structures, as illustrated in Fig 3.2. The nature of the nitrogen atom in a ligand also affects the activity the $Cu^{I}X$/L complex in the following order: imine < aliphatic amine ≤ pyridine[18].

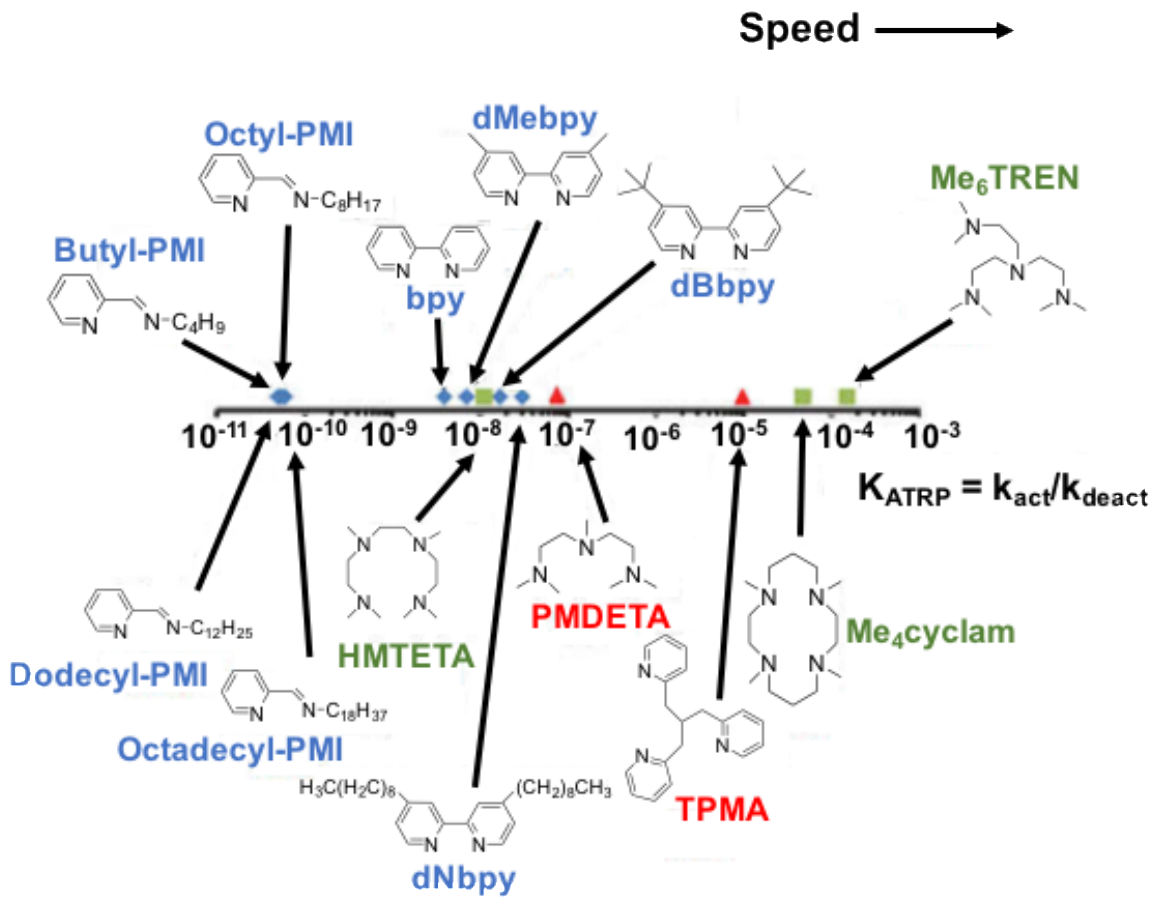

Fig. 3.2 The ATRP equilibrium constants (K_{ATRP}) plotted for common ATRP multidentate nitrogen-based ligands. The ATRP reactions were conducted at 22 °C using $Cu^{I}Br$ catalyst in acetonitrile. The direction of the black arrow indicates faster rates of ATRP[19].

3.1.2 Halogen exchange method

The halogen exchange method was regularly used in this work to optimise the blocking efficiency of block copolymers[20]. Typically, the mixed halide initiating system[21] used in this work comprised of a secondary or tertiary (macro)initiators that possessed bromo-terminal groups and a copper chloride (CuCl) catalyst. The switch of catalyst was necessary to encourage fast initiation rates and slower propagation rates (i.e. $k_i > k_p$). The higher k_i value is related to the weaker carbon-bromine bond of the initiator, whilst the lower k_p is ascribed to stronger carbon-chloride bond that form the terminus of most polymer chains following halogen exchange[22]. This results in slower rates of polymerisation whilst optimising control over the ATRP reaction. Scheme 3.2 illustrates the rates of halogen exchange for rate constant for chlorine ($k_{HE}^{\ Cl}$) and bromine ($k_{HE}^{\ Br}$) atoms in producing well defined copolymers.

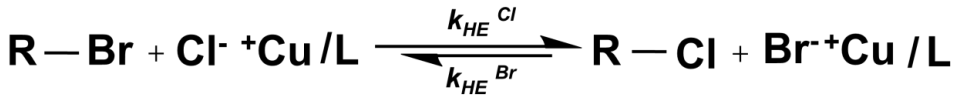

Scheme 3.2 Kinetics of the halogen exchange principle in copper mediated ATRP [20].

3.1.3 Solvent polarity and polymerisation temperature

ATRP reactions can be conducted in the presence or in the absence of a solvent. For this work, solution polymerisation in toluene was used to eliminate side reactions and solubilise the solvophobic polymers[4]. The polarity of the solvent is also known to optimise ATRP reaction constants by influencing the activity of activator species[23]. In less polar environments $Cu^{I}Br$/PMDETA can form neutral $[Cu^{I}(PMDETA)Br]$ and ion pair $[Cu^{I}(PMDETA)Br]^{+}$ $[CuBr_2]^{-}$ complexes as seen in Fig. 3.3. The latter ion forms because bromide anions are less stable and bind strongly with $Cu^{I}Br$ to form the inactive ion $[CuBr_2]^{-}$ [24]. Consequently, to obtain a high k_{act} only half of $Cu^{I}Br$ species form the ion $[Cu^{I}(PMDETA)Br]^{+}$ can participate in the activation process[25]. In this work the ratio of the $Cu^{I}Br$/PMDETA complex was often tailored to ~ 1/1 to achieve maximal k_{act} in toluene[26]. This differs for polar solvents like dimethylformamide (DMF) where the proportion of stable bromide anions in the complex $[Cu^{I}(PMDETA)]^{+}$ Br^{-} is less competitive in binding to Cu^{I} compared to PMDETA.

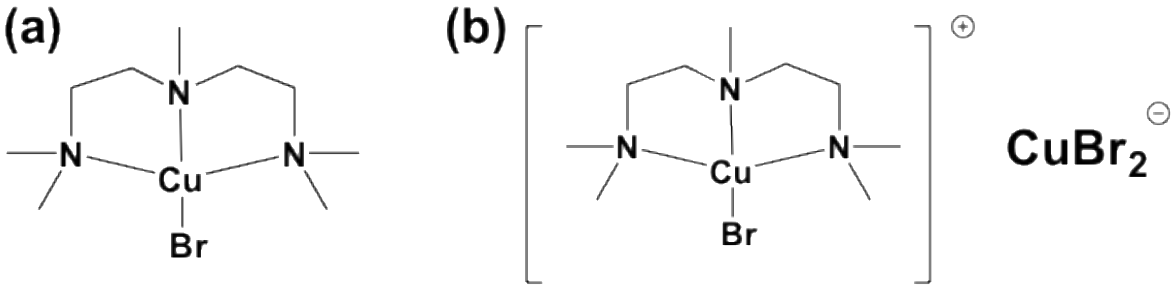

Fig. 3.3 $Cu^{I}Br$/PMDETA in a non-polar media forms a neutral complex (a) and an ion pair[25].

The polymerisation temperature also affects k_{act} of an ATRP reaction. For less reactive initiators higher temperatures increase k_{act} causing faster rates of polymerisation[27]. As initiators used for this work are already recognised as highly reactive, polymerisation reactions were not conducted above 60 °C to main high chain fidelity. This is because the stability of the (macro)initiator can be compromised at even higher temperatures[28].

3.1.4 The initial presence of deactivator species/ reducing agents

For the preparation of graft copolymers presented in this thesis, deactivator species in form of Cu^{II} species[29] were introduced at the beginning of ATRP reactions to increase k_{deact}. This is advised for ATRP reactions involving a multi-site macroinitiator. During the activation process of the multi-halogenated macroinitiator, the creation of a high local radical concentration would lead to unfavourable termination[30]. However, the presence of Cu^{II} species at the start of the reaction can react with radicals to form dormant species and reduced Cu^{I} species.

The introduction of reducing agents, such as *L*-ascorbic acid, serves the role of reducing k_{deact} in a polymerisation technique known as activators regenerated by electron transfer (ARGET) ATRP[31]. *L*-ascorbic acid does so by slowly reducing Cu^{II} species to Cu^{I} species to minimise high amounts of termination[32]. The benefits of using *L*-ascorbic are only desirable in a heterogeneous environment where it has limited solubility and a low radical concentration can be sustained[32]. ARGET ATRP was explored briefly in this thesis for its benefit of providing better control over an ATRP reaction.

3.2 Physical characterisation

This section deals with the theory and fundamental principles of the characterisation techniques used to analyse the macro(molecules) and gels investigated in this thesis.

3.2.1 Proton nuclear magnetic resonance

Proton nuclear magnetic resonance (^{1}H NMR) was used to analyse the hydrogen nuclei (i.e., protons) of (macro)molecules in this thesis to help deduce their respective structures. It also helped to determine impurities and unreacted chemicals following a chemical reaction. The following background information addresses how the protons in a sample were studied using ^{1}H NMR spectroscopy.

The atoms that make up a molecular sample consists of nuclei that comprise of protons and neutrons at the centre and surrounding electrons within their respective orbits. A hydrogen nucleus, such as a proton, is considered as a magnetic dipole. This is because it is electrically charged and in combination with its characteristic spin (I), can create a nuclear magnetic moment (μ).

When an external magnetic field (H_0) is applied, a proton can align with or against the direction of the magnetic field as shown in Fig. 3.4. This differs from the random orientation of protons in the absence of an external magnetic field. Given that a proton possesses a half-integer spin (i.e., ½), protons that align with an external magnetic field possess lower energy and exhibit + ½ spin state, whilst opposing alignment means that the protons possess higher energy with a - ½ spin state[33].

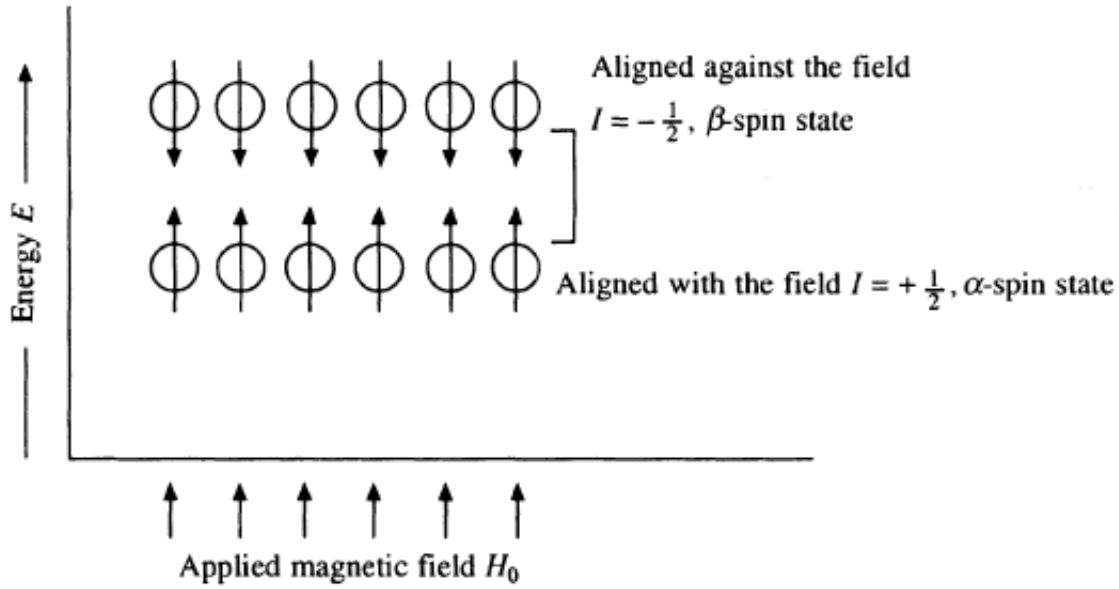

Fig. 3.4 Orientation of protons in an external magnetic field[33].

The absorption of energy by precessing protons and re-emitted energy provided information regarding the (macro)molecules investigated in this study. Radio-frequency waves are used to irradiate a sample in a varying H_0 in order to bring protons into resonance. Resonance is achieved when a proton absorbs the appropriate radio-frequency energy for it to exist in the higher energy spin state[33]. Once the resonance effect is absent, the promoted proton resumes its low energy state by re-emitting the radio-frequency in the form of an electric current, which is finally interpreted as a proton resonance signal. The deuterated solvent that is used to solubilise a given (macro)molecular sample, is expected to possess residual protons that will bear corresponding resonance signals that can be used as a reference. Thus, a ^{1}H NMR spectrum is used to identify distinct protons in (macro)molecules.

3.2.2 Gel permeation chromatography

Gel permeation chromatography (GPC) was used to measure the chain length (i.e., MW_n and MW_w) and the chain polydispersity (i.e., PDI) of polymers studied in this thesis. The method of size exclusion chromatography (SEC)[34] is synonymous with GPC, despite the latter comprising of a column made of a porous gel that behaves as a molecular filter (Scheme 3.3).

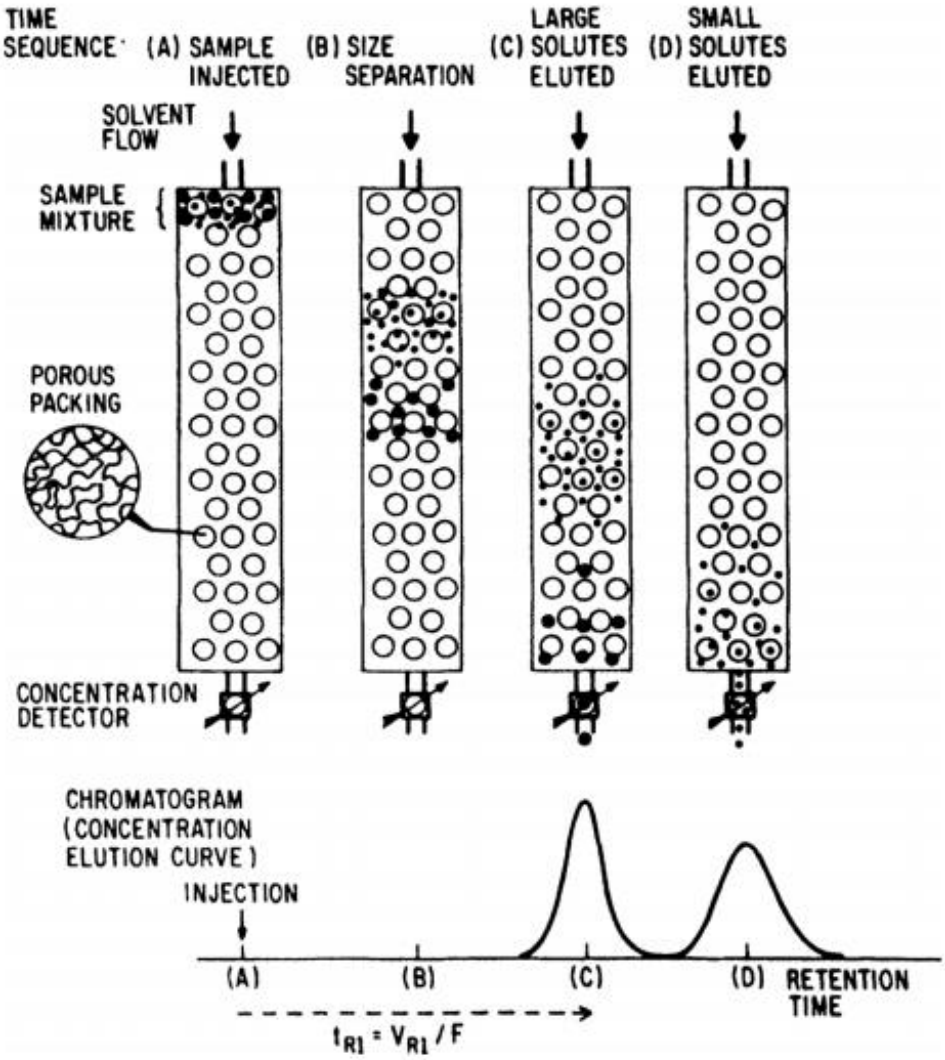

Scheme 3.3 Depiction of gel permeation chromatography[34].

Referring to the image above, once a polymer solution is introduced into a GPC instrument the dissolved macromolecules would meet with the porous gel (Scheme 3.3a). Thereafter two instances can take place depending on the size of the pores in relation to the size of the macromolecules (Scheme 3.3b). The first scenario describes larger macromolecules escaping the journey of entering the pores and therefore continuing through the column (Scheme 3.3c).

The second instance describes smaller macromolecules entering and leaving the pores *via* diffusion. Consequently, smaller macromolecules take longer to exit the column (Scheme 3.3d) whilst larger particles can pass through more quickly, and the length of time for intermediate sized polymers exists between the two extremes. Information regarding the number-average molecular weight (M_n), weight-average molecular weight (M_w) and PDI of the polymers can be provided from a computer software[35]. M_n, M_w and PDI is determined using Equations 3.1-3.3:

$$M_n = \frac{\Sigma N_i M_i}{\Sigma N_i} \qquad \textbf{(3.1)}$$

$$M_w = \frac{\Sigma N_i M_i^2}{\Sigma N_i M_i} \qquad \textbf{(3.2)}$$

where N_i is the number of chains of the molecular weight in question and M_i is the molecular weight of a chain.

$$PDI = \frac{M_w}{M_n} \qquad \textbf{(3.3)}$$

3.2.3 Dynamic light scattering

Dynamic light scattering (DLS) studies was used to characterise the size distribution of the nano-objects investigated in this thesis. Photon correlation spectroscopy (PCS), a branch of DLS studies, was used to measure the size of the nano-objects in dispersion by focusing an incident light (I_0) onto a sample (Fig 3.5). Although some light is transmitted (I_t), it is the fluctuations of scattered light (I_θ), as a function of time, that provides information regarding particle size[36].

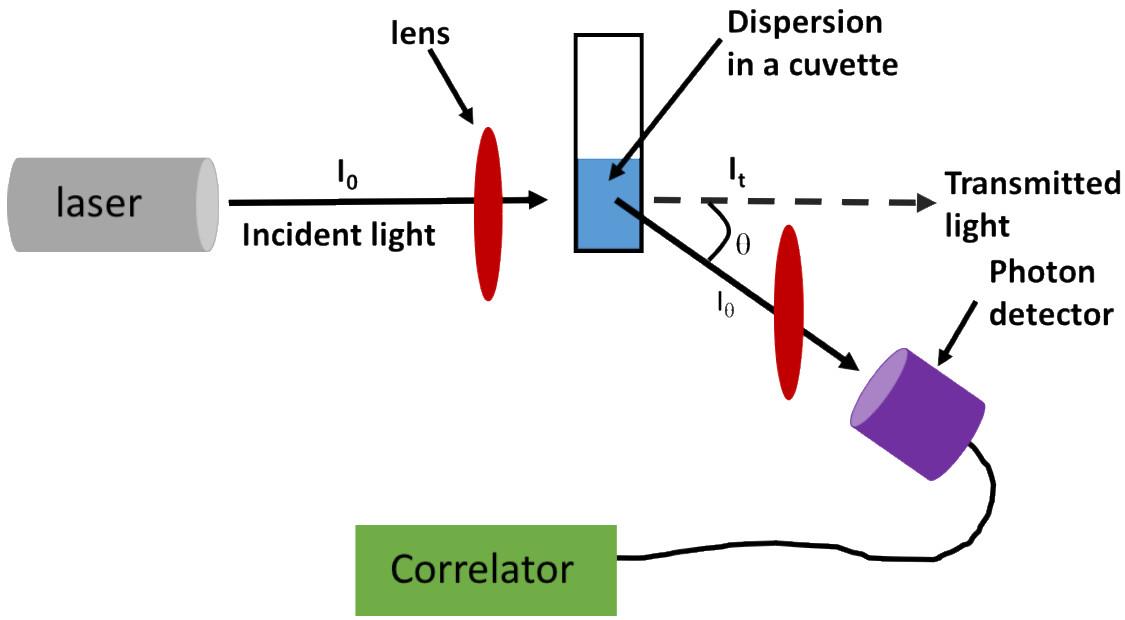

Fig. 3.5 Diagram of the dynamic light scattering theory[37].

A DLS instrument measures the Brownian motion of particles. Larger particles tend to move slower and scatter less light compared to smaller particles that move quickly. Considering Fig. 3.5, the correlator analyses the varying scattered light within a time frame to give the autocorrelation function of intensity ($G(\tau)$) that is expressed by Equation 3.4[38]:

$$G(\tau) = \langle I(t).I(t+\tau)\rangle \qquad \textbf{(3.4)}$$

where I represents the intensity scattered light, t is the time and τ corresponds to the delay time. The latter is independent of the experimental start time. For monodisperse particles, the exponential decaying function of time is expressed by Equation 3.5[38]:

$$G(\tau) = A + B\exp(-2\Gamma\tau) \qquad \textbf{(3.5)}$$

From the equation above, A and B are regarded as instrumental factors and Γ is the decay rate. The decay rate can then be related to the diffusion coefficient (D) of particles as expressed by Equation 3.6[38]:

$$\Gamma = Dq^2 \qquad \textbf{(3.6)}$$

where q^2 is the modulus of scattering vector that is expressed by Equation 3.7[38]:

$$q = \frac{4\pi n}{\lambda}\sin(\frac{\theta}{2}) \qquad \textbf{(3.7)}$$

where n is the refractive index of the dispersion fluid and λ corresponds to the wavelength of the sample fluid with a scattering angle (θ). Considering that Equation 3.6 provides D, the diameter (d) of a particle can be determined from rearranging Stokes-Einstein equation, which is expressed by Equation 3.8 [38]:

$$d = \frac{kT}{3\pi\eta D} \qquad \textbf{(3.8)}$$

where k is Boltzmann's constant, T is the temperature, and η is the viscosity of the dispersion fluid. Some of the nano-objects investigated in this thesis were non-spherical, therefore the value for d was acknowledged as an equivalent spherical diameter.

3.2.4 Rheology

Rheological studies were used to study the flow and deformation of the gels investigated in this thesis in response to applied mechanical forces. Fig. 3.6 depicts the shear force (F_p) a material can be exposed to using a rheometer.

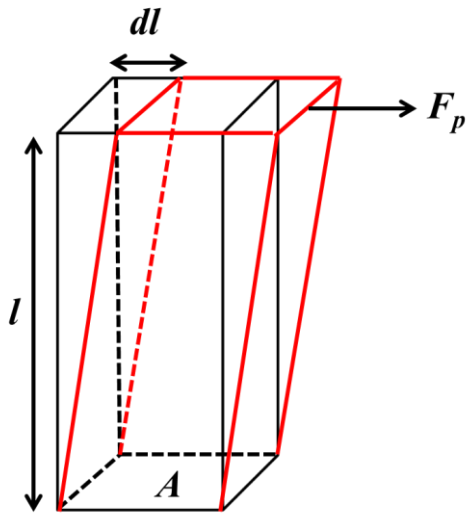

Fig. 3.6 Depiction of shear stress on an object[39].

Viscoelastic materials, such as a gel, displays the behaviours of an elastic solid and viscous fluid when subject to F_p. An elastic solids response to F_p is typified by slight deformation.

The original shape can be recovered upon removal of a force, if the force is weaker than the intermolecular interactions sustaining the solids structure. The degree of deformation, known as strain (ε), is quantified by considering the change in length (dl) and the original length (l_o) as shown by Equation 3.9[39]:

$$\varepsilon = \frac{dl}{l_o} \qquad \textbf{(3.9)}$$

Alternatively, viscous fluids irreversibly deform in response to F_p. When under shear stress, the viscosity (η) of a fluid can be measured using Equation 3.10[39]:

$$\eta = \frac{\tau}{\dot{\gamma}} \qquad \textbf{(3.10)}$$

where $\dot{\gamma}$ represents the shear strain rate. For Newtonian fluids, their viscosity remains constant irrespective of increasing shear strain rate. Conversely for non-Newtonian fluids, an increase in shear strain rate can increase or decrease the viscosity of the fluid (Fig 3.7).

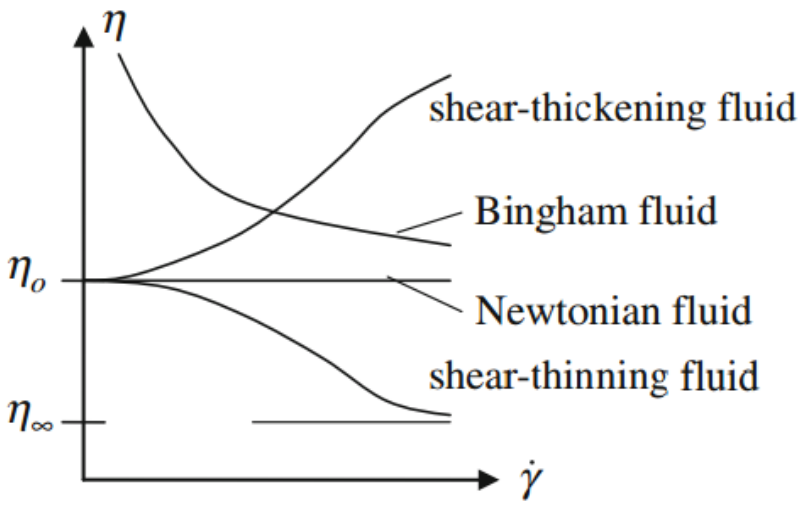

Fig. 3.7 Newtonian, non-Newtonian and Bingham fluids viscosity in response to a constant shear rate taken from ref. Bingham fluids are strictly non-Newtonian before displaying Newtonian fluid-like behaviour when under minimum stress. The symbols $\eta_0$and η_∞represent zero shear rate viscosity and infinite shear rate viscosity, respectively[39].

In a dynamic oscillatory experiment, whereby a viscoelastic material is subject to a sinusoidal stress, the viscoelastic materials strain response to is measured. The elastic modulus is accounted for by the shear modulus (G), which is a ratio of the shear stress and shear strain as expressed in Equation 3.11[39]

$$G = \frac{\tau}{\gamma} \qquad \textbf{(3.11)}$$

The shear modulus can be further classified into the storage modulus (G') and the loss modulus (G'') which corresponds to the elastic and viscous properties, respectively. The ratio of these moduli for a viscoelastic material gives $tan\ \delta$ value of 1, whereby the strain wave has a phase angle (ϕ) that is greater than 0 ° and less 90 °. This relationship is expressed by Equation 3.12[39]:

$$\tan \delta = \frac{G''}{G'} \qquad \textbf{(3.12)}$$

3.2.5 Transmission electron microscopy

Transmission electron microscopy (TEM) was used to observe characteristic features of the nano-assemblies investigated in this thesis. The TEM instrument operates on a similar principle to light microscopy except that electrons are used as the illuminating source instead of light, resulting in captured images at higher magnifications with improved resolution[40].

A positive staining method that uses the powerful oxidant, ruthenium tetra-oxide (RuO_4), was used to provide enhanced images of the structures the copolymers formed in dispersion. Once RuO_4 vapours are exposed to a specimen, it preferentially reacts with alcohol, aromatic, ether or amide groups[41]. The blackened appearance of the specimen following exposure to RuO_4 vapours is a characteristic feature. For this project, the contrasting images of the nano-assemblies were observable due to RuO_4 reacting with aromatic groups belonging to the copolymers. RuO_4 behaves as an electrophile and breaks the carbon-carbon double bond to give products that can be ketones, aldehydes or carboxylic acids and ruthenium dioxide[41]. As the reaction between RuO_4 and a benzene ring is difficult to describe, a proposed mechanism for the reaction between RuO_4 and cyclohexene is depicted below by Scheme 3.4[42].

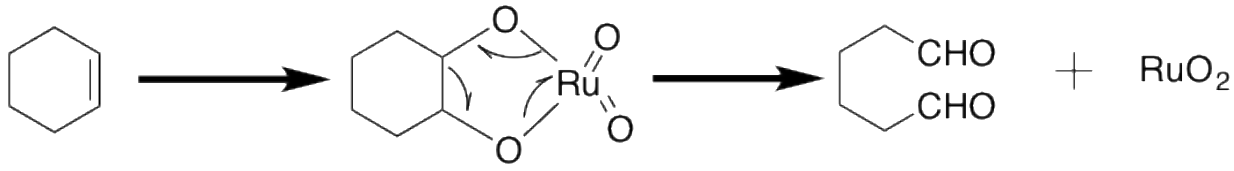

Scheme 3.4 Proposed mechanism for the reaction between cyclohexene and ruthenium tetra-oxide results in adipaldehyde and ruthenium dioxide[42]

3.2.6 Elemental analysis

Elemental analysis was used to provide a quantitative measure of the percentage of carbon (C), nitrogen (N) and hydrogen (H) in the investigated molecules studied in this thesis.

3.3 References

1. A. Muhlebach, S. G. Gaynor and K. Matyjaszewski, *Macromolecules*, 1998, **31**, 6046-6052.
2. K. Matyjaszewski, S. Coca, S. G. Gaynor, M. L. Wei and B. E. Woodworth, *Macromolecules*, 1998, **31**, 5967-5969.
3. V. A. Williams and K. Matyjaszewski, *Macromolecules*, 2015, **48**, 6457-6464.
4. K. Matyjaszewski and J. H. Xia, *Chem Rev*, 2001, **101**, 2921-2990.
5. K. Matyjaszewski, *Isr J Chem*, 2012, **52**, 206-220.
6. A. K. Nanda and K. Matyjaszewski, *Macromolecules*, 2003, **36**, 8222-8224.
7. W. Tang and K. Matyjaszewski, *Macromolecules*, 2007, **40**, 1858-1863.
8. K. Matyjaszewski, *Macromolecules*, 2012, **45**, 4015-4039.
9. M. Ishio, M. Katsube, M. Ouchi, M. Sawamoto and Y. Inoue, *Macromolecules*, 2009, **42**, 188-193.
10. Y. Wang and K. Matyjaszewski, *Macromolecules*, 2010, **43**, 4003-4005.
11. F. di Lena and K. Matyjaszewski, *Prog Polym Sci*, 2010, **35**, 959-1021.
12. A. A. Isse, A. Gennaro, C. Y. Lin, J. L. Hodgson, M. L. Coote and T. Guliashvili, *J Am Chem Soc*, 2011, **133**, 6254-6264.
13. C. Y. Lin, M. L. Coote, A. Gennaro and K. Matyjaszewski, *J Am Chem Soc*, 2008, **130**, 12762-12774.
14. J. H. Xia and K. Matyjaszewski, *Macromolecules*, 1997, **30**, 7697-7700.
15. K. L. Beers and K. Matyjaszewski, *J Macromol Sci Pure*, 2001, **38**, 731-739.
16. R. V, D. Baskaran and S. Sivaram, *Polymer*, 2004, **45**, 3149-3155.
17. W. Tang and K. Matyjaszewski, *Macromolecules*, 2006, **39**, 4953-4959.
18. W. Tang, Y. Kwak, W. Braunecker, N. V. Tsarevsky, M. L. Coote and K. Matyjaszewski, *J Am Chem Soc*, 2008, **130**, 10702-10713.
19. S. Grajales, Atom Transfer Radical Polymerization (ATRP) Tools & Techniques, http://www.sigmaaldrich.com/technical-documents/articles/technology-spotlights/tools-for-performing-atrp.html, (accessed 28th December, 2016).
20. C. H. Peng, J. Kong, F. Seeliger and K. Matyjaszewski, *Macromolecules*, 2011, **44**, 7546-7557.
21. J. S. Wang and K. Matyjaszewski, *Macromolecules*, 1995, **28**, 7901-7910.

22. K. Matyjaszewski, D. A. Shipp, J. L. Wang, T. Grimaud and T. E. Patten, *Macromolecules*, 1998, **31**, 6836-6840.
23. W. A. Braunecker, N. V. Tsarevsky, A. Gennaro and K. Matyjaszewski, *Macromolecules*, 2009, **42**, 6348-6360.
24. A. T. Levy, M. N. Olmstead and T. E. Patten, *Inorg Chem*, 2000, **39**, 1628-1634.
25. A. K. Nanda and K. Matyjaszewski, *Macromolecules*, 2003, **36**, 1487-1493.
26. A. K. Nanda and K. Matyjaszewski, *Macromolecules*, 2003, **36**, 599-604.
27. F. Seeliger and K. Matyjaszewski, *Macromolecules*, 2009, **42**, 6050-6055.
28. K. Matyjaszewski, K. Davis, T. E. Patten and M. L. Wei, *Tetrahedron*, 1997, **53**, 15321-15329.
29. K. Matyjaszewski, A. K. Nanda and W. Tang, *Macromolecules*, 2005, **38**, 2015-2018.
30. K. L. Beers, S. G. Gaynor, K. Matyjaszewski, S. S. Sheiko and M. Moller, *Macromolecules*, 1998, **31**, 9413-9415.
31. K. Min, H. F. Gao and K. Matyjaszewski, *Macromolecules*, 2007, **40**, 1789-1791.
32. T. Pintauer and K. Matyjaszewski, *Chem Soc Rev*, 2008, **37**, 1087-1097.
33. L. D. S. Yadav, in *Organic Spectroscopy*, Springer Netherlands, Dordrecht, 2005, DOI: 10.1007/978-1-4020-2575-4_5, pp. 133-194.
34. A. M. Striegel, W. W. Yau, J. J. Kirkland and D. D. Bly, in *Modern Size-Exclusion Liquid Chromatography*, John Wiley & Sons, Inc., 2009, DOI: 10.1002/9780470442876.ch2, pp. 18-48.
35. J. V. Dawkins, T. Stone and G. Yeadon, *Polymer*, 1977, **18**, 1179-1184.
36. R. Pecora, *Dynamic light scattering : applications of photon correlation spectroscopy*, 1985.
37. R. Xu, *Particle characterization : light scattering methods*, 2000.
38. N. Dejaeger, H. Demeyere, R. Finsy, R. Sneyers, J. Vanderdeelen, P. Vandermeeren and M. Vanlaethem, *Part Part Syst Char*, 1991, **8**, 179-186.
39. F. Irgens, *Rheology and non-Newtonian fluids*, 2014.
40. D. B. Williams and C. B. Carter, *Transmission electron microscopy : a textbook for materials science*, 2009.
41. J. S. Trent, J. I. Scheinbeim and P. R. Couchman, *Macromolecules*, 1983, **16**, 589-598.
42. L. M. Berkowitz and P. N. Rylander, *J Am Chem Soc*, 1958, **80**, 6682-6684.

4 Results and Discussion

This chapter discusses the obtained results from the key characterisation techniques described previously. The results are separated into three proposed publication papers.

The first proposed publication paper is titled 'Towards the synthesis of cyclo(*L*-aspartyl-*L*-phenylalanyl) containing copolymer organogelators based on poly(lauryl methacrylate) and poly(2-hydroxy ethyl methacrylate) using ATRP'. The work presented in this proposed publication was centred towards the synthesis of copolymer gelators containing the low molecular weight gelator (LMWG) cyclo(*L*-aspartyl-*L*-phenylalanyl) (CAP). The author of this thesis was responsible for conducting all experimental work, carrying out GPC studies and interpreting the characterisation data obtained from ^{1}H NMR spectroscopy, GPC studies and elemental analysis. The experimental strategies explored in this work was postponed as a simpler route to preparing a polymer gelator was investigated.

The second proposed publication paper is titled 'Self-assembly of poly(lauryl methacrylate)-*b*-poly(benzyl methacrylate) nano-objects synthesised by ATRP and their temperature-responsive dispersion properties'. This work which focused on the synthesis of amphiphilic linear copolymer gelators and has since been published (Melody *et al*., *Soft Matter*, 2017, 13, 2228). The author of this thesis was responsible for conducting all experimental work, carrying out GPC, rheology and DLS studies. The author of this thesis was also responsible for interpreting the characterisation data obtained from ^{1}H NMR spectroscopy, GPC, rheology, DLS and TEM studies. The potential of the experimental strategy employed in this work was pursued further in the next proposed publication paper.

The third proposed publication paper is titled 'Synthesis and characterisation of temperature-responsive graft copolymers based on lauryl methacrylate'. The work presented in this proposed publication was concerned with the preparation of an amphiphilic graft copolymer gelator. The author of this thesis was responsible for conducting all experimental work, carrying out GPC and DLS studies and interpreting the characterisation data obtained from ^{1}H NMR spectroscopy, GPC, DLS and TEM studies. Due to time constraints, this work is presented as a proof-of-concept study.

Proposed Publication Paper 1

Towards the synthesis of cyclo(*L*-aspartyl-*L*-phenylalanyl) containing copolymer organogelators based on poly(lauryl methacrylate) and poly(2-hydroxyethyl methacrylate) using ATRP

Towards the synthesis of cyclo(*L*-aspartyl-*L*-phenylalanyl) containing copolymer organogelators based on poly(lauryl methacrylate) and poly(2-hydroxy ethyl methacrylate) using ATRP

Melody Obeng[a*], Kyriaki Pafiti[a], Louise Farrand[b], Mark Goulding[b], Brian R. Saunders[a]
[a]School of Materials, The University of Manchester, Manchester, M13 9PL, UK
[b]Merck Chemicals Ltd, Chilworth Technical Centre, University Parkway, Southampton, SO16 7QD, UK

Abstract

This study describes two approaches to synthesise polymer-based gelators containing cyclo(*L*-aspartyl-*L*-phenylalanyl) (CAP). The first approach focused on the preparation of a diblock copolymer gelator. Lauryl acrylate (LA) and lauryl methacrylate (LMA) were both polymerised, *via* ATRP, with the LMA homopolymer selected as the first block. Subsequent chain extension of HEMA resulted in the diblock copolymer composition poly(lauryl methacrylate)-*b*-poly(2-hydroxyethyl methacrylate) ($PLMA_x$-$PHEMA_y$). ^{1}H NMR spectroscopy was used to calculate the number-average degree of polymerisation for PLMA (x) and PHEMA (y) as x =10 and y = 5. GPC characterisation was used to show controlled chain extension of HEMA from the PLMA block. The addition of trichloroacetyl isocyanate to $PLMA_{10}$-$HEMA_5$ played an important role in providing insight into the structural changes for the diblock copolymer gelator $PLMA_{10}$-*b*-$PHEMA_5$-CAP_z after esterification. The synthesis of the diblock copolymer gelator was realised and characterised *via* ^{1}H NMR spectroscopy. The second approach focused on the preparation of a graft copolymer gelator. The multibrominated macroinitiator poly(2-bromoisobutyryloxyethyl) acrylate (PBiBEA) was used in the graft copolymerisation reactions of LA and LMA. Grafted LMA repeat units *via* ATRP were preferred over LA because the growth of PLA side chains precipitated from solution. The resultant graft copolymer $(PBiBEA\text{-}PLMA_x)_{21}$ was characterised by ^{1}H NMR spectroscopy and GPC. The latter characterisation technique, was used to calculate x for $(PBiBEA\text{-}PLMA_x)_{21}$ as 33. The data showed that some success for this approach was realised. The potential of the primary approach to developing a polymer gelator could be applied in electrophoretic display (EPD) technology.

Introduction

Gels have become a valuable part of our everyday lives be it for their potential in the field of biomedical science[1-3], cosmetics[4] or other diverse[5, 6] applications. Organogelation, which describes the process in which a physical gel is formed from an organic fluid, is typified by self-assembled, low molecular weight gelators (LMWGs)[7]. The structure of the latter molecule can be based on amino acids[8, 9], cyclo(dipeptides)[10] and ureas[11], with optimised organogelation abilities described for amino acid type and cyclodipeptide based LMWGs.

The self-assembly of LMWGs is driven by non-covalent interactions such as hydrogen bonding, van der Waals forces, π-π interactions and electrostatic forces[12]. For amino acid and cyclo(dipeptide) derived LMWGs, hydrogen bonding sustains the self-assembly of the LMWGs into one-dimensional supramolecular polymers. The entanglements of supramolecular polymers then lead to fibre-like aggregates that bundle together to form a three-dimensional fibrous network that is held together by van der Waals forces. Within the interstices of the network, solvent molecules are immobilised resulting in a gel made from predominantly organic fluid (i.e., $\leq$ 1 wt. % LMWGs)[13]. The relationship between intermolecular forces dominating at different stages of gelation was essential to the development for this work[14]. This study focuses on supramolecular polymer gels formed from two components; a polymer gelator containing LMWGs and an organic solvent.

Polymer gelators are interesting gelator molecules because they consist of a LMWG that is introduced onto a polymer segment *via* esterification or hydrosilylation reactions[15]. This approach has led to the development of a new family of gelators, whereby the polymer segment prevents crystallisation of the LMWG and enhances the organogelation ability of a LMWG in various organic solvents, whilst the LMWG drives organogelation[16, 17]. These benefits popularise the use of polymer gelators for industrial purposes particularly for enhancing the performance of electronic devices[18, 19]. Here, the synthesis of polymer gelators based on poly(lauryl methacrylate) (PLMA) that contain the LMWG cyclo-(*L*-aspartyl-*L*-phenylalanyl) (CAP) were explored[10, 20]. It was hypothesised that CAP would enable gelation with non-polar solvents. The aim of this work was to develop a polymer gelator containing CAP. The motivation was to use it for application in electrophoretic paper display (EPD) technology.

The development of EPDs has popularised in display technology because the devices are malleable and re-writeable paper-like displays that operate on low power consumption[21]. Comiskey *et al.*[22] were the first to describe a microencapsulated EPD. The microencapsulated feature was developed to overcome the challenges of agglomeration and lateral drift of charged particles[23]. The context of this work was to develop a polymer gelator that would form a gel with the dielectric medium in the microcapsule.

The method for evolving a polymer gelator usually involves the initial preparation of a polymer segment. There are various versatile conventional (co)polymers that are commercially available or can be synthesised *via* controlled polymerisation techniques, such as atom transfer radical polymerisation (ATRP)[24-26]. These include poly(dimethysiloxane)-based macroinitiators that readily polymerise methyl methacrylate or 2-dimethylaminoethyl methacrylate to form well-defined block copolymers[27, 28]. Subsequent introduction of the LMWG segment can be achieved by copolymerisation, whereby the LMWG possess polymerisable groups[29] or reactive functional groups that can engage in hydrosilylation or esterification reactions[30], respectively. Hanabusa *et al.*[12] synthesised a series of polydimethylsiloxane-based gelators *via* a hydrosilylation reaction between polydimethylsiloxane and a L-isoleucine derived LMWG. It was observed that the organogelation ability of the polydimethylsiloxane-based gelators were as efficient in causing gelation from silicone oil as the individual LMWG molecule[12]. Maintaining the gelation ability of LMWGs following their introduction onto a polymer segment is important because stable transparent gels were required for this study[31].

The nature of non-covalent interactions is weaker in comparison to covalent bonds[32]. This allows the structure of a gel to breakdown temporarily in response to changes in temperature, pH and mechanical stress[33, 34]. The transient disruption of non-covalent intermolecular forces between LMWG segments results in reversible transformation of a three-dimensional network into unidirectional supramolecular polymers, and *vice versa*. This self-healing property was demonstrated by Hoshizawa *et al.*[20], whereby the investigated CAP-containing polydimethylsiloxane-based gel displayed shear thinning properties when subject to shear stress at 25 °C. When left to stand, the gel completely reformed over a matter of minutes. The rapid reversible gel-sol-gel transition was a central aim for this work. It was hypothesised that the self-healing property would assist the function of an EPD device[22].

There were two main strategies used in this study. The first strategy used a diblock copolymer approach (Scheme 1). LA (Scheme 1a) and LMA (Scheme 1b) were both polymerised via ATRP, however, it was discovered that the latter monomer was more suited for further chain extension of 2-hydroxyethyl methacrylate (HEMA) to give $PLMA_{10}$-$PHEMA_y$ (Scheme 1c). Developing the diblock copolymer gelator involved preparing CAP from Aspartame (Scheme 2), before it was introduced onto $PLMA_{10}$-$PHEMA_y$ to give the linear copolymer gelator $PLMA_{10}$-$PHEMA_y$-CAP_z (Scheme 1c). The second strategy used a graft copolymer approach that required synthesis of the multibrominated macroinitiator, $PBiBEA_{21}$ (Scheme 3). LA was first grafted from PBiBEA to give $(PBiBEA\text{-}PLA_7)_{21}$ (Scheme 4a). However, complications concerning the ATRP of LA led to the preferred grafting of LMA from PBiBEA to give $(PBiBEA\text{-}PLMA_{33})_{21}$ (Scheme 4b). The next proposed steps involved the chain extension of HEMA from $(PBiBEA\text{-}PLMA_x)_{21}$ to give $(PBiBEA\text{-}PLMA_x\text{-}PHEMA_y)_{21}$. This would occur prior to the introduction of CAP. The resultant graft copolymer gelator would be based on the composition $(PBiBEA\text{-}PLMA_x\text{-}PHEMA_y\text{-}CAP_z)_{21}$ as seen in Scheme 4c.

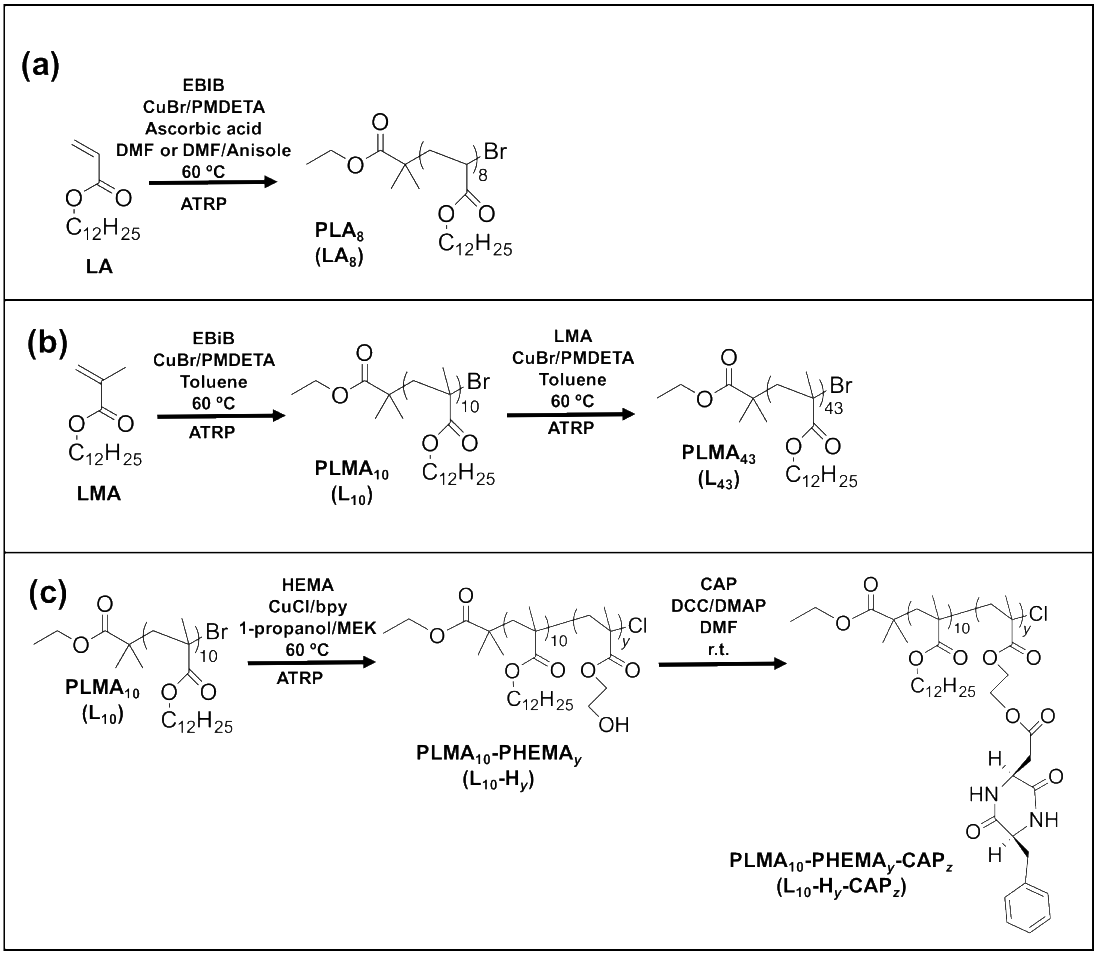

Scheme 1 Depiction of the synthesis of the diblock copolymer strategy. (a) The first step involved ATRP of LA to form PLA_8. (b) LMA was used in place of LA to form $PLMA_{10}$. Further chain extension of LMA from $PLMA_{10}$ resulted in $PLMA_{43}$. (c) Subsequent polymerisation of HEMA from $PLMA_{10}$ formed $PLMA_{10}$-$HEMA_y$ prior to the introduction of CAP that resulted in the diblock copolymer gelator, $PLMA_{10}$-$HEMA_y$-CAP_z.

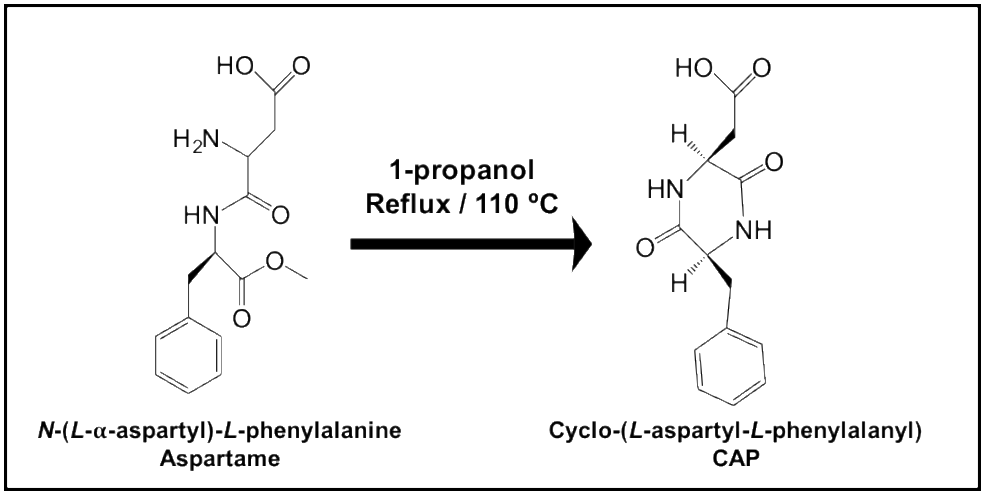

Scheme 2 Depiction of the synthesis of CAP from Aspartame.

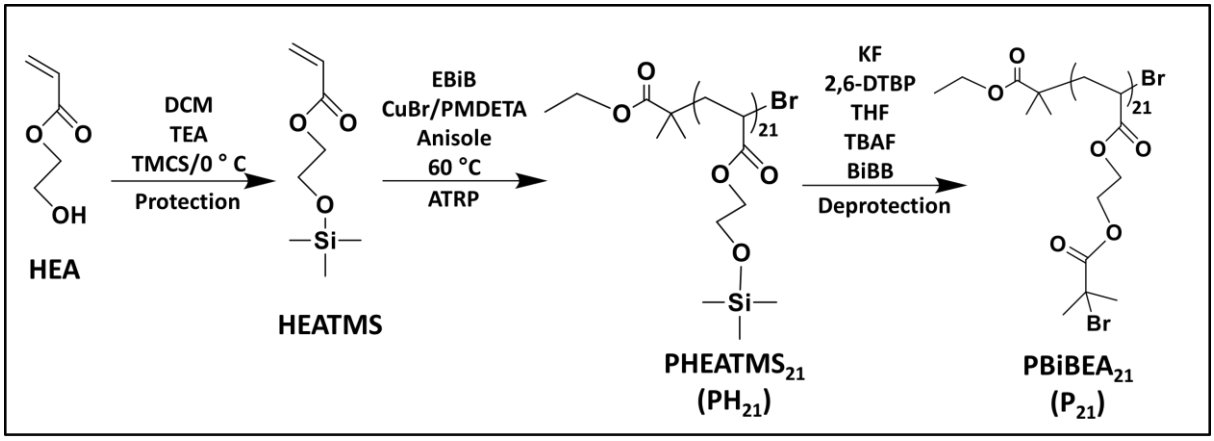

Scheme 3 Depiction of the series of steps required to synthesise PBiBEA from 2-hydroxethyl acrylate (HEA).

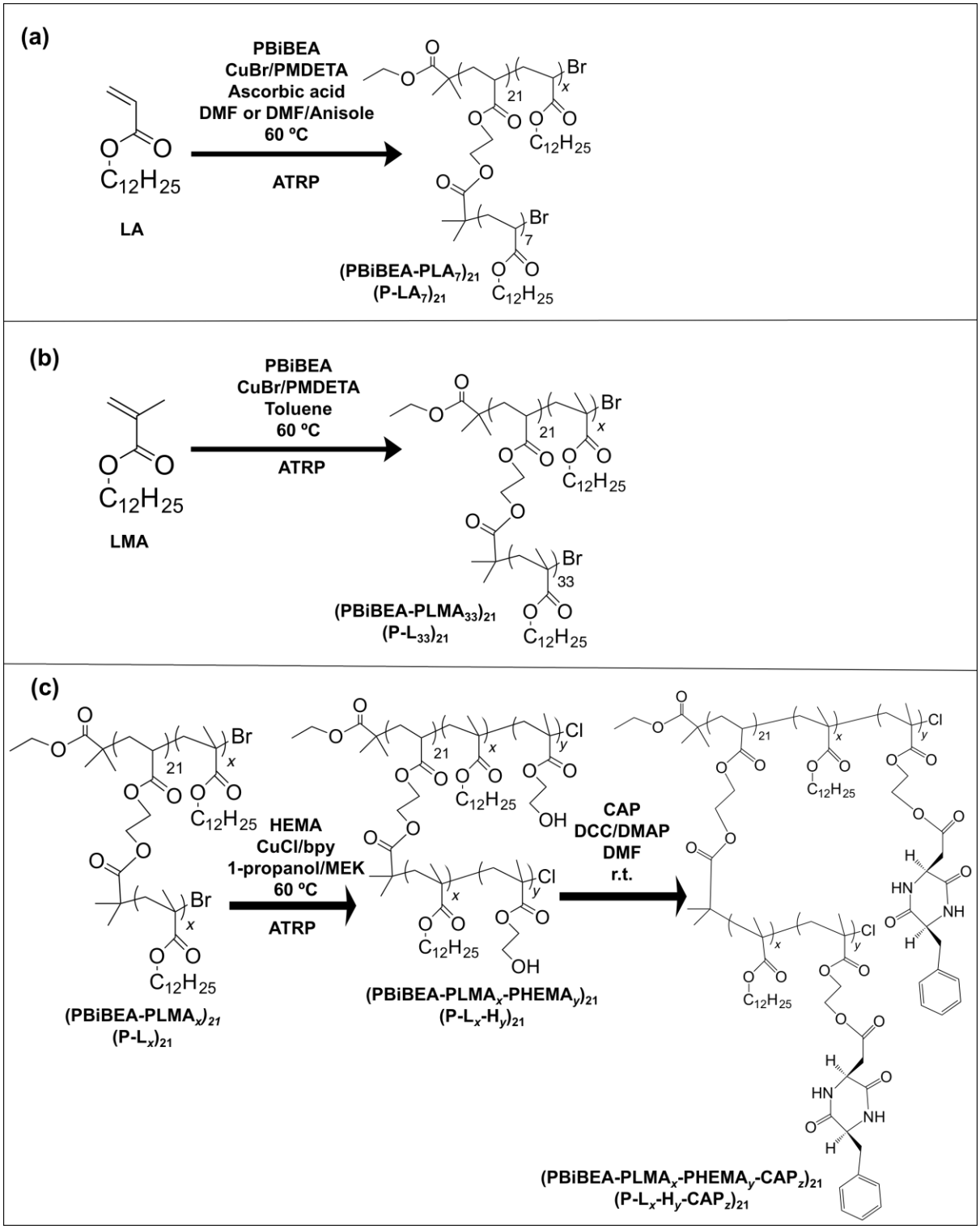

Scheme 4 Depiction of the synthesis of the graft copolymer strategy. (a) The first step involved grafting LA from PBiBEA to form $(PBiBEA\text{-}PLA_7)_{21}$. (b) LMA was also grafted from PBiBEA in place of LA to form $(PBiBEA\text{-}PLMA_{33})_{21}$. (c) The proposed steps for synthesising the graft copolymer gelator, $(PBiBEA\text{-}\ PLMA_x\text{-}HEMA_y\text{-}CAP_z)_{21}$.

In the first part of this study the homopolymers poly(lauryl acrylate) (PLA) and PLMA were characterised by GPC and ^{1}H NMR spectroscopy. The preferred copolymer composition

contained PLMA as the first block, followed by polymerisation of HEMA to form the diblock copolymer (PLMA-HEMA) that was characterised using GPC and ^{1}H NMR spectroscopy. In the second part of this study, the macroinitiator (PBiBEA) that was required for graft copolymerisation reactions was characterised by GPC and ^{1}H NMR spectroscopy. The graft copolymers (PBiBEA-PLA$_x$)$_{21}$ and (PBiBEA-PLMA$_x$)$_{21}$ were studied *via* ^{1}H NMR spectroscopy, with the latter graft copolymer also being characterised by GPC. The results of the study showed a viable route for preparing a diblock copolymer gelator.

Experimental Section

Materials

Trimethylsilyloxyethyl acrylate (HEATMS), poly(trimethylsilyloxyethyl acrylate) (PHEATMS) and PBiBEA were prepared according to literature[35] (Scheme 2). The reagents used for synthesis of HEATMS include: 2-hydroxyethyl acrylate (HEA, 96 %), trimethylamine (TEA, ≥ 99 %) and chlorotrimethylsilane (TMCS, ≥ 99 %) which were purchased from Sigma Aldrich and were used as received. Dichloromethane (DCM HLPC grade, 99.8 %) was purchased from Fischer Scientific and was used as received. The reagents used for the synthesis of PHEATMS include: ethyl α-bromoisobutyrate (EBiB, 98 %), copper bromide (CuBr, 99.999 %), *N,N,N′,N′′,N′′*-pentamethyldiethylenetriamine (PMDETA, 99 %) and Anisole (≥ 99 %) which were purchased from Sigma Aldrich, and were used as received. The reagents used for the synthesis of PBiBEA include: potassium fluoride (KF, ≥ 99 %), 2,6-di-*tert*-butylphenol (2,6-DTBP, 99 %), tetrahydrofuran (THF, anhydrous ≥ 99 %), tetrabutylammonium fluoride solution (TBAF 1.0 M in THF) and α-bromoisobutyryl bromide (BiBB, 98 %). The other reagents used in this study are listed as followed. LA (contains 60-100 ppm MEHQ as inhibitor, 90 %), LMA (contains 500 ppm MEHQ as inhibitor, 96 %), HEMA (contains ≤ 250 ppm MEHQ as inhibitor, 97 %) and methyl acrylate (MA, contains ≤ 100 ppm MEHQ as inhibitor, 99 %) were all purchased from Aldrich and were passed through a basic alumina column before use. Methyl 2-bromopropionate (97 %), allyl alcohol (AlOH, 98 + %) and *n*-hexane (99%) were all purchased from Alfa Aesar and were used as received. Copper (Cu, powder, 99.999 % trace metal basis), copper II bromide ($CuBr_2$, 99 %), tris[2-(dimethylamino)ethyl]amine, 97 %) were purchased from Sigma Aldrich and were used as received. *N,N′*-dicyclohexylcarbodiimide, 99 %), (DCC), 4-(dimethylamino)pyridine (DMAP, ≥ 99 %), 2,2-bipyridyl (bpy, ≥ 99%), copper chloride (CuCl, ≥ 99.995 %), *L*-ascorbic acid (reagent grade), *N,N*-dimethylformamide (DMF, ≥ 99.9 %), toluene (99.5 %), 1-propanol (> 99 %), 2-butanone (MEK, > 99.0 %) and methanol were purchased from Aldrich and were used as received. *N*-(*L*-α-aspartyl)-*L*-phenylalanine (Aspartame, 98 %) was purchased from Alfa Aesar and was used as received. Water was high purity grade.

PLA-Br homopolymer synthesis

LA was polymerised to form PLA (Scheme 1a). The following gives an example synthesis for $PLA_{8,}$ which is represented by LA_8. The molar ratio of monomer [M], initiator [I], copper

catalyst [Cu(I)] and ligand [L] was 30:1:1:3:1.5. A Schlenk flask was charged with DMF (20 mL), EBiB (143 μL, 0.98 mmol), LA (8 mL, 29.4 mmol) and PMDETA (602 μL, 2.94 mmol). The reagents were deoxygenated with argon (Ar) for 30 minutes whilst stirred magnetically at room temperature. The reaction mixture was degassed by repeated freeze-pump-thaw cycles. During the third cycle, the Schlenk flask was filled with Ar before CuBr (0.14 g, 0.98 mmol) and *L*-ascorbic acid (0.26 g, 1.47 mmol) were quickly added to the frozen mixture. The reaction flask was then sealed, evacuated and backfilled with Ar three times before it was immersed in a pre-heated oil bath of 60 °C for 8 h. LA_8 precipitated from DMF during the initial stages of the polymerisation reaction. This was also observed when a co-solvent blend of DMF/Anisole (1:2 v/v) was used. An LA_8 sample was taken and diluted in chloroform before being passed through a basic alumina column. The remaining chloroform was removed by evaporation and LA_8 was dried in a vacuum-oven at 30 °C for 12 h. The mass of purified L_8 was 5.2 g with a percentage yield of 64.7 %. LA_8 was confirmed *via* ^{1}H NMR. ^{1}H NMR (400MHz, $CDCl_3$): δ (ppm) = 4.0 (s, 2H, - C(=O)O-C**H$_2$**-), 2.3 (s, 1H, -CH_2-C**H**-), 1.9 (s, 1H) and 1.4 (m, 1H) (-C**H$_2$**-CH-), 1.6 (s, 2H, -C(=O)O-CH_2-C**H$_2$**-), 1.3 (s, 18H, -C_9**H$_{18}$**-), 0.9 (t, 3H, -C_9H_{18}-C**H$_3$**).

PLMA-Br homopolymer synthesis

LMA was polymerised to form PLMA (Scheme 1b). The following gives an example synthesis for $PLMA_{10,}$ which is represented by L_{10}. The molar ratio of monomer [M], initiator [I], copper catalyst [Cu(I)] and ligand [L] was 10:1:1:3. A Schlenk flask was charged with toluene (5.6 mL), EBiB (740 μL, 5 mmol), LMA (15 mL, 50 mmol) and PMDETA (3.1 mL, 15 mmol). The reagents were deoxygenated with Ar for 30 minutes whilst stirred magnetically at room temperature. The reaction mixture was degassed by repeated freeze-pump-thaw cycles. During the third cycle, the Schlenk flask was filled with Ar before CuBr (0.72 g, 5 mmol) was quickly added to the frozen mixture. The reaction flask was then sealed, evacuated and backfilled with Ar three times before it was immersed in a pre-heated oil bath of 60 °C for 5 h. L_{10} mixture was diluted in THF before it was passed through a basic alumina column and subsequently concentrated. L_{10} was purified in excess methanol and dried in a vacuum-oven at 30 °C for 12 h. The mass of purified L_{10} was 12.4 g with a percentage yield of 82.6 %. L_{10} was confirmed *via* ^{1}H NMR. ^{1}H NMR (400MHz, $CDCl_3$): δ (ppm) = 4.1 (m, 2H, CH_3-C**H$_2$**-), 4.0 (s, 2H, -C(=O)O-C**H$_2$**-), 1.8-2.0 (m, 2H, -C**H$_2$**-C-CH_3-), 1.6 (s, 2H, -C(=O)O-CH_2-C**H$_2$**-), 1.3 (s, 18H, -C_9**H$_{18}$**-), 1.1 (m, 3H, C**H$_3$**-CH_2-), 0.9 (s, t, 6H, -C-C**H$_3$**-C(=O)O-CH_2-$(CH_2)_{10}$-C**H$_3$**).

Chain extension of LMA from PLMA homopolymer

LMA was polymerised from L_{10} to provide insight for further chain extension reactions (Scheme 1b). The following gives an example synthesis for $PLMA_{43,}$ which is represented by L_{43}. The molar ratio of monomer [M], initiator [I], copper catalyst [Cu(I)] and ligand [L] used was 100:1:1:3. A Schlenk flask was charged with PLMA-Br (50 mg, 0.183 mmol) dissolved in toluene (1.0 mL) before the remainder was added (1.0 mL). LMA (5.4 mL, 18.3 mmol) and PMDETA (109 μL, 0.55 mmol) were later added. The reagents were deoxygenated with Ar for 30 minutes whilst stirred magnetically at room temperature. The reaction mixture was degassed by repeated freeze-pump-thaw cycles. During the third cycle the Schlenk flask was filled with Ar before CuCl (18.1 mg, 0.183 mmol) was quickly added to the frozen mixture. The reaction flask was then sealed, evacuated and backfilled with Ar five times before it was immersed in a pre-heated oil bath of 60 °C overnight. L_{43} mixture was diluted in THF before it was passed through a basic alumina column and subsequently concentrated. L_{43} was purified and dried as described for L_{10}. The mass of purified L_{43} was 2.2 g with a percentage yield of 41.6 %. L_{43} was confirmed *via* ^{1}H NMR. ^{1}H NMR (400MHz, $CDCl_3$): δ (ppm) = 4.0 (s, 2H, -C(=O)O-C**H$_2$**-), 1.8-2.0 (m, 2H, -C**H$_2$**-C-CH_3-), 1.6 (s, 2H, -C(=O)O-CH_2-C**H$_2$**-), 1.3 (s, 18H, -C_9**H$_{18}$**-), 1.1 (m, 3H, C**H$_3$**-CH_2-), 0.9 (s, t, 6H, -C-C**H$_3$**-C(=O)O-CH_2-$(CH_2)_{10}$-C**H$_3$**).

Chain extension of HEMA from PLMA homopolymer

HEMA chain extension from L_{10} (Scheme 1c) was adapted from a method reported in literature[36]. The following gives an example synthesis for $PLMA_{10}$-$PHEMA_{5,}$ which is represented by L_{10}-H_5. The molar ratio of monomer [M], initiator [I], copper catalyst [Cu(I)] and ligand [L] was 10:1:0.27:0.55. A Schlenk flask was charged with L_{10} (50 mg, 0.183 mmol) dissolved in 1-propanol/MEK (480 μL / 1120 μL), HEMA (224 μL, 1.83 mmol) and bpy (15.6 mg, 0.1 mmol). The reagents were deoxygenated with Ar for 30 minutes whilst stirred magnetically at room temperature. The reaction mixture was degassed by repeated freeze-pump-thaw cycles. During the third cycle the Schlenk flask was filled with Ar before CuCl (5.0 mg, 0.05 mmol) was quickly added to the frozen mixture. The reaction flask was then sealed, evacuated and backfilled with Ar five times before it was immersed in a pre-heated oil bath of 60 °C for 3 h. L_{10}-H_5 mixture was diluted in additional 1-propanol (1.5 mL) and MEK (3.5 mL) co-solvent blend before it was passed through a basic alumina column and subsequently concentrated. L_{10}-H_5 mixture was purified in excess water and was dried in

a vacuum-oven at 30 °C for 12 h. The same method described above was used to prepare L_{10}-H_{10}. For the preparation of L_{10}-H_{10} the molar ratios for [M]:[I]:[Cu(I)]:[L] were [M]:1:0.27:0.55, whereby [M] was 20. Percentage yield of purified L_{10}-H_y copolymers was ~ 42.8 %. PHEMA units in the L_{10}-H_y copolymers were confirmed *via* ^{1}H NMR with the presence of DMF. ^{1}H NMR (400MHz, $CDCl_3$): δ (ppm) = 4.8 (s, 1H, -O**H**), 4.1 (s, 2H, C(=O)O-C**H$_2$**-CH_2OH), 4.0 (s, 2H, -C(=O)O-C**H$_2$**-$(CH_2)_{10}$-), 3.8 (s, 2H, -C(=O)O-CH_2-C**H$_2$**OH), 1.7-2.0 (m, 4H, -C**H$_2$**-C-CH3-(C=O)O-CH_2-CH_2OH and -C**H$_2$**-C-CH_3-(C=O)O-C**H$_2$**-$(CH_2)_{10}$-), 1.6 (s, 2H, -C(=O)O-CH_2-**CH$_2$**-), 1.3 (s, 18H, -C_9**H$_{18}$**-), 0.9-1.2 (s, m, 9H, -CH_2-C-C**H$_3$**-C(=O)O-CH_2-CH_2OH, -CH_2-C-C**H$_3$**-C(=O)O-CH_2-$(CH_2)_{10}$-C**H$_3$**).

CAP synthesis

CAP was synthesised *via* the cyclization of Aspartame (Scheme 2) according to literature[10]. A round-bottomed flask was charged with Aspartame (10 g) dissolved in 1-propanol (800 mL). The oil bath was set to 110 ˚C with signs of 1-propanol evaporating at 100 ˚C. The reaction mixture was refluxed for 15 h before it was concentrated 200 mL and allowed to cool to room temperature. CAP was filtered and dried in a vacuum at 80 ˚C for 12 h. The mass of purified CAP was 8.2 g with a percentage yield of ~ 88.2 %. CAP was confirmed *via* ^{1}H NMR. ^{1}H NMR (400MHz, DMSO-d_6): δ (ppm) = 12.3 (s, C(=O)OHC**H$_2$**-), 8.2 (s, 1H, -N**H**-CH-CH_2-C_5H_5), 7.9 (s, 1H, C(=O)OHCH_2-CH-N**H**-), 7.3 (m, 5H, -C_5**H$_5$**), 4.3 (s, 1H, -C**H**-CH_2-C_5H_5), 4.0 (m, 1H, C(=O)OHCH_2-C**H**-), 2.7-3.3 (m, 2H, -C**H$_2$**-C_5H_5), 1.0-1.6 (m, C(=O)OHC**H$_2$**-).

Aspartame was confirmed *via* ^{1}H NMR. ^{1}H NMR (400MHz, DMSO-d_6): δ (ppm) = 8.9 (s, 2H, -N**H$_2$**-), 7.3 (m, 5H, -C_5**H$_5$**), 4.6 (m, 1H, -NH_2-C**H**-), 3.7 (m, 3H, -O-C**H$_3$**), 3.0-3.3 (m, 2H, -C**H$_2$**-C_5H_5), 2.2-2.4 (m, 2H, C(=O)OHC**H$_2$**-).

Incorporation of CAP onto PLMA-HEMA copolymer

This method involved using DCC/DMAP combination with L_{10}-H_5 to synthesise L_{10}-H_5-CAP_z (Scheme 1c), where *z* indicates the number of CAP groups per L_{10}-H_5. A three-necked round-bottomed flask was charged with L_{10}-H_5 (0.055 g, 0.135 mmol of hydroxyl groups per L_{10}-H_5), CAP (0.6 g, 2.28 mmol) dissolved in 20 mL DMF, DCC (0.52g, 1.68 mmol) dissolved in 2 mL DMF and, lastly DMAP (27.9 mg, 0.23 mmol). The reaction was stirred for 24 h at room temperature. The mixture was then filtered and the solid product was dried in a vacuum oven at 40 °C for 48 h. The mass of purified L_{10}-H_5-CAP_z was 0.02 g with a

percentage yield of ~ 38.3 %. L_{10}-H_5-CAP_z was confirmed *via* ^{1}H NMR. ^{1}H NMR (400MHz, DMSO-d_6): δ (ppm) = 8.2 (s, 1H, -N**H**-CH-CH_2-C_5H_5), 7.6 (s, 1H, -C(=O)OCH_2-CH-N**H**-), 7.3 (m, 5H, -C_5**H_5**), 4.2 (m, 2H, -C(=O)O-CH_2-C**H** and -C**H**-CH_2-C_5H_5), 3.9 (m, 2H, -CH_2-**CH_2**C(=O)O-), 2.5-3.3 (m, 4H, - C(=O)O-C**H_2**- and -C**H_2**-C_5H_5).

PMA-AlOH synthesis

PMA-AlOH macroinitiator was synthesised using a modification of a literature procedure[37]. The PMA macroinitiator was synthesised first. The following gives an example synthesis for PMA_6. The molar ratio of monomer [M], initiator [I], copper catalyst [Cu(I)] and ligand [L] used was 6:1:0.01:0.01. A Schlenk flask was charged with MA (5.0 mL, 55 mmol), methyl 2-bromopropionate (1.0 mL, 9 mmol) and PMDETA (19.0 μL, 0.09 mmol). The reagents were deoxygenated with Ar for 30 minutes whilst stirred magnetically at room temperature. The reaction mixture was degassed by repeated freeze-pump-thaw cycles. During the third cycle the Schlenk flask was filled with Ar before CuBr (13 mg, 0.09 mmol) was quickly added to the frozen mixture. The reaction flask was then sealed, evacuated and backfilled with Ar three times before it was immersed in a pre-heated oil bath of 30 °C. The reaction occurred overnight. PMA_6 mixture was diluted in THF before it was passed through a basic alumina column and subsequently concentrated. PMA_6 was purified in excess hexane and dried in a vacuum-oven at 30 °C for 12 h. The mass of purified PMA_6 was 4.4 g with a percentage yield of ~ 89.4 %. PMA_6 was confirmed *via* ^{1}H NMR. ^{1}H NMR (400MHz, $CDCl_3$): δ (ppm) = 4.2 (m, 1H, [-CH_2-C**H**-]), 3.8 (s, 3H, CH_3-CH-C(=O)O-C**H_3**), 3.7 (s, 3H, [-C(=O)O-C**H_3**]), 1.5-2.7 (m, 3H, C**H**-[C**H_2**]-), 1.2 (m, 3H, C**H_3**-CH-).

The second stage involved the addition of AlOH onto PMA_6. A Schlenk flask was charged with PMA_6 (2.0 g) dissolved in 2.5 mL MeOH and excess AlOH (2.5 mL). The reagents were deoxygenated with Ar for 30 minutes whilst stirred magnetically at room temperature. The reaction mixture was degassed by repeated freeze-pump-thaw cycles. During the third cycle the Schlenk flask was filled with Ar before $Cu/CuBr_2/Me_6TREN$ (18 mg, 0.28 mmol/ 63 mg, 0.28 mmol/ 144 μL, 0.56 mmol). The reaction flask was then sealed, evacuated and backfilled with Ar five times before it was immersed in a pre-heated oil bath of 40 °C. The reaction occurred overnight. PMA_6-$AlOH_1$ mixture was diluted in THF before it was passed through a basic alumina column and subsequently concentrated. PMA_6-$AlOH_1$ was purified in excess hexane and dried in a vacuum-oven at 30 °C for 12 h. The mass of purified PMA_6-$AlOH_1$ was 1.8 g with a percentage yield of ~ 92.2 %. PMA_6-$AlOH_1$ was confirmed *via* ^{1}H

NMR. ^{1}H NMR (400MHz, $CDCl_3$): δ (ppm) = 4.5 (m, 2H, [-CH_2-CH-C**H$_2$**-OC(=O)-]), 3.7 (s, 3H, [-C(=O)O-C**H$_3$**]), 1.5-2.7 (m, 3H, C**H**-[C**H$_2$**]-), 1.2 (m, 3H, C**H$_3$**-CH-).

PBiBEA macroinitator synthesis

PBiBEA, which is represented by P_{21}, was prepared in three steps using a modification of a literature procedure[35]. The first step (Scheme 3) involved synthesising the protected monomer HEATMS. A three-necked round-bottomed flask was charged with HEA (40.0 mL, 0.348 mol), TEA (72.6 mL, 0.522 mol) and DCM (500 mL). The reaction mixture was cooled to 0 °C before being stirred magnetically during the drop-wise addition of TMCS (66.5 mL, 0.522 mol) at a rate of 1 ml min^{-1}. The reaction mixture was maintained at a temperature of 0 °C for 1 h before it was left to stir overnight at room temperature. The reaction mixture was terminated by its exposure to the air. The salt was washed with diethyl ether as it was filtered. Pure HEATMS was obtained *via* distillation (47 °C, 2 mbar). The mass of purified HEATMS was 25.6 g with a percentage yield of ~ 64 %. HEATMS was confirmed *via* ^{1}H NMR. ^{1}H NMR (400MHz, $CDCl_3$): δ (ppm) = 5.9-6.2 (m, 3H, C**H**=C**H$_2$**), 4.2 (m, 2H, -C(=O)O-C**H$_2$**-), 3.8 (m, 2H, -C(=O)O-CH_2-C**H$_2$**), 0.1 (s, 9H, -O-Si-(C**H$_3$)$_3$**).

The second step (Scheme 3) involved polymerising HEATMS. The homopolymerisation reaction was conducted under Ar. A Schlenk flask was charged with anisole (1.30 mL), HEATMS (12.5 mL, 60 mmol), EBiB (367.0 μL, 2.5 mmol) and PMDETA (73.0 μL, 0.5 mmol). The reagents were deoxygenated with Ar for 30 minutes whilst stirred magnetically at room temperature. The reaction mixture was degassed by repeated freeze-pump-thaw cycles. During the third cycle, the Schlenk flask was filled with Ar before CuBr (71.7 mg, 0.5 mmol) was quickly added to the frozen mixture. The reaction flask was then sealed, evacuated and backfilled with Ar three times before it was immersed in a pre-heated oil bath of 60 °C for 150 minutes. The PHEATMS polymer, which is represented by PH_{21} was passed through a neutral alumina column and dried in a vacuum-oven at 30 °C for 12 h. The mass of purified PH_{21} was 9.0 g with a percentage yield of ~ 72.3 %. PH_{21} was confirmed *via* ^{1}H NMR. ^{1}H NMR (400MHz, $CDCl_3$): δ (ppm) = 4.2 (m, 2H, -C(=O)O-C**H$_2$**), 3.7 (m, 2H, -C(=O)O-CH_2-C**H$_2$**), 2.3 (s, 1H, -CH_2-C**H**-), 1.3-2.0 (s, 2H, -C**H$_2$**-CH-), 1.2 (m, 3H, C**H$_3$**-CH_2), 1.1, (d, 6H, -C-(C**H$_3$**)$_2$-), 0.1 (s, 9H, -O-Si-(C**H$_3$)$_3$**).

The third step (Scheme 3) involves substituting protective groups with brominated moieties required for graft copolymerisation reactions[38]. A three-necked flask was charged with PHEATMS (6 g, assuming 31.9 mmol of TMS groups), KF (2.26 g, 38.3 mmol) and 2,6-

DTBP (0.0657 g, 0.319 mmol). The reaction mixture was sealed flushed with Ar and the addition of dry THF (40 mL). The TBAF solution (0.0319 mL) was added in a drop-wise fashion followed by the addition of BiBB (8.82 g, 38.3 mmol) at a rate of 1 mL min^{-1}. The reaction mixture was stirred magnetically overnight at room temperature before the quenching of acid bromide by the addition of 1.0 mL de-ionised water and 1.0 mL of TEA to the reaction mixture. Centrifugation was used to separate solid products. P_{21} was dried in a vacuum-oven at 30 °C for 12 h before being dialysed against THF for 48 h (2000 g mol^{-1} average pore size). Pure P_{21} was dried in a vacuum-oven at 30 °C for 24 h. The mass of purified P_{21} was 4.5 g with a percentage yield of ~ 75.2 %. P_{21} was confirmed *via* ^{1}H NMR. ^{1}H NMR (400MHz, $CDCl_3$): δ (ppm) = 4.2-4.4 (m, 4H, -(C=O)O-C**H$_2$**C**H$_2$**-), 4.1 (m, 2H, CH_3-C**H$_2$**-), 2.4 (s, 1H, -CH_2-C**H**-), 2.0, (s, 6H, -C-(C**H$_3$**)$_2$Br), 1.4-1.8 (m, 2H, -C**H$_2$**-CH-), 1.2 (m, C**H$_3$**-CH_2-), 1.1, (d, 6H, -C-(C**H$_3$**)$_2$-), 0.1 (s, 9H, -O-Si-(C**H$_3$)$_3$**).

(PBiBEA-PLA$_7$)$_{21}$ graft copolymer synthesis

The graft copolymer approach began with grafting LA side chains from PBiBEA to form (PBiBEA-PLA$_7$)$_{21}$, which is represented by (P-LA$_7$)$_{21}$ (Scheme 4a). The molar ratio of monomer [M], initiator [I], copper catalyst [Cu(I)], ligand [L] and *L*-ascorbic acid were 30:1:0.15:0.4:1.5. For a typical reaction, a Schlenk flask was charged with P_{21} (0.5 mg, 1.82 mmol PBiBEA-Br groups) dissolved in DMF (3.0 mL) before the remainder of DMF was added (7.0 mL). LA (15 mL, 55.2 mmol) and PMDETA (165 µL, 0.79 mmol) were then added. The reagents were deoxygenated under Ar for 30 minutes whilst stirred magnetically at room temperature. The reaction mixture was degassed by repeated freeze-pump-thaw cycles. During the third cycle, the Schlenk flask was filled with Ar before CuBr (39 mg, 0.27 mmol) and *L*-ascorbic acid (0.48 g, 2.7 mmol) were quickly added to the frozen mixture. The reaction flask was then sealed, evacuated and backfilled with Ar five times before it was immersed in a pre-heated oil bath of 60 °C for 5 h. The precipitated (P-LA$_7$)$_{21}$ graft copolymer was separated by filtration and dried in a vacuum oven at 30 °C for 12 h. The same method of preparation for the graft copolymerisation reaction of LA was also employed in a co-solvent blend of DMF:Anisole (1:2 v/v). The subsequent (P-LA$_x$)$_{21}$ graft copolymer was also separated from solution by filtration and dried in a vacuum oven at 30 °C for 12 h. The mass of obtained (P-LA$_7$)$_{21}$ was 3.2 g with a percentage yield of 22.1 %. (P-LA$_7$)$_{21}$ was confirmed *via* ^{1}H NMR. ^{1}H NMR (400MHz, $CDCl_3$): δ (ppm) = 4.0 (s, 2H, -C(=O)O-C**H$_2$**-), 2.2 (s, 2H, -CH_2-C**H**-C(=O)O-CH_2-CH_2 and -

CH_2-C**H**-C(=O)O-CH_2-$(CH_2)_{10}$-CH_3), 1.6 (s, m, 6H, -C**H_2**-CH-C(=O)O-CH_2-CH_2 and -C**H_2**-CH-C(=O)O-CH_2-C**H_2**-$C_{10}H_{21}$), 1.3 (s, 18H, -C_9**H_{18}**-), 0.9 (t, 3H, -C_9H_{18}-C**H_3**).

(PBiBEA-PLMA$_{33}$)$_{21}$ graft copolymer synthesis

The second graft copolymer synthesis involved grafting LMA side chains from PBiBEA to form (PBiBEA-PLMA$_{33}$)$_{21}$, which is represented by (P-L$_{33}$)$_{21}$ (Scheme 4b). The same molar ratio of monomer [M], initiator [I], copper catalyst [Cu(I)], ligand [L] described for (P-LA$_7$)$_{21}$ was adopted. For a typical reaction, a Schlenk flask was charged with PBiBEA (25 mg, 1.82 mmol PBiBEA-Br groups) dissolved in toluene (3.0 mL) before the remainder of toluene was added (27.0 mL). This was then followed by the addition of LMA (16 mL, 55.2 mmol), and PMDETA (9.4 μL, 0.045 mmol). The reagents were deoxygenated under Ar for 30 minutes whilst stirred magnetically at room temperature. The reaction mixture was degassed by repeated freeze-pump-thaw cycles. During the third cycle the Schlenk flask was filled with Ar before CuBr (39 mg, 0.27 mmol) was quickly added to the frozen mixture. The reaction flask was then sealed, evacuated and backfilled with argon five times before it was immersed in a pre-heated oil bath of 60 °C for 5 h. (P-L$_{33}$)$_{21}$ mixture was diluted in THF before it was passed through a basic alumina column before. (P-L$_{33}$)$_{21}$ mixture was then concentrated prior to being precipitated from excess methanol. Pure (P-L$_{33}$)$_{21}$ was then dried in a vacuum-oven at 30 °C for 12 h. Percentage yield of (P-L$_{33}$)$_{21}$ was 41.7 %. (P-L$_{33}$)$_{21}$ was confirmed *via* ^{1}H NMR: ^{1}H NMR (400MHz, $CDCl_3$): δ (ppm) = 4.0 (s, 2H, -C(=O)O-C**H_2**-), 1.7-1.9 (m, 4H, -C**H_2**-CH-C(=O)O-CH_2-CH_2 and -C**H_2**-C-CH_3-C(=O)O-CH_2-$(CH_2)_{10}$-CH_3), 1.6 (s, 6H, -C**H_2**-CH-C(=O)O-CH_2-CH_2, -C**H_2**-CH-C(=O)O-CH_2-C**H_2**-$C_{10}H_{21}$), 1.3 (s, 18H, -C_9**H_{18}**-), 0.9 (t, s, 6H, -C-C**H_3**C(=O)O-CH_2-$(CH_2)_{10}$-C**H_3**).

Physical measurements

Gel permeation chromatography (GPC) was performed using an instrument that was self-built with separate parts. A Knauer smartline HPLC pump flow 1 mL min^{-1} and a Shodex RI-101 reactive index detector was used. The 3 porous columns were connected in series and comprised of a phenomenox 'phenogel' 5 μ 500. The eluent was distilled and dried THF and calibration was performed using linear polystyrene standards with molecular weights ranging of 10^3 to 2 x 10^6 g mol^{-1}. ^{1}H NMR spectroscopy was conducted using a Bruker AVI-400 MHz spectrometer and $CDCl_3$ and DMSO-d_6 were used as the deuterated solvents. Elemental analysis (*C*, *H* and *N*) was conducted at the School of Chemistry, University of Manchester.

Results and Discussion

Homopolymer characterisation

The homopolymerisation of LA *via* ATRP is shown in Scheme 1a. The ^{1}H NMR spectrum (Fig. 1a) revealed signals belonging to the oxyethylene protons (4.0 ppm, **f**) and methylene protons (1.6 ppm, **g**) as expected[39]. The presence of the protons from the polymer backbone (**d**, **e**) and the end group (1.1 ppm, **a**) further supported that PLA was synthesised.

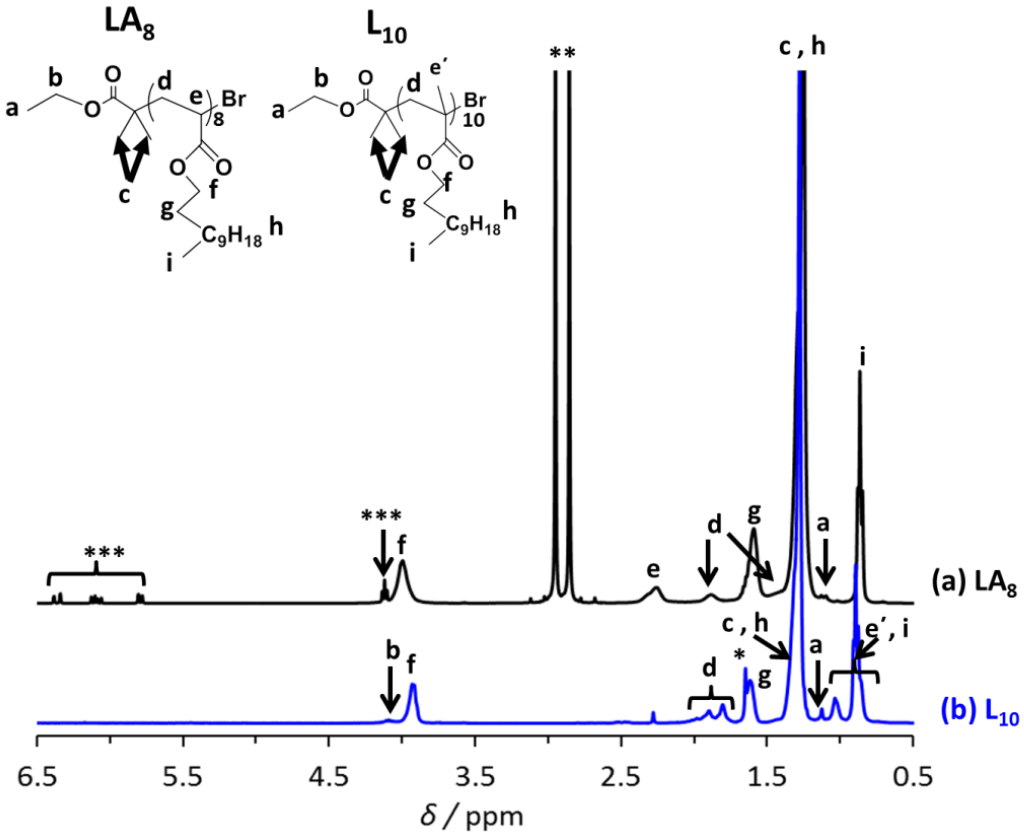

Fig. 1 ^{1}H NMR spectra for LA_8 (a) and L_{10} (b). The signals labelled with *, ** and *** signify the impurities water, DMF and vinyl groups belonging to unreacted LA, respectively.

The number-average degree of polymerisation (x) for PLA was calculated *via* end group analysis using Equation 1:

$$x = \frac{1}{6}\left(\left(\frac{A_h + A_c}{A_a}\right) - 2\right) \qquad \textbf{(1)}$$

whereby A_h, A_c and A_a corresponds to the integrals of the **h**, **c** and **a** proton signals, respectively (Fig. 1a). The value for *x* was calculated as 8.0, giving the abbreviated representation of PLA_8 as LA_8.

During the ATRP of LA it was observed that LA_8 precipitated from solution. The heterogeneous mixture was attributed to the solvophobic nature of the long alkyl chain of LA_8 in DMF. A similar observation was also reported in literature relating the insolubility of PLA in polar media when the ligand PMDETA was used[40]. The bimodal chromatograph of LA_8 (Fig. 2a) possessed a high polydispersity of 2.23 (Table 1) indicating that control over the ATRP of LA was indeed challenged. This is a probable cause for the value of *x* deviating from the targeted degree of polymerisation of 30, despite the reaction attaining a high monomer conversion of 90 %.

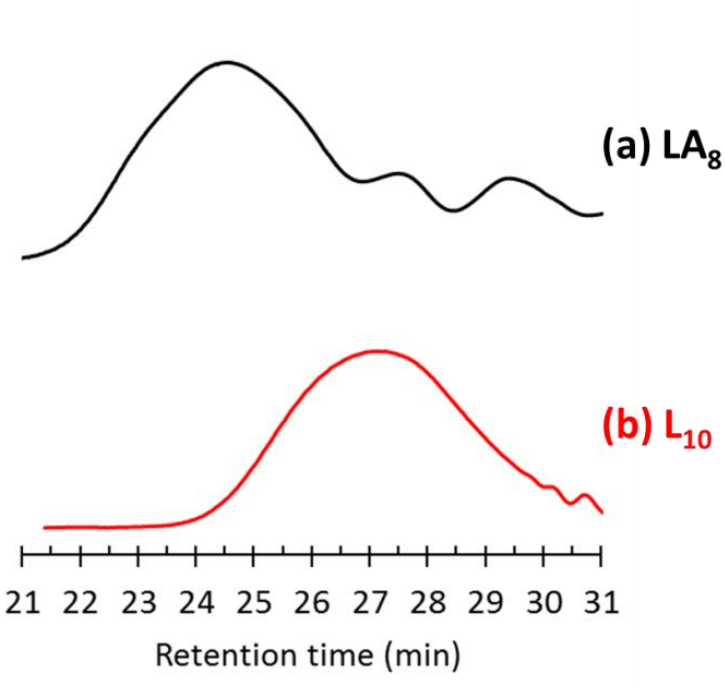

Fig. 2 GPC chromatograms for LA_8 (a) and L_{10} (b). The chromatograms were obtained using THF eluent and polystyrene standards.

Table 1 Compositions and characterisation data for the synthesised homopolymers, diblock copolymer, macroinitiator and graft copolymers.

Code	Composition[a]	$M_{n(NMR)}$ / g / mol	$M_{n(GPC)}$ / g / mol	M_w / M_n
LA_8	PLA_8	2,100	9,300	2.23
L_{10}	$PLMA_{10}$	2,700	4,400	1.56
L_{43}	$PLMA_{43}$	11,100	45,600	4.89
L_{10}-H_5	$PLMA_{10}$-$PHEMA_5$	3,300	6,300	1.27
PH_{21}	$PHEATMS_{21}$	4,100	4,300	1.25
P_{21}	$PBiBEA_{21}$	5,800	5,900	1.35
$(P\text{-}LA_7)_{21}$	$(PBiBEA\text{-}PLA_7)_{21}$	-	-	-
$(P\text{-}L_{33})_{21}$	$(PBiBEA\text{-}PLMA_{33})_{21}$[b]	59,100	180,000	2.21

Compositions determined from [a] ^{1}H NMR spectroscopy and [b] GPC studies.

For comparison, the value for *x* was also determined from GPC studies using Equation 2:

$$x = \frac{M_n - 195}{240} \qquad \textbf{(2)}$$

whereby M_n represents the number-average molecular weight of a polymer. Inserting the M_n value of 9,300 g mol^{-1} for LA_8 (Table 1) in the above equation resulted in the calculated value of *x* as 38.0, which is almost four times greater than the value of *x* calculated using Equation 1. Slight deviations of *x* determined by ^{1}H NMR and GPC are expected due to received M_n values that are dependent on molecular weights of the calibration[41]. However, major differences in values for *x* may be because LA_8 precipitated from solution during the ATRP reaction.

In contrast, the homopolymerisation of LMA in toluene (Scheme 1b) resulted in a homogeneous mixture. This is despite reports discouraging the use of the ligand PMDETA for the polymerisation of (meth)acrylate based monomers[40]. Raghunadh *et al.*[42] also describes the controlled ATRP polymerisation of LMA in non-polar media whilst using PMDETA. The ATRP of LMA was preferred for this reason. The ^{1}H NMR spectrum of PLMA (Fig. 1b) also showed signals belonging to the oxyethylene protons (4.0 ppm, **f**) and methylene (1.6 ppm, **g**)

akin to the signals observed in ^{1}H NMR of LA_8 (Fig. 1a). However, the presence of the methyl group (0.9 ppm, **e′**) was exclusive to PLMA[43]. The value for *x* was calculated using Equation 1. The value for *x* was calculated as 10.0 resulting in the abbreviated form of $PLMA_{10}$ as L_{10}. The latter value was consistent with the targeted degree of polymerisation of 10 as a high monomer conversion of 99 % was attained.

The GPC study of L_{10} (Fig. 2b) showed a monomodal chromatograph that possessed a lower polydispersity of 1.56. This suggested that better control was attained over the polymerisation of LMA. The value for *x* was calculated from the GPC study using Equation 3.

$$x = \frac{M_n - 195}{254} \qquad \textbf{(3)}$$

The M_n value of 4,400 g mol^{-1} for L_{10} (Table 1) was inserted into the above equation and *x* was calculated as 17.0. A closer comparison of the values for *x* supports the reasoning of improved polymerisation of LMA.

Diblock copolymer characterisation

Following the positive result of the ATRP of LMA, the halogen exchange principle[44] was employed to provide high block efficiency of further LMA growth from L_{10} (Scheme 1b). As expected, the signals observed in the ^{1}H NMR spectrum of L_{10} (Fig. 1b) were identical to the signals apparent in the ^{1}H NMR spectrum following further chain extension of LMA (Fig. 3a). The significant difference was the reduced intensity of the terminal methyl end group from EBiB (1.1 ppm, **a**). The value for *x* was calculated as 43.0 by using Equation 1, resulting in the abbreviated form of $PLMA_{43}$ as L_{43}. The latter calculated value of *x* was consistent with the targeted degree of polymerisation of 100 whereby a monomer conversion of 43 % was attained.

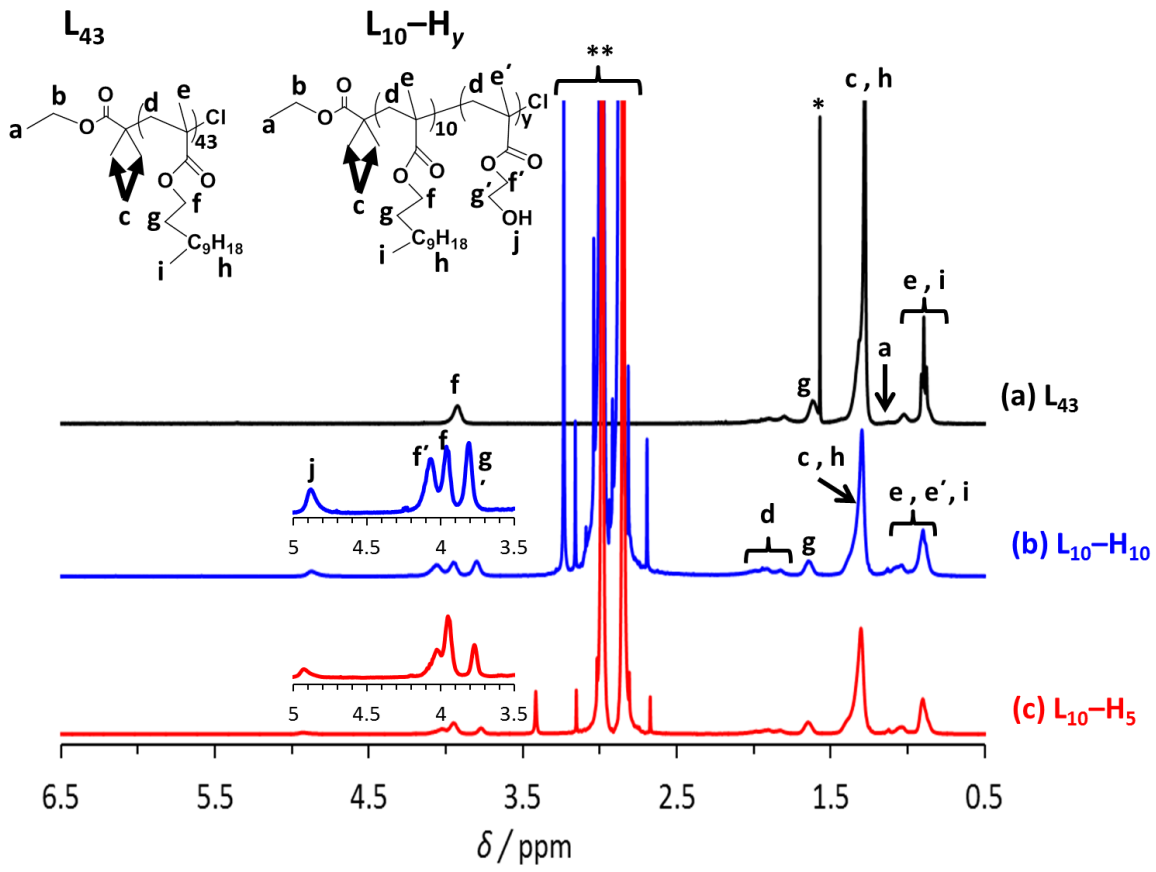

Fig. 3 ^{1}H NMR spectra for the homopolymer L_{43} (a) and the diblock copolymers L_{10}-H_{10} (b) and L_{10}-H_5 (c). The signals labelled with * and ** represent water and DMF, respectively. A co-solvent blend of the deuterated solvents $CDCl_3$ and undeuterated DMF was required for ^{1}H NMR characterisation of L_{10}-H_y copolymers.

The chromatograph for L_{43} (Fig. 4a) was expected to appear at a lower retention time as it is a larger polymer. A polydispersity of 4.89 indicates a broad molecular weight distribution (Table 1). This was related to the low chain end fidelity of L_{10} as a consequence high LMA conversion (i.e., > 85 %) prior to termination[45]. Although control over further LMA growth was challenged, the results demonstrate that chain extension from L_{10} was attainable.

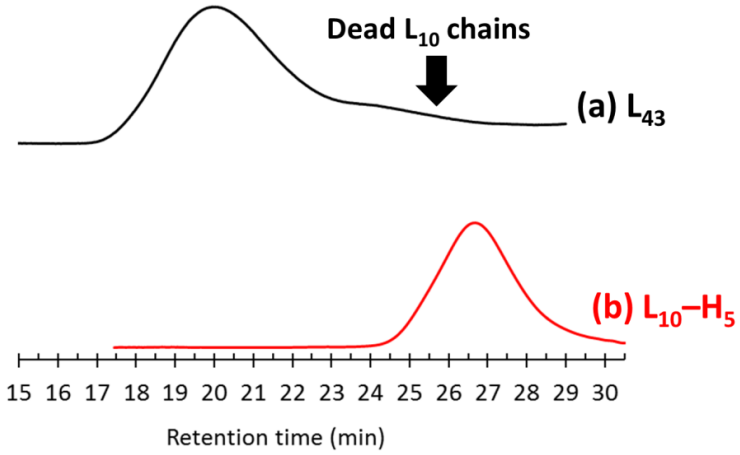

Fig. 4 GPC chromatograms for L_{43} and the diblock copolymer L_{10}-H_5. Signs of L_{10} that lacked further chain extension of LMA repeat units is indicated by the arrow. The chromatograms were obtained using THF eluent and polystyrene standards.

The value for *x* was calculated for L_{43} from the GPC study using Equation 3 and the M_n value of 45,600 g mol^{-1} (Table 1). The value for *x* was calculated as 179 which signified that the low chain end fidelity of L_{10} caused unfavourable termination. It was also reasoned that other conditions, such as the presence of oxygen, may have prevented the efficacy of the halogen exchange method. Despite challenged control over longer repeat units of LMA it was concluded that chain extension from L_{10} was attained.

The diblock copolymer organogelator approach involved preparing a diblock copolymer composition based on PLMA-PHEMA (Scheme 1c). Further chain extension of HEMA from L_{10} also utilised the halogen exchange principle[40]. Differences in solubility of the PLMA and PHEMA blocks were encountered when preparing a sample for ^{1}H NMR spectroscopy. This led to the use of a co-solvent blend of $CDCl_3$ and DMF to ensure that the protons belonging to PLMA and PHEMA were visible. The ^{1}H NMR study of the diblock copolymers (Fig. 3b-c) confirmed the presence of oxyethylene protons (4.1 ppm, **f´**), methylene protons (3.8 ppm, **g´**) and the hydroxyl proton (4.8 ppm, **j**)[36]. The number-average degree of polymerisation for PHEMA (*y*) was determined using Equation 4.

$$y = (9x + 3)\left(\frac{A_{g^*}}{A_h + A_c}\right) \qquad \textbf{(4)}$$

For the above equation, A_g^* A_h and A_c indicate the integrals of the proton signals labelled **g´**, **h** and **c**. The value for *y* was calculated as 5.0 and 10.0, respectively. This resulted in PLMA-PHEMA copolymers referred to as L_{10}-H_5 and $L_{10}H_{10}$, respectively. The values for *y* were consistent with the targeted degree of polymerisations of 10 and 20, respectively, given that the monomer conversion of both reactions were terminated at 50 %. The ^{1}H NMR spectrum of $L_{10}H_{10}$ (Fig. 3b) showed an increased intensity of the signals labelled **f´**, **g´** and **j**. This indicated the presence of more protons when compared to the same signals evidenced in the ^{1}H NMR spectrum of $L_{10}H_5$ (Fig. 3c). The copolymer composition $L_{10}H_5$ was used for further investigation as it possessed the least repeat units of PHEMA required for this study.

The GPC characterisation of L_{10}-H_5 (Fig. 4b) shows a monomodal chromatograph that possessed a low polydispersity of 1.27. This result is indicative of high blocking efficiency of HEMA from L_{10}The value for *y* was also determined from Equation 5:

$$y = \frac{M_n - (254x) - 151}{130} \qquad \textbf{(5)}$$

whereby *x* corresponds to the number-average degree of polymerisation of L_{10} determined from ^{1}H NMR spectroscopy. Inserting the M_n value of 6, 300 g mol^{-1} for L_{10}-H_5 (Table 1) resulted in *y* equating to 26.0. Despite the lowered polydispersity of L_{10}-H_5 indicating high blocking efficiency, it is clear that differences in the values for *y* is greatly impacted by the low chain end functionality of L_{10}. Another reason may relate to the use of linear polymers as standards for GPC. As PLMA type copolymers occupy a higher hydrodynamic volume and will give a higher apparent molecular weight.

Further confirmation of the presence of PHEMA repeat units were determined by the addition of a few drops of trichloroacetyl isocyanate to L_{10}-H_5 solution. This resulted in the formation of L_{10}-H_5-CONHCOC(Cl)$_3$ (Scheme 5)[37, 46, 47].

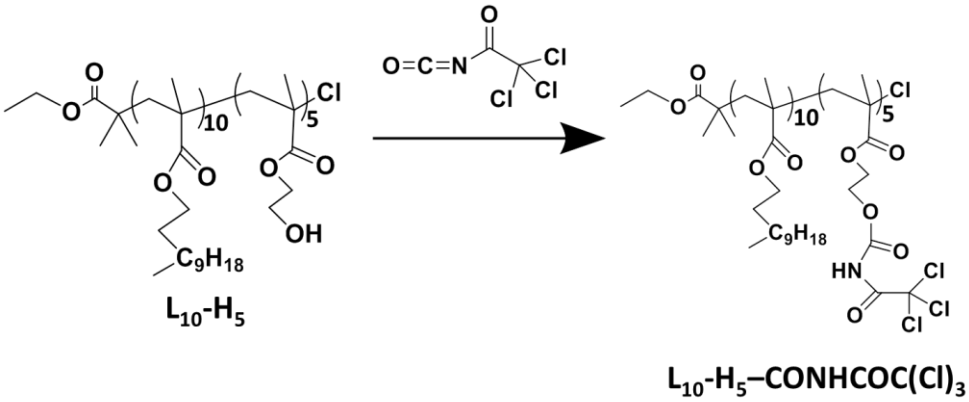

Scheme 5 Depiction of the alcoholysis reaction between L_{10}-H_5 and trichloroacetyl isocyanate, that results in a proportion OH groups being substituted with a urethane bond.

In the ^{1}H NMR spectrum of L_{10}-H_5 after alcoholysis, it is observed that the PHEMA signal representing the hydroxyl proton (**j**) is missing upon formation of a urethane bond (Fig. 5b). Interestingly, this change influenced the position of the oxyethylene protons (**f´**) and methylene protons (**g´**) causing them move to higher chemical shifts (4.20 – 4.60 ppm). It was expected that the signal corresponding to the oxyethylene protons (**f**) from PLMA would remain unaffected following the removal of the hydroxyl proton from PHEMA.

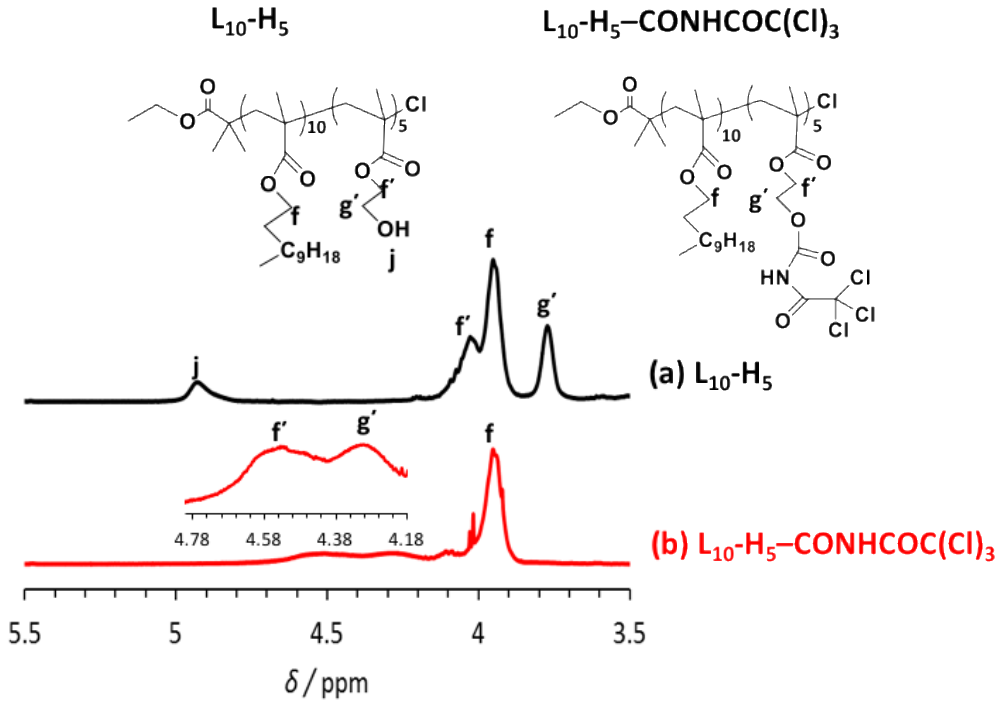

Fig. 5 ^{1}H NMR spectra for L_{10}-H_5 (a) and L_{10}-H_5-CONHCOC(Cl)$_3$ (b) following the addition of trichloroacetyl isocyanate, that results in a proportion of substituted OH groups.

To determine the number of PHEMA repeat units that were affected, Equation 6 was used to calculate the value for *y* following the alcoholysis reaction:

$$y = x(\frac{A_{g^*}}{A_f}) \qquad \textbf{(6)}$$

whereby A_{g*} and A_f corresponds to the integrals for the proton signals labelled **g´** and **f**. The value for *y* was 3, implying that 60 % of the hydroxyl protons had been replaced by a urethane bond.

The formation of the urethane bond was also supported by a physical transformation that changed the colour of the solution from transparent to pale yellow. Similarly, an intense colour change was also observed after the addition of trichloroacetyl isocyanate to poly(methyl acrylate)-*b*-poly(allyl alcohol) (PMA_6-$AlOH_1$). The PMA_6-$AlOH_1$ copolymer[37] was characterised to provide insight into the structural changes of L_{10}-H_5-$CONHCOC(Cl)_3$ *via* ^{1}H NMR spectroscopy. The ^{1}H NMR spectrum of PMA (Fig. 6a) enabled *x* to be calculated *via* end group analysis using Equation 7:

$$x = \frac{A_f}{A_a} \qquad \textbf{(7)}$$

whereby A_f and A_a represents the integrals for the methyl protons labelled **f** and **a** belonging to the PMA and the MBP end group, respectively. The value for *x* was calculated as 6.0 giving the abbreviation PMA_6. The value *y* for allyl alcohol was calculated using Equation 8:

$$y = 3x\ (\frac{A_{g^*}}{A_f}) \qquad \textbf{(8)}$$

The value for *y* was calculated as 1.0 indicating that there was one repeat unit of allyl alcohol following the PMA block. The ^{1}H NMR spectrum of PMA (Fig. 6a) showed a signal corresponding to the terminal hydroxyl proton (4.2 ppm, **e**). However, after the addition reaction of allyl alcohol the aforementioned signal became invisible, thus suggesting the successful addition of the allyl alcohol repeat unit (Fig. 6b). Once trichloroacetyl isocyanate was added, a signal emerged in the ^{1}H NMR spectrum (Fig. 6c) that was indicative of

methylene protons (4.5 ppm, **g´**). The enhanced colour transformation after alcoholysis was related to 80 % formation of urethane bonds.

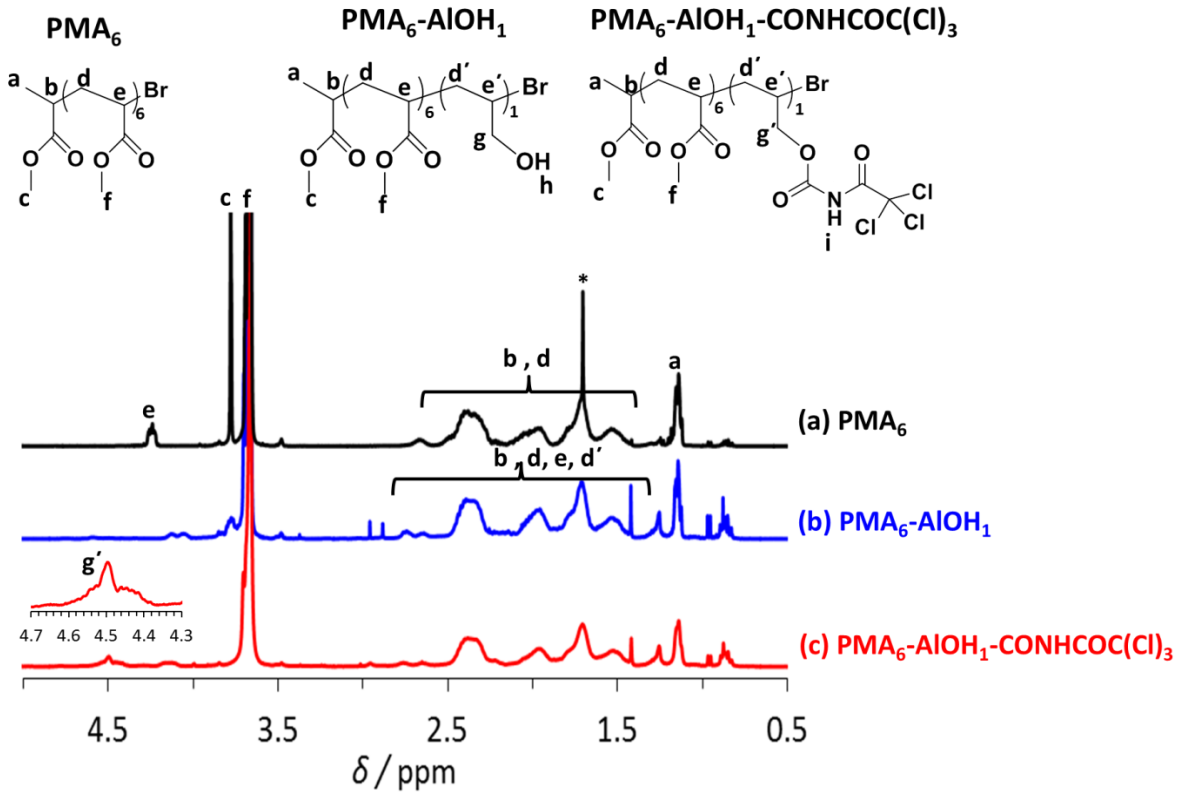

Fig. 6 ^{1}H NMR spectra for PMA_6 (a), PMA_6-$AlOH_1$ (b) PMA_6-$AlOH_1$-$CONHCOC(Cl)_3$ (c).

The reason behind the colour change is not understood. However, it appears to be a physical observation indicating that a reaction (i.e., alcoholysis) has taken place. The positive result of L_{10}-H_5-$CONHCOC(Cl)_3$ was used to predict structural changes for the diblock copolymer gelator.

Polymer organogelator characterisation

The LMWG, CAP, was prepared from the cyclisation of Aspartame (Scheme 2). The ^{1}H NMR spectrum for Aspartame (Fig 7a) was distinguished due to the presence of the signals representing the amine protons (8.9 ppm, **n**) and methyl protons (3.7 ppm, **s**). The signals corresponding to the benzene group (7.3 ppm, **u**) and methylene groups (**m** and **t**) were also apparent as expected[48].

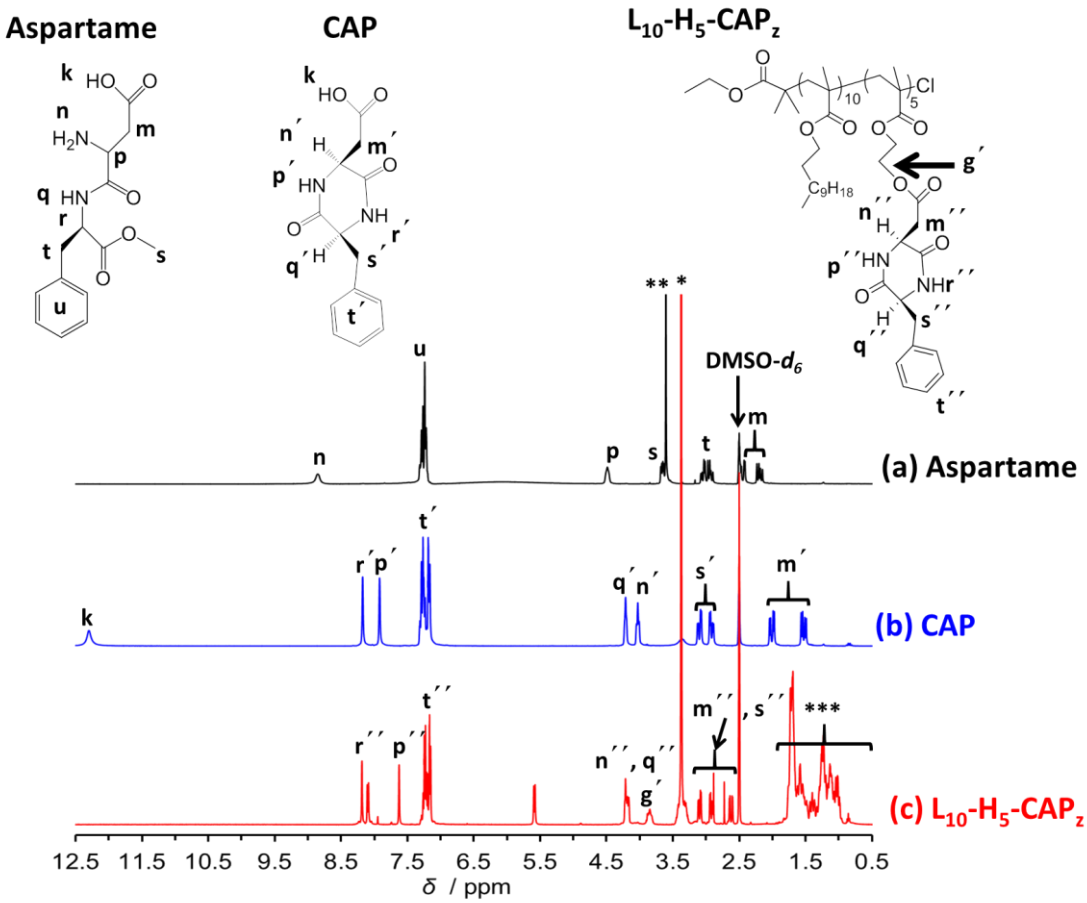

Fig. 7 ^{1}H NMR spectra for Aspartame (a) and CAP (b) and the diblock copolymer gelator, L_{10}-H_5-CAP_z (c).

The ^{1}H NMR spectrum of CAP (Fig. 7b) showed exclusive signals belonging to the amide protons (**p´** and **r´**). The presence of the signals corresponding to protons (**q´** and **n´**) and methylene protons (**s´** and **m´**) also suggest the successful cyclisation of Aspartame. Elemental analysis of CAP showed that the experimental values for **C:** 59.3, **H:** 5.3, **N:** 10.6 were within 0.40 % of the theoretical values for **C:** 59.6, **H:** 5.4, **N:** 10.7, thereby supporting the validity of the results. From the experimental result, the molecular formula for CAP was determined as $C_{13}H_{14}N_2O_4$, which in conjunction with ^{1}H NMR spectroscopy implies that a pure form of CAP was obtained[10].

From the ^{1}H NMR spectrum for CAP (Fig. 7b) the signal that indicated the presence of hydroxyl proton from the carboxylic group was of most interest for this study. This is because the absence of this signal would hint at the successful introduction of CAP onto L_{10}-H_5. The reaction between the hydroxyl group of PHEMA from L_{10}-H_5 and the carboxylic group belonging to CAP was carried out *via* Steglich esterification[49] (Scheme 1c). The ^{1}H NMR spectrum of the diblock copolymer organogelator (Fig. 7c) lacked the signal

corresponding to the hydroxyl proton that belonged to the carboxylic group from CAP. The number of CAP units that had successfully added onto L_{10}-H_5 was calculated using Equation 9.

$$z = \frac{1}{5}\left(\left(\frac{A_{t^{**}}}{A_{g^{*}}}\right) 2y\right) \qquad \textbf{(9)}$$

For the above equation A_t^{**} and A_g^{*} correspond to the integrals for the protons assigned to the benzene group (**t´´**) from CAP and the methylene group (**g´**) from PHEMA. The value for *y* calculated from ^{1}H NMR spectroscopy was inserted into the above equation. The value for *z* was 11.0 and indicated that further purification of L_{10}-H_5-CAP_z was required to remove excess CAP. A diluted acidic wash followed by a diluted basic bath is proposed to aid the removal of the urea by-product and other impurities[43].

In the ^{1}H NMR spectrum for L_{10}-H_5-CAP_z (Fig. 7c) it was expected that all the signals corresponding to PLMA groups would be unseen in a polar deuterated solvent. It is reasoned that PLMA arms would assume a collapsed state in DMSO-d_6. It is also plausible that the signals for the oxyethylene protons (**f**) from PHEMA were hidden by the collapsed state of PLMA. However, the methylene signal from PHEMA (3.9 ppm, **g´**) emerged in the ^{1}H NMR spectrum of the diblock copolymer gelator. The aforementioned signal was predicted to appear at higher chemical shifts after observations from the ^{1}H NMR study of a trichloroacetyl isocyanate reaction with L_{10}-H_5 (Fig. 5). However, the characteristic shift of the methylene signal (**g´**) now recognised at 3.9 ppm is reported to initially exist at 3.60 ppm[50] in DMSO-d_6, thus implying that the diblock copolymer gelator was successfully synthesised.

In addition, the emergence of the signal assigned to **n´´** and **q´´** (Fig. 7c) also supports the success of the reaction. The value for *z* was calculated using Equation 10 for comparative reasons:

$$z = y\left(\frac{A_{n^{**}} + A_{q^{**}}}{A_{g^{*}}}\right) \qquad \textbf{(10)}$$

For the above equation, A_n^{**} and A_q^{**} correspond to the integrals of the protons belonging to the CAP segment of the diblock copolymer gelator, which were labelled as **n´´** and **q´´**,

respectively. The value of *z* was calculated as 11.0 which is similar to the calculated value for *z* determined by Equation 9. Despite the higher than expected values for z, the results still imply that L_{10}-H_5-CAP_z was successfully synthesised.

PBiBEA macroinitiator characterisation

The macroinitiator, PBiBEA, was used to follow the graft copolymer gelator strategy. PBiBEA was prepared *via* three steps (Scheme 3). The first step involved protection of the hydroxyl group belonging to HEA, as a means of producing HEATMS. The ^{1}H NMR spectrum of HEA (Fig. 8a) demonstrated that the hydroxyl proton (**e**) was replaced by a protective TMS protons (**e´**) as seen in the ^{1}H NMR spectrum of HEATMS (Fig. 8b). Elemental analysis showed that the experimental values of **C**: 51.1, **H**: 8.7 were within 0.40 % of the theoretical values for **C:** 51.1, **H:** 8.5. The elemental analysis results and ^{1}H NMR spectroscopy confirmed that a pure form of HEATMS was obtained after distillation.

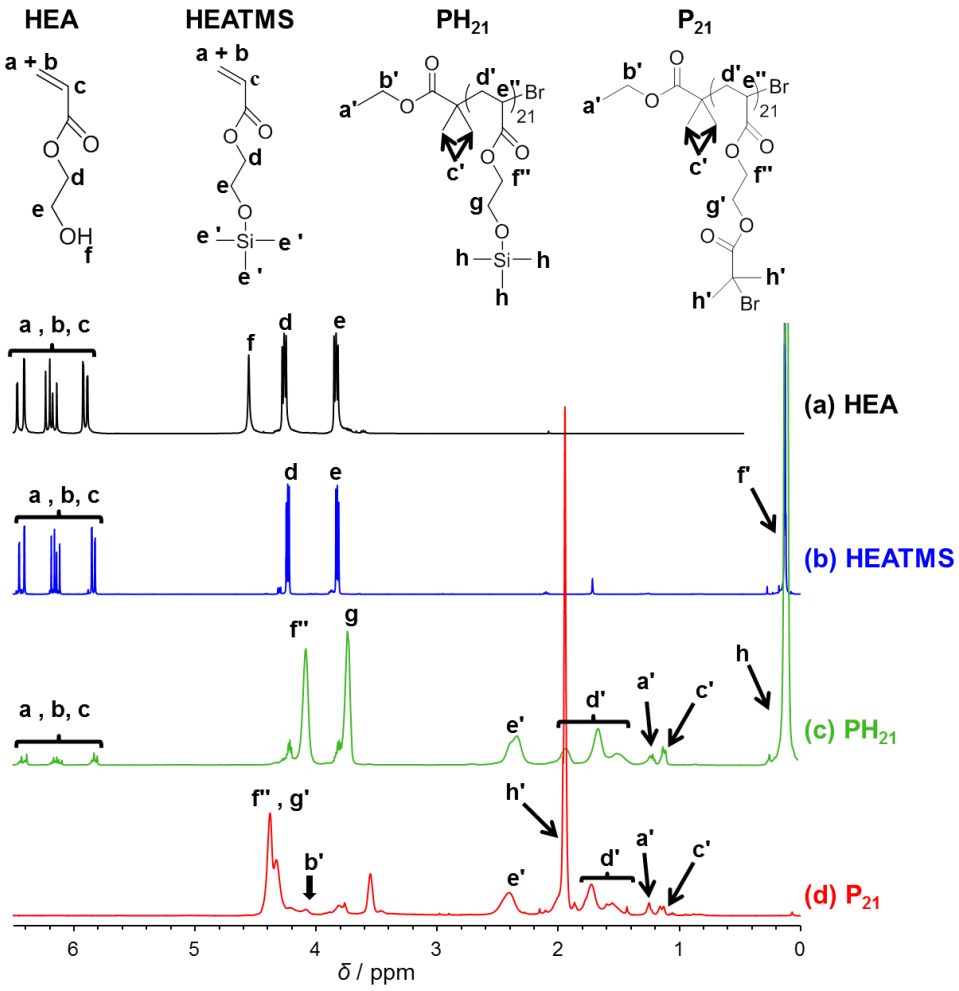

Fig. 8 ^{1}H NMR spectra for HEA (a) and HEATMS (b) $PHEATMS_{21}$ (c) and the macroinitiator P_{21} (d).

The second step involved ATRP of HEATMS to form PHEATMS (Scheme 3). The ^{1}H NMR spectrum of PHEATMS (Fig. 8c) enabled the value for *x* to be calculated *via* end group analysis using Equation 11.

$$x = 3\left(\frac{A_{f^{**}}}{A_{c^{*}}}\right) \qquad \textbf{(11)}$$

For the above equation A_f and A_c corresponds to the integrals of the protons belonging to the methylene group from PHEATMS (**f´´**) and methyl groups from EBiB (**e´**), respectively. The value for *x* was calculated as 21.0 giving $PHEATMS_{21}$ in the abbreviated form as PH_{21}. The signals representing the oxyethylene protons (4.2 ppm, **f´´**) and the methylene protons (3.7 ppm, **g**) were present as expected, as well as the signals corresponding to the polymer backbone (**d´** and **e´**)[35]. The signals belonging to the vinyl protons (**a**, **b** and **c**) from HEATMS were also apparent. This is because the polymerisation reaction was terminated at 90 % monomer conversion. The high monomer conversion was to ensure that most of the polymerised monomer units would result in grafted side chains possessing narrow molecular weight distribution. It was essential that PH_{21} still possessed the protective group (**h**) to alleviate the occurrence of unwanted side reactions[51, 52].

The GPC data for PHEATMS (Fig. 9a) was represented by a monomodal chromatograph possessing a low polydispersity of 1.25 (Table 1), that is within range for well-defined acrylate polymers prepared by ATRP[53].

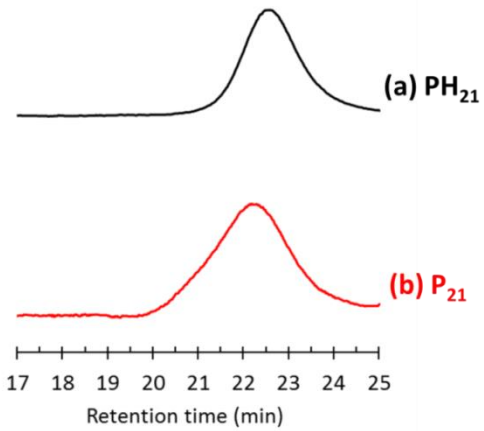

Fig. 9 GPC chromatograms for PH_{21} (a) and the macroinitiator P_{21} (b). The chromatograms were obtained using THF eluent and polystyrene standards.

The value for *x* was also calculated according to the GPC study of PH_{21} using Equation 12.

$$x = \frac{M_n - 195}{188} \qquad \textbf{(12)}$$

Inserting the M_n value of 4,300 g mol^{-1} for PH_{21} (Table 1) into the above equation resulted in the value for *x* to be calculated as 22.0, which is similar to the *x* value calculated from ^{1}H NMR spectroscopy. This result implies that there was good control over the ATRP of HEATMS.

The final step was responsible for preparing PBiBEA from PHEATMS (Scheme 3). This reaction involved substituting the protective group with terminal brominated groups to encourage subsequent graft polymerisation. The ^{1}H NMR spectrum of PBiBEA (Fig. 8d) was confirmed by the absence of the signal corresponding to the protons from the protective group (0.0 ppm) and the presence of the signal belonging to the methyl protons from the 2-bromoisobutyryl unit (**h**´)[35]. The ^{1}H NMR spectrum of PBiBEA (Fig. 8d) enabled the number-average degree of polymerisation (*n*) to be calculated for PBiBEA using Equation 13:

$$n = \frac{3}{2}\left(\frac{A_f^{**} + A_g^{*}}{A_c}\right) \qquad \textbf{(13)}$$

For the above equation, A_f^{**} and A_g^{*} correspond to the integral of the protons for the signals assigned to the oxyethylene group (**f**´´) and methylene group (**g**´), respectively. A_c represents the integral of the protons assigned to the methyl groups (**c**) from (EBiB). The value for *n* was calculated as 21.0, which is consistent with the value of *x* for PH_{21}. This resulted in the abbreviation for $PBiBEA_{21}$ as P_{21}. The chain end fidelity (%) of P_{21} was calculated using Equation 14:

$$\text{chain end fidelity} = \left(\frac{A_{h^*}}{A_{c^*}} \times \frac{1}{n}\right) \times 100 \qquad \textbf{(14)}$$

For the above equation, A_h^* and A_c^* corresponds to the integrals for the protons belonging to the methyl protons from the 2-bromoisobutyryl unit (**h´**) and methyl protons from EBiB (**c´)**. The chain end fidelity of P_{21} was 96 %, which is sufficient for subsequent graft copolymerisation reactions.

The GPC chromatograph for P_{21} (Fig 9b) showed a monomodal chromatograph that has a low polydispersity of 1.35 (Table 1). The GPC study of P_{21} also enabled the value for *n* to be calculated using Equation 15:

$$n = \frac{M_n - 195}{265} \qquad \textbf{(15)}$$

Inserting the M_n value of 5,900 g mol^{-1} for P_{21} (Table 1) resulted in *n* being equivalent to 21.0, which is consistent with the value of *n* that was determined from ^{1}H NMR spectroscopy. It was concluded from the obtained results that PBiBEA was successfully synthesised.

Graft copolymer characterisation

The second strategy for this study focused on the synthesis of a graft copolymer gelator. The first step involved grafting LA from P_{21} to give (PBiBEA-LA$_x$)$_{21}$ (Scheme 4a). In the ^{1}H NMR spectrum of (PBiBEA-LA$_x$)$_{21}$ (Fig 10a) the presence of LA repeat units were evidenced by the presence of signals corresponding to the oxyethylene protons (4.0 ppm, **f´**) and the methylene protons (1.6 ppm, **g´**). The emergence of the signals corresponding to the protons belonging to long alkyl chain (**c**, **c´**, **h**) and the terminal methyl protons (**i**) also appear as expected and provide additional support[39]. Although there was potential for PLA block copolymer growth (Scheme 4a), it was hypothesised that PLA grafted side chains would be the majority, and therefore contribute mostly to the proton signals in the ^{1}H NMR spectrum of (PBiBEA-LA$_x$)$_{21}$ (Fig 10a).

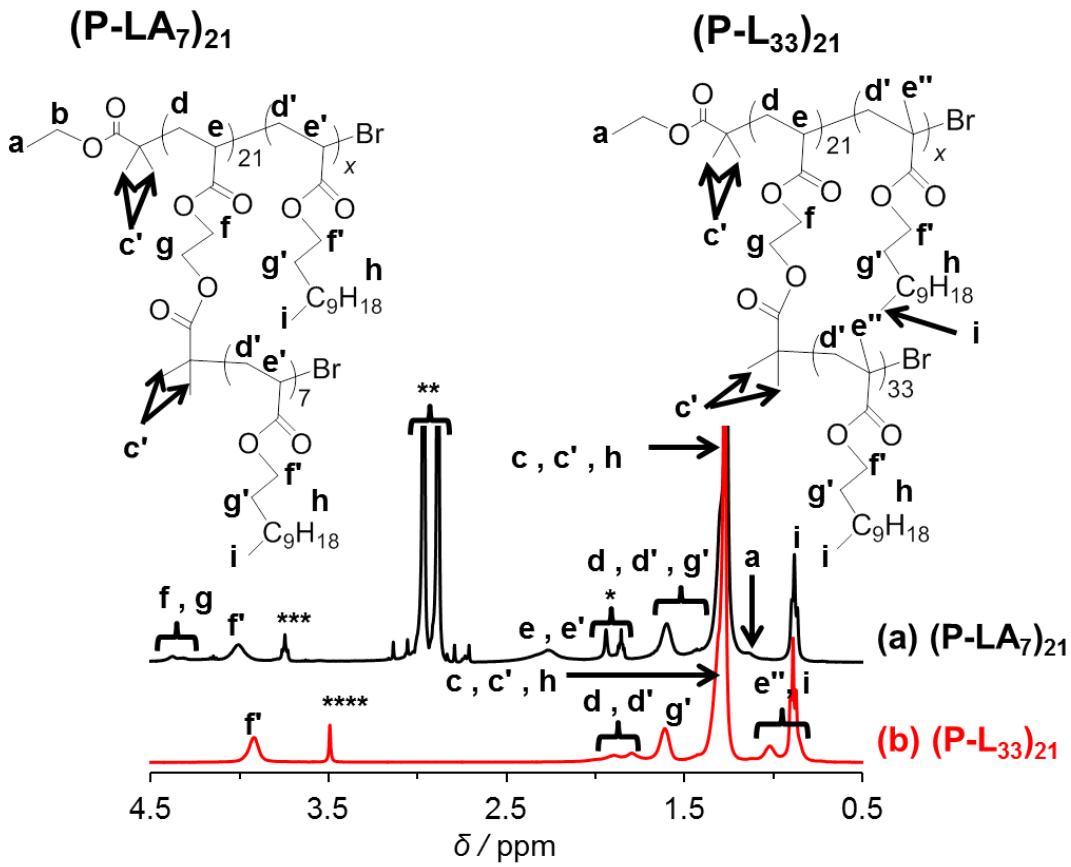

Fig. 10 ^{1}H NMR spectra for the graft copolymers (P-LA$_7$)$_{21}$ (a) and (P-L$_{33}$)$_{21}$ (b).

.

The ^{1}H NMR spectrum for (PBiBEA-LA$_x$)$_{21}$ allowed a value of x to be calculated for the LA repeat units, by considering the proton signals of the 2-bromoisobutyryl unit belonging to PBiBEA when using Equation 16:

$$x = \frac{2}{9}\left(\left(\frac{A_c + A_{c^*} + A_h}{A_f + A_g}\right) - \frac{1}{3}\left(1 + \frac{1}{n}\right)\right) \qquad \textbf{(16)}$$

For the above equation A_c and A_c^* correspond to the integrals of the methyl protons labelled **c** **c´**, respectively, that belong to EBiB. A_h represents the integral for the methylene protons labelled **h** that belong to PLA, whilst A_f and A_g represent the integral of the oxyethylene (**f**) and methylene protons (**g**) belonging to PBiBEA. The presence of the latter proton signals was helpful in determining the value for x as 7.0, giving the abbreviated form of the graft copolymer as (P-LA$_7$)$_{21}$.

A similar solubility issue described for the hompolymerisation of LA was observed for the graft copolymerisation of LA (Fig. 11).

Fig. 11 Image of the graft copolymer, $(P\text{-}LA_7)_{21}$, that precipitated from solution during polymerisation of LA from the macroinitiator P_{21}.

This was related to the insolubility of PLA side chain growth. $(P\text{-}LA_7)_{21}$ was insoluble in THF preventing further characterisation of the molecular weight and molecular weight distribution of the graft copolymer. Given the exacerbated precipitation of the graft copolymer, LMA was chosen as the suitable monomer for subsequent graft copolymerisation reactions.

Following from the positive result of the homopolymerisation of LMA, it was expected that the graft copolymer $(PBiBEA\text{-}LMA_x)_{21}$ (Scheme 4b) would be suited to the graft copolymer gelator approach for this study. In the ^{1}H NMR spectrum of $(PBiBEA\text{-}LMA_x)_{21}$ (Fig 10b) the presence of the oxyethylene protons (4.0 ppm, **f´**) and the methylene protons (1.6 ppm, **g´**) confirmed the success of the reaction. The emergence of the signals corresponding to the protons belonging to long alkyl chain (**c**, **c´**, **h**) and the terminal methyl protons (**e´´**, **i**) also appear as expected and provide further support[43]. Similar to $(PBiBEA\text{-}LA_x)_{21}$ synthesis, it was expected that most LMA repeat units would be grafted from P_{21}, despite the possibility of some block copolymer growth. The value of *x* of $(PBiBEA\text{-}LMA_x)_{21}$ according to ^{1}H NMR spectroscopy was undetermined as the distinct signals corresponding to the oxyethylene (**f**) and methylene protons (**g**) from PBiBEA were undetectable. For this reason, the value for *x* was calculated from the GPC study (Table 1) of $(PBiBEA\text{-}LMA_x)_{21}$ by using Equation 17.

$$x = \frac{M_n - (265n) - 195}{254n} \qquad \textbf{(17)}$$

For the above equation, the value for *n* that was used was according to ^{1}H NMR spectroscopy. Inserting the M_n value of 180, 000 g mol^{-1} for (PBiBEA-LMA$_x$)$_{21}$ resulted in the calculated value for *x* as 33.0, thus resulting in the abbreviated form of the graft copolymer as (P-L$_{33}$)$_{21}$. The GPC study of (P-L$_{33}$)$_{21}$ (Fig. 12) was represented by a bimodal chromatograph that possessed a high polydispersity of 2.21.

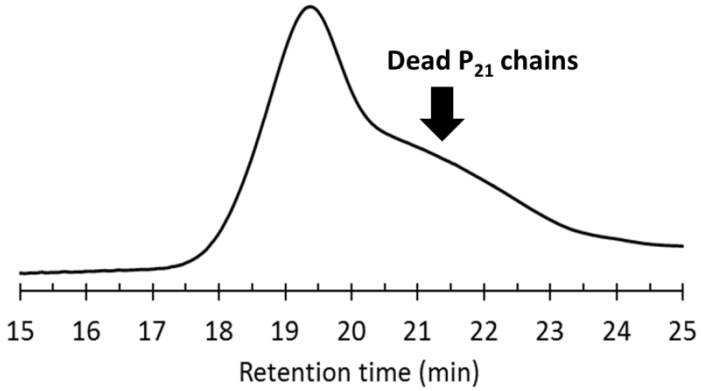

Fig. 12 GPC chromatograph of (P-L$_{33}$)$_{21}$. Signs of the macroinitiator P$_{21}$ that lacked grafted LMA repeat units is indicated by the arrow. The chromatograms were obtained using THF eluent and polystyrene standards.

This broad molecular weight distribution suggests that the graft copolymerisation of LMA was challenged. This could be improved through the introduction of Cu II species that behave as deactivators that balance the position of the equilibrium to favour the formation of dormant species[54]. It was reasoned that the high concentration of multi-initiating sites from (P-L$_{33}$)$_{21}$ caused bimolecular coupling and therefore prevented uniform chain growth of LMA[55].

There was limited time for exploring the chain extension of HEMA from (P-L$_{33}$)$_{21}$. However, given the promising results of the diblock copolymer L$_{10}$-H$_5$, it can be hypothesised that there is potential for the synthesis of (P-L$_{33}$-H$_y$)$_{21}$. This framed the proceeding steps for the graft copolymer approach shown in Scheme 4c.

Conclusions

In this work two strategies were employed to synthesise a polymer gelator containing the LMWG molecule CAP. The first was concerned with developing a diblock copolymer

gelator, whilst the second focused on the preparation of a graft copolymer gelator. Despite challenged control over ATRP of the diblock copolymer, this study successfully demonstrated that ATRP could be used to prepare the polymeric segment of the diblock copolymer gelator, provided that PLMA was the first block. ^{1}H NMR spectroscopy confirmed the presence of the PHEMA block and GPC showed good control over the ATRP of the PHEMA block. ^{1}H NMR spectroscopy confirmed that the diblock copolymer gelator was realised and required further purification to remove excess CAP. Some success of the graft copolymer gelator was achieved through the synthesis of the polymeric segment. The graft copolymerisation of LMA presented better control compared to LA. Further chain extension of HEMA from the graft copolymer and the subsequent introduction of CAP were hypothesised, given the successful synthesis of the diblock copolymer gelator. However, the graft copolymer organogelator approach was not carried out to completion as an easier route to preparing polymer gelators was explored.

Acknowledgments

We would gratefully acknowledge funding for this research through an EPSRC iCASE grant (Voucher 12220937).

References

1. D. Ma, K. Tu and L. M. Zhang, *Biomacromolecules*, 2010, **11**, 2204-2212.
2. K. Y. Lee and D. J. Mooney, *Chem Rev*, 2001, **101**, 1869-1879.
3. S. Thaiboonrod, C. Berkland, A. H. Milani, R. Ulijn and B. R. Saunders, *Soft Matter*, 2013, **9**, 3920-3930.
4. V. Jenning, A. Gysler, M. Schafer-Korting and S. H. Gohla, *Eur J Pharm Biopharm*, 2000, **49**, 211-218.
5. J. Chen and A. J. McNeil, *J Am Chem Soc*, 2008, **130**, 16496-+.
6. N. M. Sangeetha and U. Maitra, *Chem Soc Rev*, 2005, **34**, 821-836.
7. D. J. Abdallah and R. G. Weiss, *Adv Mater*, 2000, **12**, 1237-+.
8. N. Brosse, D. Barth and B. Jamart-Gregoire, *Tetrahedron Lett*, 2004, **45**, 9521-9524.
9. K. Hanabusa, H. Nakayama, M. Kimura and H. Shirai, *Chem Lett*, 2000, DOI: DOI 10.1246/cl.2000.1070, 1070-1071.
10. K. Hanabusa, M. Matsumoto, M. Kimura, A. Kakehi and H. Shirai, *J Colloid Interf Sci*, 2000, **224**, 231-244.
11. B. Isare, L. Bouteiller, G. Ducouret and F. Lequeux, *Supramol Chem*, 2009, **21**, 416-421.
12. K. Hanabusa and M. Suzuki, *Polym J*, 2014, **46**, 776-782.
13. J. K. Gupta, D. J. Adams and N. G. Berry, *Chem Sci*, 2016, **7**, 4713-4719.
14. M. Suzuki, Y. Nakajima, M. Yumoto, M. Kimura, H. Shirai and K. Hanabusa, *Langmuir*, 2003, **19**, 8622-8624.

15. M. Suzuki and K. Hanabusa, *Chem Soc Rev*, 2010, **39**, 455-463.
16. M. Suzuki, S. Owa, H. Shirai and K. Hanabusa, *Macromol Rapid Comm*, 2005, **26**, 803-807.
17. M. Suzuki, S. Owa, H. Shirai and K. Hanabusa, *J Polym Sci Pol Chem*, 2006, **44**, 3817-3824.
18. M. Yoshio, Y. Shoji, Y. Tochigi, Y. Nishikawa and T. Kato, *J Am Chem Soc*, 2009, **131**, 6763-6767.
19. L. Sardone, V. Palermo, E. Devaux, D. Credgington, M. De Loos, G. Marletta, F. Cacialli, J. Van Esch and P. Samori, *Adv Mater*, 2006, **18**, 1276-1280.
20. H. Hoshizawa, M. Suzuki and K. Hanabusa, *Chem Lett*, 2011, **40**, 1143-1145.
21. H. L. Guo and X. P. Zhao, *Opt Mater*, 2004, **26**, 297-300.
22. B. Comiskey, J. D. Albert, H. Yoshizawa and J. Jacobson, *Nature*, 1998, **394**, 253-255.
23. P. Murau and B. Singer, *J Appl Phys*, 1978, **49**, 4820-4829.
24. K. Matyjaszewski, *Isr J Chem*, 2012, **52**, 206-220.
25. K. Matyjaszewski, *Progress in Controlled Radical Polymerization: Mechanisms and Techniques*, 2012, **1100**, 1-13.
26. K. Matyjaszewski, *Macromolecules*, 2012, **45**, 4015-4039.
27. K. Huan, L. Bes, D. M. Haddleton and E. Khoshdel, *J Polym Sci Pol Chem*, 2001, **39**, 1833-1842.
28. Y. Nakagawa, P. J. Miller and K. Matyjaszewski, *Polymer*, 1998, **39**, 5163-5170.
29. H. Ihara, M. Takafuji, T. Sakurai, M. Katsumoto, N. Ushijima, T. Shirosaki and H. Hachisako, *Org Biomol Chem*, 2003, **1**, 3004-3006.
30. E. P. Boden and G. E. Keck, *J Org Chem*, 1985, **50**, 2394-2395.
31. D. J. Adams, K. Morris, L. Chen, L. C. Serpell, J. Bacsa and G. M. Day, *Soft Matter*, 2010, **6**, 4144-4156.
32. Y. B. Huang, I. Szleifer and N. A. Peppas, *Macromolecules*, 2002, **35**, 1373-1380.
33. N. Mohmeyer and H. W. Schmidt, *Chem-Eur J*, 2005, **11**, 863-872.
34. T. Kar, S. Debnath, D. Das, A. Shome and P. K. Das, *Langmuir*, 2009, **25**, 8639-8648.
35. A. Nese, J. Mosnacek, A. Juhari, J. A. Yoon, K. Koynov, T. Kowalewski and K. Matyjaszewski, *Macromolecules*, 2010, **43**, 1227-1235.
36. K. L. Beers, S. Boo, S. G. Gaynor and K. Matyjaszewski, *Macromolecules*, 1999, **32**, 5772-5776.
37. X. M. Tong, B. H. Guo and Y. B. Huang, *Chem Commun*, 2011, **47**, 1455-1457.
38. D. Neugebauer, B. S. Sumerlin, K. Matyjaszewski, B. Goodhart and S. S. Sheiko, *Polymer*, 2004, **45**, 8173-8179.
39. J. F. J. Coelho, E. Y. Carvalho, D. S. Marques, A. V. Popov, P. M. Goncalves and M. H. Gil, *Macromol Chem Physic*, 2007, **208**, 1218-1227.
40. K. L. Beers and K. Matyjaszewski, *J Macromol Sci Pure*, 2001, **38**, 731-739.
41. S. R. Holding, *Endeavour*, 1984, **8**, 17-20.
42. R. V, D. Baskaran and S. Sivaram, *Polymer*, 2004, **45**, 3149-3155.
43. D. P. Chatterjee and B. M. Mandal, *Macromolecules*, 2006, **39**, 9192-9200.
44. K. Matyjaszewski, D. A. Shipp, J. L. Wang, T. Grimaud and T. E. Patten, *Macromolecules*, 1998, **31**, 6836-6840.
45. P. Cacioli, D. G. Hawthorne, R. L. Laslett, E. Rizzardo and D. H. Solomon, *J Macromol Sci Chem*, 1986, **A23**, 839-852.
46. G. Raspoet, M. T. Nguyen, M. McGarraghy and A. F. Hegarty, *J Org Chem*, 1998, **63**, 6878-6885.
47. P. A. Hedin, R. C. Gueldner and A. C. Thompson, *Anal Chem*, 1970, **42**, 403-&.

48. M. Mukai, H. Minamikawa, M. Aoyagi, M. Asakawa, T. Shimizu and M. Kogiso, *Soft Matter*, 2012, **8**, 11979-11981.
49. B. Neises and W. Steglich, *Angew Chem Int Edit*, 1978, **17**, 522-524.
50. G. D. Pizarro, O. G. Marambio, M. Jeria-Orell, M. E. Flores and B. L. Rivas, *J Appl Polym Sci*, 2010, **118**, 3649-3657.
51. C. A. Roth, *Ind Eng Chem Prod Rd*, 1972, **11**, 134-&.
52. C. Cheng and J. F. Hartwig, *Chem Rev*, 2015, **115**, 8946-8975.
53. S. Coca, C. B. Jasieczek, K. L. Beers and K. Matyjaszewski, *J Polym Sci Pol Chem*, 1998, **36**, 1417-1424.
54. K. Matyjaszewski and J. H. Xia, *Chem Rev*, 2001, **101**, 2921-2990.
55. K. Ohno, A. Goto, T. Fukuda, J. H. Xia and K. Matyjaszewski, *Macromolecules*, 1998, **31**, 2699-2701.

Proposed Publication Paper 2

Self –assembly of poly(lauryl methacrylate)-*b*-poly(benzyl methacrylate) nano-objects synthesised by ATRP and their temperature-responsive dispersion properties

Self-assembly of poly(lauryl methacrylate)-*b*-poly(benzyl methacrylate) nano-objects synthesised by ATRP and their temperature-responsive dispersion properties

Melody Obeng[a*], Amir H. Milani[a], Muhamad S. Musa[a], Zhengxing Cui[a], Lee A. Fielding[a], Louise Farrand[b], Mark Goulding[b], Brian R. Saunders[a]
[a]School of Materials, The University of Manchester, Manchester, M13 9PL, UK
[b]Merck Chemicals Ltd, Chilworth Technical Centre, University Parkway, Southampton, SO16 7QD, UK

Abstract

Poly(lauryl methacrylate)-*b*-poly(benzyl methacrylate) ($PLMA_x$-$PBzMA_y$) diblock copolymers were synthesised for the first time using solution ATRP. The PLMA degree of polymerisation (x) was fixed at 14 and the PBzMA degree of polymerisation (y) was varied from 34 to 74. Post-polymerisation transfer of this new series of diblock copolymers from chloroform into *n*-dodecane (a poor solvent for PBzMA) resulted in self-assembly of polymeric nano-objects. The morphologies for the latter (spheres, worms and vesicles) were controlled by y. The observed morphologies generally agreed with those reported for related $PLMA_x$-$PBzMA_y$ diblock copolymers ($x \geq 16$) prepared by polymerisation induced self-assembly (PISA) *via* reversible addition-fragmentation chain transfer (RAFT) polymerisation (Fielding *et al., J. Amer. Chem. Soc.*, 136, 5790, 2014). However, a number of differences were observed such as de-gelation behaviour and the phase boundary positions compared to those expected from Fielding *et al.* Variable-temperature dynamic light scattering studies for the $PLMA_{14}$-$PBzMA_{34}$ spheres revealed that the aggregation number was unaffected by a temperature increase over the range of 20 – 90 ^{o}C which differed from the behaviour observed for $PLMA_{14}$-$PBzMA_{64}$ worms. This difference is a new observation with mechanistic importance for the worm-to-sphere breakdown mechanism. It was demonstrated that concentrated $PLMA_{14}$-$PBzMA_y$ dispersions (20 % w/w) in *n*-dodecane can be prepared using post-polymerisation transfer. The dispersion with a mixed spherical and worm-like copolymer phase showed reversible de-gelation when heated; whereas, the dispersions containing pure worm phase remained as white gels at all temperatures up to 90 °C. This study presents a new and potentially versatile ATRP method for preparing temperature-responsive nano-objects and gels in organic solvents that decouples chain growth and self-assembly

Introduction

Self-assembly of amphiphilic diblock copolymers into nano-objects is an important area of soft matter science, forming sophisticated nanomaterials with potentially useful properties[1-9], which includes new Pickering emulsifiers[8] and superflocculants[9]. The use of a selective solvent that is a good solvent for one of the blocks but a poor solvent for the other block triggers copolymer nano-object formation by self-assembly[10]. Depending on the packing parameter of the block copolymer a wide array of nano-objects can be obtained which include spheres, worms, and vesicles[5]. A common method for preparing such nano-objects is by means of polymerisation induced self-assembly (PISA) *via* reversible addition-fragmentation chain transfer (RAFT) polymerisation[10]. However, variations of RAFT polymerisation and alternative methods for preparing nano-objects are being actively pursued[11, 12] in order to expand architectural versatility and property performance. The majority of diblock copolymers prepared by PISA contain one block that has a glass transition temperature (T_g) higher than room temperature. This raises the question of the extent to which these nano-objects can be regarded as "living" in terms of their ability to reversibly disassemble. The latter question led us to investigate an alternative solution-based synthetic method to prepare a self-assembling organic solvent dispersible diblock copolymer. In this study poly(lauryl methacrylate)-*b*-poly(benzyl methacrylate) diblock copolymers (PLMA-PBzMA) prepared using atom transfer radical polymerisation (ATRP) were investigated. The hypothesis for this study was that self-assembly of PLMA-PBzMA nano-objects would be independent of the copolymer synthesis method. The motivation for this study was to develop concentrated (gel-forming) dispersions of self-assembled nano-objects with morphologies and properties that could have potential application in electronic paper display (EPD) technology.

The self-assembly of amphiphilic copolymers into cylindrical (worm-like) polymer micelles using RAFT-based PISA in aqueous[13-16] and non-polar solvents[17-21] is well established. For this work diblock copolymers that self-assembled into gel-forming nano-objects in a non-polar solvent (*n*-dodecane) were of prime concern. Physical gels formed from an organic fluid have a range of potential applications which includes delivery[22, 23], cosmetics[24] and energy transfer[25]. Fielding *et al.* synthesised a series of $PLMA_x$-$PBzMA_y$ ($x \geq 16$) diblock copolymers using RAFT-based PISA in *n*-dodecane[26]. Systematic variation of the PLMA and PBzMA block lengths enabled spherical, worm-like and vesicle morphologies to be prepared. The worms formed temperature-responsive gels, which reversibly de-gelled at temperatures

above 50 °C. Derry *et al.* investigated similar diblock copolymers whilst focusing on the effect of solvent nature on nano-object morphology[27]. Whilst the PISA approach has achieved a considerable success[10] there are some limitations which may constrain versatility. Firstly, the corona-forming block must be soluble in the selective solvent used and the latter must be a thermodynamically bad solvent for the core-forming block. Furthermore, the sulphur-based end groups may be undesirable for some industrial applications as they confer colour and a degree of toxicity[28]. Whilst end-group modification methods are known[29], additional synthetic steps are required which would add to cost. Here, we use a potentially versatile solution based ATRP method to synthesise PLMA-PBzMA copolymers in a good solvent for both blocks. Because our new approach to PLMA-PBzMA nano-object preparation decouples copolymer synthesis from self-assembly, and should apply to other copolymers, it offers new versatility for nano-object formation.

ATRP and other living polymerisation methods such as ring-opening polymerisation have been widely used to prepare a number of self-assembled copolymers[30-34]. ATRP is a versatile method for the synthesis of diblock copolymers and enables high blocking efficiencies with targeted block lengths, well-defined architectures and is well-suited to the polymerisation of many vinyl monomers with diverse functionalities[35]. However, there have been relatively few reports of the use of ATRP to prepare polymer worms. Banerjee *et al.* described using ATRP in xylene to prepare worm-like nanostructures from poly(chloromethyl styrene)-*g*-poly(benzyl methacrylate)[36] with average lengths less than 100 nm. Worm-like nanostructures were also reported to self-assemble in bulk films of poly(methyl methacryate)-*b*-poly(azobenzene methacrylate)[37]. There have not been any reports using ATRP to prepare PLMA-based nano-objects to the best of our knowledge.

The approach used in the present study is depicted in Scheme 1a. A $PLMA_{14}$-Br macroinitiator (abbreviated as L_{14}) was prepared *via* ATRP of lauryl methacrylate (LMA), followed by solution ATRP of benzyl methacrylate (BzMA) to give $PLMA_{14}$-$PBzMA_y$. The copolymer was dissolved in a low boiling point good solvent for both blocks (chloroform, Scheme 1b) and then added to a high boiling point selective solvent (*n*-dodecane), which is a good solvent for the PLMA block. The chloroform was then removed by evaporation. The PBzMA and PLMA blocks formed, respectively, the core and corona of the nano-objects. In this study, we investigate the effect of PBzMA degree of polymerisation, i.e., *y*, on the

morphology and response to temperature of the self-assembled $PLMA_{14}$-$PBzMA_y$ nano-objects and gels.

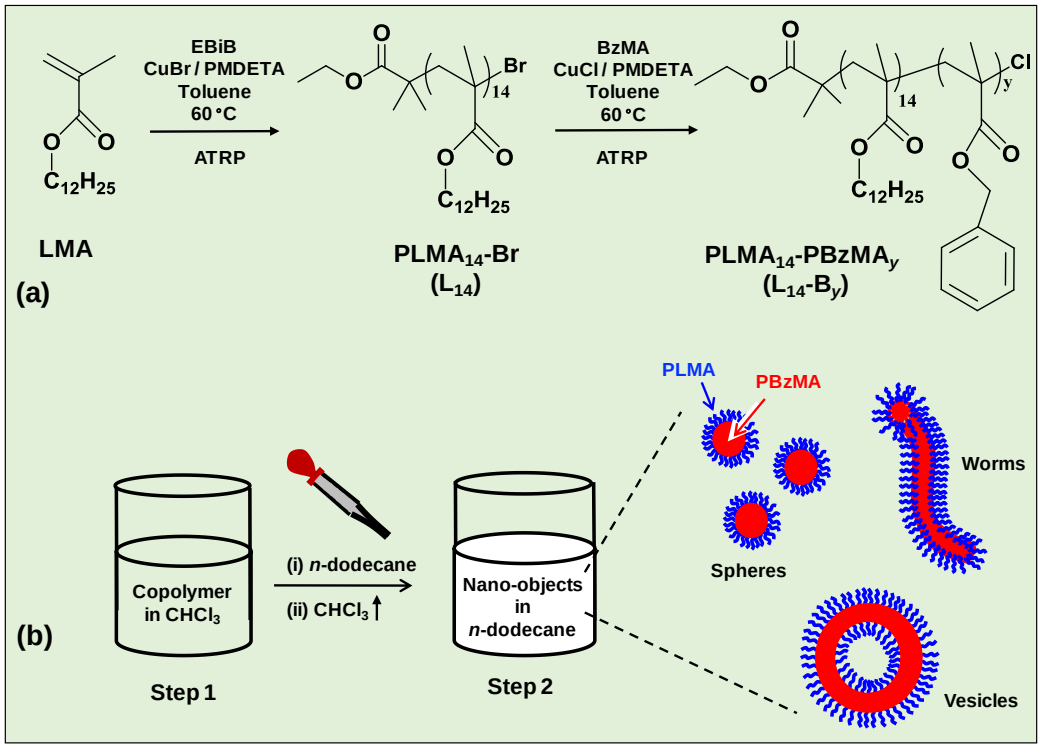

Scheme 1 (a) Depiction of the synthesis of poly(lauryl methacrylate) macroinitiator ($PLMA_{14}$-Br) *via* solution ATRP using α-bromoisobutyrate (EBiB) and subsequent addition of benzyl methacrylate (BzMA) *via* halogen exchange through the use of CuCl/PMDETA to form $PLMA_{14}$-$PBzMA_y$. (b) Self-assembly of nano-objects was achieved by post-polymerisation transfer which involved replacing a volatile good solvent for both blocks (chloroform, Step 1) with a selective solvent (*n*-dodecane) for PLMA (Step 2). Spherical, worm-like or vesicle-like nano-objects assembled depending on the value for *y*.

The factors governing the self-assembly of non-ionic diblock copolymers in water are well understood[38]. The two dominant free energy contributions are the elastic energy (entropic) of the corona and surface energy of the core. The elastic energy of stretched chains within the core also contributes to the total free energy of the system. As the morphology changes from spheres, to worms and then to vesicles the stretching of the chains in the core decreases; however, the crowding of the chains within the corona increases[39]. The design rules governing nano-object morphology for diblock copolymers in non-polar solvents are still being established and the extent to which the nano-objects are at equilibrium is of considerable interest[10]. In the present study, we systematically vary the degree of polymerisation of the core-forming block (PBzMA) and probe temperature-triggered PLMA-

PBzMA nano-object morphology and gelation changes in dilute and concentrated *n*-dodecane dispersions.

In the first part of the study the diblock copolymers are characterised by GPC and ^{1}H NMR spectroscopy. Nano-object morphology and self-assembly behaviours are then explored using TEM and variable temperature ^{1}H NMR spectroscopy and dynamic light scattering (DLS). Physical observations and dynamic rheology studies involving concentrated dispersions prepared using post-polymerisation transfer are then considered. These studies show that the mixed spherical and worm-like compositions are capable of forming temperature responsive physical gels. By comparing the temperature-triggered nano-object and gel-to-fluid transformations of the spheres and worms it was found that the PBzMA degree of polymerisation controls the extent of reversibility. The results of this study show that the self-assembly of PLMA-PBzMA copolymers is generally independent of the synthesis method. However, the copolymers used in this study also show differences in the morphologies and properties which are discussed.

Experimental Section

Materials

LMA (96 %) was purified using a basic alumina column before use. BzMA, (96 %) was passed through a 1/1 neutral/basic alumina column before use. Toluene (99.5 %), ethyl α-bromoisobutyrate (EBiB, 98 %), *N*,*N*,*N′*,*N″*,*N‴* - pentamethyldiethylenetriamine (PMDETA, 99 %), copper bromide (CuBr, 99.999 %) and copper chloride (CuCl, ≥ 99.995 %) were all purchased from Aldrich and used as received. Chloroform (ACS reagent grade), methanol (HPLC grade), tetrahydrofuran (HLPC grade) were all purchased from Fisher and used as received. Chloroform-d (99.8 atom % D), dodecane-d_{26} (98 atom % D) and *n*-dodecane (99+ %) were purchased from Aldrich and Alfa Aesar, respectively, and were used as received..

Synthesis of PLMA-Br macroinitiator

The $PLMA_{14}$-Br macroinitiator (L_{14}) synthesis was adapted from a literature method[40]. The ATRP homopolymerisation was terminated at 64 % monomer conversion to retain a high percentage of bromo-terminated moieties for the subsequent diblock growth step[41]. A Schlenk flask was charged with toluene (2 ml), LMA (10 mL, 34.1 mmol), EBiB (220.0 μL, 1.55 mmol) and PMDETA (323.0 μL, 1.55 mmol). The reagents were deoxygenated with Ar whilst stirring magnetically at room temperature and subjected to repeated freeze-pump-thaw cycles. CuBr (0.22 g, 1.55 mmol) was quickly added to the frozen mixture under Ar during the final cycle. The sealed reaction flask was immersed in a pre-heated oil bath at 60 °C for 150 min. The reaction mixture was passed through a basic alumina column and precipitated from excess methanol to isolate L_{14}. L_{14} was then dried in a vacuum oven at 30 °C for 12 h. The mass of purified L_{14} was 6.2 with a percentage yield of 61.9 %. L_{14} was confirmed *via* ^{1}H NMR. ^{1}H NMR (400MHz, $CDCl_3$): δ (ppm) = 4.1 (m, 2H, CH_3-C**H$_2$**-), 4.0 (s, 2H, -C(=O)O-C**H$_2$**-), 1.8-2.0 (m, 2H, -C**H$_2$**-C-CH_3-), 1.6 (s, 2H, -C(=O)O-CH_2-C**H$_2$**-), 1.3 (s, 18H, -C_9**H$_{18}$**-), 1.1 (m, 3H, C**H$_3$**-CH_2-), 0.9 (s, t, 6H, -CC**H$_3$**-C(=O)O-CH_2-$(CH_2)_{10}$-C**H$_3$**).

PLMA-PBzMA diblock copolymer synthesis

Table 1 shows the compositions and codes for the $PLMA_{14}$-$PBzMA_y$ copolymers. L_{14}-B_{34} represents the $PLMA_{14}$-$PBzMA_{34}$ copolymer. The following gives an example synthesis for L_{14}-B_{34}. The molar ratio of monomer [M], initiator [I], Cu(I) [Cu(I)] and ligand [L] used were

37:1:0.8:0.8. Accordingly, a Schlenk flask was charged with the L_{14} (0.5 g, 0.133 mmol) that had been dissolved in toluene (3.63 mL), followed by BzMA (1.50 mL, 8.911 mmol) and PMDETA (23.0 μL, 0.11 mmol). The reagents were deoxygenated with Ar whilst stirring magnetically at room temperature before being subjected to repeated freeze-pump-thaw cycles. CuCl (11 mg, 0.11 mmol) was quickly added to the frozen mixture under Ar during the final cycle. The sealed reaction flask was immersed in an oil bath at 60 °C for 15 h. The resulting copolymer was passed through a 1/1 neutral/basic alumina column before being purified and dried as described for L_{14}. The same method as described above was used to prepare L_{14}-B_{46}, L_{14}-B_{64} and L_{14}-B_{74}. For those copolymers the molar ratios for [M]:[I]:[Cu(I)]:[L] were [M]:1:0.8:0.8 with [M] = 50, 67 and 80, respectively. The monomer conversions for all copolymers were in the range of 92 to 96%. Percentage yield of L_{14}-B*y* copolymers were 78 to 83 %. High purity of L_{14}-B*y* copolymers was confirmed *via* ^{1}H NMR. ^{1}H NMR (400MHz, $CDCl_3$): δ (ppm) = 7.3 (m, 5H, -$C_5\mathbf{H_5}$), 4.9 (d, 2H, -C(=O)O-C$\mathbf{H_2}$-), 1.5-2.1 (m, 6H, -C$\mathbf{H_2}$-CCH_3-C(=O)O-CH_2-C$\mathbf{H_2}$-$C_{10}H_{21}$, -C$\mathbf{H_2}$$CCH_3$-C(=O)O-$CH_2$-$C_5H_5$), 1.3 (s, 18H, -$C_9\mathbf{H_{18}}$-) and 0.9-1.2 (s, m, 6H, -CC$\mathbf{H_3}$C(=O)O-CH_2-$(CH_2)_{10}$-C$\mathbf{H_3}$)

Table 1 Compositions and characterisation data for the macroinitiator and copolymers.

Code	Composition[a]	$M_{n(NMR)}$ / g / mol	$M_{n(GPC)}$ / g / mol	M_w / M_n	d_z / nm [b]	Morphology [c]
L_{14}	$PLMA_{14}$	3,800	4,900	1.31	-	-
L_{14}-B_{34}	$PLMA_{14}$-$PBzMA_{34}$	9,700	13,700	1.50	39	Spheres
L_{14}-B_{46}	$PLMA_{14}$-$PBzMA_{46}$	11,800	15,400	1.50	-	Spheres & Worms
L_{14}-B_{64}	$PLMA_{14}$-$PBzMA_{64}$	15,000	20,900	1.58	480	Worms
L_{14}-B_{74}	$PLMA_{14}$-$PBzMA_{74}$	16,700	22,600	1.55	-	Vesicles

[a] Compositions determined from ^{1}H NMR spectroscopy. [b] Apparent sphere-equivalent *z*-average diameter of the diblock copolymers measured at 20 ^{o}C. [c] Morphologies based on TEM data (Fig. 2).

Physical measurements

Gel permeation chromatography (GPC) was performed using a Max Viscotek instrument that comprised two mixed B columns (average porosity of 500 Å). The eluent was THF and calibration was performed using linear polystyrene standards. The standards had molecular

weights ranging of 1 x 10^3 to 2 x 10^6 g mol^{-1} and a Viscotek VE 3580 refractive index detector was used. ^{1}H NMR spectroscopy was conducted using a Bruker AVI-400 MHz spectrometer and $CDCl_3$ as the solvent. Variable-temperature ^{1}H NMR spectroscopy was conducted using a Bruker Instrument (AVI-500 MHz spectrometer) using dodecane-d_{26}. The copolymer dispersion was prepared by dissolving neat copolymer in chloroform (20 μL). The solution was then transferred into the appropriate volume of dodecane-d_{26} and chloroform evaporated with stirring at 40 ^{o}C for 48 h to give a dispersion (5.0 % w/w). DLS studies were conducted using a Zetasizer Nano-ZS instrument (Malvern Instruments, UK) at a fixed scattering angle of 173^o. The copolymer dispersions underwent 20 to 90 to 20 ˚C temperature cycles with an equilibration time of 5 min at each temperature. The *z*-average diameters (d_z) correspond to sphere-equivalent values for the worm-containing systems. The dispersions used for DLS (0.1 % w/w) used *n*-dodecane and were prepared in a similar method as described above. For transmission electron microscopy (TEM) samples diluted dispersions in *n*-dodecane (0.05 % w/w) were used. The dispersion was deposited on a carbon-coated grid before being exposed to ruthenium tetra-oxide vapour for 10 min. TEM measurements were obtained using a Philips CM20 200 kV instrument. Average sizes determined from TEM were obtained by counting 94 spheres, 27 worms and 32 vesicle shells. Dynamic rheology measurements were conducted using an AR-G2 rheometer equipped with aluminium cone geometry (2° and 20 mm diameter). Measurements were conducted using a strain of 1.0 % and gap of 800 - 1200 μm. Variable-temperature studies were conducted at a frequency of 1 Hz with a ramping rate of 1 ◦C min^{-1} and an equilibration of 5 min for each step. The dispersions (20 % w/w in *n*-dodecane) measured by rheology were prepared as described above using concentrated copolymer solutions in chloroform (~ 45 % w/w) and subsequent chloroform removal.

Results and Discussion

Macroinitiator and diblock copolymer characterisation

The macroinitiator was synthesised *via* solution ATRP of LMA in toluene (Scheme 1a). The ^{1}H NMR spectrum (Fig. 1a) enabled calculation of the number-average degree of polymerisation (x) *via* end group analysis using Equation 1.

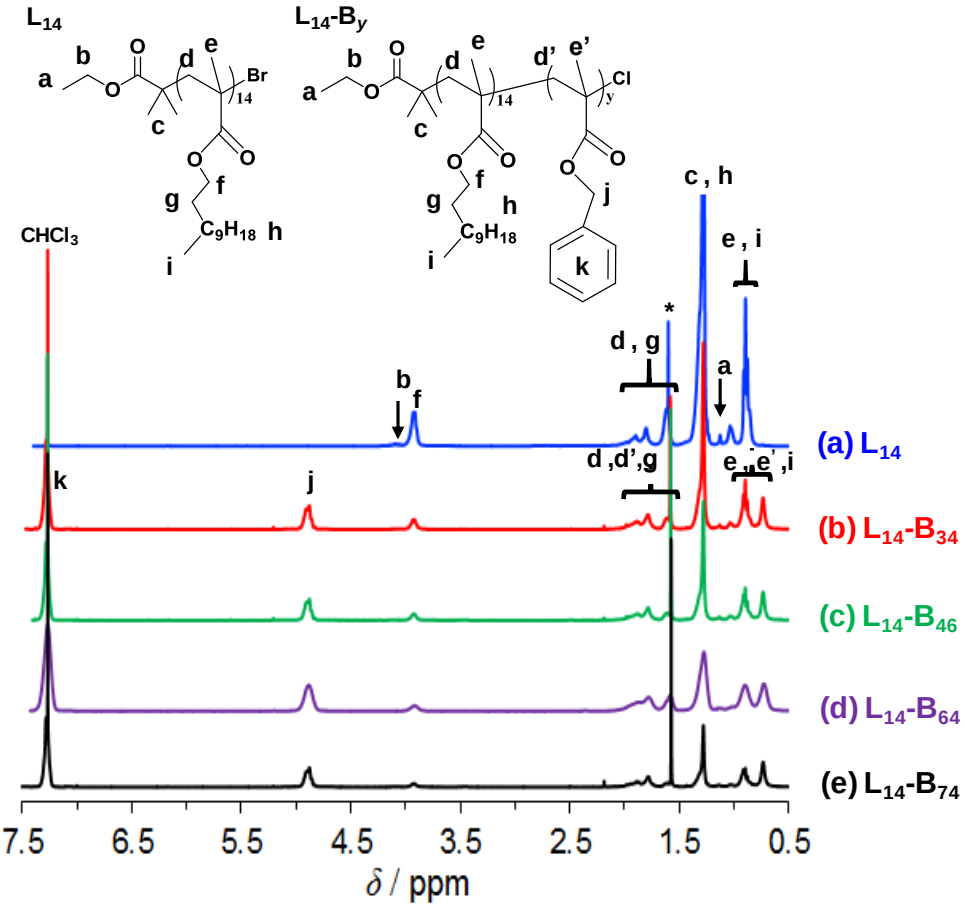

Fig. 1 ^{1}H NMR spectra for the macroinitiator (L_{14}) and the diblock copolymers. The identities are shown. The peak labelled with * was due to water.

$$x = \frac{1}{6}\left(\left(\frac{A_h + A_c}{A_a}\right) - 2\right) \qquad (1)$$

For the above equation A_h, A_c and A_a correspond to the integrals of the proton signals from PLMA (**h**), the methyl groups of EBiB **(c**) and the terminal methyl group of EBiB (**a**). The calculated x was 14.0, which was significantly lower than those reported previously for PLMA-PBzMA diblock copolymers prepared *via* RAFT-based PISA (x > 16) by Fielding *et al.*[26] and Derry *et al.*[27]. Consequently, the diblock $PLMA_{14}$-$PBzMA_y$ copolymers reported

here are a new series of copolymers. The GPC data (Fig. S2 and Table 1) gave an M_n of 4,900 g mol^{-1} and a polydispersity of 1.31. The latter value is in the range reported for other PLMA homopolymers prepared by ATRP[40, 42, 43].

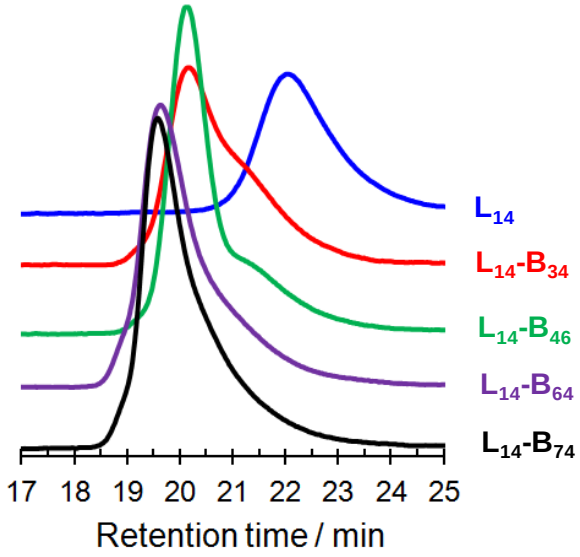

Fig. 2 GPC chromatograms for the macroinitiator (L_{14}) and the diblock copolymers (L_{14}-B_{34} – L_{14}-B_{74}). The chromatograms were obtained using THF eluent and polystyrene standards.

$PLMA_{14}$-$PBzMA_y$ copolymer synthesis was conducted using L_{14} and Cu(I)Cl following the halogen exchange method[44, 45] (Scheme 1a). It was discovered that the latter approach[46, 47] was essential to prepare the diblock copolymers and minimise their polydispersity (see Chapter 3). After PBzMA polymerisation the ^{1}H NMR spectra (Fig. 1b - e) showed that signals from the BzMA methylene protons (4.7 ppm, **j**) and aromatic protons (7.3 ppm, **k**) were present, as expected[48]. The relative intensity from the PLMA oxyethylene group (4.0 ppm, **f**) decreased after the growth of the PBzMA block. The number-average value for *y* was calculated using the integration values for the methylene PBzMA group (**j**) and the values for the methylene groups from PLMA (**h**) and the methyl groups from EBiB **(c**) using Equation 2.

$$y = (9x + 3)\left(\frac{A_j}{A_h + A_c}\right) \qquad (2)$$

The *y* values can be seen from the $PLMA_{14}$-$PBzMA_y$ compositions shown in Table 1. The GPC chromatograms indicated that the diblock copolymers were mostly monomodal (Fig. 2) with polydispersities in the range of 1.50 - 1.58 (Table 1). It was challenging to gain control over BzMA chain growth and consequently a switch of catalyst was used in this work

(Scheme 1a). It is likely that a minor proportion of dead PLMA chains were present which subsequently contributed to the polydispersity of the copolymers.

Temperature-responsive nano-objects assembled from $PLMA_{14}$-PBzMA*y*

A key difference between the method used here and PISA[18] is that the ATRP approach used copolymer synthesis under good solvency conditions. The formation of nano-objects involved the transfer of the diblock copolymer from a chloroform solution (which is a good solvent for both blocks) into the selective solvent *n*-dodecane (Scheme 1b) followed by chloroform removal (See Experimental section). ^{1}H NMR analysis indicated a very low content of residual chloroform (less than 0.2 vol.%) remained after this treatment. TEM data for L_{14}-B_{34} deposited from *n*-dodecane showed spheres with low size polydispersity (Fig. 3a). The other three systems showed mixtures of spheres and worms (L_{14}-B_{46}, Fig. 3b), worms (L_{14}-B_{64}, Fig. 3c) and vesicles (L_{14}-B_{74}, Fig. 3d).

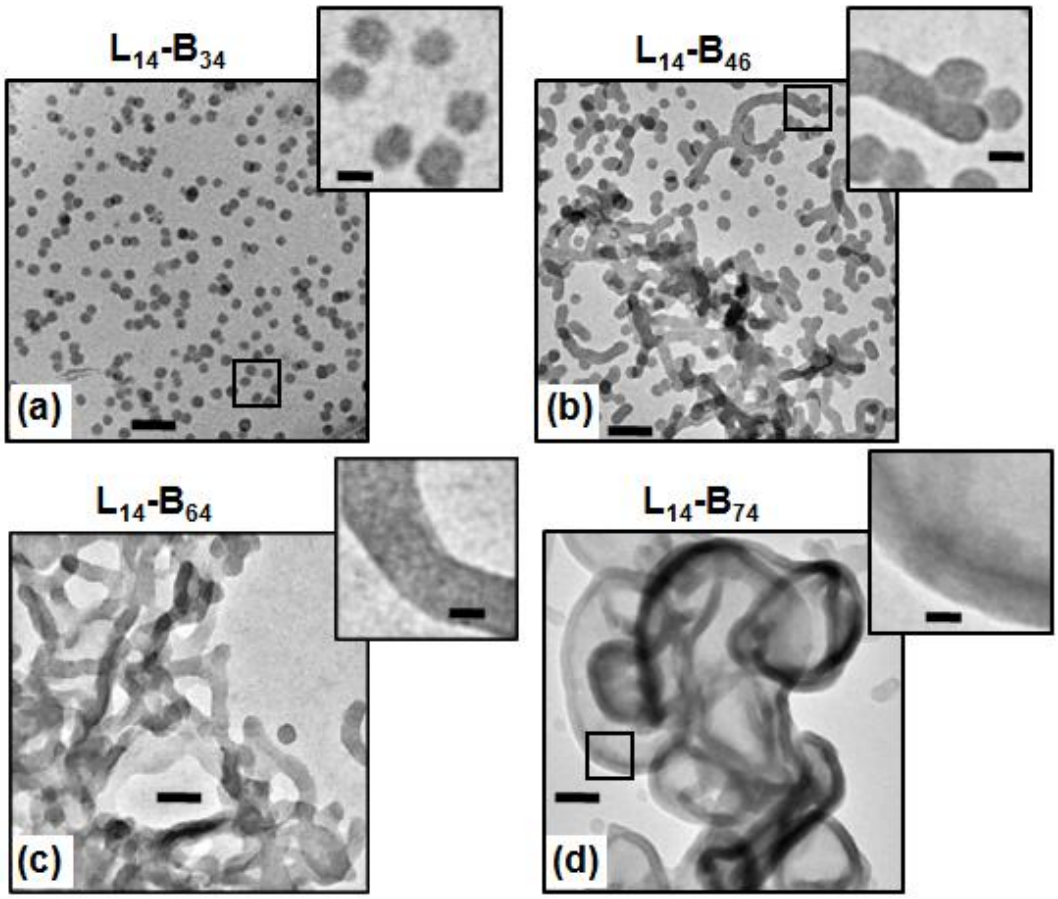

Fig. 3 TEM images of diblock copolymer nano-objects deposited from *n*-dodecane dispersions. The samples were stained with ruthenium tetra-oxide. The scale bars in the main and inset figures represent 200 and 20 nm, respectively.

Additional TEM images obtained using lower magnifications are shown in Fig. 4. Whilst there were occasional spheres present for L_{14}-B_{64} and L_{14}-B_{74} the overwhelming majority of the copolymer was present as worms or vesicles, respectively. The vesicles had a range of sizes with some less than 100 nm (Fig. 4d).

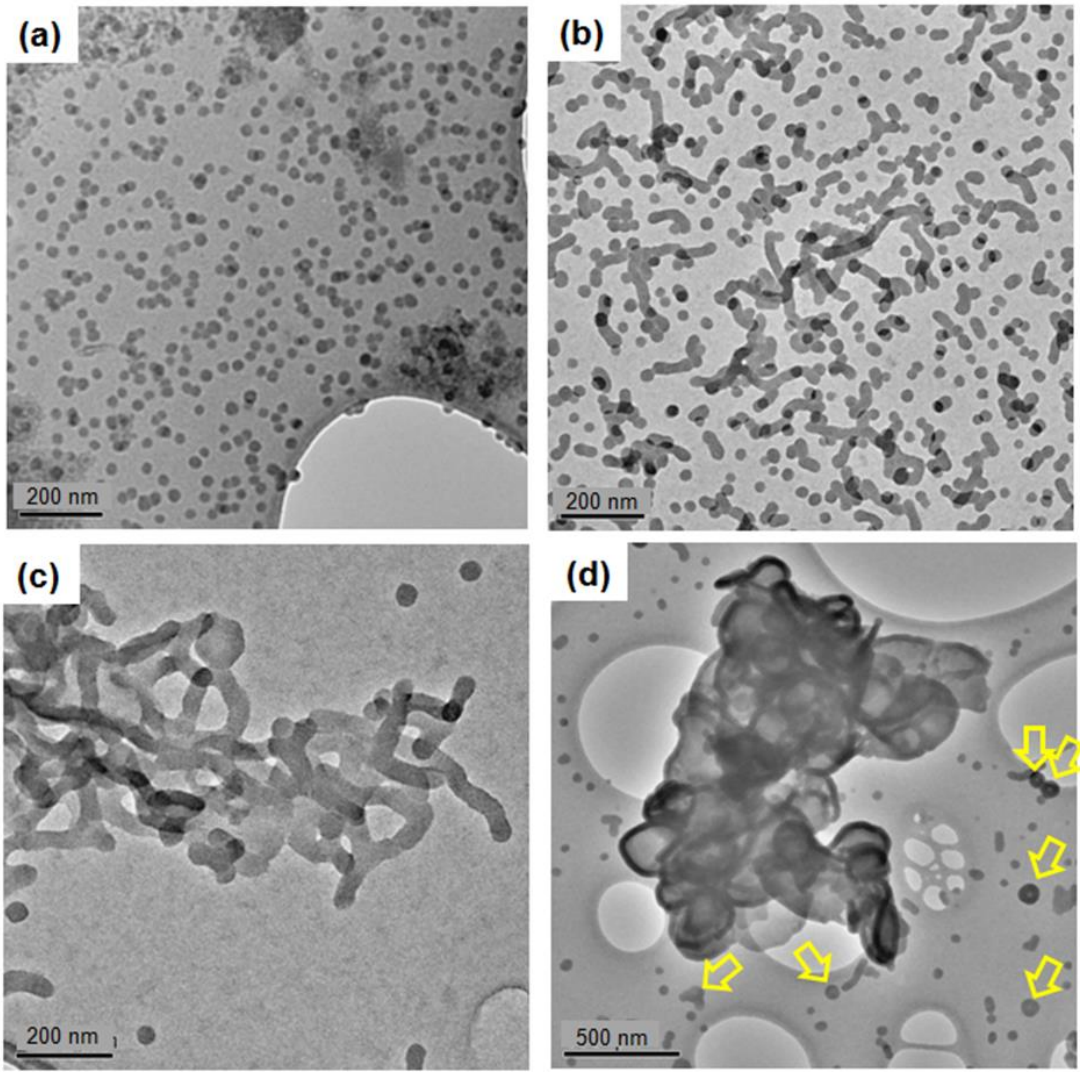

Fig. 4 Low magnification TEM images of diblock copolymer nano-objects deposited from *n*-dodecane dispersions containing (a) L_{14}-B_{34}, (b) L_{14}-B_{46}, (c) L_{14}-B_{64} and (d) L_{14}-B_{74}. The samples were stained with ruthenium tetra-oxide. The arrows in (d) highlight small vesicles.

The number-average diameter of the spheres (L_{14}-B_{34}) was 20.5 ± 2.3 nm whilst the worms (L_{14}-B_{64}) had an average cross-sectional diameter of 38.5 ± 3.4 nm. The vesicles (from L_{14}-B_{74}) had diameters larger than 200 nm and an average wall thickness of 24.0 ± 1.6 nm. These morphologies are in accord with the reduction of strain for the PBzMA core chains afforded by the decrease in curvature associated with the transitions from spheres to worms and then vesicles[5, 49]. The TEM images show that the PLMA-PBzMA nano-objects prepared *via*

ATRP had the same *general* morphologies as those reported for $PLMA_x$-$PBzMA_y$ ($x \geq 16$) diblock copolymers prepared by PISA[26]. It follows that thermodynamics had a strong role in controlling PLMA-PBzMA nano-object morphology.

To provide a better comparison of the morphologies of $PLMA_{14}$-$PBzMA_y$ nano-objects prepared here by ATRP with the $PLMA_x$-$PBzMA_y$ ($x \geq 16$) nano-objects prepared using PISA,[26] the morphological data from both studies were plotted on a common phase diagram (Fig. 5).

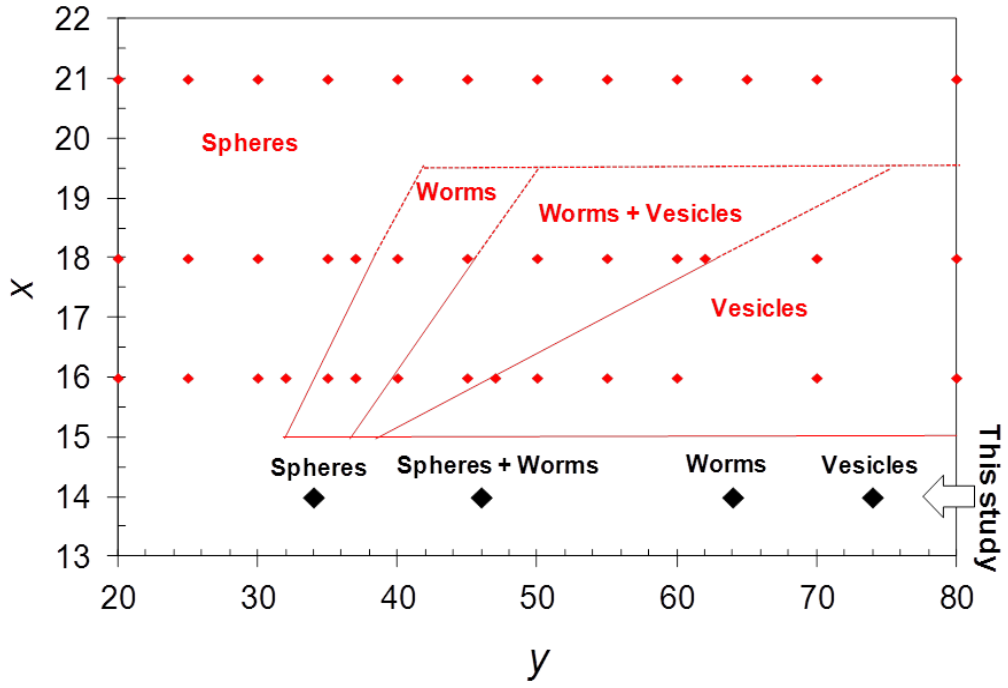

Fig. 5 Phase diagram comparing ATRP-based $PLMA_{14}$-$PBzMA_y$ diblock copolymer nano-objects from the present study (black diamonds and labels) with those prepared by non-aqueous RAFT dispersion polymerisation from Fielding *et al.* [26] (red diamonds and labels).

In agreement with the results of Fielding *et al.*[26], as *y* increased the morphology changed from spheres, to worms and then vesicles. However, the positions of the nano-object phases identified from this study are not in the positions expected if the phase boundary lines from Fielding *et al.*[26] are extrapolated to the PLMA degree of polymerisation value of 14.0. For example, L_{14}-B_{64} existed as worms at a much higher *y* value than expected. Furthermore, L_{14}-B_{34} existed as spheres in this work; whereas L_{16}-B_{37} from Fielding *et al.*[26] formed worms. Considering these morphological differences, it was plausible to question whether the *x* or *x*/*y* values were the more pertinent parameter. The *x*/*y* values for L_{14}-B_{34} (this study) and L_{16}-B_{37}

(from Ref. [26]) were 0.41 and 0.43, respectively. These *x*/*y* values were within 5% of each other and are not considered distinguishable. Therefore, the differences in morphologies for these two systems cannot be explained using *x*/*y* values. However, the *x* values were significantly different.

Whilst differences in copolymer polydispersities and possibly end group effects may have contributed to the morphological differences it does appear that the phase boundary positions for these self-assembling copolymers depends on the manner in which the copolymers are synthesised. The presence of a mixed phase for L_{14}-B_{46} (Fig. 3b) is a feature frequently reported for this family of self-assembling copolymers[27, 50, 51]. Worm formation and growth is believed to involve fusion of cores which is a relatively slow process[52]. Consequently, it is suggested that incomplete sphere fusion, due to the relatively low value for *y*, was responsible for the mixed phase (Fig. 3b). However, we cannot rule out a morphological contribution from chain polydispersity.

Ruthenium tetra-oxide reacts preferentially with double bonds and enables contrast to be enhanced for TEM[53, 54]. Here, we used this species to stain the PBzMA blocks within the spheres (Fig. 3a), which enabled the number-average diameter (d_{TEM}) of 20.5 nm to be used as a measure of the L_{14}-B_{34} core diameter. The repeat unit length (l) for BzMA was calculated using Equation 3.

$$l = 0.125 \times 2 \qquad \textbf{(3)}$$

From the above equation l is estimated as ~ 0.25 nm. The fully stretched length ($l_{stretch}$) for a $PBzMA_{34}$ was calculated using Equation 4.

$$l_{stretch} = yl \qquad \textbf{(4)}$$

From the above equation, y was taken as 34 resulting in the fully stretched length for a $PBzMA_{34}$ chain as ~ 8 nm. The diameter of a micelle core (d_{max}) of fully stretched PBzMA chains was calculated using Equation 5:

$$d_{max} = 2l_{stretch} \qquad \textbf{(5)}$$

Consequently, the diameter of a micelle core of fully stretched PBzMA chains would be ~ 16 nm, which is close to d_{TEM}. It follows that the PBzMA chains were highly stretched in the L_{14}-B_{34} micelle cores. The number of aggregated L_{14}-B_{34} chains of a sphere could be

determined from considering the mass of one PBzMA chain (m_{PBzMA}) and the mass of an average sphere (m_{sphere}). The value for m_{sphere} was determined using Equation 6:

$$m_{sphere} = \frac{\pi \rho_{PBzMA} d_{TEM}^3}{6} \qquad \textbf{(6)}$$

whereby the density of PBzMA (ρ_{PBzMA}) was taken as[55] 1.18 g/cm^3 and the number-average diameter of the sphere obtained from TEM (d_{TEM}) was 20.5 nm. Also, the value for m_{PBzMA} was determined using Equation 7:

$$m_{PBzMA} = \frac{MW_{PBzMA}}{N_A} \qquad \textbf{(7)}$$

whereby MW_{PBzMA} is molecular weight of the PBzMA segment (34 x 176 g/mol = 5984 g/mol) and N_A is Avogadro's number. Thus, it follows that the value for m_{sphere} is 5.3 x 10^{-18} g and m_{PBzMA} is 1.0 x 10^{-20} g. Furthermore, the values for m_{PBzMA} and m_{sphere} were used to determine the aggregation number (N_{agg}) of PBzMA chains using Equation 8:

$$N_{agg} = \frac{m_{sphere}}{m_{PBzMA}} \qquad \textbf{(8)}$$

From the above equation N_{agg} was calculated as 530. This estimation assumed that solvation of the core did not occur at room temperature which is consistent with ^{1}H NMR data (below) and has previously been shown for related systems[21].

From the average surface area of the L_{14}-B_{34} spheres and the N_{agg} value an average separation of the PLMA chains could be determined. Firstly, the surface area of a sphere (A_{sphere}) was calculated using Equation 9.

$$A_{sphere} = \pi d_{TEM}^2 \qquad \textbf{(9)}$$

From the above equation A_{sphere} was calculated as 1.3 x 10^{-15} m^2. Secondly, the area per chain (A_{chain}) was calculated as 2.5 nm^2 by using Equation 10.

$$A_{chain} = \frac{A_{sphere}}{N_{agg}} \qquad \textbf{(10)}$$

Considering the above equation, the average separation of the PLMA chains at the surface would be ~ 1.6 nm assuming a cubic lattice. The latter value can be compared to the diameter of a cross-sectional slice of a PLMA cylinder which can be shown to be ~ 6 nm. This

geometric analysis suggests that the PLMA chains were sterically crowded in the micelle corona. It follows that both blocks of the copolymer that formed the spheres were in somewhat entropically unfavourable environments. It is likely that the micelles were preferred because of the strong (enthalpic) incompatibility between PBzMA and *n*-dodecane at room temperature.

Temperature-triggered morphology transitions

The effect of temperature on the local environments of the PBzMA and PLMA blocks was probed using variable-temperature ^{1}H NMR spectroscopy for the L_{14}-B_{34} (spheres) and L_{14}-B_{64} (worms) dispersed in dodecane-d_{26} (Fig. 6). With increasing temperature, both the methylene signal from PBzMA at 4.9 ppm (**j**) and the PLMA oxyethylene group (**f**) increased in intensity (Fig. 6a and b). The latter trend is consistent with related data reported for $PLMA_{16}$-$PBzMA_{37}$ prepared by PISA[26]. The increases in the signal intensities apparent from scrutiny of Fig. 6a and b indicate that solvation increased for both blocks with temperatures greater than or equal to 40 ^{o}C. Interestingly, relatively enhanced solvation occurred for the PBzMA block at higher temperatures as can be seen from Fig. 6c which shows the ratio of the integrals (A_j/A_f) for the PBzMA and PLMA signals. The onset temperatures for enhanced PBzMA solvation were about 55 and 70 ^{o}C, respectively, for both L_{14}-B_{34} and L_{14}-B_{64}. This may indicate that the shorter $PBzMA_{14}$ chains were more easily solvated. Upon cooling the signals corresponding to PBzMA groups were not detectable (Fig 6a and b) which shows that the solvation changes were fully reversible for both the spheres and worms.

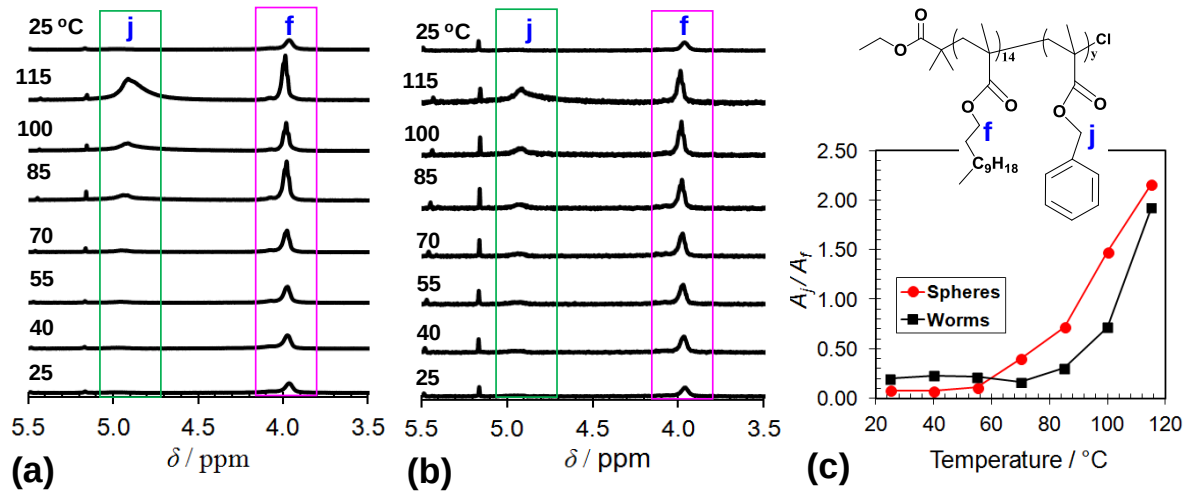

Fig. 6 Variable-temperature ^{1}H NMR spectra for dilute dispersions of (a) L_{14}-B_{34} and (b) L_{14}-B_{64} in dodecane-d_{26}. The temperature was increased from 25 to 115 °C before cooling to 25 °C. (c) Signal integral ratios of **j** to **f** for the dispersions containing L_{14}-B_{34} spheres (red circles) and L_{14}-B_{64} worms (black squares).

The response of the dispersions of spheres (L_{14}-B_{34}) and worms (L_{14}-B_{64}) to elevated temperatures was also studied using variable temperature DLS. Whilst related data were published for $PLMA_{16}$-$PBzMA_{37}$ worms prepared by PISA[26], variable d_z data for spheres have not been reported. Considering the spheres first (Fig. 7a) the d_z range of 37 - 39 nm at 20 °C is larger than the TEM-derived number-average core diameter of 20.5 nm. A sphere consisting of a 20.5 nm core and corona of $PLMA_{14}$ chains with a fully extended backbone would have a calculated total diameter of 27 nm. If the LMA chains were forced to protrude outwards due to lateral crowding (as discussed above) an extra 6 nm could be added, resulting in a total diameter of ~ 33 nm. Taking into account chain polydispersity and the fact that the d_z values are strongly weighted by the largest spheres, which scatter more light, it is reasonable to attribute the d_z range at 20 °C to spherical L_{14}-B_{34} micelles.

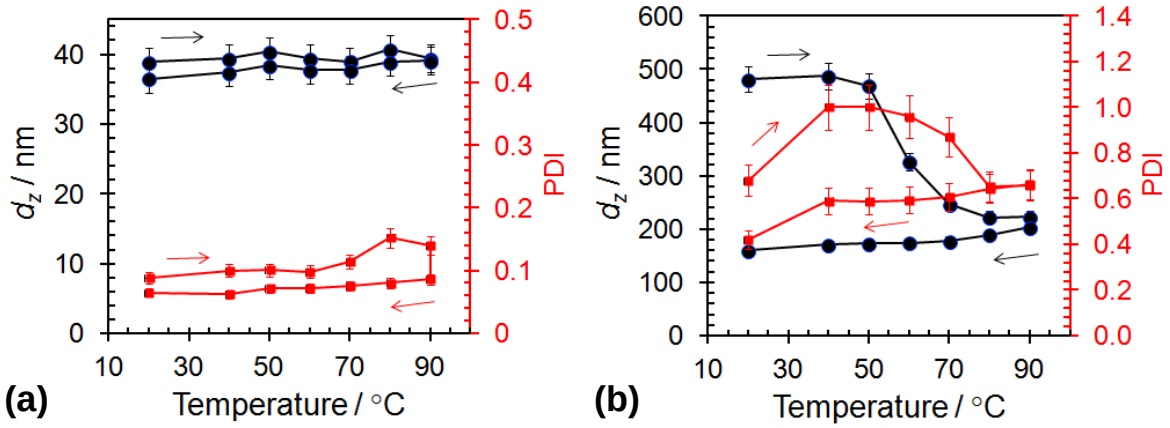

Fig. 7 Variable-temperature DLS data for dispersions of (a) L_{14}-B_{34} spheres and (b) L_{14}-B_{64} worms. The *z*-average diameter is represented by blue circles, while the polydispersity index is represented by red squares. The arrows indicate the directions of temperature ramps. The initial and final temperatures were 20 °C.

The variable-temperature DLS data for the spheres (Fig. 7a) shows that d_z did not change significantly over the temperature range of 20 – 90 °C. The polydispersity of the spheres decreased slightly due to heating. The invariance of d_z with temperature is noteworthy because the core PBzMA chains became increasingly solvated with increasing temperature (as discussed above in connection with Fig. 6) and must, therefore, have occupied an increasingly larger (average) volume. An increase in diameter of 2 nm for the spheres (from 39 nm at 20 °C to 41 nm at 80 °C during the temperature increase) would be too small to detect using DLS. However, this diameter increase would equate to a 16 % increase in

volume. Therefore, ^{1}H NMR spectroscopy was more sensitive to small solvation changes than DLS. Because the d_z values were not significantly affected by heating, the data suggest that the spheres were in a thermodynamically stable state and not kinetically trapped.

By contrast to the L_{14}-B_{34} spheres, the L_{14}-B_{64} worms demonstrated irreversible changes for d_z when heated (Fig. 7b). For the latter species at 20 °C, d_z was 481 nm and decreased to 223 nm upon heating to 90 °C. However, upon subsequent cooling to 20 °C a d_z of only 159 nm was measured. Whilst this trend agrees with that reported for $PLMA_{16}$-$PBzMA_{37}$ worms prepared using PISA[26] the d_z values for the present worms were a factor of ~ 3 larger and the onset of the d_z decrease occurred at a much lower temperature (50 ^{o}C here cf. 70 ^{o}C[26]). Moreover, the d_z values for our L_{14}-B_{64} worms decreased at temperatures well below that where solvation of the PBzMA core was detectable by ^{1}H NMR (~ 84 ^{o}C from Fig. 3c). This behaviour differs greatly to that for the spheres and indicates that the worms were relatively unstable and fragmented before the majority of the PBzMA had been solvated. A process akin to fracture can be envisaged whereby the worms cleaved into smaller segments, presumably moving toward spheres[26]. The latter conclusion is generally supported by the PDI data which decreased due to heating.

As the temperature subsequently decreased the formation of worms was favoured. However, worm formation was relatively slow because worms tend to grow by core-core fusion[52, 56]. These differences in temperature-triggered nano-object behaviours for the spheres (Fig. 7a) and the worms (Fig. 7b) have contributions from the PBzMA degree of polymerisation as well as dispersion concentration. The increased y value for the L_{14}-B_{64} worms resulted in them being metastable with possibly less favourable solvation (Fig. 6c). The low worm concentration used for the DLS studies will also have contributed to the lack of reversibility[26]. In a study on a related poly(stearyl-methacrylate-*b*-phenylpropyl methacrylate) system Pei *et al.*[57] observed good worm-to-sphere reversibility using DLS of samples taken from concentrated dispersions. It is likely that the proposed kinetic trapping contributes most to DLS for dilute dispersions because the fragment collision rate is low.

Temperature-triggered gelation

The properties of concentrated L_{14}-B_y dispersions (20% w/w) prepared using the post-polymerisation transfer method illustrated in Scheme 1b were investigated. The L_{14}-B_{34}, L_{14}-B_{46} and L_{14}-B_{64} dispersions became more opaque with increasing y value (Fig. 8a). The use

of solution ATRP afforded gels that were white, which contrasts to the *pink* colour normally associated with RAFT copolymers. This lack of colour is an inherent advantage for the present ATRP approach compared to RAFT because it would facilitate inclusion of chromophores to prepare coloured or fluorescent responsive gels[58] without the complication of end group removal. Tube inversion tests for the diblock copolymers in *n*-dodecane showed that L_{14}-B_{46} and L_{14}-B_{64} formed self-supporting physical gels (Fig. 8a). By contrast, the L_{14}-B_{34} (spheres) and L_{14}-B_{74} (vesicles) copolymers exhibited behaviour of free-flowing liquids.

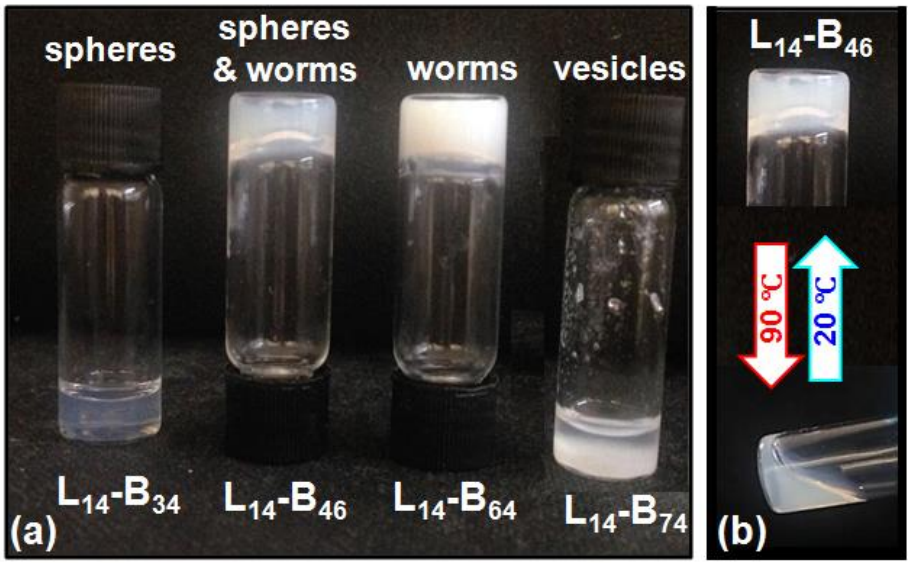

Fig. 8 (a) Concentrated dispersions of $PLMA_{14}$-$PBzMA_y$ diblock copolymers in *n*-dodecane (20 % w/w) at room temperature. Dispersions of L_{14}-B_{34} and L_{14}-B_{74} were free-flowing liquids. The vesicles in L_{14}-B_{74} showed evidence of sedimentation. L_{14}-B_{46} and L_{14}-B_{64} formed self-supporting gels with the former being less turbid. (b) L_{14}-B_{46} de-gelled when heated to 90 ^{o}C to form a free-flowing liquid which subsequently re-gelled when cooled.

Only the L_{14}-B_{46} dispersion showed reversible gel formation behaviour. Heating this gel to 90 °C for 4 h resulted in a free-flowing viscous fluid that could reform into a physical gel upon cooling to 20 °C over a 24 h period (Fig. 5b). Surprisingly, the gel formed from L_{14}-B_{64} did not show reversible gel formation when tested by tube inversion even after 16 h of heating at 90°C. It is likely that the relatively high PBzMA degree of polymerisation of 64 for L_{14}-B_{64} was responsible for the lack of reversibility. The longer PBzMA chains had stronger intra-core attractive interactions. This conclusion implies that temperature-triggered de-gelation (and hence reversibility of gel formation) of L_{14}-B_y is tuneable via *y*.

To gain insight into the gelation behaviour dynamic rheology was used to probe concentrated L_{14}-B_{46} and L_{14}-B_{64} dispersions at 20 ^{o}C. Fig. 9 shows frequency-sweep data and it can be seen that the G' (storage modulus) and tan δ values (= G'' / G', where G'' is the loss

modulus) for both physical gels were frequency-dependent. These data imply that the gels were soft and viscoelastic. The physical gel formed from L_{14}-B_{64} had a greater *G'* value (1,450 Pa) compared to the gel formed from L_{14}-B_{46} (1,180 Pa) at 1 Hz indicating the former system had about 20% more elastically-effective chains. The latter conclusion is from rubber elasticity theory wherein the modulus is proportional to the number-density of elastically effective chains[59]. For the present gels the details of the network are not fully resolved. Nevertheless, the trend of the *G'* values above is expected because of the higher proportion of anisotropic worms which are undoubtedly the load bearing element of these networks. The fact that the gels had tan δ values (Fig. 9b) that were significantly larger than zero (the value for an ideal elastic solid) shows that viscous dissipation mechanisms were operative. We speculate that these involved breaking and reforming of worms based on the trends in Fig. 9b.

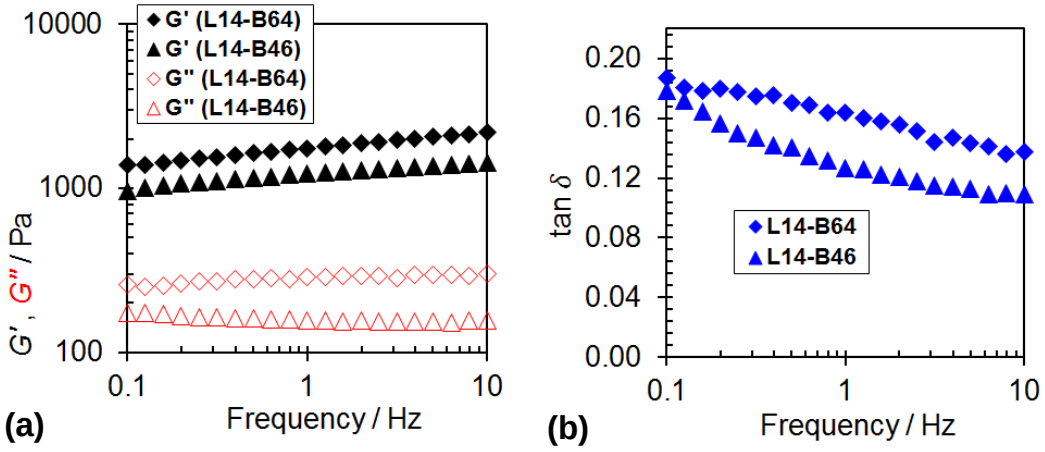

Fig. 9 (a) Dynamic frequency-sweep rheology data for the physical gels formed from L_{14}-B_{64} and L_{14}-B_{46} dispersed in *n*-dodecane (20 % w/w). The *G′* (storage modulus) and *G″* (loss modulus) values are indicated by closed and open data points, respectively. (b) Variation of tan δ (= *G"* / *G′*) with frequency for L_{14}-B_{64} and L_{14}-B_{46}. All data were measured at 20 ^{o}C.

Variable-temperature rheological data were measured to probe the temperature-triggered changes in the gel networks for L_{14}-B_{46} and L_{14}-B_{64} (Fig. 10). The critical gelation temperature (CGT) describes the temperature at which the worm-to-sphere transition occurs to a sufficient extent whereby *G'* becomes equal to *G"* and tan δ = 1.0. Following Fielding *et al.* the CGT values during the first heating cycle could be estimated as 55 ^{o}C for L_{14}-B_{46}.

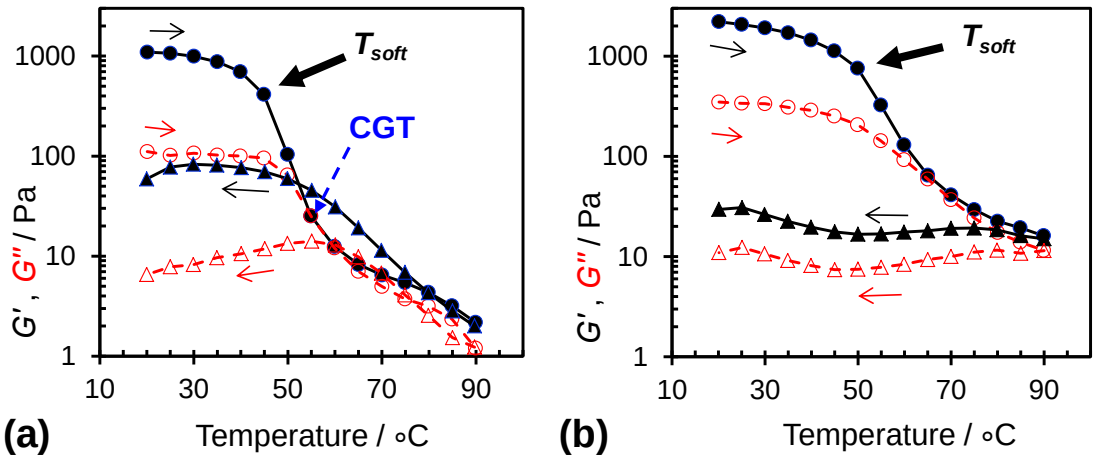

Fig. 10 Variable temperature dynamic rheological data for (a) L_{14}-B_{46} and (b) L_{14}-B_{64} dispersed in *n*-dodecane (20 % w/w). The *G'* (storage modulus) and *G"* (loss modulus) values are indicated by closed data points and open data points, respectively. T_{soft} and CGT are the gel softening temperature and critical gelation temperatures, respectively (See text).

However, close inspection of the data for the variation of tan δ with temperature (Fig. 11) shows that the tan δ values fluctuated with temperature and became less than 1.0 at higher temperatures. This behaviour is a combination of a weak de-gelation process, possible structural rearrangement, and the difficulty of measuring small *G'* and *G"* values. It is noted that the tan δ values for L_{14}-B_{64} remained less than 1.0 at all temperatures (Fig. 11b) and this system did not exhibit a CGT. Of greater significance than the CGT value is the onset of the pronounced *G'* decreases for both systems (Fig. 10). These values occurred at ~ 45 and 50 ^{o}C, respectively for L_{14}-B_{46} and L_{14}-B_{64}, respectively. These values can be considered as "softening temperatures (T_{Soft})". The latter values reside within the temperature range where solvation of the PBzMA blocks was first detectable from the ^{1}H NMR spectroscopy data ($\geq$ 40 ^{o}C, Fig. 6a and b). The beginning of temperature-triggered solvation of the PBzMA cores strongly decreased the load distribution abilities of the worm-based networks.

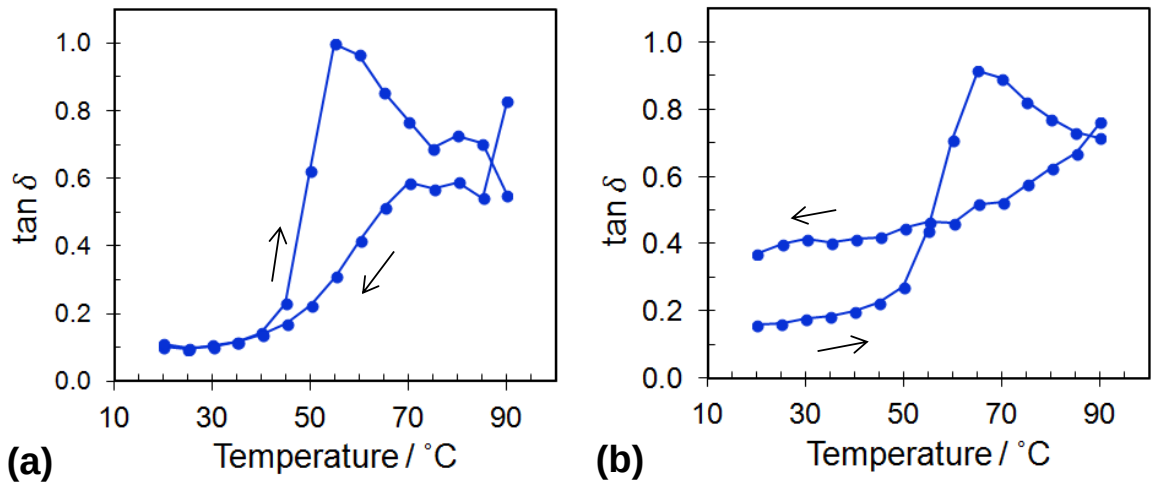

Fig. 11 Variation of tan δ (= G'' / G', where G'' and G' are the loss and storage modulus, respectively) with temperature for (a) L_{14}-B_{46} and (b) L_{14}-B_{64} dispersed in *n*-dodecane (20 % w/w). The measurements started at 20 °C.

It is noteworthy that temperature-triggered reversibility was not observed the L_{14}-B_{64} gels because the G' values remained higher than G'' (and tan δ < 1.0) after the samples were held at 90 °C and then cooled (Fig. 8a and Fig. 11b). This behaviour is consistent with the DLS data (Fig. 7b) and tube inversion study (Fig. 8) as discussed above. However, the lack of gel reversibility contrasts to the reversible gel formation reported for RAFT-based PLMA-PBzMA worm gels[26]. The lack of reversibility for the L_{14}-B_{64} gels was related to the relatively long timescales involved in the reformation of worms which probably involved core fusion. These results lead to the suggestion that $PLMA_x$-$PBzMA_y$ copolymers with higher BzMA contents (such as L_{14}-B_{64}) are more kinetically frozen systems. This claim is supported by the delayed and weaker solvation of the PBzMA chains evident from Fig. 6c. Thus, the mechanical properties of these concentrated worm-based dispersions are tuneable in terms of their reversibility and G' variation with temperature through control of *y*.

Conclusions

The present study is not the first to investigate $PLMA_x$-$PBzMA_y$ nano-objects. However, it is the first to successfully use ATRP combined with post-polymerisation transfer to prepare $PLMA_{14}$-$PBzMA_y$ spheres, worms, and vesicles. This work has demonstrated that PISA *via* RAFT dispersion polymerisation is *not* a prerequisite for preparing self-assembling PLMA-PBzMA nano-objects at high concentrations (20 % w/w). Furthermore, the temperature-responsive behaviour of the spheres was examined for the first time. Variable-temperature ^{1}H

NMR spectra for L_{14}-B_{34} and L_{14}-B_{64} showed that reversible solvation of the PBzMA occurred with increasing temperature. Temperature-triggered worm breakdown did, however, occur and was poorly reversible. Variable-temperature DLS data showed the sphere diameter was not affected by temperature over the range of 20 – 90 ^{o}C and they were considered to be equilibrium systems. Concentrated dispersion studies of the gels revealed that only the mixed phase system (L_{14}-B_{46}) showed reversible temperature-triggered gelation behaviour as measured by tube inversion, whilst the pure L_{14}-B_{64} worms softened (but did not de-gel) at 90 ^{o}C. It was proposed that as *y* increased the morphological transition changed from being largely thermodynamically controlled to having a greater kinetic contribution which is likely a consequence of the sphere-fusion mechanism. The ability to use ATRP and post-polymerisation transfer to achieve concentrated (20 % w/w) nano-object dispersions demonstrated here should also apply to other diblock copolymer / solvent combinations and may bring forward the application of worm-based dispersions for next generation lubricants and gels suited towards to EPD technology. It is noted, however, that the present approach may have some disadvantages compared to PISA because removal of a toxic catalyst and chlorinated solvent was required and the copolymers were less well-defined. Nevertheless, the study opens the door for future systems where decoupling of copolymer synthesis and assembly is desirable.

Acknowledgments

We would gratefully acknowledge funding for this research through an EPSRC iCASE grant (Voucher 12220937).

References

1. N. P. Truong, M. R. Whittaker, A. Anastasaki, D. M. Haddleton, J. F. Quinn and T. P. Davis, *Polym Chem-Uk*, 2016, **7**, 430-440.
2. L. Bes, S. Angot, A. Limer and D. M. Haddleton, *Macromolecules*, 2003, **36**, 2493-2499.
3. K. Matyjaszewski and N. V. Tsarevsky, *Nat Chem*, 2009, **1**, 276-288.
4. Y. C. Chen, K. Zhang, X. J. Wang, F. W. Zhang, J. H. Zhu, J. W. Mays, K. L. Wooley and D. J. Pochan, *Macromolecules*, 2015, **48**, 5621-5631.
5. L. F. Zhang and A. Eisenberg, *Science*, 1995, **268**, 1728-1731.
6. F. L. Baines, N. C. Billingham and S. P. Armes, *Macromolecules*, 1996, **29**, 3416-3420.
7. P. Chambon, A. Blanazs, G. Battaglia and S. P. Armes, *Macromolecules*, 2012, **45**, 5081-5090.
8. C. J. Mable, K. L. Thompson, M. J. Derry, O. O. Mykhaylyk, B. P. Binks and S. P. Armes, *Macromolecules*, 2016, **49**, 7897-7907.

9. N. J. W. Penfold, Y. Ning, P. Verstraete, J. Smets and S. P. Armes, *Chem Sci*, 2016, **7**, 6894-6904.
10. S. L. Canning, G. N. Smith and S. P. Armes, *Macromolecules*, 2016, **49**, 1985-2001.
11. J. Tan, C. Huang, D. Liu, X. Zhang, Y. Bai and L. Zhang, *Acs Macro Lett*, 2016, **5**, 894-899.
12. L. Xiao, Y. Chen and K. Zhang, *Macromolecules*, 2016, **49**, 4452-4461.
13. J. Rieger, C. Grazon, B. Charleux, D. Alaimo and C. Jerome, *J Polym Sci Pol Chem*, 2009, **47**, 2373-2390.
14. S. Boisse, J. Rieger, K. Belal, A. Di-Cicco, P. Beaunier, M. H. Li and B. Charleux, *Chem Commun*, 2010, **46**, 1950-1952.
15. N. J. Warren and S. P. Armes, *J Am Chem Soc*, 2014, **136**, 10174-10185.
16. J. Rosselgong, A. Blanazs, P. Chambon, M. Williams, M. Semsarilar, J. Madsen, G. Battaglia and S. P. Armes, *Acs Macro Lett*, 2012, **1**, 1041-1045.
17. L. A. Fielding, M. J. Derry, V. Ladmiral, J. Rosselgong, A. M. Rodrigues, L. P. D. Ratcliffe, S. Sugihara and S. P. Armes, *Chem Sci*, 2013, **4**, 2081-2087.
18. M. J. Derry, L. A. Fielding and S. P. Armes, *Prog Polym Sci*, 2016, **52**, 1-18.
19. D. Zehm, L. P. D. Ratcliffe and S. P. Armes, *Macromolecules*, 2013, **46**, 128-139.
20. M. Semsarilar, V. Ladmiral, A. Blanazs and S. P. Armes, *Polym Chem-Uk*, 2014, **5**, 3466-3475.
21. M. J. Derry, L. A. Fielding, N. J. Warren, C. J. Mable, A. J. Smith, O. O. Mykhaylyk and S. P. Armes, *Chem Sci*, 2016, DOI: 10.1039/C6SC01243D.
22. V. K. Singh, K. Pal, D. K. Pradhan and K. Pramanik, *J Appl Polym Sci*, 2013, **130**, 1503-1515.
23. S. Sahoo, N. Kumar, C. Bhattacharya, S. S. Sagiri, K. Jain, K. Pal, S. S. Ray and B. Nayak, *Designed Monomers and Polymers*, 2011, **14**, 95-108.
24. M. E. Morales, V. Gallardo, B. Clares, M. B. Garcia and M. A. Ruiz, *J. Cosmetic Sci.*, 2009, **60**, 627-636.
25. A. Ajayaghosh, V. K. Praveen and C. Vijayakumar, *Chem Soc Rev*, 2008, **37**, 109-122.
26. L. A. Fielding, J. A. Lane, M. J. Derry, O. O. Mykhaylyk and S. P. Armes, *J Am Chem Soc*, 2014, **136**, 5790-5798.
27. M. J. Derry, L. A. Fielding and S. P. Armes, *Polym. Chem.*, 2015, **6**, 3054-3062.
28. S. Perrier, P. Takolpuckdee and C. A. Mars, *Macromolecules*, 2005, **38**, 2033-2036.
29. A. B. Lowe, B. S. Sumerlin, M. S. Donovan and C. L. McCormick, *J Am Chem Soc*, 2002, **124**, 11562-11563.
30. Z. C. Li, Y. Z. Liang, G. Q. Chen and F. M. Li, *Macromol Rapid Comm*, 2000, **21**, 375-380.
31. W. L. Zhang, J. L. He, Z. Liu, P. H. Ni and X. L. Zhu, *J Polym Sci Pol Chem*, 2010, **48**, 1079-1091.
32. N. Karanikolopoulos, M. Zamurovic, M. Pitsikalis and N. Hadjichristidis, *Biomacromolecules*, 2010, **11**, 430-438.
33. D. J. Siegwart, J. K. Oh and K. Matyjaszewski, *Prog Polym Sci*, 2012, **37**, 18-37.
34. J. Wang, P. Gao, L. Ye, A. Y. Zhang and Z. G. Feng, *Polym Chem-Uk*, 2011, **2**, 931-940.
35. K. Matyjaszewski and N. V. Tsarevsky, *J Am Chem Soc*, 2014, **136**, 6513-6533.
36. S. Banerjee, T. Maji and T. K. Mandal, *Colloid Polym Sci*, 2014, **292**, 2217-2226.
37. H. Yu, A. Shishido, T. Iyoda and T. Ikeda, *Macromol Rapid Comm*, 2007, **28**, 927-931.
38. E. B. Zhulina, M. Adam, I. LaRue, S. S. Sheiko and M. Rubinstein, *Macromolecules*, 2005, **38**, 5330-5351.

39. Z. Li, M. A. Hillmyer and T. P. Lodge, *Langmuir*, 2006, **22**, 9409-9417.
40. V. Raghunadh, D. Baskaran and S. Sivaram, *Polymer*, 2004, **45**, 3149-3155.
41. P. Cacioli, D. G. Hawthorne, R. L. Laslett, E. Rizzardo and D. H. Solomon, *J Macromol Sci Chem*, 1986, **A23**, 839-852.
42. D. P. Chatterjee and B. M. Mandal, *Macromolecules*, 2006, **39**, 9192-9200.
43. W. J. Xu, X. L. Zhu, Z. P. Cheng and J. Y. Chen, *J Appl Polym Sci*, 2003, **90**, 1117-1125.
44. C. H. Peng, J. Kong, F. Seeliger and K. Matyjaszewski, *Macromolecules*, 2011, **44**, 7546-7557.
45. J. S. Wang and K. Matyjaszewski, *Macromolecules*, 1995, **28**, 7901-7910.
46. K. Matyjaszewski, D. A. Shipp, J. L. Wang, T. Grimaud and T. E. Patten, *Macromolecules*, 1998, **31**, 6836-6840.
47. S. Munirasu, J. Ruhe and R. Dhamodharan, *J Polym Sci Pol Chem*, 2006, **44**, 2848-2861.
48. Q. B. Li, Y. Y. Bao, H. Wang, F. F. Du, Q. Li, B. K. Jin and R. K. Bai, *Polym Chem-Uk*, 2013, **4**, 2891-2897.
49. J. N. Israelachvili, D. J. Mitchell and B. W. Ninham, *J Chem Soc Farad T 2*, 1976, **72**, 1525-1568.
50. M. Semsarilar, E. R. Jones, A. Blanazs and S. P. Armes, *Adv Mater*, 2012, **24**, 3378-3382.
51. S. Sugihara, A. Blanazs, S. P. Armes, A. J. Ryan and A. L. Lewis, *J Am Chem Soc*, 2011, **133**, 15707-15713.
52. L. Wang, Y. Wang, H. Miao and D. Chen, *Soft Matter*, 2016, **12**, 4891-4895.
53. J. S. Trent, J. I. Scheinbeim and P. R. Couchman, *Macromolecules*, 1983, **16**, 589-598.
54. P. P. Soo, B. Huang, Y.-I. Jang, Y.-M. Chiang, D. R. Sadoway and A. M. Mayes, *J. Electrochem. Soc.*, 1999, **146**, 32-37.
55. P. Ranitovic, X. M. Tong, C. W. Hogle, X. Zhou, Y. Liu, N. Toshima, M. M. Murnane and H. C. Kapteyn, *Phys Rev Lett*, 2011, **106**.
56. M. Williams, N. J. W. Penfold, J. R. Lovett, N. J. Warren, C. W. I. Douglas, N. Doroshenko, P. Verstraete, J. Smets and S. P. Armes, *Polym. Chem.*, 2016, **7**, 3864-3873.
57. Y. Pei, O. R. Sugita, L. Thurairajah and A. B. Lowe, *RSC Advances*, 2015, **5**, 17636-17646.
58. J. Hu and S. Liu, *Macromolecules*, 2010, **43**, 8315-8330.
59. L. R. G. Treloar, *The physics of rubber elasticity*, Clarendon, Oxford, 3rd edn., 2005.

Proposed Publication Paper 3

Synthesis and characterisation of temperature-responsive graft copolymers based on lauryl methacrylate

Synthesis and characterisation of temperature-responsive graft copolymers based on lauryl methacrylate

Melody Obeng[a*], Amir H Milani, Lee A. Fielding[a], Muhamad S. Musa[a], Zhengxing Cui[a]
Louise Farrand[b], Mark Goulding[b], Brian R. Saunders[a]
[a]School of Materials, The University of Manchester, Manchester, M13 9PL, UK
[b]Merck Chemicals Ltd, Chilworth Technical Centre, University Parkway, Southampton, SO16 7QD, UK

Abstract

Temperature responsive organic soluble graft copolymers based on poly(lauryl methacrylate)-*b*-poly(benzyl methacrylate) ($PLMA_x$-$PBzMA_y$) were prepared using the multibrominated macroinitiator poly(2-bromoisobutyryloxyethyl acrylate) (PBiBEA) *via* solution ATRP. The degree of polymerisation for PBiBEA (*n*) and PLMA side chain (*x*) were confined to 21 and 15, respectively. Further chain extension of BzMA using the halogen exchange method resulted in graft copolymers, whereby the length of final block (*y*) were 4 and 31, respectively. Transfer of these PBzMA terminated graft copolymers into a selective solvent for PBiBEA and PLMA blocks resulted in spherical macromicelles that formed clusters that were observed by transmission electron microscopy (TEM). Variable-temperature ^{1}H NMR studies showed the onset of enhanced PBzMA solvation was at 70 °C and the extent of thermo-sensitivity of the graft copolymers relied on the length of the solvophobic (PBzMA) block. Variable-temperature dynamic light scattering (DLS) studies revealed evidence of kinetically frozen spheres up to 90 °C. For spheres with shortened PBzMA lengths, the diameters of 195 – 230 nm at 90 °C measured by DLS were significantly larger than the diameters of 97 – 129 nm measured by TEM. This difference was attributed to solvated PLMA-PBzMA side chains at elevated temperature. This proof-of-study concept may provide a route for preparing a new temperature responsive copolymer with potential gelation capability with organic solvents.

Introduction

Temperature-responsive copolymers are versatile materials with growing promise for varied applications[1]. In response to changes in temperature, improved solvation or turbidity in varying degrees can be evident depending on the ratio of the insoluble block to the solvophillic block. The temperature-responsive behaviour of water-soluble graft copolymers is most widely studied[2-5] with fewer reports for organic soluble graft copolymers[6, 7]. The latter formed the basis of this investigation to explore the influence of temperature on a graft copolymer with AB diblock methacrylate polymeric arms. Here, we grafted poly(lauryl methacrylate)-*b*-poly(benzyl methacrylate) (PLMA-*b*-PBzMA) from poly(2-bromoisobutyryloxyethyl acrylate) (PBiBEA) macroinitiator using atom transfer radical polymerisation (ATRP). The hypothesis for this study was that the solvophobic effect of the PBzMA block would result in temperature-responsive behaviour. The second hypothesis was that the graft copolymer design with the PBzMA on the periphery would result in macromicelle formation and temperature sensitivity. The practical motivation for this work was to show that a reversible physical gel would form from concentrated dispersions of the graft copolymer. Due to time constraints, this work was limited to study the temperature-responsiveness of amphiphilic graft copolymers in dilute dispersions.

The thermo-sensitivity of linear PLMA-PBzMA block copolymers is well known[8, 9]. Spherical, worm-like and vesicle nano-objects were synthesised in a selective non-polar solvent (i.e., *n*-dodecane), which encouraged the aforementioned self-assemblies that were dictated by the length of the insoluble (PBzMA) block[10]. Fielding *et al.*[9] reported the mechanistic breakdown of worms at elevated temperatures and attributed it to a worms-to-sphere transition. The morphological change into less strained spherical nano-objects was possible due to improved solubility of the insoluble (PBzMA) block in hot *n*-dodecane. In our previously reported work[11], dilute and concentrated dispersion studies of PLMA-PBzMA copolymers prepared by ATRP were described. The copolymers resulted in concentrated gels composed from the worms and mixed spherical and worms phases, whereby reversible temperature responsive behaviour of the gels were tuneable by the length of the PBzMA block. The earlier study was preliminary work to the present study because the target graft copolymer bears a comparable composition to PLMA-PBzMA side chains, that are grafted from the multibrominated macroinitiator poly(2-bromoisobutyryloxyethyl) acrylate (PBiBEA) (see Fig. 1). It was hypothesised that the present graft copolymers when placed in

n-dodecane would form less turbid stable gels suited for its application in electrophoretic display (EPD) technology.

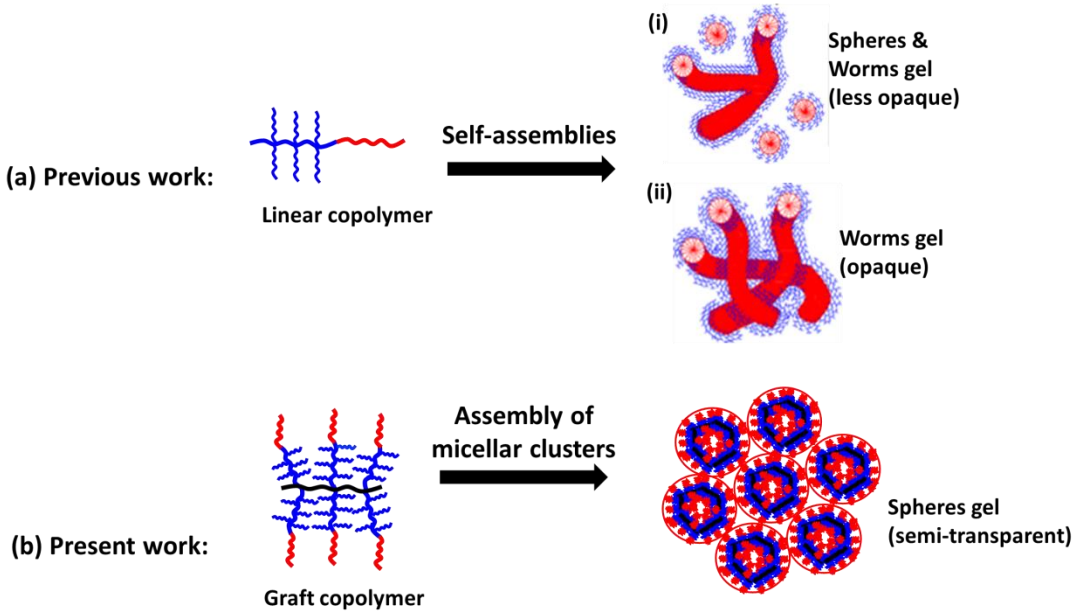

Fig. 1 Design strategies for previous work (a) described in the second proposed publication in Chapter 4 and current work (b). The solvophilic and solvophobic blocks are represented by the blue and red segments, respectively. The solvophilic core (PBiBEA) is exclusive to the graft copolymer and represented by the black segment.

The potential of a polymer gelator envisaged from this study would form a physical gel with the dielectric medium within microencapsulated EPDs. This type of display technology possesses the advantage of being more energy efficient compared to liquid crystal displays[12]. EPDs operate on the principle of bistability[13], which ensures that energy is consumed only when an image is being formed. It was reasoned that the potential of this study could develop a physical gel that can comply with the requirements of bistability, as well as, support the design of reflective displays.

Several (meth)acrylate multi-site initiators[14-16] have been used to synthesise graft copolymers by ATRP. Nese *et al.*[17] reported using PBiBEA to graft poly(*n*-butyl acrylate)-*b*-poly(methyl methacrylate) side chains. The self-assembly of the graft copolymers in this present study was expected to differ from linear block copolymers[10] due to the existence of a PBiBEA backbone. The latter polymer block is assumed to impose conformational limitations as reported in related studies, [18, 19] thus leading to intricate hierarchal structures. The work of Zhang *et al.*[20] and others[21] showed that crowded side chains result in an increase in entropic

energy and interfacial energy between the polymer backbone and polymers arms. Lowering the free energy of the graft copolymer is attainable through convex morphologies, whereby the side chains stretch away from each other. In addition, architectural and interaction parameters of a graft copolymer in an organic solvent can contribute to the energetically preferred morphology[22, 23]. For these reasons structure-property mechanisms concerning the self-assembly of graft copolymer are continuously being developed[24, 25].

Controlled living polymerisation techniques, such as ATRP[26], is a versatile method that has enabled the preparation of diverse graft copolymers. Depending on the length of the core to side chain, star-like[17, 27] or brush-like[28-30] architectures can be produced. With increasing side chain length and quality of the solvent, further stretching of the polymer core is enforced due to repulsion of neighbouring side chains[31]. Typically, there are three routes that can be taken for the creation of graft copolymers structures: grafting-through[32], grafting-from[33] and grafting-to[34]. The grafting-from strategy refers to the core-first approach, whereby side chains are grown[35]. This approach is favoured for the synthesis of densely grafted high molecular weight copolymers with low polydispersity indices. Xu *et al.*[15] reported the synthesis of densely grafted copolymer brushes with PLMA side chains. However, control over the ATRP of PLMA side chains was challenging given the bulky disposition of lauryl methacrylate (LMA)[15].

The temperature-responsive graft copolymers were of interest to this study as the stimulus responsive property is envisaged towards its application in EPD technology. Yamamoto *et al.*[3] described using ATRP to prepare dual responsive graft copolymers based on di(ethylene glycol) methyl ether methacrylate (MEO_2MA) arms grafted from poly (2-(2-bromoisobutyroyloxy) ethyl methacrylate macroinitiators. The temperature triggered association behaviour to temperature was studied in water. When methacrylic acid (MAA) was the terminating block the lower critical solution temperature (LCST) decreased with increasing MAA lengths. Conversely, substituting MAA for *N*-*N*-dimethylaminoethyl methacrylate (DMAEMA) increased the LCST in relation to increasing DMAEMA content. The present study differs from the few reported thermoresponsive organic soluble graft copolymers due to insolubility of PBzMA side chain, and the solubility of the core and PLMA side chain in a selective organic solvent.

The approach used in this study is illustrated in Scheme 1a. LMA was grown from a multibrominated macroinitiator (PBiBEA) *via* solution ATRP, followed by chain extension using BzMA to give the final graft copolymer (PBiBEA-*g*-PLMA$_{15}$-*b*-PBzMA$_y$)$_{21}$. Scheme 1b depicts the steps involved in preparing a graft copolymer dispersion. Firstly, the graft copolymer was dissolved in chloroform which is a good solvent for all polymer blocks. The solution was then transferred into a selective solvent (*n*-dodecane) which is suitable for the PBiBEA and PLMA blocks. Subsequent evaporation of chloroform left spherical-like nanoassemblies made up of PBiBEA, PLMA and PBzMA blocks that form clusters. It is proposed below that PBiBEA and PLMA formed the core whilst PBzMA takes the place of the shell. In this proof-of-concept study, the lengths of the PBzMA block were varied and the degree to which it dictated the morphology and temperature-responsive property of the dispersed graft copolymer was investigated.

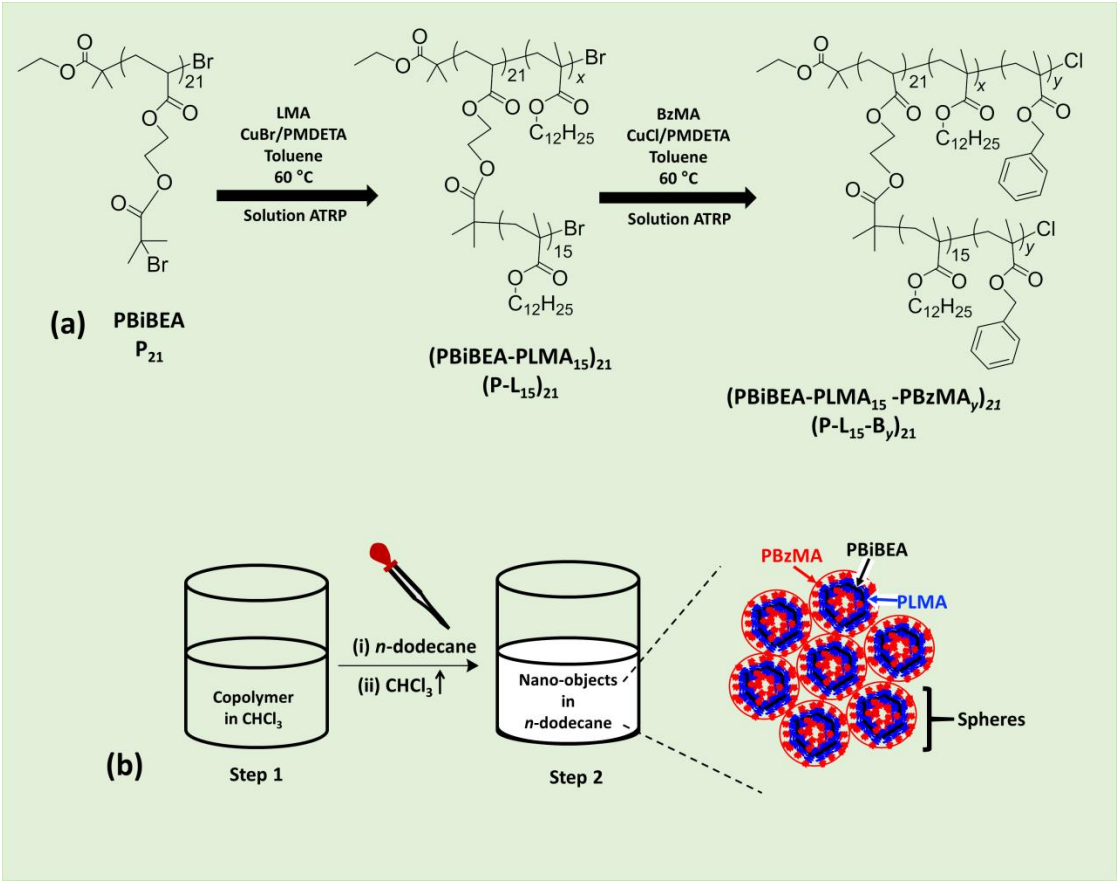

Scheme 1 (a) The synthesis of the graft copolymer (PBiBEA-PLMA$_{15}$-PBzMA$_y$)$_{21}$. The first step was the ATRP-based graft solution polymerisation of LMA from the multibrominated macroinitator (PBiBEA$_{21}$). The next step was chain extension using BzMA and halogen exchange. (b) Macromicelles assemblies of the graft copolymer obtained by post-polymerisation transfer involved replacing a good solvent for all three blocks (chloroform, Step 1) with a selective solvent (*n*-dodecane) for PLMA (Step 2).

The study begins with ^{1}H NMR and GPC characterisation of the polymer backbone and the side chains. TEM studies showed core-shell structure of the graft copolymers and gave insight into the association behaviour of unimolecular graft copolymers to form macromicelle spheres. Variable-temperature ^{1}H NMR spectroscopy illustrated the temperature-responsive behaviour of the graft copolymers. Variable-temperature dynamic light scattering (DLS) studies were used to probe changes of nano-assembly dispersions. The results of this study illustrate that the temperature-responsive behaviour of (PBiBEA-PLMA$_{15}$-PBzMA$_{y}$)$_{21}$ graft copolymers, based on a short polymer backbone, is dependent on concentration

Experimental Section

Materials

PBiBEA was synthesised according to adapted methodology[17] and the reagents used are described in the experimental section of the first proposed publication paper (Chapter 4). LMA (96 %) was purified using a basic alumina column before use. BzMA, 96 %,) was passed through a 1/1 neutral/basic alumina column before use. Toluene (99.5 %,), *N,N,N′,N″,N‴*- pentamethyldiethylenetriamine (PMDETA, 99 %), copper (I) bromide (CuBr, 99.999 %), copper (I) chloride (CuCl, ≥ 99.995 %) and copper (II) chloride ($CuCl_2$, 99.999 %) were purchased from Aldrich and used as received. Chloroform (ACS regent grade), methanol (HPLC grade), tetrahydrofuran (HLPC grade) were all purchase from Fisher and used as received. Chloroform-*d* (99.8 % atom D), dodecane-d_{26} (98 %, atom D) and *n*-dodecane (99+ %) were purchased from Aldrich and Alfa Aesar, respectively, and were used as received

PBiBEA macroinitiator synthesis

A similar method of preparing the PBiBEA macroinitiator (P_{21}) was described in the first proposed publication paper (Chapter 4). A series of three steps were carried out that was adapted to literature[17]. The mass of purified P_{21} was 4.5 g with a percentage yield of ~ 75.2 %. P_{21} was confirmed *via* ^{1}H NMR. ^{1}H NMR (400MHz, $CDCl_3$): δ (ppm) = 4.2-4.4 (m, 4H, -C(=O)O-C**H$_2$**C**H$_2$**-), 4.1 (m, 2H, CH_3-C**H$_2$**-), 2.4 (s, 1H, -CH_2-C**H**-), 2.0, (s, 6H, -C(C**H$_3$**)$_2$Br), 1.4-1.8 (m, 2H, -C**H$_2$**-CH-), 1.2 (m, C**H$_3$**-CH_2-), 1.1, (d, 6H, -C(C**H$_3$**)$_2$-), 0.1 (s, 9H, -O-Si(C**H$_3$**)**$_3$**).

(PBiBEA-PLMA)$_{21}$ graft copolymer synthesis

The first graft copolymer was synthesised from grafting LMA from P_{21} to give (PBiBEA-$PLMA_{15})_{21}$, which is represented by $(P\text{-}L_{15})_{21}$ (Scheme 1a). The molar ratio of monomer [M], initiator [I], copper catalyst [Cu(I)], ligand [L] were 45:1:0.5:0.5. For a typical reaction, a Schlenk flask was charged with P_{21} (25 mg, 0.091 mmol P_{21}-Br groups) dissolved in toluene (1.5 mL) before the remaining toluene (500 μL) was used to dissolve remaining P_{21}. The addition of LMA (1187 μL, 4.05 mmol) and PMDETA (9.4 μL, 0.045 mmol) followed. The reagents were deoxygenated with argon (Ar) whilst stirring magnetically at room temperature before being subjected to repeated freeze-pump-thaw cycles. During the third cycle,

the Schlenk flask was filled with Ar before CuBr (6.4 mg, 0.045 mmol) was quickly added to the frozen mixture. The reaction flask was then sealed, evacuated and backfilled with Ar five times before it was immersed in a pre-heated oil bath of 60 °C for 40 minutes. $(P\text{-}L_{15})_{21}$ mixture was diluted in THF before it was passed through a basic alumina column. $(P\text{-}L_{15})_{21}$ mixture was then concentrated prior to being precipitated from excess methanol. Purified $(P\text{-}L_{15})_{21}$ was finally dried in a vacuum oven at 30 °C for 12 h. The mass of purified P_{21} was 0.7 g with a percentage yield of 65.3 %. $(P\text{-}L_{15})_{21}$ was confirmed *via* ^{1}H NMR. ^{1}H NMR (400MHz, $CDCl_3$): δ (ppm) = 4.0 (s, 2H, -C(=O)O-C**H$_2$**-), 1.7-1.9 (m, 4H, -C**H$_2$**-CH-C(=O)O-CH_2CH_2 and -C**H$_2$**-CCH_3-C(=O)O-CH_2-$(CH_2)_{10}$-CH_3), 1.6 (s, 6H, -C**H$_2$**-CHC(=O)O-CH_2CH_2, -C**H$_2$**-CHC(=O)O-CH_2-C**H$_2$**$C_{10}H_{21}$), 1.3 (s, 18H, -C_9**H$_{18}$**-), 0.9 (s, t, 6H, -CC**H$_3$**C(=O)O-CH_2-$(CH_2)_{10}$-C**H$_3$**).

$(PBiBEA\text{-}PLMA_{15}\text{-}PBzMA_y)_{21}$ copolymer synthesis

A series of graft copolymers were synthesised using BzMA and the halogen exchange method to give $(PBiBEA\text{-}PLMA_{15}\text{-}PBzMA_y)_{21}$, which is abbreviated as $(P\text{-}L_{15}\text{-}B_y)_{21}$ (Scheme 1a). The following is an example for synthesis of $(P\text{-}L_{15}\text{-}B_{31})_{21}$. The molar ratio of monomer [M], initiator [I], ligand [L], CuCl [Cu(I)] and $CuCl_2$ [Cu(II)] were 288:1:1.3:2.6:0.06. A Schlenk flask was charged with $(P\text{-}L_{15})_{21}$ (25 mg, 0.139 mmol $(P\text{-}L_{15})_{21}$-Br groups) dissolved in toluene (1.5 mL) before additional toluene (500 μL) was used to dissolve remaining $(P\text{-}L_{15})_{21}$. The addition of BzMA (6.15 mL, 36.4 mmol), PMDETA (37.3 μL, 0.182 mmol) and $CuCl_2$ (1.2 mg, 0.009 mmol) in the reaction flask followed. The reagents were deoxygenated with Ar whilst stirring magnetically at room temperature before being subjected to repeated freeze-pump-thaw cycles. During the third cycle, the Schlenk flask was filled with Ar before CuCl (36 mg, 0.364 mmol) was quickly added to the frozen mixture. The reaction flask was then sealed, evacuated and backfilled with Ar five times before it was immersed in a pre-heated oil bath of 60 °C for 10 h. $(P\text{-}L_{15}\text{-}B_{31})_{21}$ mixture was diluted in THF before it was passed through a 1/1 neutral/basic alumina column. The same purification method described for $P\text{-}(L_{15})_{21}$ was carried out for $(P\text{-}L_{15}\text{-}B_{31})_{21}$ mixture. The same method described above was used to prepare $P_{21}\text{-}(L_{15}\text{-}B_4)_{21}$. For the preparation of the latter graft copolymer the molar ratio of [M], [I], [L], [Cu(I)] and [Cu(II)] were 785:1:1.3:2.6:0.06. Percentage yield of purified $(P\text{-}L_{15}\text{-}B_y)_{21}$ was ~ 2.1 %. $(P\text{-}L_{15}\text{-}B_y)_{21}$ was confirmed *via* ^{1}H NMR. ^{1}H NMR (400MHz, $CDCl_3$): δ (ppm) = 7.3 (m, 5H, -C_5**H$_5$**), 4.9 (d, 2H, -C(=O)O-C**H$_2$**-C_5H_5-), 1.6-2.0 (m, 8H, -C**H$_2$**-CH-, -C**H$_2$**-CCH_3C(=O)O-CH_2-C**H$_2$**-$C_{10}H_{21}$ and C**H$_2$**-CCH_3-C(=O)O-CH_2-

C_5H_5), 1.3 (s, 18H, -C_9**H_{18}**-) and 0.9-1.2 (m, 9H, -CH_2-CC**H_3**-C(=O)O-CH_2-C_5H_5 and CH_2-CC**H_3**C(=O)O-CH_2-CH_2-C_9H_{18}-C**H_3**).

Physical measurements

The characterisation methods used in the present study were gel permeation chromatography (GPC), ^{1}H NMR spectroscopy, Variable-temperature ^{1}H NMR spectroscopy and dynamic light scattering (DLS). The characterisation conditions were the same as that described in the experimental section of the second proposed publication paper (Chapter 4). Transmission electron microscopy (TEM) measurements of deposited diluted dispersions in *n*-dodecane (0.1 % w/w) were used to measure the average size using 29 graft copolymer particles. The preparation of graft copolymer dispersions and the subsequent TEM staining method was the same as that described the experimental section of the second proposed publication paper (Chapter 4).

Results and Discussion

Graft copolymer characterisation

The PBiBEA macroinitiator (P_{21}) that was used to prepare the graft copolymers shown in Scheme 1a was synthesised first. The ^{1}H NMR spectrum of P_{21} (Fig. 2a) revealed a signal belonging to the 2-bromoisobutyryl unit (1.96 ppm, **h**)[17] that was essential for graft copolymer synthesis. Furthermore, the presence of the proton signal (2.4 ppm, **e**) contained a brominated moiety that can encourage block copolymer growth. This was supported by the absence of this signal following LMA chain growth (see Fig. 2b). However, chain fidelity from this active site was expected to be low due to preparation method for P_{21} (see the experimental section of the first proposed publication paper, Chapter 4). Henceforth, this study focused on the addition of monomer units from 2-bromoisobutyryl units (**h**).

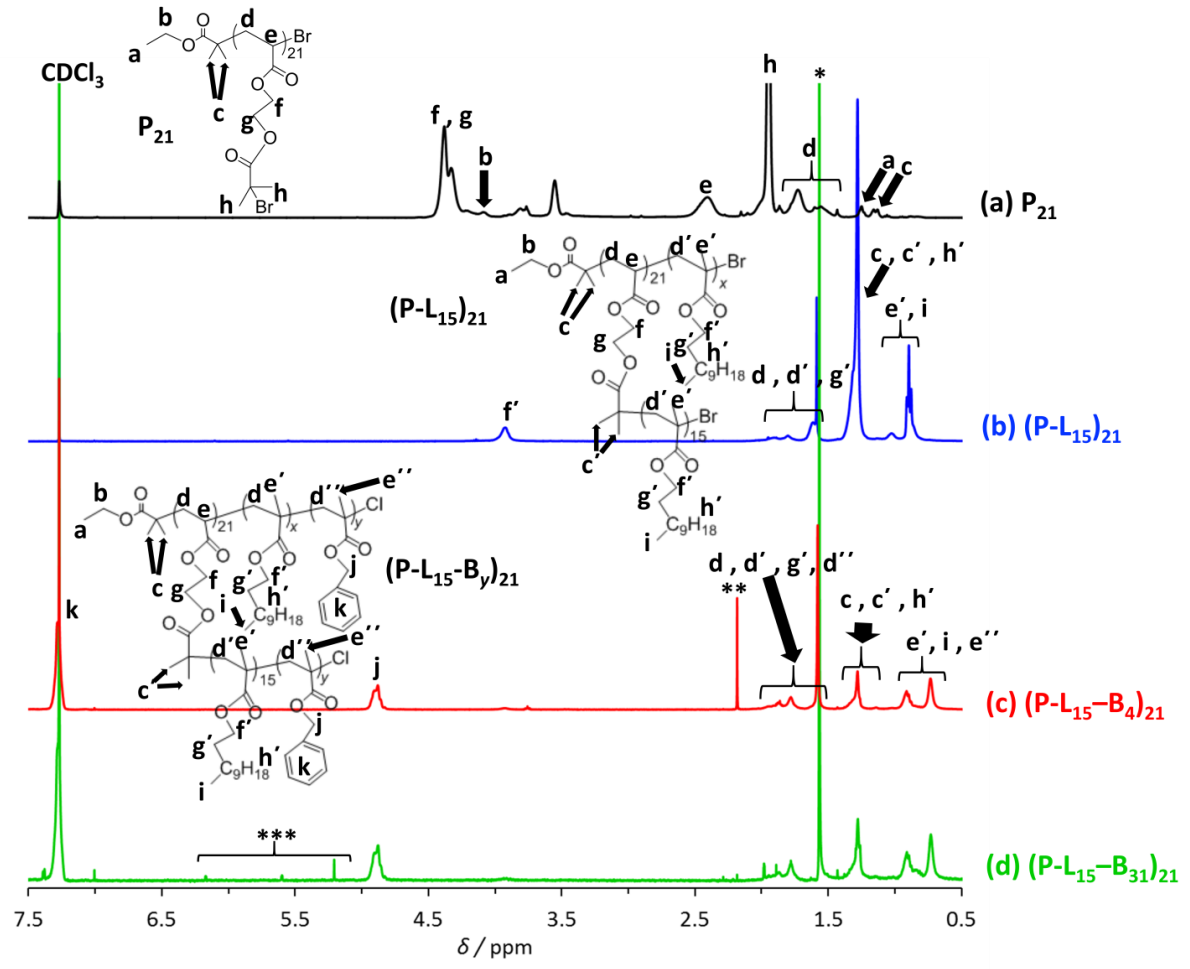

Fig. 2 ^{1}H NMR for the macroinitiator P_{21} (a) and the graft copolymers $(P\text{-}L_{15})_{21}$ (b), $(P\text{-}L_{15}\text{-}B_{4})_{21}$ (c) and $(P\text{-}L_{15}\text{-}B_{31})_{21}$ (d). The peaks labelled with an asterix are identified as residual water (*), acetone (**) and benzyl methacrylate vinyl groups (***), respectively.

The ^{1}H NMR spectrum of P_{21} enabled calculation of the number-average degree of polymerisation (n) through end group analysis using Equation 1:

$$x = \frac{3}{2}\left(\frac{A_f + A_g}{A_c}\right) \qquad \textbf{(1)}$$

whereby A_f , A_g and A_c correspond to the integrals of the protons **f**, **g** and **c**, respectively. The value for n was calculated as 21.0. This latter value was compared with an experimental value for n according to GPC data using Equation 2:

$$n = \frac{M_n - 195}{265} \qquad \textbf{(2)}$$

Including the number-average molecular weight (M_n) of 5,700 g mol^{-1} from Table 1, n was calculated as 21.0 resulting in the abbreviated form of PBiBEA macroinitiator as P_{21}. The consistency of the values of n determined from end group analysis and GPC chromatography indicates good control over the synthesis of P_{21}, which is supported by the monomodal chromatograph (Fig. 3) and a low polydispersity index (PDI) of 1.24 (Table 1). The latter value was comparable with related studies[17] and other polymers prepared *via* ATRP[36].

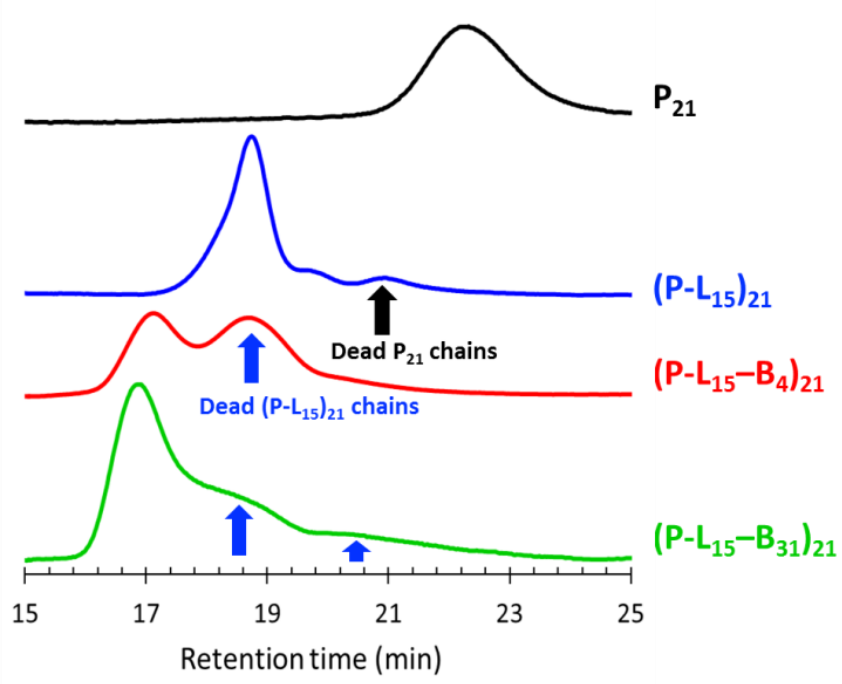

Fig. 3 GPC chromatograms for the macroinitiator P_{21} and the graft copolymers $(P\text{-}L_{15})_{21}$, $(P\text{-}L_{15}\text{-}B_4)_{21}$ and $(P\text{-}L_{15}\text{-}B_{31})_{21}$. The chromatograms were obtained using THF and linear polystyrene standards. The arrows indicate evidence of dead polymeric chains.

Table 1. Compositions and characterisation data for the multibrominated macroinitiator and graft copolymers.

Code	Composition [a]	$M_{n\ (GPC)}$ / g / mol	M_w / M_n	d_z nm [b]	Morphologies [c]
P_{21}	$PBiBEA_{21}$	5,700	1.24	-	-
$(P\text{-}L_{15})_{21}$	$(PBiBEA\text{-}PLMAL_{15})_{21}$	86,500	1.28	-	-
$(P\text{-}L_{15}\text{-}B_4)_{21}$	$(PBiBEA\text{-}PLMA_{15}\text{-}PBzMA_4)_{21}$	102,000	4.01	264	spheres
$(P\text{-}L_{15}\text{-}B_{31})_{21}$	$(PBiBEA\text{-}PLMA_{15}\text{-}PBzMA_{31})_{21}$	199,300	2.40	208	spheres

[a] Compositions of P_{21} and the graft copolymers determined from GPC studies. [b] The spheres z-average diameters were measured at 20 °C *via* DLS. [c] The graft copolymer morphologies were determined from TEM data (Fig. 4).

The chain end fidelity of P_{21} corresponding to the relevant active site (**h**) was calculated using Equation 3:

$$\text{chain end fidelity} = \left(\frac{A_h}{A_c} \times \frac{1}{n}\right) \times 100 \qquad \textbf{(3)}$$

whereby A_h and A_c are the integrals of the protons **h** and **c**. The value for n was 21.0 taken from GPC data (Table 1). The high chain end fidelity[37] calculated here as 96 % implied that efficient grafted side chains would form.

The first graft copolymer was synthesised from polymerising LMA from P_{21} to form the graft copolymer $(P\text{-}L_{15})_{21}$ (Scheme 1a). The ^{1}H NMR spectrum of (Fig. 1b) indicated a successful reaction by the emergence of signals belonging to PLMA side chains (1.5-2.1 ppm) that have replaced the methyl protons of the 2-bromoisobutyryl side chain units belonging to P_{21}. Furthermore, the presence of signals for the long alkyl chain (1.27 ppm, **h´**), oxyethylene protons (4.0 ppm, **f´**) and methyl protons (**e´**, **i**) appear as expected[38-40].

The grafting of PLMA arms was terminated at < 50 % monomer conversion to retain a high percentage of bromo-terminated moieties for the chain extension growth step and to decrease coupling[17]. In the ^{1}H NMR spectrum (Fig. 1b) it was found that the signals that were indicative of P_{21} protons were invisible. Consequently, the number-average degree of polymerisation for $(P\text{-}L_{15})_{21}$ (whereby x = 15.0) was tentatively determined *via* end group analysis. GPC studies were used to calculate the value of x as 15.0 by using Equation 4:

$$x = \frac{M_n - (265n) - 195}{254n} \qquad \textbf{(4)}$$

For the above equation *n* was 21.0. The value for *n* was determined using Equation 2 and the M_n value of 86,500 g mol^{-1} was obtained from GPC studies (Table 1). The value for *x* closely relates to the $PLMA_{14}$ macroinitiator used our previous study[11] which was reported in the second proposed publication paper (Chapter 4). This enabled the present work to demonstrate structure-property differences of the graft copolymers with PLMA-PBzMA side chains.

The bimodal GPC chromatograph of $(P\text{-}L_{15})_{21}$ shows evidence of challenged growth of PLMA arms from dead P_{21} chains (Fig. 3) rather than bimolecular termination. The conclusion was drawn from firstly calculating the number of moles of P_{21} (n_{MI}) by using Equation 5:

$$n_{MI} = \frac{m_{MI}}{M_n} \qquad \textbf{(5)}$$

whereby m_{MI} corresponds to the mass of P_{21} used for $(P\text{-}L_{15})_{21}$ synthesis and M_n value of 5,700 g mol^{-1} for P_{21} obtained from Table 1. This resulted in the value for n_{MI} as 0.0044 mmol. Assuming a cubic lattice, this latter value was used to determine the number of molecules of P_{21} ($\bar{n}_{MI}$) per meter cubed using Equation 6:

$$\bar{n}_{MI} = \frac{N_A\, n_{MI}}{V} \qquad \textbf{(6)}$$

whereby N_A is avogadro's number and V represents the volume of the reaction mixture for $(P\text{-}L_{15})_{21}$ synthesis. Furthermore, Equation 7 was used to determine the distance between neighbouring P_{21} molecules (*H*) from their respective centres.

$$H = \left(\frac{1}{\bar{n}_{MI}}\right)^{\frac{1}{3}} \qquad \textbf{(7)}$$

From the above equation, *H* was 100 Å. The length of PLMA side chains was determined by first calculating the unit length (*x'*) of PLMA using Equation 8:

$$x' = \sin(54.75)Q \qquad \textbf{(8)}$$

whereby *Q* represents the bond length which is equivalent to 1.5 Å for a single carbon-carbon bond. Thus, the length of side chains (*L*) that had LMA repeat units was calculated using Equation 9:

$$L = xm \qquad \textbf{(9)}$$

whereby *x* was 15.0 determined by GPC studies (Table 1), and *m* corresponds to the number of segments that is calculated by Equation 10:

$$m = 1(0.8Q) \qquad \textbf{(10)}$$

Considering Equations 8 -10 led to the value for *L* as 18 Å and 2*L* equating to 36 Å. Therefore, since $H >> 2L$, it was concluded that there was no coupling between neighbouring P_{21} molecules during LMA graft copolymerisation.

Further arm growth was encouraged using BzMA and the halogen exchange method[41, 42] to give $(P\text{-}L_{15}\text{-}B_y)_{21}$ (Scheme 1a). The ^{1}H NMR spectrum for the latter graft copolymer (Fig. 1c-d) presented signals belonging to the oxyethylene protons (4.9 ppm, **j**) and benzene group (7.3 ppm, **k**) as expected[43]. After growth of the BzMA block the relative intensity of PLMA oxyethylene signal (4.0 ppm, **f´**) decreased significantly with respect to BzMA groups (**j** and **k**). Thus, supporting the success of the reaction.

The number-average degree of polymerisation for BzMA block (*y*) was calculated from GPC studies (Table 1) rather than end group analysis due to a lack of the signals belonging to P_{21}. The latter observation was expected given that the P_{21} core would be surrounded by densely grafted PLMA-PBzMA side chains. The value for *y* was calculated using Equation 11:

$$y = \frac{M_n - (265n) - (254xn) - 195}{176} \qquad \textbf{(11)}$$

whereby the M_n value for the $(P\text{-}L_{15}\text{-}B_y)_{21}$ graft copolymer was taken from Table 1. The symbols *x* and *n* corresponded to the number-average degree of polymerisation for PLMA and P_{21}, respectively, which were obtained from GPC studies (Table 1). Considering the

above equation led to the abbreviated graft copolymers $(P\text{-}L_{15}\text{-}B_4)_{21}$ and $(P\text{-}L_{15}\text{-}B_{31})_{21}$, whereby their respective *y* values were calculated as 4.0 and 31.0.

Despite the application of a catalyst switch to increase initiation efficiency, GPC studies of $(P\text{-}L_{15}\text{-}B_4)_{21}$ and $(P\text{-}L_{15}\text{-}B_{31})_{21}$ exhibited bimodal chromatographs (Fig. 3), which were the likely effect of steric congestion[44]. The existence of bulky PLMA groups and nearby densely grafted copolymers may challenge uniform BzMA chain growth, as evidenced by the high polydispersity values which were 4.01 and 2.40 for $(P\text{-}L_{15}\text{-}B_4)_{21}$ and $(P\text{-}L_{15}\text{-}B_{31})_{21}$, respectively.

The length of PLMA-PBzMA side chains for the $(P\text{-}L_{15}\text{-}B_y)_{21}$ copolymers were calculated using Equation 12:

$$L = (x + y)m \qquad \textbf{(12)}$$

whereby *x* was 15.0 and *y* was 4.0 or 31.0 for $(P\text{-}L_{15}\text{-}B_4)_{21}$ and $(P\text{-}L_{15}\text{-}B_{31})_{21}$, respectively. The introduction of the BzMA segment would double the value of *m* determined from Equation 10. This would result in the value for *L* as 46 Å for $(P\text{-}L_{15}\text{-}B_4)_{21}$ and 110 Å for $(P\text{-}L_{15}\text{-}B_{31})_{21}$ when using Equation 12. Therefore, 2*L* for $(P\text{-}L_{15}\text{-}B_4)_{21}$ would be equal to 92 Å which is slightly less than the value for *H* which was calculated as 100 Å. However, the low monomer conversion of 8 % for $(P\text{-}L_{15}\text{-}B_4)_{21}$ suggests that biomolecular termination may have occurred because of a high local concentration of radicals [45]. The same reasoning was applied to $(P\text{-}L_{15}\text{-}B_{31})_{21}$ possessing a value for 2*L* equivalent to 220 Å. These calculations were supported by the high polydispersity values in Table 1 for the graft copolymers. Based on all the results there is strong evidence for the preparation of the graft copolymers. However, it is likely that were impure due to residual dead chains of $(P\text{-}L_{15})_{21}$.

Graft copolymer self-assembly

The self-assembly of graft copolymers was expected to differ significantly when compared to diblock copolymers. When placed in a selective solvent, a linear copolymer self-assembles in order to shield the solvophobic block from unfavourable solvent molecules[46]. Depending on the packing parameter, self-assembled nano-objects such as spheres, worms and vesicles[47] are observed as evidenced for the diblock copolymers discussed in our previous work[11] that is

reported in the second proposed publication paper (Chapter 4). In the present study, the morphological features of (P-L_{15}-B_y)$_{21}$ graft copolymers were studied. The post-polymerisation method that was used (Scheme 1b) involved transferring the graft copolymers under good solvency conditions (in chloroform solution) to *n*-dodecane. With the subsequent removal of chloroform the samples were deposited onto TEM grids. TEM studies of the assemblies of (P-L_{15}-B_4)$_{21}$ and (P-L_{15}-B_{31})$_{21}$ showed assemblies of spherical-like macromicelles (Fig. 4).

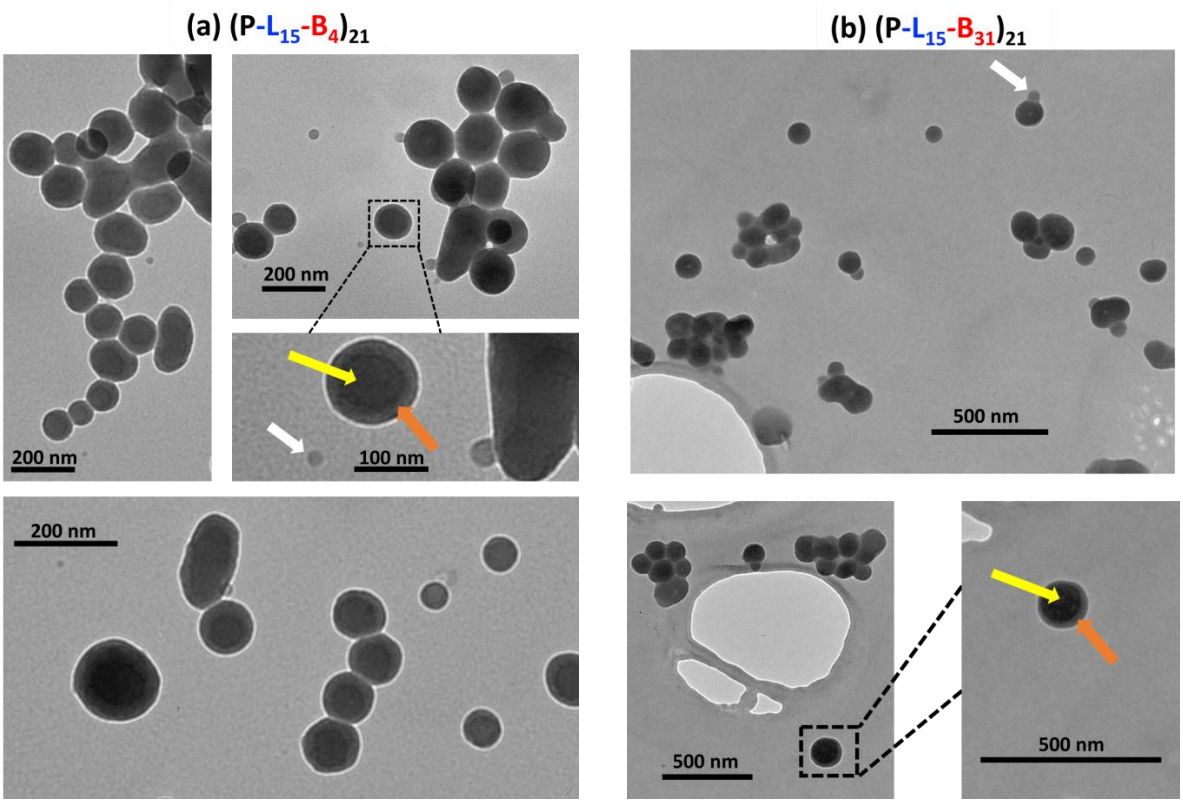

Fig. 4 TEM images for (P-L_{15}-B_4)$_{21}$ (a) and (P-L_{15}-B_{31})$_{21}$ (b) graft copolymer assemblies. Scrutiny of the core-shell morphology is indicated by a yellow arrow (core) and an orange arrow (shell). The white arrow specifies smaller assemblies.

The positive staining method using ruthenium tetra-oxide vapour enhanced contrast of the aromatic group in PBzMA[48, 49]. The number-average diameters (d_{TEM}) of the graft copolymers were 129 ± 16 nm and 97 ± 15 nm for (P-L_{15}-B_4)$_{21}$ and (P-L_{15}-B_{31})$_{21}$, respectively. The diameter (d_{cal}) of a (P-L_{15}-B_y)$_{21}$ particle was estimated using Equation 13:

$$d_{cal} = \left(\frac{6m_{chain}}{\rho\pi}\right)^{\frac{1}{3}} \qquad \textbf{(13)}$$

whereby the density (ρ) of a (P-L_{15}-B_y)$_{21}$ chain was taken as 1.0 g cm^{-3}, and the mass of the chain (m_{chain}) was calculated by inserting relevant information from Table 1 and avagadros number (N_A) into Equation 14:

$$m_{chain} = \frac{M_n}{N_A} \qquad \textbf{(14)}$$

Using the above equations, the diameter of (P-L_{15}-B_4)$_{21}$ and (P-L_{15}-B_{31})$_{21}$ particles were 7 nm and 9 nm, respectively. Although (P-L_{15}-B_{31})$_{21}$ consists of more PBzMA units, the values for d_{cal} suggest similar sized particles for (P-L_{15}-B_4)$_{21}$. This was supported by the narrow size range of d_{TEM} values for the graft copolymers.

Assuming P_{21} and PLMA blocks are fully extended due to its solubility in *n*-dodecane, and repulsive interactions of the side chains[31], the diameters at most may reach 14 nm for (P-L_{15}-B_4)$_{21}$ and 18 nm for (P-L_{15}-B_{31})$_{21}$. In addition, it follows that the PBzMA block would be in a collapsed state in *n*-dodecane, which implies that the length of the particles may be less than the estimated values of diameters. Despite considering this reduction, it is clear the d_{TEM} (Fig 4) is significantly larger than the estimated values of diameters determined from the above equations. This strongly implies that the macromicelles comprise of multiple graft copolymer chains as postulated by Figure 1b. This is supported by closer scrutiny of TEM images for (P-L_{15}-B_4)$_{21}$ (Fig 4a) where smaller particles indicated by a white arrow has a d_{TEM} of 20 nm, which is close to the theoretical size if the soluble blocks were stretched. However, it is also likely that the broad molecular weight distribution (Table 1) of the graft copolymers contributed to the various sized spherical assemblies.

Inspection of the TEM images (Fig 4) shows a core-shell structure for the graft copolymers. For (P-L_{15}-B_{31})$_{21}$, the high coefficient of variation for the cross-sectional length of the core and shell, respectively, deterred the use of the values for further consideration. Nevertheless, the TEM images for (P-L_{15}-B_4)$_{21}$ were used to measure the diameter of the core as 80 ± 12 nm and the shell thickness to be 24 ± 24 nm. It is likely that high polydispersity index values of the graft copolymer played a role in forming less defined structures[50].

It was proposed above that multiple (P-L_{15}-B_y)$_{21}$ particles associate to form spherical assemblies as depicted in Scheme 1. As ruthenium tetra-oxide vapours favour the contrast of

the solvophobic PBzMA block, it was reasoned from the TEM images that the darker regions indicate the association of neighbouring particles with respective PBzMA peripheries touching each other. Darker regions present in vesicular nano-objects reported in our previous work[11] were also concluded to comprise of PBzMA groups in the core. Thus, supporting the above proposal. In the present study, the formation of micellar clusters suggests that the spherical assemblies may prefer to shield outer PBzMA groups from unfavourable solvent molecules. This type of association behaviour is speculated to encourage microgel formation through the entrapment of solvent molecules within the interstices of arranged spheres.

Temperature responsive behaviour of graft copolymers

Given that the graft copolymers comprised of terminating PBzMA groups, it was hypothesised that these assemblies would demonstrate temperature-responsive behaviour in a selective solvent. The effects on varying lengths of the insoluble PBzMA block in concentrated dispersions of $(P\text{-}L_{15}\text{-}B_4)_{21}$ and $(P\text{-}L_{15}\text{-}B_{31})_{21}$ were studied using variable-temperature ^{1}H NMR (Fig. 5 a-b). As the temperature was periodically raised, the signals indicating the aromatic group from PBzMA (7.3 ppm, **k**) and the oxyethylene group from PLMA (4.0 ppm, **f´**) intensified for both graft copolymers. The impurity labelled with * was due to residual monomer and interfered with observing the full extent of the raised **k** proton signal for $(P\text{-}L_{15}\text{-}B_{31})_{21}$.

The ratio of the integrals for the **k** and **f´** proton signals (A_k /A_f´) was calculated and shown in Fig. 5c as a function of temperature. A closer examination of (A_k /A_f´) demonstrates that above 70 ^{o}C the PBzMA block became increasingly soluble in hot dodecane. A similar observation of improved solvation of the PBzMA block was described for the diblock spheres discussed in our previous work[11], that was addressed in the second proposed publication paper. The increased onset temperature for enhanced solvation of the PBzMA block in the present work, could suggest that the spherical macromicelles discourage stretching of the PBzMA block at temperatures below 70 ^{o}C.

The results of the diblock spheres presented in our previous work[11] displayed an intensified oxyethylene proton signal belonging to the PBzMA block. Therefore, it was surprising that the latter signal labelled as **j**, in Fig. 5c, was absent. A clear explanation for this cannot be

provided at this point. However, differences in association for BzMA units within the graft copolymer and the PLMA-PBzMA side chains may be responsible.

Importantly, when the temperature returned to 25 ^{o}C the signal belonging to PBzMA groups were no longer visible. This proves that the graft copolymers response to temperature changes was fully reversible, despite the presence of impurities. Furthermore, the greater values of (A_k /A_f´) for (P-L_{15}-B_4)$_{21}$ has shown that the extent of thermosensitivity is dependent on the length of the BzMA block.

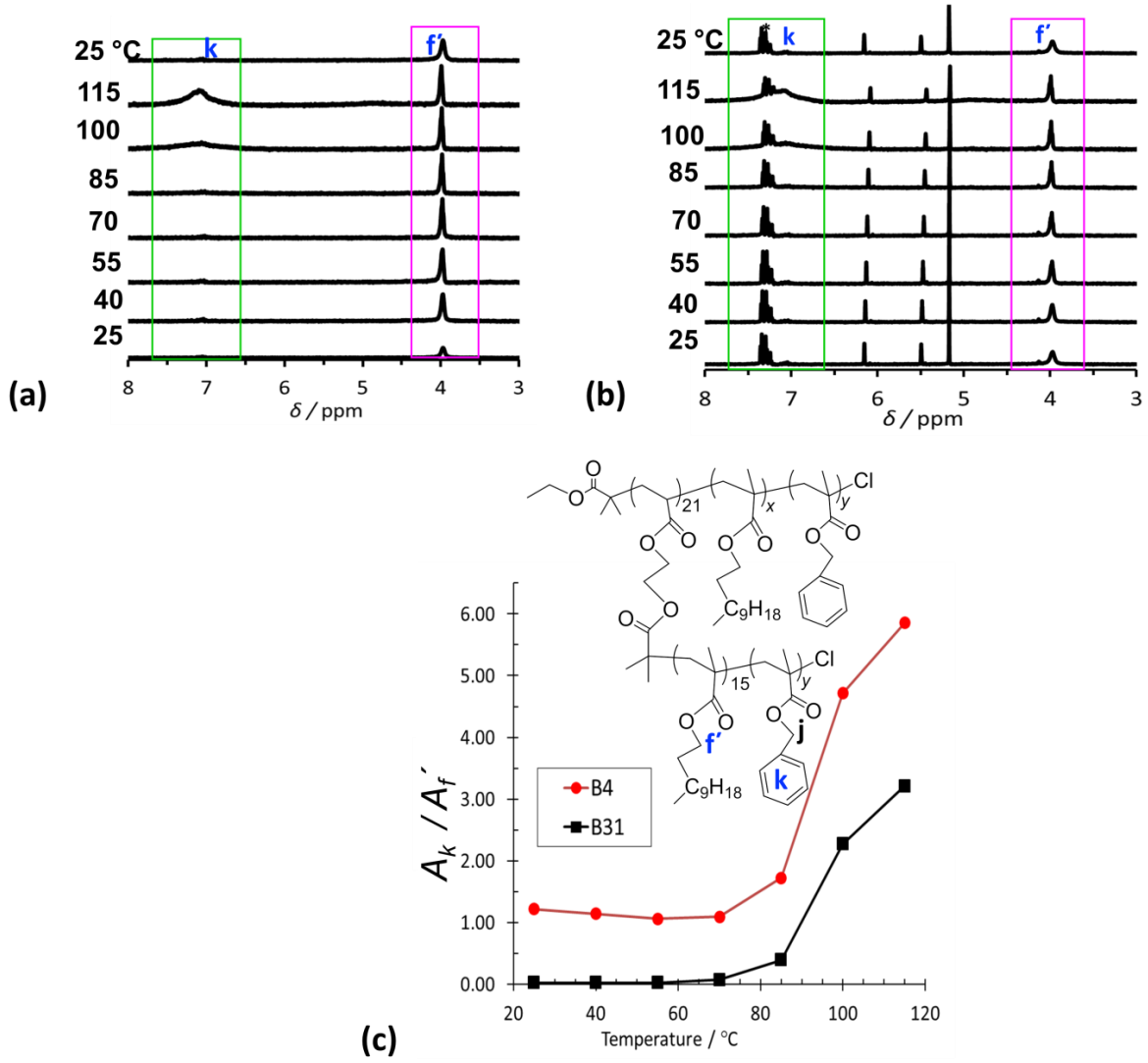

Fig. 5 Variable-temperature ^{1}H NMR studies for dilute dispersions of the graft copolymers (P-L_{15}-B_4)$_{21}$ (a) (P-L_{15}-B_{31})$_{21}$ (b). The temperature increased every 15 ^{o}C from 25 ^{o}C to 115 ^{o}C before returning to the starting temperature. (c) Signal integral ratio for **k** and **f**´ for (P-L_{15}-B_4)$_{21}$ (B4) and (P-L_{15}-B_{31})$_{21}$ (B31).

Variable-temperature DLS measurements were also used to investigate the influence of temperature on the particle size of the graft copolymers. The samples were subjected to a 20 to 90 to 20 °C variable-temperature cycle (Fig. 6). It follows, that the diameter of $(P\text{-}L_{15}\text{-}B_4)_{21}$ and $(P\text{-}L_{15}\text{-}B_{31})_{21}$ at 20 °C were 264 nm and 208 nm, respectively. The smaller diameter for the latter graft copolymer may be related to thermodynamically driven self-assembly into more compact spheres due to increased length of the PBzMA block. The obtained d_z values for $(P\text{-}L_{15}\text{-}B_4)_{21}$ and $(P\text{-}L_{15}\text{-}B_{31})_{21}$ at 90 °C reduced to 230 nm and 195 nm, respectively. There is a significant difference between the overall d_z and d_{TEM} values, whereby the latter values were 129 nm and 97 nm for $(P\text{-}L_{15}\text{-}B_4)_{21}$ and $(P\text{-}L_{15}\text{-}B_{31})_{21}$, respectively. It can be suggested that the PLMA-PBzMA blocks, and in particular the PBzMA units within the spheres, became solvated and prefer to extend their length with increasing temperature. Therefore, it may be speculated from DLS studies that swollen spherical assemblies exist with improved solvation of PLMA-PBzMA side chains.

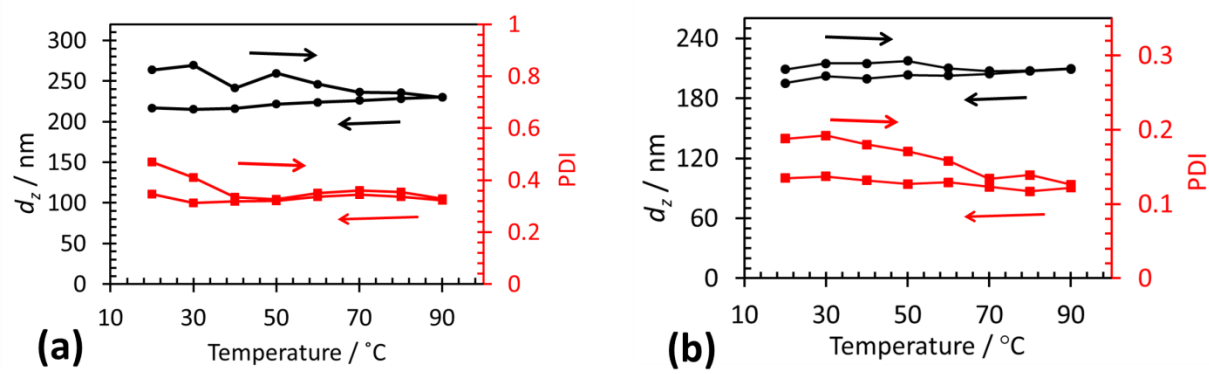

Fig. 6 Variable-temperature DLS studies of the graft copolymers $(P\text{-}L_{15}\text{-}B_4)_{21}$ (a) and $(P\text{-}L_{15}\text{-}B_{31})_{21}$ (b). The *z*-average diameter is represented by black circles, whilst the PDI is represented by red squares. The arrows indicate the direction of the temperature ramps. The temperature ramp began and ended at 20 °C.

Drawing attention to the range of d_z values for $(P\text{-}L_{15}\text{-}B_4)_{21}$, an apparent reduction in size and PDI values that was not reversible upon cooling over the given experimental time may be due to slow association (Fig. 6a). In accordance with the discussed method of association, one could propose that assemblies partly dissociated upon heating. As PBzMA has improved solubility in hot *n*-dodecane, the graft copolymer is more able to exist as mono-molecular micelles independently from the sphere, which may result in its size reduction.

It is interesting to observe that the range of d_z values remains relatively constant for the graft copolymer $(P\text{-}L_{15}\text{-}B_{31})_{21}$ despite increasing temperatures (Fig. 6b). A similar trend was described in the DLS studies of the diblock spheres discussed in our previous work[11] discussed in the second proposed publication paper (Chapter 4). The results for the present study gives one reason to believe that the spheres are equilibrium structures, as an increase in temperature had no effect on the aggregation extent. The lack of temperature responsiveness may relate to longer PBzMA blocks in $(P\text{-}L_{15}\text{-}B_{31})_{21}$ that can exhibit stronger solvophobic association.

In summary, the variable-temperature studies suggest that shorter PBzMA blocks in graft copolymer composition demonstrated greater temperature-responsive behaviour, as the PBzMA blocks are likely to be kinetically trapped. These results lead one to speculate that an associative microgel formed by graft copolymer units is plausible (Scheme 1). Furthermore, it can be speculated that the responsiveness of the graft copolymer with shortest PBzMA units would be greatest.

Conclusions

ATRP was used to prepare organic soluble graft copolymers that assembled into spherical micellar clusters after post-polymerisation transfer from a good solvent to a selective solvent. Variable-temperature ^{1}H NMR spectroscopy demonstrated reversible temperature-responsive behaviour of the graft copolymers. The extent of the latter property was tuneable by the length of the PBzMA block. The relatively constant diameter of the graft copolymer composition with the longest PBzMA block, measured *via* variable-temperature DLS, suggested that the spherical macromicelles might have been effectively frozen equilibrium structures. The enhanced solvation of PLMA-PBzMA side chains probed by variable-temperature studies resulted in larger diameters of the spheres, which proposes that at higher temperatures PLMA-PBzMA side chains within the spheres can extend. Thermodynamically speaking, this can cause some mono-molecular micelles to dissociate from macromicelles. This association behaviour of the graft copolymer offers the potential for microgel formation from *n*-dodecane that may be semi-transparent. Indeed, it maybe suggested that concentrated dispersions have potential to form gels through microgel overlap. This holds promise towards future smart copolymer materials that can be suited for application in electronic paper display technology. However, improvement of the synthetic approach and composition optimisation

are required. In addition, the high polydispersities of the present copolymers means that conclusions must remain tentative.

Acknowledgments

We would gratefully acknowledge funding for this research through an EPSRC iCASE grant (Voucher 12220937).

References

1. E. S. Gil and S. M. Hudson, *Prog Polym Sci*, 2004, **29**, 1173-1222.
2. S. J. Zhai, B. D. Wang, C. Feng, Y. J. Li, D. Yang, J. H. Hu, G. L. Lu and X. Y. Huang, *J Polym Sci Pol Chem*, 2010, **48**, 647-655.
3. S. Yamamoto, J. Pietrasik and K. Matyjaszewski, *Macromolecules*, 2008, **41**, 7013-7020.
4. J. Rueda, S. Zschoche, H. Komber, D. Schmaljohann and B. Voit, *Macromolecules*, 2005, **38**, 7330-7336.
5. J. P. Zhao, G. Z. Zhang and S. Pispas, *J Polym Sci Pol Chem*, 2010, **48**, 2320-2328.
6. C. F. Song, S. R. Yu, C. Liu, Y. M. Deng, Y. T. Xu, X. L. Chen and L. Z. Dai, *Mat Sci Eng C-Mater*, 2016, **62**, 45-52.
7. M. M. Li, P. J. Pan, G. R. Shan and Y. Z. Bao, *Polym Int*, 2015, **64**, 389-396.
8. L. A. Fielding, J. A. Lane, M. J. Derry, O. O. Mykhaylyk and S. P. Armes, *J Am Chem Soc*, 2014, **136**, 5790-5798.
9. A. Blanazs, R. Verber, O. O. Mykhaylyk, A. J. Ryan, J. Z. Heath, C. W. I. Douglas and S. P. Armes, *J Am Chem Soc*, 2012, **134**, 9741-9748.
10. Y. Y. Mai and A. Eisenberg, *Chem Soc Rev*, 2012, **41**, 5969-5985.
11. M. Obeng, A. H. Milani, M. S. Musa, Z. X. Cui, L. A. Fielding, L. Farrand, M. Goulding and B. R. Saunders, *Soft Matter*, 2017, **13**, 2228-2238.
12. D. G. Yu, J. H. An, J. Y. Bae, D. J. Jung, S. Kim, S. D. Ahn, S. Y. Kang and K. S. Suh, *Chem Mater*, 2004, **16**, 4693-4698.
13. B. Comiskey, J. D. Albert, H. Yoshizawa and J. Jacobson, *Nature*, 1998, **394**, 253-255.
14. W. F. M. Daniel, J. Burdynska, M. Vatankhah-Varnoosfaderani, K. Matyjaszewski, J. Paturej, M. Rubinstein, A. V. Dobrynin and S. S. Sheiko, *Nat Mater*, 2016, **15**, 183-+.
15. Y. Y. Xu, H. Becker, J. Y. Yuan, M. Burkhardt, Y. Zhang, A. Walther, S. Bolisetty, M. Ballauff and A. H. E. Muller, *Macromol Chem Physic*, 2007, **208**, 1666-1675.
16. M. F. Zhang, T. Breiner, H. Mori and A. H. E. Muller, *Polymer*, 2003, **44**, 1449-1458.
17. A. Nese, J. Mosnacek, A. Juhari, J. A. Yoon, K. Koynov, T. Kowalewski and K. Matyjaszewski, *Macromolecules*, 2010, **43**, 1227-1235.
18. M. Pitsikalis, J. Woodward, J. W. Mays and N. Hadjichristidis, *Macromolecules*, 1997, **30**, 5384-5389.
19. G. L. Cheng, A. Boker, M. F. Zhang, G. Krausch and A. H. E. Muller, *Macromolecules*, 2001, **34**, 6883-6888.
20. L. S. Zhang, J. P. Lin and S. L. Lin, *J Phys Chem B*, 2008, **112**, 9720-9728.
21. M. Xenidou, F. L. Beyer, N. Hadjichristidis, S. P. Gido and N. B. Tan, *Macromolecules*, 1998, **31**, 7659-7667.

22. Z. W. Xu, J. P. Lin, Q. Zhang, L. Q. Wang and X. H. Tian, *Polym Chem-Uk*, 2016, **7**, 3783-3811.
23. J. F. Wang and M. Muller, *J Phys Chem B*, 2009, **113**, 11384-11402.
24. H. Liu, S. Zhang, C. Feng, Y. J. Li, G. L. Lu and X. Y. Huang, *Polym Chem-Uk*, 2015, **6**, 4309-4318.
25. G. D. Fu, S. J. Phua, E. T. Kang and K. G. Neoh, *Macromolecules*, 2005, **38**, 2612-2619.
26. K. Matyjaszewski, *Macromolecules*, 2012, **45**, 4015-4039.
27. A. Juhari, J. Mosnacek, J. A. Yoon, A. Nese, K. Koynov, T. Kowalewski and K. Matyjaszewski, *Polymer*, 2010, **51**, 4806-4813.
28. H. I. Lee, W. Jakubowski, K. Matyjaszewski, S. Yu and S. S. Sheiko, *Macromolecules*, 2006, **39**, 4983-4989.
29. H. G. Borner, K. Beers, K. Matyjaszewski, S. S. Sheiko and M. Moller, *Macromolecules*, 2001, **34**, 4375-4383.
30. J. P. Zhao, G. Mountrichas, G. Z. Zhang and S. Pispas, *Macromolecules*, 2010, **43**, 1771-1777.
31. K. Fischer and M. Schmidt, *Macromol Rapid Comm*, 2001, **22**, 787-791.
32. G. Morandi, G. Mantovani, V. Montembault, D. M. Haddleton and L. Fontaine, *New J Chem*, 2007, **31**, 1826-1829.
33. A. Nese, Y. C. Li, S. Averick, Y. Kwak, D. Konkolewicz, S. S. Sheiko and K. Matyjaszewski, *Acs Macro Lett*, 2012, **1**, 227-231.
34. B. Zdyrko and I. Luzinov, *Macromol Rapid Comm*, 2011, **32**, 859-869.
35. K. L. Beers, S. G. Gaynor, K. Matyjaszewski, S. S. Sheiko and M. Moller, *Macromolecules*, 1998, **31**, 9413-9415.
36. T. E. Patten, J. H. Xia, T. Abernathy and K. Matyjaszewski, *Science*, 1996, **272**, 866-868.
37. J. Pyun, T. Kowalewski and K. Matyjaszewski, *Macromol Rapid Comm*, 2003, **24**, 1043-1059.
38. R. V, D. Baskaran and S. Sivaram, *Polymer*, 2004, **45**, 3149-3155.
39. D. P. Chatterjee and B. M. Mandal, *Macromol Symp*, 2006, **240**, 224-231.
40. W. J. Xu, X. L. Zhu, Z. P. Cheng and J. Y. Chen, *J Appl Polym Sci*, 2003, **90**, 1117-1125.
41. D. A. Shipp, J. L. Wang and K. Matyjaszewski, *Macromolecules*, 1998, **31**, 8005-8008.
42. K. Matyjaszewski, D. A. Shipp, J. L. Wang, T. Grimaud and T. E. Patten, *Macromolecules*, 1998, **31**, 6836-6840.
43. Q. B. Li, Y. Y. Bao, H. Wang, F. F. Du, Q. Li, B. K. Jin and R. K. Bai, *Polym Chem-Uk*, 2013, **4**, 2891-2897.
44. D. Neugebauer, B. S. Sumerlin, K. Matyjaszewski, B. Goodhart and S. S. Sheiko, *Polymer*, 2004, **45**, 8173-8179.
45. C. Waldron, A. Anastasaki, R. McHale, P. Wilson, Z. D. Li, T. Smith and D. M. Haddleton, *Polym Chem-Uk*, 2014, **5**, 892-898.
46. R. Nagarajan and K. Ganesh, *Macromolecules*, 1989, **22**, 4312-4325.
47. A. Blanazs, J. Madsen, G. Battaglia, A. J. Ryan and S. P. Armes, *J Am Chem Soc*, 2011, **133**, 16581-16587.
48. J. S. Trent, J. I. Scheinbeim and P. R. Couchman, *Macromolecules*, 1983, **16**, 589-598.
49. P. P. Soo, B. Y. Huang, Y. I. Jang, Y. M. Chiang, D. R. Sadoway and A. M. Mayes, *J Electrochem Soc*, 1999, **146**, 32-37.

50. B. S. Sumerlin, D. Neugebauer and K. Matyjaszewski, *Macromolecules*, 2005, **38**, 702-708.

5 Conclusions and future work

5.1 Work overview

The motivation for this study was to design and prepare a polymer organogelator that could be applied in an electrophoretic paper display (EPD). This framed the vision of Merck's goal of producing the next generation of EPDs that can one day be commercially available. It was envisaged that the polymer organogelator can form a transparent physical gel from a non-polar organic fluid (i.e., *n*-dodecane) and that the gel would exhibit rapid self-healing properties to adhere to the energy efficient mechanism of EPD technology. Three studies, that employed atom transfer radical polymerisation (ATRP) as the main method of synthesis, were carried out to address the aim of the project in this thesis.

The work from the first proposed publication paper worked towards developing a polymer gelator containing a low molecular weight gelator (LMWG) portion. The latter molecule would be responsible for encouraging gelation through intermolecular interactions as described in Chapter 2. The first strategy, which was driven to prepare a linear copolymer gelator based on poly(lauryl methacrylate)-*b*-poly(2-hydroxyethyl methacrylate) (PLMA-PHEMA), was realised. This accomplishment provided insight into designing a graft copolymer gelator with a similar composition for the polymeric side chains. It was envisaged that the graft copolymer approach would further increase the stability of the gel by preventing crystallisation of the LMWG portion. However, towards the end of the investigation, an easier approach was selected that might appeal to better industrial scale synthesis.

The second proposed publication paper focused on preparing a polymer gelator that would cause gelation from *n*-dodecane due to the differing solubilities of the polymer segments in the diblock copolymer. The diblock copolymer comprised of poly(lauryl methacrylate)-*b*-poly(benzyl methacrylate) (PLMA-PBzMA), whereby PBzMA formed the insoluble block in *n*-dodecane. For the first-time, solution ATRP was used to prepare PLMA-PBzMA amphiphilic copolymers. Subsequently, that following a post-polymerisation technique enabled the self-assembly of PLMA-PBzMA amphiphilic copolymers into various morphologies in *n*-dodecane. This provided a versatile method for synthesising spherical, worm-like and vesicle polymeric nano-objects that were observed by electron microscopy. Concentrated dispersions of the pure worms and the mixed spherical and worms resulted in

gels. However, they were opaque and therefore unsuitable for EPD application. In addition, the gels exhibited a slow self-healing ability (i.e., over a 24 h period) that would hinder the energy efficient mechanism in EPD technology. Nonethless, it is noteworthy to mention that the mechanical properties and reversible temperature-responsive behaviour of the gels were tuneable by the length of the PBzMA block. Overall, this approach did present some advantages to using ATRP over reversible addition-fragmentation chain transfer (RAFT) for the preparation of gels, in particular, the absence of colour.

The third proposed publication paper was a proof-of-concept study that investigated the temperature-responsive behaviour of a polymer organogelator based on an amphiphilic graft copolymer architecture. The graft copolymer possessed PLMA-PBzMA side chains, thereby relating this work to the study described above. Electron microscopy images revealed spherical macromolecular micelles that further associated to form clusters. The size of the spheres formed in this study suggested that multiple graft copolymers make up a macromolecular micelle. Variable-temperature studies demonstrated that thermosensitivity of the graft copolymers also relied on the length of the PBzMA block. At elevated temperatures, the size of the graft copolymer with the shortest PBzMA length were larger than the measured diameters obtained from electron microscopy. Due to associative formation having occurred for these assemblies, there is reason to suppose that concentrated dispersions from *n*-dodecane may form gels.

In summary, the cumulative findings of the studies discussed in this thesis can lead one to conclude that ATRP is a versatile technique that can produce gels that exhibit stimulus responsive behaviour. This is despite the challenges of control over polymerisation. Gelation driven by self-assembled diblock copolymers was the most successful in providing temperature-responsive gels. The data allows tentative suggestion for the formation of less turbid gels by tuning the length of the solvophobic portion in the polymer gelator.

5.2 Future work

The use of ATRP for this study provided scope to synthesise robust polymer organogelators. The most successful approach involved the preparation of amphiphillic diblock copolymer gelators because it led to the formation of concentrated gels, whereby the temperature-responsive behaviour of a concentrated gel was tuneable by the length of the solvophobic

block. Tailoring the ratio of the solvophobic block to the solvophillic block could be explored in future work. Whilst keeping the solvophillic block at a fixed length (i.e., DP of 14), reducing the length of the solvophobic block to obtain the lowest mixed spheres and worms composition would be of interest, as this mixed phase bears good gelation ability. It is important that for a mixed phase composition a critical worms concentration is present to enable gelation. In addition, the presence of isotropic spheres would imply that a near-transparent dispersion would be obtainable. The influence of these nano-objects could result in concentrated gel that can exhibit faster rates of breakdown and reformation compared to analogous gels based on predominately worms.

It is well known that the slow temperature-responsiveness of such amphiphilic copolymer gelators is dependent on slower kinetic contributions, which would imply their overall method of self-assembly is less ideal for dynamic EPD technology. Furthermore, the lack of transparency for the resultant gels would be problematic in EPD technology. However, the lowest mixed spheres composition may be able to circumvent the latter disadvantage and the resultant gel could be applied in passive EPD devices. The stability of the gels would be able to support information being displayed over a long period of time.

The diblock copolymer organogelator approach could also be a useful template for the preparation of Pickering emulsifiers synthesised *via* ATRP. Their well-defined nanostructures and stimuli-responsiveness could be useful in controlled release studies such as drug delivery, where slower rates of drug release at a specific target area would be desirable. The vesicle morphology would be of interest for such an application due to its large surface area and hollow region for drug encapsulation. In the context of biomedicine, it would be important that the chosen block copolymers and the organic fluid are biocompatible. In addition, given that copper is a toxic metal, exploring ATRP methods that utilise an alternative catalyst (i.e., iron) or purification methods that can efficiently remove ppm amounts of copper, should be considered. It is probable that the latter suggestion for future work would attract academic research before industrial efforts due to the high expense of wastage.

The versatility of ATRP implies that, optimising the ATRP conditions for the (co)polymerisation of lauryl methacrylate and benzyl methacrylate could be tailored to the polymerisation of other methacrylate monomers. Altering the type of monomer and non-polar

solvent could result in less translucent dispersions. In summary, the adaptability of solution ATRP gives opportunity for future smart materials that can be easily stored and used closer to the time of application.